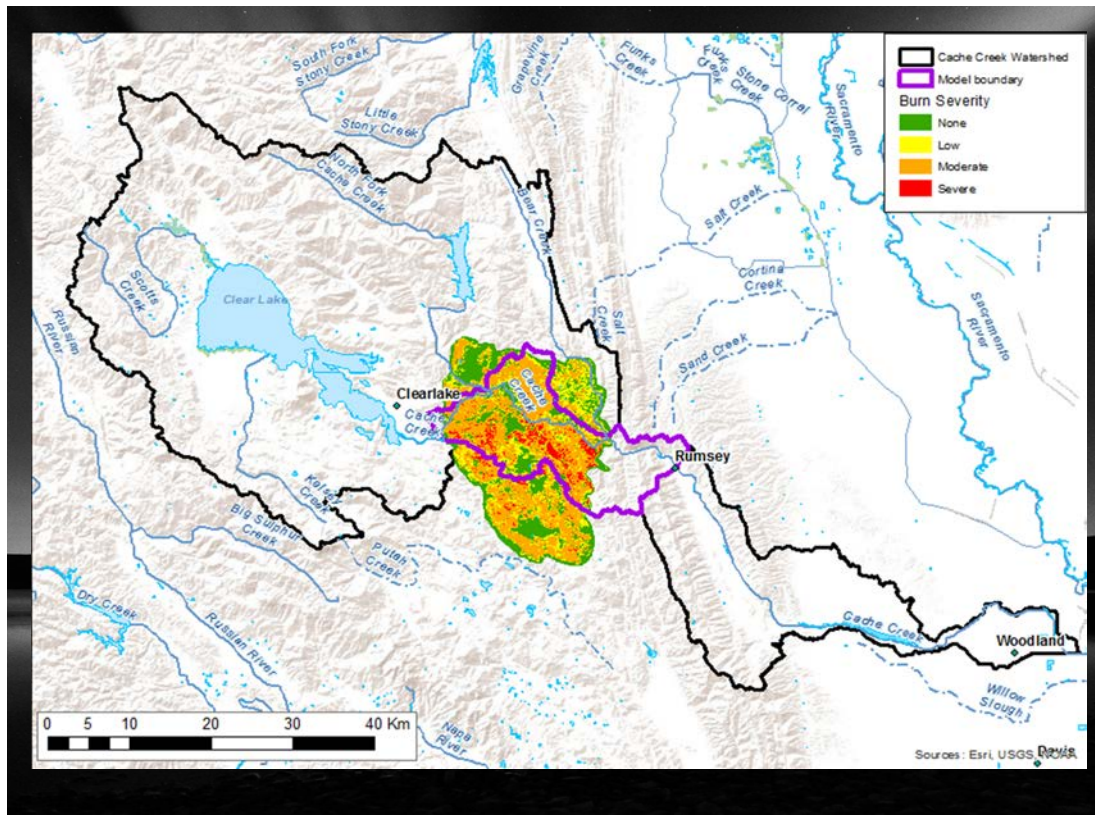


RECLAMATION

Managing Water in the West

Research and Development of a Watershed-Scale Model/Tool for Simulating the Effects of Wildfires on Mercury Contamination of Land and Water

Research and Development Office
Science and Technology Program
(Final Report) ST-2019-7112-01



U.S. Department of the Interior
Bureau of Reclamation
Research and Development Office

09/30/2019

Mission Statements

Protecting America's Great Outdoors and Powering Our Future

The Department of the Interior protects and manages the Nation's natural resources and cultural heritage; provides scientific and other information about those resources; and honors its trust responsibilities or special commitments to American Indians, Alaska Natives, and affiliated island communities.

Disclaimer:

This document has been reviewed under the Research and Development Office Discretionary peer review process https://www.usbr.gov/research/peer_review.pdf consistent with Reclamation's Peer Review Policy CMP P14. It does not represent and should not be construed to represent Reclamation's determination, concurrence, or policy.

REPORT DOCUMENTATION PAGE		<i>Form Approved</i> <i>OMB No. 0704-0188</i>
T1. REPORT DATE: SEPTEMBER 2019	T2. REPORT TYPE: RESEARCH	T3. DATES COVERED October 2016 – September 2019
T4. TITLE AND SUBTITLE Research and Development of a Watershed-Scale Model/Tool for Simulating the Effects of Wildfires on Mercury Contamination of Land and Water		5a. CONTRACT NUMBER WBS: RY.15412017.CC27112
		5b. GRANT NUMBER N/A
		5c. PROGRAM ELEMENT NUMBER 1541 (S&T)
6. AUTHOR(S) Jun Wang, junwang@usbr.gov , Michelle Stern, mstern@usgs.gov Charles N. Alpers, cnalpers@usgs.gov , Vanessa M. King, vking@usbr.gov , Jackson Webster, jwebster13@csuchico.edu , Nigel W.T. Quinn, nwquinn@lbl.gov , Yong Lai, ylai@usbr.gov		5d. PROJECT NUMBER ST-2019-7112-01
		5e. TASK NUMBER N/A
		5f. WORK UNIT NUMBER MP-740
7. PERFORMING ORGANIZATION NAME(S) AND ADDRESS(ES) Jun Wang United States Bureau of Reclamation Mid-Pacific Region 2800 Cottage Way, Sacramento, CA 95825 Email: junwang@usbr.gov , Phone: (916) 978-5189		8. PERFORMING ORGANIZATION REPORT NUMBER
9. SPONSORING / MONITORING AGENCY NAME(S) AND ADDRESS(ES) Research and Development Office U.S. Department of the Interior, Bureau of Reclamation, PO Box 25007, Denver CO 80225-0007		10. SPONSOR/MONITOR'S ACRONYM(S) R&D: Research and Development Office BOR/USBR: Bureau of Reclamation DOI: Department of the Interior
		11. SPONSOR/MONITOR'S REPORT NUMBER(S) ST-2019-7112 -01
12. DISTRIBUTION / AVAILABILITY STATEMENT Final report can be downloaded from Reclamation's website: https://www.usbr.gov/research/		
13. SUPPLEMENTARY NOTES		
14. ABSTRACT (Maximum 200 words) Project goals were achieved by constructing a relatively simple watershed-scale model to simulate wildfire effects on runoff, and loads of sediment, mercury (Hg) and methylmercury (MeHg) at the watershed outlet. Runoff increases after wildfires that burn vegetation and create a condition of soil-water repellence (SWR). A new post-fire watershed hydrological model, PFHydro, was created to simulate vegetation interception and SWR effects for four burn-severity categories: high, medium, and low severity and unburned. The model was applied successfully to the upper Cache Creek watershed in California by simulating two years pre-fire (water year (WY) 2015, 2016) and two years post-fire (WYs 2016-17). The PFHydro-WQ model was created and applied successfully in the Cache Creek watershed for WYs 2015-2017 by simulating daily sediment erosion and load with input of surface runoff from PFHydro. A one-dimensional soil-heating model was used to estimate fire-related Hg loss from soils as a function of burn severity and vegetation. Land use/land cover data were used to estimate post-fire soil Hg concentrations. Daily sediment loads were used to make reasonable estimates of Hg and MeHg loads, which were dominantly particulate.		

15. SUBJECT TERMS Wildfire, Effects, flow, sediment, Hg/MeHg, Modeling					
16. SECURITY CLASSIFICATION OF:			17. LIMITATION OF ABSTRACT	18. NUMBER OF PAGES	19a. NAME OF RESPONSIBLE PERSON Jun Wang
a. REPORT	b. ABSTRACT	c. THIS PAGE	U		19b. TELEPHONE NUMBER (916) 978-5189
U	U	U			

S Standard Form 298 (Rev. 8/98)
P Prescribed by ANSI Std. 239-18

BUREAU OF RECLAMATION

Research and Development Office
Science and Technology Program

Final Report ST-2019-7112-01

Title: Research and Development of a Watershed-Scale Model/Tool for Simulating the Effects of Wildfires on Mercury Contamination of Land and Water

Prepared by: Jun Wang, PhD, PE
Civil Engineer/Water Resources Modeler
Interior Region 10, California-Great Basin, Division of Planning

Peer Review: Daniel Deeds, PhD
Regional Water Quality Coordinator
Interior Region 10, California-Great Basin, Division of Planning

For Reclamation disseminated reports, a disclaimer is required for final reports and other research products, this language can be found in the peer review policy:

This document has been reviewed under the Research and Development Office Discretionary peer review process https://www.usbr.gov/research/peer_review.pdf consistent with Reclamation's Peer Review Policy CMP P14. It does not represent and should not be construed to represent Reclamation's determination, concurrence, or policy.

Executive Summary

Mercury (Hg) is a toxic metal that is found both naturally and as an introduced contaminant in aquatic environments. Methylation is the most important step in the mercury cycle because it greatly increases toxicity and potential for accumulation in aquatic biota. Methylmercury (MeHg) is the most toxic form and even at very low concentrations can lead to bioaccumulation within the aquatic food web and cause high levels of mercury contamination in fish. The behavior of Hg depends on numerous chemical, physical, and biological processes that vary in space as a function of the biogeochemical and hydrodynamic environment. Mercury can also vary in time over different scales (e.g. inter-annual, seasonal, diurnal, tidal). Wildfire is known to affect Hg cycling in watersheds by mobilizing volatile Hg into the atmosphere and allowing Hg to be carried off attached to sediments when mobilized by rainfall-runoff. Increases in MeHg in water, sediment, and biota have been documented as an aftermath of wildfire.

In California, Reclamation will be required to comply with new mercury TMDL objectives and both develop and implement various reservoir mercury management practices to help control MeHg mobilization and export to downstream water bodies. Research has indicated that each aquatic water body should be evaluated individually; similar conditions in separate reservoirs have been shown to produce different rates of mercury bioaccumulation. Management practices should be evaluated on an individual reservoir basis, although, at present there are currently no reliable procedures to make such an evaluation. Hence Reclamation, the U.S. Geological Survey, the Bureau of Land Management, the U.S. Army Corps of Engineers and Berkeley National Laboratory are collaborating on a joint effort to understand the effects of fire on Hg and MeHg cycling in important watersheds in California in order to develop an integrated and comprehensive modeling approach.

This report has been written to document progress toward the development of an integrated mathematical model to simulate mercury and methylmercury loads in watersheds subject to wildfire. The modeling took place in three phases. In the first phase, a new model called PFHydro was developed to simulate the effects of wildfire on runoff generation (Ch. 2). The PFHydro was calibrated and validated successfully in simulating post-fire runoff for water year 2016, 2017. In the second phase, the PFHydro-WQ model was developed to simulate the daily sediment load under pre- and post-fire conditions (Ch. 3). In the third phase, the pre- and post-fire levels of total mercury and methylmercury loads were modeled (Ch. 4). The PFHydro and PFHydro-WQ were successfully applied to Upper Cache Creek Watershed in modeling post-fire runoff, sediment load and get reasonable results in modeling mercury and methyl mercury load.

The end goal is the development of a comprehensive decision support tool to guide actions that might be taken by Reclamation in reducing mercury loading to Reclamation-owned and operated reservoirs – such as Lake Berryessa in Solano County, California. Although this final stage of model development is beyond the scope of this three-year initial effort, the component pieces, supported by state-of-the-art technical review and employment of best scientific practices, will be in place to catalyze and support this effort.

Table of Contents

Title: Research and Development of a Watershed-Scale Model/Tool for Simulating the Effects of Wildfires on Mercury Contamination of Land and Water	iv
1 Background	1
1.1 Report Organization	2
1.2 Literature Review Summary	3
1.3 References	15
1.4 References specific to Putah and Cache Creek watersheds	26
1.4.1 Upper Cache Creek Basin (including Clear Lake)	26
1.4.2 Lower Cache Creek Watershed, including Settling Basin	28
2 PFHydro: A New Watershed-Scale Model for Post-Fire Runoff Simulation (Journal Manuscript)	30
3 Sediment Load Simulation at Cache Creek	31
3.1 Introduction	31
3.2 Summary description of the USLE (Wischmeier and Smith, 1978)	31
3.3 Specific Models for Cache Creek Modeling	35
3.4 Wildfire Impact	37
3.5 Using HSPF results as sediment load boundary conditions	38
3.6 Pre- and post-fire modeling results	39
3.7 Discussion and break-down of KLSCP under pre- and post-fire conditions	44
3.7.1 A break-down of the combined coefficient KLSCP	45
3.8 References	47
4 Modeling Pre- and Post-fire Mercury Load Using PFHydro-WQ	49
4.1 Overview of mercury in the Cache Creek watershed	49
4.1.1 Forms of mercury	49
4.1.2 Mercury in soils	50
4.1.3 Mercury in sediment	50
4.1.4 Mercury in water	51
4.1.5 Methylmercury in soils, sediment, and water	52
4.2 Observed changes in post-fire in-stream mercury and conceptual model for transport	52
4.2.1 Total mercury	52
4.2.2 Methylmercury	54
4.3 Characterizing Cache Creek soils for post-fire mercury transport modeling	55
4.3.1 Vegetation	55
4.3.2 Modeling soil mercury concentrations	56
4.4 Modeling of Mercury and methyl mercury using HSPF	63
4.4.1 Development of HSPF Mercury boundary conditions	63
4.4.2 Soils	64
4.4.3 Streambed Sediment	64
4.4.4 Geothermal inputs	65
4.4.5 Modeling effects of wildfire in HSPF	65
4.5 Mercury simulation method in PFHydro-WQ	66
4.5.1 Mercury load calculation method and soil mercury concentrations	66
4.5.2 Pre- and post-fire total mercury (Hg) load simulations	66

4.5.3	Pre- and post-fire total methylmercury (MeHg) load simulations	71
4.5.4	Summary of PFHydro modeling results	77
4.6	Summary of mercury modeling approach and results.....	78
4.7	References	80
5	Future Work	84
5.1	Extend modeling of Cache Creek watershed through Water Year 2020 to include effects of 2018 fires	84
5.2	Gather hydrologic and soils data to support modeling.....	86
5.3	Perform process-oriented studies to improve knowledge of fire effects on Hg methylation and transport	87
5.4	Collect data for water flow, suspended sediment, total mercury, and methylmercury in watersheds of interest.....	88
5.4.1	Prioritizing watersheds: Mercury impairment in Reclamation reservoirs	88
5.4.2	Quantifying mercury and methylmercury loads into Reclamation reservoirs	92
5.5	Update PFHydro and PFHydro-WQ algorithms for the model to be applied in a heterogeneous watershed and simulate SWR effects, simulate Hg/MeHg load more effectively	92
5.6	Construct a user-friendly interface for PFHydro and PFHydro-WQ and publish documentation.....	92
5.7	References	93
Appendix 1: Accepted Manuscript for Publication		95

1 Background

Mercury (Hg) is a toxic metal that is found both naturally and as an introduced contaminant in aquatic environments. Methylation is the most important step in the mercury cycle because it greatly increases toxicity and the potential for accumulation in aquatic biota.

Monomethylmercury (MeHg) is the most toxic form and even at very low concentrations can lead to bioaccumulation within the aquatic food web and cause high levels of mercury contamination in fish. Hg makes its way into our aquatic ecosystem through one of two major routes: point/non-point source discharges and atmospheric deposition. Atmospheric deposition is the primary source to most aquatic ecosystems (Wentz et al., 2014). According to the U.S. Environmental Protection Agency, emissions from coal-fired power plants are the largest source of mercury to the atmosphere. Mercury is deposited from the atmosphere primarily as inorganic mercury. Mercury is closely associated with sulfur and selenium in the environment and has the ability to change state rapidly with consequences for its reactivity and mobility. The behavior of Hg depends on numerous chemical, physical, and biological processes that vary in space as a function of the biogeochemical and hydrodynamic environment. Mercury can also vary in time over different scales (e.g. inter-annual, seasonal, diurnal, tidal).

Wildfire is known to affect Hg cycling in watersheds by mobilizing volatile Hg into the atmosphere and allowing Hg to be carried off attached to sediments when mobilized by rainfall-runoff. Increases in MeHg in water, sediment, and biota have been documented as an aftermath of wildfire. In California, Reclamation will be required to comply with new mercury TMDL objectives and both develop and implement various reservoir mercury management practices that help to control MeHg mobilization and export to downstream water bodies. Research has indicated that each aquatic water body should be evaluated individually; similar conditions in separate reservoirs have been shown to produce different rates of mercury bioaccumulation. Therefore, management practices should be evaluated on an individual reservoir basis. There are currently no reliable procedures to make such an evaluation. Hence Reclamation, the U.S. Geological Survey, the Bureau of Land Management, the U.S. Corps of Engineers and Berkeley National Laboratory have collaborated on this joint effort to better understand the effects of fire on Hg and MeHg cycling in important watersheds in California by developing an integrated and comprehensive modeling approach.

Wildfire can significantly increase runoff and erosion. In addition to effects on water quality, such as Hg and MeHg, increased runoff and erosion can endanger lives and property, and can lead to decreased reservoir capacity. For example, sediment from flooding after the 1996 Buffalo Creek Fire in Colorado reduced Denver's municipal reservoir capacity by roughly a third (Agnew et al., 1997).

The first-order effect of fire on runoff and erosion is decreased vegetation interception and protection. Additionally, post-wildfire infiltration into the unsaturated zone is controlled by fire-induced changes in soil-water storage and soil hydraulic properties. After a fire, water repellency is typically found as a discrete layer of variable thickness and spatial continuity found on the soil surface or a few centimeters below and parallel to the mineral soil surface. This soil condition can dramatically reduce infiltration, stimulate overland flow, and, consequently, increase the risk of severe erosion.

Following an extensive literature review, the need was identified to develop a model that could simulate the effects of wildfire on runoff, accounting for (1) both infiltration-excess and saturation-excess overland flow, (2) vegetation rainfall interception for pre- and post-fire conditions, and (c) post-fire soil water repellent behavior. Following the development of such a model, it was then necessary to develop a model to simulate the pre- and post-fire sediment load, using the simulated runoff and other factors. Finally, the model needed to be modified to simulate pre-and post-fire total mercury (Hg) and methyl mercury (MeHg) loads which are associated with sediment erosion and total sediment load.

Accordingly, the modeling for this project included three phases. In the first phase, a new model called PFHydro (post-fire hydrological model) was developed to simulate the effects of wildfire on runoff generation (Ch. 2). In the second phase, the PFHydro-WQ model, based on the Generalized Water Loading Function (GWLF), was developed to simulate the daily sediment load under pre-and post-fire conditions (Ch. 3). In the third phase, the pre- and post-fire levels of total mercury and methylmercury load were modeled (Ch. 4). While these three models were developed to be used in an integrated fashion, the first two models also have value on their own, for applications beyond modeling mercury levels. For example, sediment load can significantly reduce reservoir capacity, and being able to anticipate the effects of a wildfire on sediment load can help Reclamation operators to better plan their operations under these conditions. This report documents the progress in all three of these modeling phases.

The end goal of this study was the development of a comprehensive decision-support tool to guide actions that might be taken by Reclamation in reducing mercury loading to Reclamation-owned and operated reservoirs — such as Lake Berryessa in Solano County, California. Although this final stage of model development is beyond the scope of this three-year initial effort, the component pieces, supported by state-of-the-art technical review and employment of best scientific practices, will be in place to catalyze and support this effort.

1.1 Report Organization

This report is divided into four major chapters. The first is a review chapter that draws from the Year One Progress Report: SRH-2017-xx entitled “Integrated modeling of mercury transformation and transport in watersheds subject to wildfire” by J. Wang, C.N. Alpers, Y. Lai, N.W.T. Quinn, J. Weigand and J. Sholtes which supplied a comprehensive literature review of the three major modeling components of this enterprise. The next three chapters (Chapters 2, 3 and 4) cover (a) rainfall runoff modeling in areas subject to wildfire; (b) soil erosion and sediment transport processes in areas subject to wildfire; and (c) total mercury and methylmercury load associated with runoff and soil erosion from wildlands subject to wildfire. Chapter 5 provides a roadmap for future work and discusses the authors’ recommendations for decision-support system development.

Chapter 2 consists of a manuscript accepted by the peer-reviewed Journal of Environmental Modelling and Software for publication. The manuscript, PFHydro: A New Watershed-Scale Model for Post-Fire Runoff Simulation, was attached as an appendix.

1.2 Literature Review Summary

For a more comprehensive review of literature and scientific foundation for the model development chapters in this report the reader is referred to the report referenced above — SRH-2017-xx “Integrated modeling of mercury transformation and transport in watersheds subject to wildfire” by J. Wang, C.N. Alpers, Y. Lai, N.W.T. Quinn, J. Weigand and J. Sholtes. The Modeling Review Summary presented below summarizes the major topics covered in the ten chapters of this prior report with emphasis on the key concepts and building blocks for development of the rainfall-runoff, soil erosion and sediment transport and mercury hydrochemistry covered in the current final project report.

In Chapters 1 and 2 of Wang et al. (2017) the objectives of the report were expounded and some of the tools and techniques available for making mercury measurements in the field at the watershed level were described in detail. Owing to the complexity of mercury hydrochemistry a complete ontology of mercury species in both dissolved and suspended phases was provided along with the major techniques used for their assessment.

Given the expense and difficulty of making mercury measurements in the field, especially in remote areas where mercury export from these poorly vegetated areas after wildfire is more common, alternate methods for mercury data acquisition are being adopted. These innovations were discussed in Chapter 3 of Wang et al. (2017). Of particular note for detection are mercury species that are sources for mercury methylation, including: metallic mercury (Hg^0), cinnabar (HgS), mercury (I) chloride (Hg_2Cl_2), mercury (II) chloride (HgCl_2), and mercury (II) oxide (HgO), as well as anthropogenic metacinnabar (HgS). Remote-sensing systems with multi- and hyperspectral capabilities can potentially locate source areas and track movements of mercury from source areas. However, the concentration of mercury compounds is in most cases too small to detect with airborne instruments. With use of a satellite or aircraft, one option would be to map associated minerals, such as advanced argillic altered rock within hydrothermal deposits. Although for the current research project conventional field sampling and analytical techniques were largely utilized, any future decision-support system would benefit from a lower cost and quicker access to mercury concentration and loading data needed to make resource-management decisions.

Conceptual models of mercury fate and transport were discussed in detail in Chapter 4 of Wang et al., (2017) with an emphasis on the processes that affect mercury mobilization and transport in watersheds subject to wildfire. The U.S. Geological Survey (USGS) in California has been at the forefront of developing conceptual models for mercury hydrochemistry in both terrestrial and aquatic environments. Although in many parts of the world atmospheric deposition is the dominant anthropogenic source of mercury to aquatic systems, in northern and central California research has shown that atmospheric deposition is a relatively minor source of Hg and MeHg to aquatic environments compared with historical mining sources. Anthropogenic sources to the atmosphere include fossil fuel combustion, especially coal, and other industrial emissions. For rivers draining the northwestern Sierra Nevada, Alpers et al. (2016) showed that MeHg bioaccumulation in invertebrates and fish increased by a factor of 3 to 5 while passing from zones upstream of historical gold mining to zones affected by mining, which indicated that

mining was the source of most bioaccumulated methylmercury (MeHg). Other USGS researchers (Domagalski et al., 2016) compared Hg river loads to total atmospheric deposition (wet and dry) for 27 watersheds in the western U.S. and found that watersheds with historical mining of mercury, gold, or silver less than 500 km² in area typically had Hg loads well in excess of atmospheric Hg deposition rates, consistent with non-atmospheric (mining) Hg sources. In forested watersheds without anthropogenic Hg sources, Hg in runoff was about 10 to 30% of atmospheric inputs, consistent with the hypothesis that Hg transport is attenuated by forest vegetation and soils. In contrast, urban watersheds with impermeable surfaces had Hg in runoff representing 50 to 90% of atmospheric Hg deposition. Another important finding reported from USGS studies was that Hg deposited by wet and dry atmospheric deposition was more reactive than other sources and therefore was more easily converted to MeHg (Wentz et al., 2004). The presence of vegetation facilitates mercury concentration in soil, as Hg has an affinity for organic matter (OM), and vegetated soils with higher OM content will thus tend to collect more Hg over time (Schlüter, 2000). Well-vegetated areas with organic horizons were found to have the highest concentrations of mercury (2.5x greater than bare soils), whereas bare soil environments with sparse vegetation had the lowest concentrations (Obrist et al., 2016). Soils with clay minerals and iron oxides were also shown to contain greater concentrations of Hg. These factors help establish the baseline levels of Hg and its distribution in the soil profile prior to a wildfire event.

Past research on the transport of mercury from terrestrial to aquatic environments was also reviewed in the prior report (Wang et al., 2017) because modeling mercury loading to waterbodies requires a conceptual understanding of the erosional, hydrologic, and biogeochemical processes involved in releasing Hg from soils, often in association with sediment organic matter (SOM), and transporting it to a receiving waterbody. Past studies suggested that mercury loading was highly variable on a regional scale, and understanding its conceptual deposition, storage, and transport pathways for a given region is critical for realistic modeling.

In watersheds drained by Cache Creek and Putah Creek, California, likely dominant drivers of mercury loading local are Hg contamination from mining or industrial sources, bank and floodplain sediments, and the fluvial processes that expose and erode these sediments (Domagalski et al., 2004 a,b). In general, in undisturbed watersheds, <1% of deposited Hg is delivered to lakes indicating that these areas serve as Hg sinks unless these watersheds are burned. Post-fire surface erosion of ash-laden sediment is typically the dominant driver of Hg loads (Kelly et al., 2006; Webster, 2015). Likewise forest wildfires release Hg from terrestrial pools into the atmosphere in both gaseous and particulate form from burned fuels with higher water content (Obrist et al., 2007). Mercury released from soil represents the largest forest fire emission source followed by burning vegetation. Higher-severity fires, which may burn hotter and longer, release more Hg to the atmosphere than low-intensity fires due to greater soil heating and more combustion of duff, litter, wood, and foliage (Biswas et al., 2007; Woodruff and Canon, 2010). Nearly all soil Hg may be volatilized in areas of high-intensity and high-temperature fires (Webster et al., 2016). Though all fires release some Hg into the environment, a series of lower-intensity prescribed fires may reduce fire-related Hg emissions to the atmosphere and reduce runoff of Hg associated with eroded sediments over time.

While marked decreases in soil Hg concentrations were observed in burned areas, these Hg-poor regions were shown to decrease over time through new atmospheric deposition and sequestration (Engle et al., 2006; Burke et al., 2010; Woodruff and Cannon, 2010). Though fires reduce soil

reservoirs of Hg, ash in the soil has been found to accumulate Hg from atmospheric sources at a higher rate than unburned soils (Engle et al., 2006; Burke et al., 2010). The higher rates of accumulation on burned soils are not related to SOM concentrations; rather Burke et al. (2010) hypothesized that fire-induced chemical alterations of carbon compounds in ash result in greater adsorption of Hg. Highly productive forests in mountainous and coastal areas in western North America have high Hg deposition and accumulation rates and burn infrequently. These areas were thought to have high potential for large Hg emissions from wildfire as they, and western forests in general, become subject to increased wildfire occurrence due to climate change (Westerling et al., 2006).

Fire results in increased runoff volumes and rates, and concomitant increases in terrestrial sediment erosion and associated organic carbon erosion (Moody and Martin, 2001a; Benavides-Solorio et al., 2005). Increases in runoff from burned areas are largely due to loss of ground cover (litter and duff), in addition to other soil surface impacts, all of which contribute to reduced infiltration rates in burned vs. unburned soils (Moody and Martin, 2001b). Runoff in recently-burned landscapes transports mercury complexes with dissolved OM and particulate OM in ash-laden sediment. In general fires result in increased Hg loading to waterbodies manifesting as spikes in Hg loading in the weeks immediately following the fire as well as elevated loads recorded over subsequent years (Caldwell et al., 2000; Kelly et al., 2006; Webster, 2015).

Chapter 4 of the review report (Wang et al., 2017) also summarized topical literature on the methylation process that produces methylmercury (MeHg) from inorganic Hg(II) through the action of anaerobic, sulfate-reducing microbes present in soils and aquatic sediments. Methylmercury is much more bio-available than inorganic Hg species and is therefore the primary environmental toxicant of concern (Boening, 2000). The presence of total mercury THg in aquatic bed sediment is weakly but positively correlated with MeHg concentrations. This indicates that the mere presence of Hg in a waterbody does not necessarily correlate with higher concentrations of bioavailable MeHg. Rather, other biogeochemical processes within the watershed and waterbody contribute to the production of MeHg, including appropriate temperature and redox environments, pH, the presence of organic carbon, which serves as electron donors, as well as the presence of electron receivers such as sulfate and iron (Boening, 2000; Benoit et al., 2003). Methylation in reservoirs with fluctuating pool levels is often enhanced over those with minimal change in pool elevation. Enhanced breakdown of OM in the sediment experiencing water-level fluctuations results in more dissolved Hg in pore water and more DOM, which may in turn encourage methylating microbial activity. Wildfire typically has led to an increase in nutrient loads to waterbodies draining fire-impacted areas (Smith et al., 2011) and these elevated nutrient levels in runoff often remain elevated for several weeks to months after the event (Gresswell, 1999; Spencer et al., 2003; Kelly et al., 2006). In Alberta, CA, increased nutrient levels post-fire lengthened the aquatic food web, resulted in higher concentrations of bio-accumulated Hg in piscivorous fish (Kelly et al., 2006).

A summary review of the mercury conceptual models of Alpers et al. (2008), originally developed for the CALFED Bay-Delta Regional Ecosystem Restoration Implementation Plan (DRERIP) was provided in Chapter 4 of the literature review document (Wang et al., 2017) and was specifically designed to describe fate and transport of mercury and methylmercury in the Sacramento-San Joaquin Delta. The original conceptual model was modified to include the effects of wildfire on Hg and MeHg with a focus on the upper reaches of watersheds (upstream

of reservoirs). Readers should refer to the Wang et al. (2017) report for a detailed review of these linked conceptual models covering mercury transformation and transport from watersheds affected by wildfire.

Chapter 5 of the review report (Wang et al., 2017) provides a detailed overview of a suite of numerical models published in reports and in peer-reviewed journals that describe various post-wildfire runoff and erosion processes that need to be linked to rainfall-runoff and sediment-transport models for any integrated model of mercury fate and transport at the watershed level. Empirical and physically-based rainfall-runoff models and models relating hydrology, suspended sediment, turbidity, organic matter and particulate mercury were included in this review. Watershed rainfall-runoff and erosion models deal with watershed hydrology and the associated soil erosion and transport by flow runoff. They provide answers on how the sediment is delivered to streams and reservoirs. For mercury simulation modeling in complex, undisturbed watersheds choice of appropriate model is an important, yet difficult, process. Historically, watershed erosion models have mostly been developed for agricultural applications such as soil conservation and land management and planning purposes. Watershed erosion models were classified into three categories: (1) empirical models such as the Universal Soil Loss Equation (USLE) (Wischmeier and Smith, 1978); (2) process-based models such as the Water Erosion Prediction Project (WEPP) (Flanagan et al., 1995) and the Kinematic runoff and Erosion model (KINEROS) (Goodrich et al., 2005). In general, empirical, lumped models are better suited for long-term soil erosion estimation, applicable to large watersheds, and are computationally economical. These models, however, are restricted primarily to average sediment yield over a basin with similar characteristics to the basins which were used to generate the equations and cannot be used to assess spatial variability of erosion or to dynamically model the erosion process. Process models rely more on the physical principles underlying the modeled processes, have the potential to be more general once validated, capable of modeling spatial variation and event-specific erosion processes. Such models tend to require significant input data and are computationally intensive, limited to smaller watersheds and shorter time scales.

Chapter 5 of Wang et al. (2017) provides a detailed description of the theory and application of a number of empirical, process based and mixed models applicable to the current integrated modeling project. The review also notes that most watershed erosion models are limited in their ability to simulate post-fire effects on mercury and methylmercury export from watersheds and its transport to receiving waters. A number of public-domain and proprietary models have been described in the research literature that are capable of simulating post-fire effects on runoff generation and soil erosion. Much of this literature has focused on predicting peak discharge of post-fire runoff by using techniques such as the paleo-flood method (e.g. Jarrett and England, 2002), the curve number method (Hawkins and Greenberg, 1990; Cerrelli, 2005; Foltz et al., 2009), or direct measurements from burned basins (Moody and Martin, 2001a; Moody et al., 2008; Foltz et al., 2009; Kean et al., 2011; Moody, 2012). Little research has covered predicting flood timing relative to rainfall (Elliot et al., 2010).

A review of five models for post-fire peak discharge predictions was made by Kinoshita et al. (2014) that include: the Rowe Countryman and Storey (RCS) (Rowe et al., 1949), United States Geological Survey (USGS) Linear Regression Equations (Foltz et al., 2009), USDA Windows Technical Release 55 (USDA, 2009), Wildcat5 (Hawkins and Munoz, 2011), and U.S. Army Corps of Engineers (USACE) Hydrologic Modeling System (HEC-HMS) (USACE, 2000). The TR_55, HEC-HMS and Wildcat5 are curve number-based models. These models were applied to

eight diverse basins in the western United States affected by wildfires. According to Kinoshita et al. (2014), no one model is versatile enough for application to all study sites. The review results show inconsistency between model predictions for events across the sites and less confidence with larger return periods (25- and 50-year events) and post-fire predictions.

The capability of four models representing empirical, semi-empirical, and process-oriented methods were evaluated by Chen et al. (2013) for simulating post-fire hydrograph using data from the San Dimas Experimental Forest (SDEF), San Dimas, California. The four models are: empirical based Rule of Thumb by Kuyumjian (Foltz et al., 2008) and Rational Method (MODRAT) (LACDPW, 1991), semi-empirical HEC-HMS, and physical, process-oriented KINematic Runoff and EROSion Model 2 (KINEROS2) (Canfield and Goodrich, 2005). These modeling studies showed that simple, empirical peak flow models may perform acceptably if calibrated correctly. However, these models may not be applicable for predictions outside the area where they were calibrated when they do not incorporate pertinent hydrological factors. The Chen et al. (2013) review maintained that the watershed runoff generation mechanism can be changed due to fire effects and convert from a saturation-excess runoff to an infiltration-excess dominated runoff process. Physically-based, process-oriented models show promise for in-depth analysis of pre- and post-fire hydrographs and are capable of providing reliable results (Chen et al., 2013).

In Chapter 6 of the Wang et al. (2017) review report, water-quality factors were introduced, in particular mercury fate and transport and the use of surrogate measurements to help calibrate process-based watershed water-quality simulation models. The majority of watershed-based mercury water-quality models recognize four categories of mercury transport in the environment: (a) suspended mineral particles, (b) particulate organic carbon, (c) dissolved organic carbon, and (d) inorganic complexes and ions.

The first five models reviewed were those mostly used in a research context and include: (1) the Yin-Balogh (2002) model, a statistical analytical framework that can be turned into a quantitative loading model; (2) the LOADEST model (Runkel et al., 2004) that computes multiple constituent loading using a linear least-squares regression approach with up to seven variables; (3) the Visualizing Ecosystems for Land Management Assessment (VELMA) Model for Hg (Golden et al. 2012) which uses a three-dimensional distributed column framework to simulate both lateral and vertical transport of water, heat, N, C, and Hg in soils; (4) the Grid-based Mercury Model (GBMM) (Dai et al. 2005), which is a raster-based watershed model formulated to perform water, sediment and mercury mass balances using DEM data, soil and land use information model inputs. The GBMM model calculates daily water, sediment and mercury fluxes and routes these through a channel network to the receiving water. Runoff is calculated using a modified National Resource Conservation Service (NRCS) curve number (NRCS-CN) approach for each grid cell. Total mercury (THg) is partitioned in the model between its solid and aqueous forms using a partition coefficient (K_d) (ratio of the equilibrium concentration in the soil particle to the concentration in soil water). Model-simulated THg dynamics were associated with sediment production and transport to receiving waters (Golden et al., 2012). (5) The TOPLOAD and TOPMODEL models (Beven and Kirkby, 1979) models have also been used in tandem to simulate Hg transport in small watersheds (Feaster et al., 2010).

The other models reviewed are those that are mostly used in decision-making applications and which have more widespread use. These models include: (6) the HSPF (Hydrologic Simulation

Program FORTRAN) model (Donigian et al., 1995), which is the main hydrologic driver of the BASINS GIS-based TMDL modeling framework endorsed by the Environmental Protection Agency. A large number of HSPF model applications were described that involve mercury fate and transport. Those of relevance to the current research study include the HSPF streamflow and sediment transport study in the Sacramento River watershed (Stern et al., 2016). Stern et al. (2016) developed a daily HSPF watershed model of the Sacramento River Basin to simulate both streamflow and suspended sediment transport to the San Francisco Bay-Delta. The model simulations showed decreasing sediment concentrations and loads consistent with the observed decline in sediment delivery from the upper watershed to the Bay-Delta. As expected, sediment discharge from the Sacramento River Basin increased with increased storm magnitude and frequency and decreased when air temperatures were elevated, independent of changes in precipitation. As part of this modeling study, the Sacramento River reach downstream of Clear Lake was analyzed, incorporating the area impacted by the 2015 Rocky Fire (although the model did not specifically include fire impacts). For Putah Creek, the reach downstream of Lake Berryessa was included but did not include the area impacted by the 2015 Valley Fire and Jerusalem Fire. The HSPF model has been used to simulate flows of water, sediment, and mercury in a number of locations around the US. Several of these models were used to investigate whether mercury-contaminated flood-plain soils along riverbanks were the important sources of mercury loading to the rivers (e.g. Eggleston, 2009).

The Watershed Analysis Risk Management Framework (WARMF) TMDL Model (7) is a water-quality simulation model for watersheds that has been used extensively for salinity and phytoplankton simulation modeling in the San Joaquin River Basin and has mercury hydrochemistry modeling capability. The WARMF model accounts for the contributions of various watershed contaminants and constituents that drain into a river system. A submodel to simulate Hg hydrochemistry (Chen and Herr, 2010) considers elemental Hg [Hg(0)], inorganic Hg [Hg(II)], and MeHg, with parameterized reactions for atmospheric Hg deposition using available precipitation data, Hg adsorption to total suspended solid and complexation with dissolved organic carbon, Hg methylation, MeHg absorption by algae, photo-demethylation of MeHg to Hg(II), and photo-reduction of Hg(II) to Hg(0) (Chen, 2005). Hg methylation is primarily a bacterial process linked to sulfate reduction and/or iron reduction, with MeHg concentrations proportional to the concentration of dissolved neutral Hg complexes (e.g. HgS and Hg(HS)₂) (Drott et al., 2007; Bessinger et al., 2012) and thiol-complexed Hg and nano-HgS that may be bioavailable to methylating bacteria (Schaefer and Morel, 2009; Schaefer et al., 2011; Hsu-Kim et al., 2013). Similarly, rates of MeHg demethylation depend on temperature, pH, and other environmental variables (Ullrich et al., 2001).

A mercury module has also been developed for the EPA Water Analysis Simulation Program (WASP) model (8). The mercury module was developed as a companion to WASP water quality sub-models: EUTRO and TOXI. The WASP mercury module simulates the transport and fate of three mercury components: Hg⁰, Hg(II), and MeHg in surface water. Hg(II) and MeHg are partitioned to suspended and benthic solids and to dissolved organic carbon (DOC) with user-specified partition coefficients for each sorbent or ligand type. Mercury transformation reactions simulated in WASP include: oxidation of Hg⁰ in the water column, reduction and methylation of Hg(II) in the water column and sediment layers, and demethylation of MeHg in the water column and sediment layers. These transformation processes are represented as first-order reactions operating on the total pool of the reactants with rate constants that can vary spatially and have temperature correction coefficients that adjust the rates with variations in water temperature.

Water column reduction and demethylation reactions are driven by sunlight, and so their input surface rate constants are attenuated through the water column using specified light extinction coefficients. Rate constants are applied to the dissolved, DOC-complexed, and sorbed phases on solids at varying strengths (0 to 1), as specified by the user. WASP computes mercury species and solids concentrations in the water column and sediments along individual river reaches throughout the simulation period.

The Dynamic Mercury Cycling Model (D-MCM) (9) is a proprietary, time-dependent mechanistic mass-balance model for mercury cycling and bioaccumulation. D-MCM simulates inorganic Hg(II), elemental Hg(0), and MeHg in water, sediments (solids and pore water) and employs a simplified food web that includes phytoplankton, zooplankton, benthos and three fish species. MeHg dynamics in individual fish cohorts are followed for each species using a bioenergetics approach (Harris and Bodaly, 1998).

The HgSM model (Zhang and Johnson, 2016) (10) was designed to model three species in the water column: Hg⁰, Hg(II), and MeHg and two species in the sediment layer: Hg(II) and MeHg. In HgSM, Hg(II) is used to represent inorganic mercury that can exist as Hg²⁺ such as HgCl₂, Hg(OH)₂, HgS, etc. MeHg is used to represent methylmercury. Hg(II) and MeHg can be adsorbed by DOC, algae, POM and inorganic solids. Physical and biochemical processes modeled in HgSM include (a) adsorption and desorption of mercury, (b) volatilization, (c) atmospheric deposition, (d) diffusive exchange between the water column and sediment layer, (e) deposition and resuspension, (f) sediment burial of sorbed mercury, and (7) biogeochemical transformations among three species. The HgSM simulates transformations of mercury cycling in the water column and sediment layer. Figure 1-1 provides an overview of the HgSM representation of mercury species and major processes involved in aquatic systems, with the exception of transport and external sources. The transformation processes of Hg⁰, Hg(II) and MeHg and their rates are described using simple kinetic equations adopted from the WASP mercury module (Wool et al., 2006) and Dynamic Mercury Cycling Model (D-MCM) (ERPI 2006; 2013).

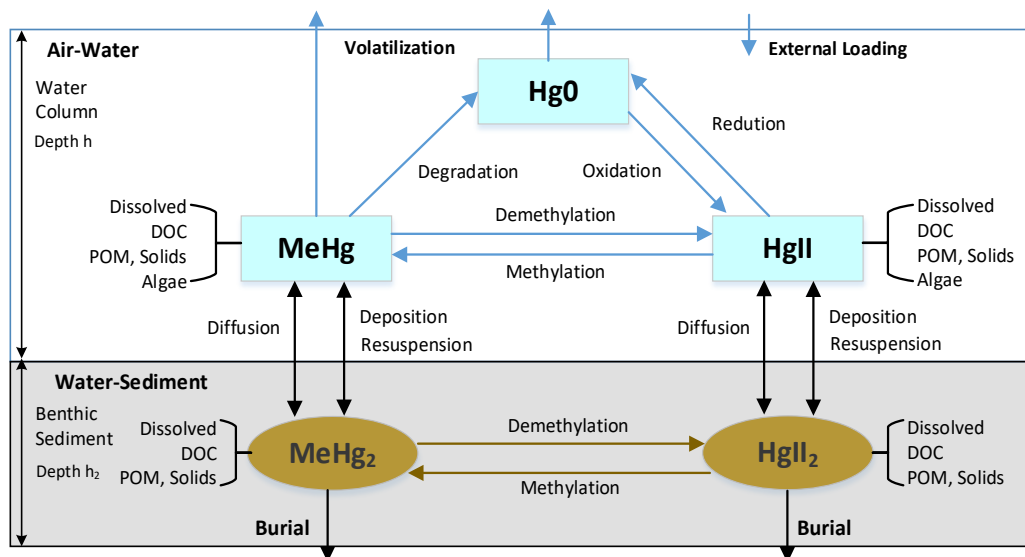


Figure 1-1. Mercury speciation and major processes simulated in the HgSM mercury hydrochemistry model (Zhang and Johnson, 2016).

Other, more limited coupled thermodynamic and kinetic reaction models have been developed such as Bessinger et al. (2012) and Helmrich et al. (2017) to simulate net MeHg production in wetlands during wet and dry cycles. These biogeochemical reaction models provide a quantitative framework describing the processes affecting partitioning, transformation, and fate of Hg and MeHg in the terrestrial and aquatic environment. Several of these models build upon the USGS-supported PHREEQC model, (Parkhurst and Appelo, 2013), which focused on the impact of biogeochemical redox zonation on the fate of Hg and Me-Hg in capped sediments (Bessinger et al., 2012). The accuracy of all biogeochemical reaction models depends on: (a) the establishment of a reliable, internally consistent thermodynamic database for relevant reactions between aqueous, solid and gaseous species; and (b) on a biogeochemical reaction matrix related by kinetic rate laws incorporating mechanistic descriptions of the processes (Helmrich et al. (2017)). Databases should include the best available equilibrium constants for Hg aqueous inorganic complexes (except sulfur-based ligands, which are difficult to measure), Hg and MeHg sorption to sediment organic matter (SOM) and complexation with dissolved organic matter (DOM) (Skylberg et al., 2006; Helmrich et al., 2017), and precipitation of mercuric sulfides (cinnabar and metacinnabar) (Bessinger et al., 2012). Hg-sulfide complex stability constants and HgS solubility products were recently critically reevaluated (Drott et al., 2013). The reaction matrix for Hg methylation is being expanded to include rate laws for methylation by iron-reducing bacteria as well as sulfate-reducing bacteria (Helmrich et al., 2017).

Summary of the review (Ch. 5 – Ch. 6)

Wildfire can significantly change watershed hydrological processes resulting in increased risks for flooding, erosion, and debris flow. Wildfire is also known to affect Hg cycling in watersheds by mobilizing volatile Hg into the atmospheric and allowing Hg to be carried off attached to sediments

mobilized in increased post-fire runoff. Increases in MeHg in water, sediment, and biota have been documented as an aftermath of wildfire.

There is no single model available capable of universally simulating Hg and MeHg fate and transport under impacts of wildfire at a watershed scale. Most hydrological models simulating post-fire runoff are event-based for peak discharge using curve-number or regression methods. The curve-number-based models should be applied to a small watershed in which infiltration dominates. The regression-method-based model is limited to use in watersheds with similar conditions to the watershed for which the regression equation was developed. Burn severity that represents the fire effects on vegetation and soil characteristics and thus subsequently determines the runoff response should be incorporated into the modeling approach. The physically based WEPP/GeoWEPP model with burn severity considered was applied in some watersheds to simulate post-fire runoff and soil erosion in a hillslope and watershed scale. However, there is no clear explanation in published manuscripts of how to simulate post-fire runoff with altered vegetation and soil properties, such as decreased vegetation interception and evapotranspiration, and increased soil water repellency.

A physically-based model that can quantify burn severity to vegetation interception, evapotranspiration, and water repellency is necessary to simulate wildfire effects on runoff generation, and thus provide a good foundation to simulate post-fire soil erosion and the fate and transport of Hg and MeHg on a watershed scale.

Sediment and mercury delivery from watersheds to streams and reservoirs has been estimated or simulated in the past as discussed in Chapter 6 of the review by Want et al. (2017). However, monitoring the effects of wildfire on sediment erosion and mercury transport is rarely performed. Simple statistical and regression-based models such as the Yin and Balogh (2002) model, the LOADEST model (Runkel et al., 2004), or the Inverse model by Burns et al. (2014) can be used for fast qualitative assessment for planning purposes. However, they require a large amount of site-specific observation data collected over a wide range of flow conditions to be useful.

Semi-physically based models, such as the GBMM (Dai et al., 2005) and HSPF models, represent watershed features within subareas delineated using a coarse model mesh and a series of mass-balance equations that are then applied to simulate the physical and biochemical processes within each grid cell and the transfer of constituents between adjacent grid cells. Water, sediment, and mercury fluxes among the grid network are often computed using simple empirical equations. For example, water runoff is calculated using the NRCS curve-number approach by GBMM. Mercury is often partitioned in a simple manner with limited mercury cycling dynamic processes incorporated in the model. Simple models can be run with a relatively large time step (e.g., hourly or daily) and a scaled-back number of input parameters.

The WASP, D-MCM, and HgSM models provide the most comprehensive mercury cycling simulation capabilities. The D-MCM model has mostly been applied to lakes and reservoirs and less often to watershed-scale problems. HgSM is not a full-fledged mercury model but rather a mercury module that must be linked to watershed hydrology models and mercury transport (routing) routines to provide useful information. There remains a need for a comprehensive, process-based, watershed-scale mercury model to address the scope and scale of mercury management in watersheds serving Reclamation facilities.

Chapter 7 of the prior literature review report (Wang et al, 2017) concentrates on post-fire rainfall-runoff modeling and the selection of a modeling approach to cope with fire-induced changes in soil infiltration characteristics. Subsequent integrated model development combines elements of some of the numerical models and model algorithms that were discussed earlier with new modeling approaches best suited to the intended initial model application in Putah and Cache Creek watersheds in Solano, Lake, and Yolo counties, California. These watersheds have been subjected to unusually large wildfires in the past 5 years and have been the focus of interagency research activities including detailed monitoring of Hg and MeHg since 2010. It is important when developing new integrated models and modeling approaches to be mindful of existing data resources and to tailor model data requirements to the data resource. The Putah Creek and Cache Creek watersheds have been the focus of study by several agencies and university researchers over the past decade including the U.S. Geological Survey and the California Resources Agency (Dept. of Water Resources) which are responsible for the current inventory of water quality and sediment Hg data.

Experimental plot and hillslope-scale studies have demonstrated that wildfires may increase event runoff or erosion by factors of 2–40 over small-plot scales and more than 100-fold over large-plot to hillslope scales (Williams et al., 2014). Additionally, annual suspended sediment yields can increase by a factor of between 1 and 1459 times the pre-fire or unburned quantities (Smith et al., 2011). The runoff response from burned watersheds is a function of rainfall (amount and intensity), burn severity, and properties of the impacted soils and vegetation cover. Burn severity classes (unburned, low, moderate, and high burn severity) were assumed to reflect the degree of removal of the canopy layer, which intercepts rainfall. Burn severity classes also account for the removal of the understory, ground cover, litter, and duff layers, all of which normally reduce the erosive potential of rainfall and which can increase the frictional drag (Gilley et al., 1992) of surface runoff, reducing rill and inter-rill erosion.

Besides rainfall interception, post-wildfire infiltration into the unsaturated zone is controlled by fire-induced changes in soil-water storage and soil hydraulic properties. After a fire, water repellency is typically found as a discrete layer of variable thickness and spatial continuity found on the soil surface or a few centimeters below and parallel to the mineral soil surface. It was shown that water repellency was created and intensified by soil heating that occurred during a fire (DeBano, 1966; DeBano and Krammes, 1966). This soil condition dramatically reduced infiltration, stimulated overland flow, and, consequently increased the risk of severe erosion. Under field conditions, the water-repellent soil layer is not typically continuous, so irregular wetting patterns are common (Bond, 1964; Meeuwig, 1971; DeBano, 1981; Dekker and Ritsema, 1995). Soil patches of different size with variable soil-hydraulic properties, when combined with scattered depressions, burnt-out stumps, and root holes after burn, make it necessary to consider spatial connectivity of overland flow when estimating soil erosion potential. An increase in bare ground post-fire results in an increase in the connectivity of water-repellent soil patches (Shakesby et al., 2000; Doerr and Moody, 2004; Cawson et al., 2010; Nyman et al., 2010). A possible threshold of 60–70% bare ground was found to be related to the connectivity of the bare patches (Johansen et al., 2001) and seemed to explain much of the post-wildfire erosion caused by increased runoff (Moody et al., 2013). The SWR significantly decreased with increased surface soil moisture (MacDonald & Huffmann 2004).

The conceptual model of post-fire infiltration and hillslope runoff contribution to channels is key to the performance of any watershed mercury transport model. Depending on the post-fire response domain, hillslope-runoff-generating processes may switch between infiltration-excess and saturation-excess overland flow (Dunne, 1978; Wondzell and King, 2003; Keizer et al., 2005; Onda et al., 2008; Ebel et al., 2012). The relative weight of the two runoff-generating processes can vary on steep hillslopes. Hence the candidate model described for simulation of post-fire runoff for use at a watershed scale for mercury management should include the following key components: (a) contain both saturation-excess and infiltration-excess overland flow algorithms; (b) explicitly simulate vegetation rainfall interception both pre- and post-fire; and (c) explicitly simulate post-fire soil water repellent behavior.

The candidate model for simulation of Hg/MeHg load as a result of post-fire runoff will utilize algorithms from two existing models TOPMODEL (Beven and Kirkby, 1979) and UFORE-Hydro (now i-tree Hydro) (Wang et al., 2005, Wang et al., 2008). TOPMODEL (Beven and Kirby, 1979, Beven, 1997) is a semi-distributed hydrological model based on the concept that topography exerts a dominant control on flow routing through upland catchments. TOPMODEL is a variable-contributing-area conceptual model, in which the major factors affecting runoff generation are the catchment topography and the soil transmissivity, which decreases with soil depth (Montesinos-Barrios and Beven, 2004). The original TOPMODEL code was applied to catchments with shallow soils and moderate topography that do not suffer from excessively long dry periods (Montesinos-Barrios and Beven, 2004) - these are circumstances when saturation-excess overland flow dominates. A more recent version of TOPMODEL used the exponential Green-Ampt model of Beven (1984) to calculate infiltration-excess runoff.

A major advantage of TOPMODEL is its simplicity which comes from the use of the topographic index, $TI = \ln(a/\tan\beta)$, where a is the upslope contributing area per unit contour length and $\tan\beta$ represents the local slope. TI is used as an index of hydrological similarity. All points on the watershed with the same index value are assumed to respond in a hydrologically similar way. Hence it is only necessary to make calculations for points with different index values, spanning the index distribution function for a catchment. Three major conceptual enhancements to the original TOPMODEL concepts were introduced into UFORE-Hydro as alternative algorithms: (a) the soil topographic index; (b) a power function for the decay of transmissivity with soil depth; and (c) a vegetation interception routine (Wang et al., 2008). The Topographic Index approach recognizes that the saturated surface transmissivity $T(z)$ of the soil varies widely over the area of the catchment. The topographic index TI ($\ln(a/\tan\beta)$) for each point in the catchment can be replaced by a soil topographic index STI ($\ln(a/T_0\tan\beta)$). This provides model flexibility and allows the model to deal with catchment heterogeneity more readily. Users are required to provide an initial T_0 (saturated surface soil transmissivity) value for each cell, or provide T_0 for several blocks of cells representing different soil types. This feature is useful for simulating post-fire runoff from a burned watershed with random soil water repellent patches. Unburned or burned soils (represented by DEMs) with different burn severities can be assigned unique T_0 values. T_0 simulate the decline of transmissivity with soil depth. TOPMODEL uses an exponential function that results in the indices TI ($\ln(a/\tan\beta)$) and STI ($\ln(a/T_0\tan\beta)$).

Summary of the review (Ch. 7):

The updated runoff simulation algorithm in UFORE-Hydro (now i-tree Hydro) contains several important enhancements that improve its suitability for watershed management of post-fire mercury and methylmercury contamination. The new model permits both saturation- and infiltration-excess overland flow mechanism, contains an interception routine and has a proposed enhancement for SWE simulation – all which provide a unique way to describe and simulate post-fire hydrological process and runoff in a watershed scale that no other available models can do.

Chapters 8 and 9 of the previous literature review report by Wang et al. (2017) discuss the data requirements for model calibration and testing and detail data gathered and inferred from past studies in the Cache Creek and Putah Creek watersheds. It is recognized when developing new modeling approaches to be mindful of existing data resources and to tailor model data requirements to existing data resources to the extent possible. Both the Putah Creek and Cache Creek watersheds have been the focus of study by several agencies and university researchers over the past decade including the US Geological Survey and the California Resources Agency (Dept. of Water Resources) which is responsible for the current inventory of water quality and sediment Hg data. A review of these studies shows more comprehensive field data collection and a longer hydrologic record in Cache Creek than in Putah Creek. The authors therefore decided to use research findings and model parameter coefficients from the Cache Creek watershed as a proxy for model development and calibration in the Putah Creek watershed. The hydrology, sediment transport and hydrochemical aspects of the project related to the effects of wildfire are not well understood or covered in the scientific literature, as described in the earlier chapters – hence the analysis in Chapter 9 of Wang et al. (2017) made inferences on likely outcomes based on extrapolation of the available science. The literature review, previously developed Hg conceptual models, and the planned modeling effort consider the sequence of important hydrochemical processes beginning in the upper watersheds and ending in a terminal reservoir. Lake Berryessa, being a Reclamation owned and operated facility, is an appropriate candidate exemplar for this study.

The science supporting Hg and MeHg modeling is relatively advanced; however, the integration of models necessary for the formulation and development of a decision-support system that has utility for mercury management in these watersheds still requires additional work, which the authors plan to conduct in future years (see Section 5 of this report).

Summary of the literature review by Wang et al., (2017) (Chs. 8 and 9):

Based on available data, the Cache Creek Watershed appears to be an excellent place to calibrate and test the mercury mobility, transport and fire effects model. Although Cache Creek does not have a reservoir managed by the Bureau of Reclamation, once the Hg-fire model is calibrated and tested it could be applied in the future to the Upper Putah Creek Watershed including the main tributaries to Lake Berryessa.

Some first-order processes affecting THg and MeHg transport were described that can serve as a basis for preliminary modeling efforts. In addition, some second-order processes were described that can be used to fine-tune the model after its initial development.

1.3 References

- Aastrup, M., Johnson, J., Bringmark, E. et al. 1991. Water, Air, and Soil Pollution, 56: 155. doi:10.1007/BF00342269
- Abdelnour, A., McKane, R., Stieglitz, M., Pan, F., Cheng., Y., 2013. Effects of harvest on carbon and nitrogen dynamics in a Pacific Northwest forest catchment. *Water Resour. Res.* 49. <http://dx.doi.org/10.1029/2012WR012994>
- Abdelnour, A., Stieglitz, M., Pan, F., McKane, R., 2011. Catchment hydrological responses to forest harvest amount and spatial pattern. *Water Resour. Res.* 47, W09521. <http://dx.doi.org/10.1029/2010WR010165>
- Agnew, W., Labn, R.E., and Harding, M.V. (1997). Buffalo Creek, Colorado, fire and flood of 1996. *Land and Water*, 41, 27-29.
- Alpers, C.N., Eagles-Smith, C., Foe, C., Klasing, S., Marvin-DiPasquale, M.C., Slotton, D.G., and Windham-Myers, L., 2008, Mercury conceptual model. Sacramento, Calif.: Delta Regional Ecosystem Restoration Implementation Plan, 62 p. http://www.science.calwater.ca.gov/pdf/drerip/DRERIP3_mercury_conceptual_model_final_012408.pdf
- Alpers, CN, Hunerlach, MP, May, JT, Hothem, RL. 2005a. Mercury contamination from historical gold mining in California. U.S. Geological Survey Fact Sheet 2005-3014, 6 p. <http://water.usgs.gov/pubs/fs/2005/3014/>
- Alpers, C.N., Yee, J.L., Ackerman, J.A., Orlando, J.L., Slotton, D.G., and Marvin-DiPasquale, M., 2016, Prediction of fish tissue mercury using geospatial data including historical mining: *Science of the Total Environment*, v. 571, p. 364-379. <http://www.sciencedirect.com/science/article/pii/S004896971631018X> <http://dx.doi.org/10.1016/j.scitotenv.2016.05.088>
- Alpers CN, Hunerlach MP, Marvin-DiPasquale MC, Antweiler RC, Lasorsa BK, De Wild JF, Snyder NP, 2006, Geochemical data for mercury, methylmercury, and other constituents in sediments from Englebright Lake, California, 2002: U.S. Geological Survey Data Series 151, 95 p. <https://pubs.usgs.gov/ds/2006/151/>
- Benavides-Solorio, JDD., MacDonald, L.H., 2005. Measurement and prediction of post-fire erosion at the hillslope scale, Colorado Front Range. *International Journal of Wildland Fire* 14, 457–474. doi:10.1071/WF05042
- Benoit, J. M., Gilmour, C. C., Heyes, A., Mason, R. P., Miller, C. L., 2003. Geochemical and biological controls over methylmercury production and degradation in aquatic ecosystems. In Cai, Y., Olin, B. C., (eds.) *Biogeochemistry of important trace elements*. ACS Symposium Series 835, 262-297.
- Bergamaschi BA, Krabbenhoft DP, Aiken GR, Patino E, Rumbold DG, Orem WH (2012), Tidally Driven Export of Dissolved Organic Carbon, Total Mercury, and Methylmercury from a Mangrove-Dominated Estuary. *Env Sci Tech* 46: 1371–1378. <http://dx.doi.org/10.1021/es2029137>
- Bessinger, B.A., Vlassopoulos, D., Serrano, S., and O’Day, P.A., 2012, Reactive transport modeling of subaqueous sediment caps and implications for the long-term fate of arsenic, mercury, and methylmercury: *Aquatic Geochemistry*, v. 18(4), p. 297-326. <https://doi.org/10.1007/s10498-012-9165-4>

- Beven, K., 1997. TOPMODEL: A critique. *Hydrological Processes* 11, 1069-1085.
- Beven, K.J., 1984. Infiltration into a class of vertically non-uniform soils. *Hydrology Science Journal* 29, 425–434.
- Beven, K. J., and M. J. Kirkby (1979), A physically based, variable contributing area model of basin hydrology, *Hydrol. Sci. Bull.*, 24, 43–69, <http://dx.doi.org/10.1080/02626667909491834>
- Biswas A, Blum JD, Klaue B, Keeler GJ, 2007, Release of mercury from Rocky Mountain forest fires. *Global Biogeochem Cycles* 13 pages. <http://dx.doi.org/10.1029/2006GB002696>
- Biswas, A, Blum, Joel D., and Gerald J. Keeler, Gerald J., 2008, Mercury storage in surface soils in a central Washington forest and estimated release during the 2001 Rex Creek Fire: *Science of The Total Environment*, v. 404, no. 1, p. 129-138.
- Boening, D.W., 2000, Ecological effects, transport, and fate of mercury: a general review: *Chemosphere*, v. 40(12), p. 1335-1351. [https://doi.org/10.1016/S0045-6535\(99\)00283-0](https://doi.org/10.1016/S0045-6535(99)00283-0)
- Bond, R.D., 1964. The influence of the microflora on the physical properties of soils. II. Field studies on water repellent sands. *Aust. J. Soil Res.* 2, 111–122.
- Bradley, PM, Jouney, CA, Brigham ME, Burns, DA, Button DT, Riva-Murray K, 2013, Intra- and inter-basin mercury comparisons: Importance of basin scale and time-weighted methylmercury estimates. *Environmental Pollution* 172: 42-52.
- Brigham ME, Wentz DA, Aiken GR, Krabbenhoft DP, 2009, Mercury cycling in stream ecosystems. 1. Water column chemistry and transport. *Environ. Sci. Technol.* 43:2720–2725.
- Burke, MP, Hogue TS, Ferreira M, Mendez CB, Navarro B, Lopez S, Jay JA, 2010, The Effect of Wildfire on Soil Mercury Concentrations in Southern California Watersheds. *Water Air and Soil Pollution* 212: 369-385. <http://dx.doi.org/10.1007/s11270-010-0351-y>
- Burns DA, Nystrom EA, Wolock, DM, Bradley PM, Riva-Murray K, 2014, An empirical approach to modeling methylmercury concentrations in an Adirondack stream watershed. *Journal of Geophysical Research: Biogeosciences* v. 119. <http://dx.doi.org/10.1002/2013JG002481>
- Bushey JT, Driscoll CT, Mitchell MJ, Selvendiran P, Motesdeoca MR, 2008, Mercury transport in response to storm events from a northern forest landscape. *Hydrological Processes*. <http://dx.doi.org/10.1002/hyp.7091>
- Caldwell, CA, Canavan, CM, Bloom NS, 2000. Potential effects of forest fire and storm flow on total mercury and methylmercury in sediments of an arid-lands reservoir. *The Science of The Total Environment* 260: 125-133. [http://dx.doi.org/10.1016/S0048-9697\(00\)00554-4](http://dx.doi.org/10.1016/S0048-9697(00)00554-4)
- Canfield, H.E. and D.C. Goodrich, 2005. Suggested Changes to AGWA to Account for Fire (V2.1). Southwest Watershed Research Center, USDA-ARS, Tucson, Arizona.
- Cawson, J., Sheridan, G., Lane, P., Smith, H., 2010. Characterising fire severity patches to understand how burn patchiness affects runoff connectivity and erosion. *Geophysical Research Abstracts* 12, EGU2010-3009.
- Cerrelli, G.A., 2005. FIRE HYDRO, a simplified method for predicting peak discharges to assist in the design of flood protection measures for western wildfires. In ‘Proceedings of the 2005 Watershed Management Conference – Managing Watersheds for Human and Natural Impacts: Engineering, Ecological, and Economic Challenges’, July 2005, Williamsburg, VA. (Ed. GE Moglen) 935–941. (American Society of Civil Engineers: Alexandria, VA).
- Chen, C. W., Herr, J., and Tsai, W., 2005, Enhancement of WARMF for mercury watershed management and TMDLs.” Technical Rep. No. 1005470, Electric Power Research Institute, Palo Alto, Calif.

- Chen, C.W., and Herr, J.W., 2010, Simulating the effect of sulfate addition on methylmercury output from a wetland: *Journal of Environmental Engineering*, v, 136(4), p. 354-362.
- Chen, L., Berli, M., and Karletta, C. (2013). "Examining modeling approaches for the rainfall-runoff process 18 in wildfire-affected watersheds: using San Dimas Experimental Forest." *Journal of the American Water Resources Association* 1-16, doi:10.1111/jawr.12043.
- Curtis JA, Flint LE, Alpers CN, Wright SA, Snyder NP, 2006, Use of Sediment Rating Curves and Optical Backscatter Data to Characterize Sediment Transport in the Upper Yuba River Watershed, California, 2001–03: U.S. Geological Survey Scientific Investigations Report 2005–5246, 74 p. <https://pubs.usgs.gov/sir/2005/5246/>
- Dai, T., R. B. Ambrose, K. Alvi, T. Wool, H. Manguerra, M. Chokshi, H. Yang, and S. Kraemer (2005), Characterizing spatial and temporal dynamics: Development of a grid-based watershed mercury loading model, in *Managing Watersheds for Human and Natural Impacts: Engineering, Ecological, and Economic Challenges*, edited by G. E. Moglen, Am. Soc. of Civ. Eng., Reston, Va., [http://dx.doi.org/10.1061/40763\(178\)56](http://dx.doi.org/10.1061/40763(178)56)
- DeBano, L.F., 1966. Formation of non-wettable soils...involves heat transfer mechanism. USDA Forest Service Research Note PSW-132, 8p.
- DeBano, L.F., 1981. Water repellent soils: a state of the art, Gen. Tech. Rpt. PSW-46. USDA For. Serv., Pacific Southwest Forest and Range Exp. Sta., Berkeley, CA, 21pp.
- DeBano, L.F., Krammes, J.S., 1966. Water repellent soils and their relation to wildfire temperatures. *International Association of Scientific Hydrology Bulletin* 11, 14–19.
- DiCosty, RJ, Callaham, MA, and Stanturf, JA, 2006, Atmospheric deposition and re-emission of mercury estimated in a prescribed forest-fire experiment in Florida, USA: *Water, Air, and Soil Pollution* 176: 77-91. <http://dx.doi.org/10.1007/s11270-006-9149-3>
- Dittman JA, Driscoll CT, 2009, Factors influencing changes in mercury concentrations in lake water and yellow perch (*Perca Xavescens*) in Adirondack lakes, *Biogeochemistry* 93:179-196. <http://dx.doi.org/10.1007/s10533-009-9289-9>
- Dittman JA, Shanley JB, Driscoll CT, Aiken GR, Chalmers AT, Towse JE, Selvendiran P, 2010, Mercury dynamics in relation to dissolved organic carbon concentration and quality during high flow events in three northeastern U.S. streams. *Water Resources Research*. <http://dx.doi.org/10.1029/2009WR008351>
- Domagalski, J.L., Alpers, C.N., Slotton, D.G., Suchanek, T.H., Ayers, S.M., 2004a, Mercury and methylmercury concentrations and loads in the Cache Creek Watershed, California: *Science of the Total Environment*. v. 327, p. 215–237. <http://www.sciencedirect.com/science/article/pii/S0048969704000543> doi: 10.1016/j.scitotenv.2004.01.013
- Domagalski, J.D., Majewski, M.S., Alpers, C.N., Eckley, C.S., Eagles-Smith, C.A., Schenk, L., and Wherry, S., 2016, Comparison of mercury mass loading in streams to atmospheric deposition in watersheds in the western U.S.: Evidence for non-atmospheric mercury sources: *Science of the Total Environment*, v. 568, p. 638–650. <http://www.sciencedirect.com/science/article/pii/S0048969716303229> doi:10.1016/j.scitotenv.2016.02.112
- Domagalski, J.L., Slotton, D.G., Alpers, C.N., Suchanek, T.H., Churchill, R., Bloom, N., Ayers, S.M., and Clinkenbeard, J., 2004b, Summary and Synthesis of Mercury Studies in the Cache Creek Watershed, California, 2000-2001. U.S. Geological Survey Water –Resources Investigations Report 03-4355, 30 p. <http://water.usgs.gov/pubs/wri/wri034335/>

- Donigian, A.S., Bicknell, B.R. and Imhoff, J.C., 1995. Hydrological simulation program—Fortran (HSPF). *Computer Models of Watershed Hydrology*, 12, 395-442.
- Drott, A., Lambertsson, L., Björn, E., Skjällberg, U., 2007, Importance of dissolved neutral mercury sulfides for methyl mercury production in contaminated sediments. *Environ. Sci. Technol.*, v. 41 (7), p. 2270– 2276.
- Drott, A., Bjorn, E., Bouchet, S., and Skjällberg, U., 2013, Refining thermodynamic constants for mercury(II)-sulfides in equilibrium with metacinnabar at sub-micromolar aqueous sulfide concentrations: *Environmental Science & Technology*, v. 47 (9), p. 4197-4203.
<https://doi.org/10.1021/es304824n>
- Ebel, B.A., Moody, J.A., 2012. Rethinking infiltration in wildfire-affected soils. *Hydrological Processes*. <http://dx.doi.org/10.1012/hyp.9696>
- Eckley, C.S., Tate, M.T., Lin, C.J., Gustin, M., Dent, S., Eagles-Smith, C., Lutz, M.A., Wickland, K.P., Wang, B., Gray, J.E. and Edwards, G.C., 2016. Surface-air mercury fluxes across Western North America: A synthesis of spatial trends and controlling variables. *Science of The Total Environment*, 568, pp.651-665.
- Eggleston, J, 2009, Mercury loads in the South River and simulation of mercury total maximum daily loads (TMDLs) for the South River, South Fork Shenandoah River, and Shenandoah River—Shenandoah Valley, Virginia: U.S. Geological Survey Scientific Investigations Report 2009–5076, 80 p., <http://pubs.usgs.gov/sir/2009/5076/>
- Elliot, W.J., Hall, D.E., Robichaud, P.R., 2010. FS Peak Flow Calculator. Version 2010.10.28. U.S. Department of Agriculture, Forest Service, Rocky Mountain Research Station, Moscow, ID (online at <http://forest.moscowfsl.wsu.edu/fswapp/ermit/peakflow>, last accessed 30 January 2012).
- Engle, MA, Gustin, MS, Johnson, DW, and others, 2006, Mercury distribution in two Sierran forest and one desert sagebrush steppe ecosystems and the effects of fire: *Science of The Total Environment*, v. 367, no. 1, p. 222-233.
- Eggleston, J., 2009, Mercury loads in the South River and simulation of mercury total maximum daily loads (TMDLs) for the South River, South Fork Shenandoah River, and Shenandoah River—Shenandoah Valley, Virginia: U.S. Geological Survey Scientific Investigations Report 2009–5076, 80 p., <http://pubs.usgs.gov/sir/2009/5076/>
- EPRI (Electric Power Research Institute). 2006. Enhancement of watershed analysis risk management framework (WARMF) for mercury watershed management and total maximum daily loads (TMDLs).
<http://www.epri.com/abstracts/Pages/ProductAbstract.aspx?ProductId=00000000001005470>. (Accessed 2 February, 2016).
- EPRI (Electric Power Research Institute). 2013. Dynamic mercury cycling model for Windows 7/Vista/XP. D-MCM v4.0 user's guide and technical support.
<http://www.epri.com/abstracts/Pages/ProductAbstract.aspx?ProductId=000000003002002518>. (Accessed 2 February, 2016).
- Erickson, B.E., 2003, Clear cutting increases mercury in runoff: *Environmental Science and Technology*, v. 37, no. 11, p. 200A-201A.
- Feaster, T. D., H. E. Golden, K. R. Odom, M. A. Lowery, P. A. Conrads, and P. M. Bradley (2010), Simulation of streamflow in the McTier Creek watershed, South Carolina, U.S. Geol. Surv. Sci. Invest. Rep., 2010-5202, 61 pp. <http://pubs.usgs.gov/sir/2010/5202/pdf/sir2010-5202.pdf>
- Flanagan, D. C., Nearing, M. A., 1995. USDA-Water Erosion Prediction Project: Hillslope profile

- Flannigan, M. D., and B. M. Wotton (2001), Climate, weather, and area burned, in *Forest Fires: Behavior and Ecological Effects*, edited by E. A. Johnson and K. Miyanishi, pp. 351–373, Elsevier, New York.
- Fleck, J.A., Alpers, C.N., Marvin-DiPasquale, M., Hothem, R.L., Wright, S.A., Ellett, K., Beaulieu, E., Agee, J.L., Kakouros, E., Kieu, L.H., Eberl, D.D., Blum, A.E., and May, J.T., 2011, The effects of sediment and mercury mobilization in the South Yuba River and Humbug Creek confluence area, Nevada County, California: Concentrations, speciation, and environmental fate—Part 1: Field characterization. U.S. Geological Survey Open-File Report 2010-1325A, 104 p. <http://pubs.usgs.gov/of/2010/1325A>
- Foltz, R.B., P.R. Robichaud, and H. Rhee, 2008. A Synthesis of Post-Fire Road Treatments for BAER Teams: Methods, Treatment Effectiveness, and Decision Making Tools for Rehabilitation. USDA FS Rocky Mountain Research Station, Moscow, Idaho
- Foltz, R.B., Robichaud, P.R., Rhee, H., 2009. A synthesis of post-fire road treatments for BAER teams: methods, treatment effectiveness, and decision making tools for rehabilitation. US Department of Agriculture, Forest Service, Rocky Mountain Research Station. General Technical Report RMRS-GTR-228 (Fort Collins, CO).
- Friedli, H. R., L. F. Radke, and J. Y. Lu (2001), Mercury in smoke from biomass fires, *Geophys. Res. Lett.*, 28, 3223– 3226.
- Frankenberger, J.R., S. Dun, D.C. Flanagan, J.Q. Wu and W.J.Elliot, 2011. Development of a GIS interface for WEPP model application to Great Lakes forested watersheds, Paper No. 11139. Presented at the International Symposium on Erosion and Landscape Evolution, 18-21 September, 2011, Anchorage, AL. St. Joseph, MI: Am. Soc. Ag & Bio Engrs. 8
- Friedli HR, Radke LF, Lu JY, Banic CM, Leitch WR, MacPherson JI, 2003, Mercury emissions from burning of biomass from temperate North American forests laboratory and airborne measurements. *Atmos Environ* 37: 253 267.
- Fu, X. 2004 A physical model of dry ravel movement. (Master's thesis). Retrieved from https://research.wsulibs.wsu.edu:8443/jspui/bitstream/2376/444/1/xiangyang_Fu_122105.pdf
- Garcia E, Carignan R, 1999, Impact of wild-fire and clear-cutting in the boreal forest on methylmercury in zooplankton *Can. J. Fish. Aquat. Sci.* **56** 339 345.
- Garcia, E, Carignan, R, Lean DRS, 2007, Seasonal and Inter-Annual Variations in Methylmercury Concentrations in Zooplankton from Boreal Lakes Impacted by Deforestation or Natural Forest Fires. *Environmental Monitoring and Assessment* Volume 131 Numbers 1-3 p. 1-11 <http://dx.doi.org/10.1007/s10661-006-9442-z>
- Gilley et al., 1992
- Golden HE, Knightes CD, Conrads PA, Davis GM, Feaster TD, Journey CA, Benedict ST, Brigham, ME, Bradley, PM, 2012, Characterizing mercury concentrations and fluxes in a Coastal Plain watershed: Insights from dynamic modeling and data. *Journal of Geophysical Research* 117: G01006. <http://dx.doi.org/10.1029/2011JG001806>
- Golden, HE, Knightes CD, Conrads PA, Feaster, TD, Davis GM, Benedict ST, Bradley PM, 2013, Climate change and watershed mercury export: a multiple projection and model analysis. *Env Toxicol Chem* 32: 2165-2174. <http://onlinelibrary.wiley.com/doi/10.1002/etc.2284/abstract;jsessionid=35FC024A553867F0DBA937C7D0D1241D.f03t03>
- Goodrich, D.C., Canfield, H.E., Burns, I.S., Semmens, D.J., Hernandez, M., Levick, L.R., Guertin,

- D.P., Kepner, W. 2005. [Rapid post-fire hydrologic watershed assessment using the AGWA GIS-based hydrologic modeling tool](#). Proc. ASCE Watershed Manage. Conf., July 19-22, Williamsburg, VA., 12p., CD-ROM.
- Gresswell, R.E., 1999, Fire and aquatic ecosystems in forested biomes of North America: Transactions of the American Fisheries Society, v. 128(2), p. 193-221.
[https://doi.org/10.1577/1548-8659\(1999\)128<0193:FAAEIF>2.0.CO;2](https://doi.org/10.1577/1548-8659(1999)128<0193:FAAEIF>2.0.CO;2)
- Grigal, DF, 2002, Inputs and outputs of mercury from terrestrial watersheds: a review. Environ Rev 10:1–39.
- Grigal DF, 2003, Mercury Sequestration in Forests and Peatlands: A Review. J. Environ. Qual. 32:393–405.
- Gustin, MS, Lindberg SE, Weisberg PJ, 2008, An update on the natural sources and sinks of atmospheric mercury Applied Geochemistry 23: 482-493.
- Hall B. D., St. Louis V. L., Rolffhus K. R., Bodaly R. A., Beaty K. G., Paterson M., 2005. The impact of reservoir creation on the biogeochemical cycling of methyl and total mercury in boreal upland forests. Ecosystems 8 3.
- Harden, J. W., J. C. Neff, D. V. Sandberg, M. R. Turetsky, R. Ottmar, G. Gleixner, T. L. Fries, and K. L. Manies (2004), Chemistry of burning the forest floor during the FROSTFIRE experimental burn, interior Alaska, 1999, Global Biogeochem. Cycles, 18, GB3014, <http://dx.doi.org/10.1029/2003GB002194>
- Harris, R.C., and Bodaly, R.A., 1998, Temperature, growth and dietary effects on fish mercury dynamics in two Ontario lakes: Biogeochemistry, v. 40, p. 175-187.
- Hawkins, R.H., Greenberg, R.J., 1990. WILDCAT4 Flow Model. University of Arizona, School of Renewable Natural Resources, Tucson, AZ.
- Hawkins, R.H. and A.B. Munoz, 2011. Wildcat5 for Windows (W5W): Documentation and Manual. School of Natural Resources and Environment. University of Arizona, Tucson, Arizona.
- Helmrich, S., Vlassopoulos, D., and O'Day, P. A. (2017) Development and application of a biogeochemical reaction-transport model for simulating mercury methylation in sediments at two mercury-impacted sites in California. *13th International Conference on Mercury as a Global Pollutant*, July 16-21. Providence, RI, USA.
- Homann, P. S., Darbyshire, R. L., Bormann, B. T., & Morrissette, B. A. (2015). Forest Structure Affects Soil Mercury Losses in the Presence and Absence of Wildfire. *Environmental Science & Technology*, 49(21), 12714-12722. <http://dx.doi.org/10.1021/acs.est.5b03355>
<http://ir.library.oregonstate.edu/xmlui/bitstream/handle/1957/57897/MorrissetteBrettForestEcosystemSocForestStructureAffects.pdf?sequence=1>
- Hsu-Kim, H., K.H. Kucharzyk, T. Zhang, and M.A. Deshusses. 2013, Mechanisms regulating mercury bioavailability for methylating microorganisms in the aquatic environment: A critical review. *Environmental Science and Technology* 47: 2441–2456.
- Hurley, J. P., Cowell, S. E., Shafer, M. M., & Hughes, P. E. (1998a). Tributary loading of mercury to Lake Michigan: Importance of seasonal events and phase partitioning. *The Science of the Total Environment*, 213(1–3), 129–137.
- Hurley, J. P., Cowell, S. E., Shafer, M. M., & Hughes, P. E. (1998b). Partitioning and transport of total and methylmercury in the Lower Fox River, Wisconsin. *Environmental Science & Technology*, 32(10), 1424–1432.

- Iordache, M.D., Bioucas-Dias, J.M. and Plaza, A., 2011. Sparse unmixing of hyperspectral data. *IEEE Transactions on Geoscience and Remote Sensing*, 49(6), pp.2014-2039.
- Jarrett, R.D., England, J.F., 2002, Reliability of paleostage indicators for paleoflood studies: in House, P.K., Webb, R.H., Baker, V.R., and Levish, D.R., (eds), *Ancient Floods, Modern Hazards, Principles and Applications of Paleoflood Hydrology*, American Geophysical Union, Water and Science Application 5, Washington, D.C., p. 99-110.
- Johansen, M.P., Hakonson, T.E., Breshears D.D., 2001, Post-fire runoff and erosion from rainfall simulation: contrasting forests with shrub lands and grasslands. *Hydrological Processes* 15: 2953– 2965.
- Kahl, J. S. et al., 2007, Watershed nitrogen and mercury geochemical fluxes integrate landscape factors in long-term research watersheds at Acadia National Park, Maine, USA: *Environmental Monitoring and Assessment*, v. 126, p. 9-25.
- Kean, J.W., Staley, D.M., Cannon, S.H., 2011. In situ measurements of post-fire debris flows in southern California: Comparisons of the timing and magnitude of 24 debris-flow events with rainfall and soil moisture conditions. *Journal of Geophysical Research* 116, F04019, 1–21. <http://dx.doi.org/10.1029/2011JF002005>
- Kelly, EN, Schindler, DW, St. Louis, VL, Donald, DB, and Vladicka, KE, 2006, Forest fire increases mercury accumulation by fishes via food web restructuring and increased mercury inputs: *PNAS*, v. 103, no. 51, p. 19380-19385.
- Kinoshita, A.M., Hogue, T.S., and Napper, C. (2014). “Evaluating pre- and post-fire peak discharge predictions across western U.S. watersheds,” *J. of the Am. Water Resources Association*, 1-18, doi:10.1111/jawr.12226.
- Knightes, CD, Golden HE, Journey CA, Davis GM, Conrads PA, Marvin-DiPasquale M, Brigham ME, Bradley PM (2014) Mercury and methylmercury stream concentrations in a Coastal Plain watershed: A multi-scale simulation analysis. *Environ Pollut* 187: 182-192.
- LACDPW, 1991. *Hydrology Manual*. Los Angeles County Department of Public Works (LACDPW), Water Resources Division, Los Angeles, California.
- Lent M, and McKee L (2011) *Guadalupe River Watershed Loading HSPF Model: Year 3 final report*. A technical progress report prepared for the Regional Monitoring Program for Water Quality in San Francisco Bay (RMP), Sources Pathways and Loading Workgroup (SPLWG). San Francisco Estuary Institute, Richmond, California., 22 p.
- MacDonald, L.H., Huffman, E.L., 2004. Post-fire soil water repellency: persistence and soil moisture threshold. *Soil Science Society of America Journal* 68, 1729–1734.
- Mailman, M., and Bodaly, R. A., 2005, Total mercury, methylmercury, and carbon in fresh and burned plants and soil in Northwestern Ontario: *Environmental Pollution*, v. 138, no. 1, p. 161-166.
- Mallik, A. U., Gimingham, C. H., and Rahman, A. A., 1984, Ecological effects of heather burning I. Water infiltration, moisture retention and porosity of surface soil: *Journal of Ecology*, v. 72, no. 3, p. 767-776.
- Marvin-DiPasquale, M., Agee, J.L., Kakouros, E., Kieu, L.H., Fleck, J.A., and Alpers, C.N., 2011, The effects of sediment and mercury mobilization in the South Yuba River and Humbug Creek confluence area, Nevada County, California: Concentrations, speciation and environmental fate—Part 2: Laboratory experiments: U.S. Geological Survey Open-File Report 2010–1325B, 54 p. <http://pubs.usgs.gov/of/2010/1325B>

- Marvin-DiPasquale, M, Hall, BD, Flanders, JR, Ladizinski, N, Agee, JL, Kieu, LH, Windham-Myers, L. 2006. Ecosystem investigations of benthic methylmercury production: a tin-reduction approach for assessing the inorganic mercury pool available for methylation. In: Mercury 2006 Abstracts Book; Eighth International Conference on Mercury as a Global Pollutant; 2006 Aug 6–11; Madison (WI).
- Meeuwig, R.O., 1971. Infiltration and water repellency in granitic soils. Res. Paper INT-111. USDA For. Serv., Intermountain Res. Sta., Ogden, UT, 10 p.
- Montesinos-Barrios, P. and Beven, K., 2004. Evaluation of TOPMODEL. Southern Cooperative Series Bulletin. <http://www3.bae.ncsu.edu/Regional-Bulletins/Modeling-Bulletin/TOPMODEL.html#837359>.
- Moody, J.A., 2012. An analytical method for predicting post wildfire peak discharges. U.S. Geological Survey Scientific Investigations Report 2011–5236, 36 p.
- Moody, J. A., Martin, D. A., 2001a. Initial hydrologic and geomorphic response following wildfire in the Colorado Front Range. *Earth Surface Processes and Landforms* 26, 1049–1070.
- Moody JA, Martin DA (2001b) Post-fire, rainfall intensity-peak discharge relations for three mountainous watersheds in the western USA. *Hydrological Processes* 15, 2981–2993. doi:10.1002/HYP.386
- Moody, J.A., Martin, D.A., Haire, SL, and Kinner, DA. 2008. Linking runoff response to burn severity after a wildfire. *Hydrological Processes* 22, 2063–2074.
- Moody JA, Shakesby RA, Robichaud PR, Cannon SH, Martin DA. 2013. Current research issues related to post-wildfire runoff and erosion processes. *Earth-Science Reviews* 122, 10– 37. DOI: 10.1016/j.earscirev.2013.03.004
- Nyman, P., Sheridan, G., Lane, P.N.J., 2010. Synergistic effects of water repellency and macropore flow on the hydraulic conductivity of a burned forest soil, south-east Australia. *Hydrological Processes* 24, 2871–2887.
- Nelson, S. J. K. B. Johnson J. S. Kahl T. A. Haines and I. J. Fernandez, 2007, Mass Balances of Mercury and Nitrogen in Burned and Unburned Forested Watersheds at Acadia National Park Maine USA: Environmental Monitoring and Assessment, 126: 69-80.
- Obrist, D., Johnson, D.W., Edmonds, R.L., 2012. Effects of vegetation type on mercury concentrations and pools in two adjacent coniferous and deciduous forests. *J. Plant Nutr. Soil Sci.* 175, 68–77.
- Obrist, D., Moosmüller, H., Schürmann, R., Chen, L. W. A., Kreidenweis, S. M., 2007. Particulate-phase and gaseous elemental mercury emissions during biomass combustion: Controlling factors and correlation with particulate matter emissions. *Environmental Science & Technology* 42, 721-727.
- Obrist, D., Pearson, C., Webster, J., Kane, T., Lin, C.-J., Aiken, G.R., and Alpers, C.N., 2016. A synthesis of terrestrial mercury in the western United States: Spatial distribution defined by land cover and plant productivity. *Sci. Total Environ.* 568, 522–535.
- Ouyang Y, Higman J, Hatten J, 2012, Estimation of dynamic load of mercury in a river with BASINS-HSPF model. *Soils and Landscape Ecology* 12:207-216. <http://dx.doi.org/10.1007/s11368-011-0426-4>
- Nouri, T. and Oskouei, M.M., 2016. Processing of Hyperion data set for detection of indicative minerals using a hybrid method in Dost-Bayli, Iran. *International Journal of Remote Sensing*, 37(20), pp.4923-4947.

- Parkhurst, D.L., and Appelo, C.A.J., 2013, Description of input and examples for PHREEQC version 3—A computer program for speciation, batch-reaction, one-dimensional transport, and inverse geochemical calculations: U.S. Geological Survey Techniques and Methods, book 6, chap. A43, 497 p. <https://pubs.usgs.gov/tm/06/a43/>
- Peckenham, J. M. J. S. Kahl S. J. Nelson K. B. Johnson and T. A. Haines 2007 Landscape Controls on Mercury in Streamwater at Acadia National Park USA Environmental Monitoring and Assessment Volume 126 Numbers 1-3 p. 97-104.
- Peng, Y., Kheir, R.B., Adhikari, K., Malinowski, R., Greve, M.B., Knadel, M. and Greve, M.H., 2016. Digital Mapping of Toxic Metals in Qatari Soils Using Remote Sensing and Ancillary Data. *Remote Sensing*, 8(12), p.1003.
- Pyne, S. J., P. L. Andrews, and R. D. Laven (1996), *Introduction to Wildland Fire*, 769 pp., John Wiley, Hoboken, N. J.
- Riscassi AL, Scanlon TM (2011) Controls on stream water dissolved mercury in three mid-Appalachian forested headwater catchments. *Water Resour Res* 47:W12512. <http://dx.doi.org/10.1029/2011WR010977>
- Rowe, P.B., C.M. Countryman, and H.C. Storey, 1949. Probably Peak Discharge and Erosion Rates from Southern California Watersheds as Influenced by Fire. Department of Agriculture, Forest Service, Pacific Southwest Forest and Range Experiment Station, Berkeley, California.
- Roth, DA, Taylor, HE, Domgalaski, J, Dileanis, P, Peart, DB, Antweiler, RC, Alpers, CN. 2001. Distribution of inorganic mercury in Sacramento River water and suspended colloidal sediment material. *Arch Environ Contam Toxicol* 40(2):161–172.
- Rothenberg, Sarah E. Matthew E. Kirby Broxton W. Bird Margie B. DeRose Chu-Ching Lin Xinbin Feng Richard F. Ambrose and Jennifer A. Jay, 2010, The impact of over 100 years of wildfires on mercury levels and accumulation rates in two lakes in southern California, USA : *Earth and Environmental Science*. 60: *Issue 5*, 993–1005
- Runkel, R.L., Crawford, C.G., Cohn, T.A., 2004. Load Estimator (LOADEST) -- FORTRAN Program for Estimating Constituent Loads in Streams and Rivers. U.S. Geological Survey, p. 69.
- Rytuba, JJ. 2003. Mercury from mineral deposits and potential environmental impact, *Environ Geol* 43:326–338.
- Schaefer JK, and Morel FMM (2009) High methylation rates of mercury bound to cysteine by *Geobacter sulfurreducens*. *Nat Geosci* 2:123–126.
- Schaefer, J.K., S.S. Rocks, W. Zheng, L. Liang, B. Gu, and F.M.M. Morel. 2011. Active transport, substrate specificity, and methylation of Hg(II) in anaerobic bacteria. *Proceedings of the National academy of Sciences of the United States of America*, v. 108, p. 8714–8719.
- Schauffler, M. S. J. Nelson J. S. Kahl G. L. Jacobson T. A. Haines W. A. Patterson and K. B. Johnson 2007 Paleocological Assessment of Watershed History in PRIMENet Watersheds at Acadia National Park USA. *Environmental Monitoring and Assessment*, 126: 39-53.
- Schelker J, Burns DA, Weiler M, Laudon H, 2011, Hydrological mobilization of mercury and dissolved organic carbon in a snow-dominated, forested watershed: Conceptualization and modeling, *J. Geophys. Res.*, 116, G01002. <http://dx.doi.org/10.1029/2010JG001330>
- Schlüter, K., 2000. Review: evaporation of mercury from soils. An integration and synthesis of current knowledge. *Environ. Geol.* 39, 249–271.
- Schuster, P.F., Shanley, J.B., Marvin-DiPasquale, M., Reddy, M.M., Aiken, G., Roth, D.A., Taylor, H.E., Krabbenhoft, D.P., and DeWild, J.F., 2008, Mercury and organic carbon

- dynamics during runoff episodes from a Northeastern USA watershed: *Wat. Air Soil Pollut.*, v. 187, p. 89-108. <http://dx.doi.org/10.1007/s11270-007-9500-3>
- Seeger M, Errea M-P, Begueria S, Marti C, Garcia-Ruiz JM, Arnáez, J, 2004, Catchment soil moisture and rainfall characteristics as determinant factors for discharge/suspended sediment hysteretic loops in a small headwater catchment in the Spanish Pyrenees, *Journal of Hydrology* 288: 299-311.
- Shakesby, R.A., Doerr, S.H., Walsh, R.P.D., 2000. The erosional impact of soil hydrophobicity: current problems and future research directions. *Journal of Hydrology* 231–232, 178–191.
- Shanley, J. B., Schuster, P. F., Reddy, M. M., Taylor, H. E., & Aiken, G. R. (2002). Mercury on the move during snowmelt in Vermont. *EOS Transactions*, 83(5), 45–48.
- Shanley, JB, Kamman, NC, Clair, TA, Chalmers, A. 2005. Physical controls on total and methylmercury concentrations in streams and lakes of the northeastern USA. *Ecotoxicol* 14:125–134.
- Shanley, J.B., Moore, R., Smith, R.A., Miller, E.K., Simcox, A., Kamman, N., et al., 2012. MERGANSER: an empirical model to predict fish and loon mercury in New England Lakes. *Environ. Sci. Technol.* 46, 4641–4648. <http://dx.doi.org/10.1021/es300581p>
- Sharpley, A.N., and J.R. Williams, eds. 1990. EPIC-Erosion/Productivity Impact Calculator: 1. Model Documentation. U.S. Department of Agriculture Technical Bulletin No. 1768. 235 pp.
- Sigler, J. M., Lee, X., and Munger, W., 2003, Emission and long-range transport of gaseous mercury from a large-scale Canadian boreal forest fire: *Environmental Science and Technology*, v. 37, no. 19, p. 4343-4347.
- Skylberg, U., Bloom, P.R., Quian, J., Lin, C-M., and Bleam, W.F., 2006, Complexation of mercury(II) in soil organic matter: EXAFS evidence for linear two-coordination with reduced sulfur groups: *Environmental Science & Technology*, v. 40, p. 4174-4190. Doi: 10.1021/es0600577
- Smith HG, Sheridan GJ, Lane PN, Nyman P, Haydon S (2011) Wildfire effects on water quality in forest catchments: a review with implications for water supply. *Journal of Hydrology* 396(1–2), 170–192. doi:10.1016/J.JHYDROL.2010.10.043
- Spencer, C.N., Gabel, K.O., and Hauer, R., 2003, Wildfire effects on stream food webs and nutrient dynamics in Glacier National Park, USA: *Forest Ecology and Management*, v. 178(1-2), p. 141-153. [https://doi.org/10.1016/S0378-1127\(03\)00058-6](https://doi.org/10.1016/S0378-1127(03)00058-6)
- Webster, J.P., Kane, T.J., Obrist, D., Ryan, J.N., Aiken, G.R., 2016. Estimating mercury emissions resulting from wildfire in forests of the western United States. *Sci. Total Environ.* 568, 578–586.
- Stern M, Flint L, Minear J, Flint A, Wright S, 2016, Characterizing Changes in Streamflow and Sediment Supply in the Sacramento River Basin, California, Using Hydrological Simulation Program—FORTRAN (HSPF). *Water* 8: 432 (21 p.) <http://dx.doi.org/10.3390/w8100432>
- Ullrich, S.M., Tanton, T.W., Abdrashitova, S.A., 2001. Mercury in the aquatic environment: a review of factors affecting methylation. *Crit. Rev. Environ. Sci. Technol.* 31, 241–293.
- U.S. Army Corps of Engineers (USACE), 2000. Hydrologic Modeling System HEC-HMS — Technical Reference Manual. U.S. Army Corps of Engineers, Hydrologic Engineering Center, Davis, California.
- U.S. Department of Agriculture (USDA), Natural Resources Conservation Service, 2009. Small Watershed Hydrology: WinTR-55 User Guide. Conservation Engineering Division.
- Wang, J., Endreny, T.A. and Hasset, J.M., 2005. A Flexible Modeling Package for Topographically Based Watershed Hydrology. *Journal of Hydrology* 314(1-4):78-91.

- Wang, J., Endreny TA., Nowak, DJ., 2008. Mechanistic simulation of tree effects in an urban water balance model. *J. Am. Water. Resour. Assoc.* 44:75–85.
- Wang, J., Alpers, C.N., Lai, Y., Quinn, N.W.T., Weigand, J., and Sholtes, J., 2017, Integrated modeling of mercury transformation and transport in watersheds subject to wildfire, Draft Year One Progress Report, Bureau of Reclamation.
- Webster, J.P., 2015, Effects of wildfire on mercury, organic matter, and sulfur in soils and sediments. Ph.D. thesis, Univ. of Colorado, Boulder, CO, 140 p.
- Webster, J.P., Kane, T.J., Obrist, D., Ryan, J.N., and Aiken, G.R., 2016, Estimating mercury emissions resulting from wildfire in forests of the western United States: *Science of the Total Environment*, v. 568, p. 578-586.
- Wentz, D.A., Brigham, M.E., Chasar, L.C., Lutz, M.A., and Krabbenhoft, D.P., 2014, Mercury in the Nation's streams—Levels, trends, and implications: U.S. Geological Survey Circular 1395, 90 p. <http://dx.doi.org/10.3133/cir1395>
- Westerling, A. L., Hidalgo, H. G., Cayan, D. R., Swetnam, T. W., 2006. Warming and earlier spring increase western US forest wildfire activity. *Science* 313, 940-943.
- Wiedinmyer, C., Friedli, H. 2007, Mercury Emission Estimates from Fires: An Initial Inventory for the United States: *Environ. Sci. Technol.* v. 41(23), p, 8092-8098.
<http://dx.doi.org/10.1021/es071289o>
- Williams J.R., 1990, The Erosion-Productivity Impact Calculator (EPIC) Model: A Case History. *Philosophical Transactions of the Royal Society*. 29 September 1990 Volume 329, issue 1255, London, England.
- Williams CJ, Pierson FB, Robichaud PR, Boll J (2014) Hydrologic and erosion responses to wildfire along the rangeland–xeric forest continuum in the western US: a review and model of hydrologic vulnerability. *International Journal of Wildland Fire* 23, 155–172.
- Wischmeier, W. H., and D. D. Smith (1978) Predicting Rainfall-Erosion Losses. *Agricultural Handbook Number 537*. Washington, DC: United States Department of Agriculture-Science and Education Administration.
- Wood, M.L., Foe, C., Cooke, J., and Louie, S.J., 2010, Sacramento – San Joaquin Delta Estuary TMDL for Methylmercury. Staff Report. Draft Report for Public Review. Regional Water Quality Control Board – Central Valley Region. February 2010, 233 p.
http://www.swrcb.ca.gov/rwqcb5/water_issues/tmdl/central_valley_projects/delta_hg/
- Wool, T. A., R. B. Ambrose, J. L. Martin, and E. A. Comer. 2006. Water quality analysis simulation program (WASP) version 6.0 draft: user's manual.
<http://www.epa.gov/athens/wwqts/html/wasp.html>. (accessed on 2 February, 2016.)
- Woolhiser et al., 1990
- Woodruff, L.G., Cannon, W.F., 2010. Immediate and long-term fire effects on total mercury in forests soils of northeastern Minnesota. *Environ. Sci. Technol.* 44, 5371–5376.
- Yin X, and Balogh SJ (2002) Mercury concentrations in stream and river water: an analytical framework applied to Minnesota and Wisconsin. *Water Air Soil Pollut* 138:79–100
- Zhang, Z., and Johnson, B.E., 2016, Aquatic Contaminant and Mercury Simulation Modules Developed for Hydrologic and Hydraulic Models. U.S. Army Corps of Engineers, Engineer Research and Development Center, ERDC/EL TR-16-8.

1.4 References specific to Putah and Cache Creek watersheds

1.4.1 Upper Cache Creek Basin (including Clear Lake)

- Ackerman, J.T., Hartman, C.A., Eagles-Smith, C.A., Herzog, M.P., Davis, J., Ichikawa, G., and Bonnema, A., 2015, Estimating exposure of piscivorous birds and sport fish to mercury in California lakes using prey fish monitoring—A predictive tool for managers: U.S. Geological Survey Open-File Report 2015-1106, 48 p., <http://dx.doi.org/10.3133/ofr20151106>
- Alpers, C.N., Eagles-Smith, C., Foe, C., Klasing, S., Marvin-DiPasquale, M.C., Slotton, D.G., and Windham-Myers, L., 2008, Mercury conceptual model. Sacramento, Calif.: Delta Regional Ecosystem Restoration Implementation Plan, 62 p. http://www.science.calwater.ca.gov/pdf/drerip/DRERIP3_mercury_conceptual_model_final_012408.pdf
- Anderson, D.W., Suchanek, T.H., Eagles-Smith, C.A., and Cahill., T., 2008, Mercury residues in ospreys and grebes in a mine-dominated ecosystem: Clear Lake, California: Ecological Applications, v. 18(8) Supplement, p. A227-A238. <http://www.esajournals.org/toc/ecap/18/sp8>
- Domagalski, J.L., Alpers, C.N., Slotton, D.G., Suchanek, T.H., Ayers, S.M., 2003, Mercury and methylmercury concentrations and loads in the Cache Creek Watershed, California, January 2000 through May 2001: U.S. Geological Survey Water-Resources Investigations Report 03-3047, 105 p. <http://loer.tamug.tamu.edu/calfed/Report/Final/USGSCacheloadings.pdf>
- Domagalski, J.L., Slotton, D.G., Alpers, C.N., Suchanek, T.H., Churchill, R., Bloom, N., Ayers, S.M., and Clinkenbeard, J., 2003, Summary and synthesis of mercury studies in the Cache Creek Watershed, California, 2000-2001: U.S. Geological Survey Water-Resources Investigations Report 03-4355, 30 p. <http://water.usgs.gov/pubs/wri/wri034335/>
- Domagalski, J.L., Alpers, C.N., Slotton, D.G., Suchanek, T.H., Ayers, S.M., 2004, Mercury and methylmercury concentrations and loads in the Cache Creek Watershed, California: Science of the Total Environment. v. 327, p. 215–237. <http://loer.tamug.tamu.edu/calfed/Report/Publications/Cachestoen.pdf>
- Eagles-Smith, C.A., Suchanek, T.H., Colwell, A.E., Anderson, N.L., and Moyle, P.B., 2008, Changes in fish diets and food web mercury bioaccumulation induced by an invasive planktivorous fish: Ecological Applications, v. 18(8) Supplement, p. A213-A226. <http://www.esajournals.org/toc/ecap/18/sp8>
- Eagles-Smith, C.A., Suchanek, T.H., Colwell, A.E., and Anderson, N.L., 2008, Mercury trophic transfer in a eutrophic lake: the importance of habitat-specific foraging: Ecological Applications, v. 18(8) Supplement, p. A196-A212. <http://www.esajournals.org/toc/ecap/18/sp8>
- Lowry, G.V., Shaw, S., Kim, C.S., Rytuba, J.J., and Brown Jr., G.E., 2004, Macroscopic and microscopic observations of particle-facilitated mercury transport from New Idria and Sulphur Bank mercury mine tailings: Environmental Science and Technology, v. 38(19), p. 5101-5111.

- Osleger, D.A., Zierenberg, R.A., Suchanek, T.H., Stoner, J.S., Morgan, S., and Adam, D.P., 2008, Clear Lake sediments: anthropogenic changes in physical sedimentology and magnetic response: *Ecological Applications*, v. 18(8) Supplement, p. A239-A256.
<http://www.esajournals.org/toc/ecap/18/sp8>
- Richerson, P.J., Suchanek, T.H., Zierenberg, R., Osleger, D., Heyvaert, A., Slotton, D., Eagles-Smith, C.A., and Vaughn, C., 2008, Anthropogenic stressors and changes in the Clear Lake ecosystem as recorded in sediment cores: *Ecological Applications*, v. 18(8) Supplement, p. A257-A283. <http://www.esajournals.org/toc/ecap/18/sp8>
- Sparks, G. (2016) Mercury and methylmercury related to historical mercury mining in three tributaries to Lake Berryessa, upper Putah Creek watershed, California: M.Sc. thesis, California State University, Sacramento, 278 p.
- Suchanek, T.H., 2008, Special Issue - Mercury cycling and bioaccumulation in a mine-dominated aquatic ecosystem: Clear Lake, California: *Ecological Applications*, v. 18(8) Supplement, p. A1-A2. <http://www.esajournals.org/toc/ecap/18/sp8>
- Suchanek, T.H., Cooke, J., Keller, K., Jorgensen, S., Richerson, P.J., Eagles-Smith, C.A., Harner, E.J., and Adam, D.P., 2009, A mass balance mercury budget for a mine-dominated lake: Clear Lake, California: *Water, Air and Soil Pollution*, v. 196, p. 51-73.
<http://www.esajournals.org/toc/ecap/18/sp8>
- Suchanek, T.H., Eagles-Smith, C.A., Slotton, D.G., Harner, E.J., Colwell, A.E., Anderson, N.L., Mullen, L., Flanders, J., Adam, D., and McElroy, K., 2008, Spatio-temporal trends of mercury in fish from a mine-dominated ecosystem at Clear Lake, California: individual, species, and population trends: *Ecological Applications*, v. 18(8) Supplement, p. A177-A195.
<http://www.esajournals.org/toc/ecap/18/sp8>
- Suchanek, T.H., Eagles-Smith, C.A., Slotton, D.G., Harner, E.J., Adam, D., Colwell, A.E., Anderson, N.L., and Woodward, D., 2008, Mine-derived mercury: effects on lower trophic species in Clear Lake, California. *Ecological Applications*, v. 18(8) Supplement, p. A158-A176. <http://www.esajournals.org/toc/ecap/18/sp8>
- Suchanek, T.H., Eagles-Smith, C.A., Harner, E.J., and Adam, D., 2008, Mercury in abiotic compartments of Clear Lake, California: human health and ecotoxicological implications. *Ecological Applications*, v. 18(8) Supplement, p. A128-A157.
<http://www.esajournals.org/toc/ecap/18/sp8>
- Suchanek, T.H., Eagles-Smith, C.A., Harner, E.J., 2008, Is Clear Lake methylmercury decoupled from bulk mercury loading? Implications for lake management and TMDL implementation: *Ecological Applications*, v. 18(8) Supplement, p. A107-A127.
<http://www.esajournals.org/toc/ecap/18/sp8>
- Suchanek, T.H., Richerson, P.J., Nelson, D.C., Eagles-Smith, C.A., Anderson, D.W., Cech, Jr., J.J., Zierenberg, R., Schladow, G., Mount, J.F., McHatton, S.C., Slotton, D.G., Webber, L.B., Swisher, B.J., and Sexton, M., 2003, Evaluating and managing a multiply stressed ecosystem at Clear Lake, California: A holistic ecosystem approach. In: D.J. Rapport, W.L. Lasley, D.E. Rolston, N.O. Nielsen, C.O. Qualset, and A.B. Damania (eds.) *Managing for Healthy Ecosystems*, Lewis Publishers, Boca Raton, Florida USA, Chapter 121, p. 1239-1271,

- Suchanek, T.H., Richerson, P.J., Zierenberg, R.A., Eagles-Smith, C.A., Slotton, D.G., Harner, E.J., Osleger, D.A., Anderson, D.W., Cech Jr., J.J., Schladow, S.G., Colwell, A.E., Mount, J.F., King, P.S., Adam, D.P., and McElroy, K.J., 2008. The legacy of mercury cycling from mining sources in an aquatic ecosystem: from ore to organism: *Ecological Applications*, v. 18(8) Supplement, p. A12-A28. <http://www.esajournals.org/toc/ecap/18/sp>
- SWRCB (2016) The Integrated Report - 303(d) List of Water Quality Limited Segments and 305(b) Surface Water Quality Assessment. http://www.swrcb.ca.gov/centralvalley/water_issues/tmdl/impaired_waters_list/#newproposed
- Weiner, J.G., and Suchanek, T.H., 2008, The basis for ecotoxicological concern in aquatic ecosystems contaminated by historical mercury mining: *Ecological Applications*, v. 18(8) Supplement, p. A3-A11. <http://www.esajournals.org/toc/ecap/18/sp8>.
- 1.4.2 Lower Cache Creek Watershed, including Settling Basin**
- Domagalski, J.L., Alpers, C.N., Slotton, D.G., Suchanek, T.H., Ayers, S.M., 2003, Mercury and methylmercury concentrations and loads in the Cache Creek Watershed, California, January 2000 through May 2001: U.S. Geological Survey Water-Resources Investigations Report 03-3047, 105 p. <http://loer.tamug.tamu.edu/calfed/Report/Final/USGSCacheloadings.pdf>
- Domagalski, J.L., Alpers, C.N., Slotton, D.G., Suchanek, T.H., Ayers, S.M., 2004, Mercury and methylmercury concentrations and loads in the Cache Creek Watershed, California: *Science of the Total Environment*. v. 327, p. 215-237. <http://loer.tamug.tamu.edu/calfed/Report/Publications/Cachestoen.pdf>
- Domagalski, J.L., Slotton, D.G., Alpers, C.N., Suchanek, T.H., Churchill, R., Bloom, N., Ayers, S.M., and Clinkenbeard, J., 2003, Summary and synthesis of mercury studies in the Cache Creek watershed, California, 2000–2001: U.S. Geological Survey Water–Resources Investigations Report 03-4355, 30 p. <http://water.usgs.gov/pubs/wri/wri034335/>
- Holloway, J.M., Goldhaber, M.B., and Morrison, J.M., 2009, Geomorphic controls on mercury accumulation in soils from a historically mined watershed, Central California Coast Range, USA: *Applied Geochemistry*, v. 24, p. 1538-1548.
- Labiosa, W.B., Leckie, J.O., Mumley, T., Rytuba, J.J., and Bernknopf, R., 2003, A decision analysis approach to TMDL implementation decisions: mercury TMDLs in the San Francisco Bay Area: *Proceedings of TMDL 2003 Specialty Conference*, 23 p.
- Labiosa, W.B., Leckie, J.O., Shachter, R., Freyberg, D., and Rytuba, J.J., 2005, Incorporating uncertainty in watershed management decision-making: a mercury TMDL case study. *ASCE Watershed Management Conference, Managing Watersheds for Human and Natural Impacts: Engineering, Ecological, and Economic Challenges*, Williamsburg, VA, July 19–22, 2005.
- Marvin Di Pasquale, M., Alpers, C.N., and Fleck, J.A., 2009, Mercury, methylmercury, and other constituents in sediment and water from seasonal and permanent wetlands in the Cache Creek Settling Basin and Yolo Bypass, Yolo County, California, 2005–06: U.S. Geological Survey, Open File Report 2009-1182, 69 p. <http://pubs.usgs.gov/of/2009/1182/>

- Slowey, A.J., and Rytuba, J.J., 2008, Mercury release from the Rathburn Mine, Petray Mine, and Bear Valley saline springs, Colusa County, California 2004–2006, U.S. Geological Survey Open-File Report 2008-1179, 49 p. <http://pubs.usgs.gov/of/2008/1179/>
- Wentz, D.A., Brigham, M.E., Chasar, L.C., Lutz, M.A., and Krabbenhoft, D.P., 2014, Mercury in the Nation's streams—Levels, trends, and implications: U.S. Geological Survey Circular 1395, 90 p. <http://dx.doi.org/10.3133/cir1395>
- Wood, A.W., Bernknopf, R., Rytuba, J.J., Labiosa, W.B., Singer, D.A., and Kapla, R., Champion, R., 2004, Incorporating uncertainty into mercury-offset decisions with a probabilistic network for National Pollutant Discharge Elimination System permit holders: An interim report: U.S. Geological Survey Open-File Report 2004-1408, 75 p. <http://pubs.usgs.gov/of/2004/1408/>
- Wood, A.W., Bernknopf, R., Rytuba, J.J., Singer, D.A., and Champion, R., 2005, Offset-based decision support models for mitigating mercury sources in the Cache Creek watershed, north central California: Proceedings of the Water Environment Federation, no. 3, p. 1496-1516.

2 PFHydro: A New Watershed-Scale Model for Post-Fire Runoff Simulation (Accepted Journal Manuscript)

A new watershed-scale model for post-fire runoff simulation was developed, called PFHydro. In lieu of a chapter on this subject, a manuscript is provided that was accepted by the Journal of Environmental Modeling and Software for publication. Environmental Modeling and Software has an impact factor of 4.55 in 2018 and is one of the most influential journals focused on environmental modeling.

In keeping with the formatting requirements of Reclamation's Science and Technology Program the accepted manuscript is included in **Appendix 1** of this report.

3 Sediment Load Simulation at Cache Creek

3.1 Introduction

Watershed erosion models deal with the simulation of soil detachment and subsequent transport by flowing water. They provide predictions of how soil is eroded and then delivered to streams and reservoirs at specified locations. Historically, watershed erosion models have mostly been developed for agricultural applications for soil conservation and land management and planning. In practice, however, models have been extended and applied to general watersheds beyond the original intended applications. Different erosion models have been developed for different applications and with differing model complexity. In this project - simulating the soil erosion and delivery at Cache Creek - a specific erosion approach is adopted and implemented in our new watershed model, which is derived from the Universal Soil Loss Equation (USLE) (Wischmeier and Smith, 1978). The new model is then demonstrated by simulating the soil erosion and delivery at Cache Creek. In the following chapter, the USLE approach is briefly described, and the specific erosion model implemented in this project for the Cache Creek simulation is reported, along with the model results.

3.2 Summary description of the USLE (Wischmeier and Smith, 1978)

The USLE was initially developed from the statistical analyses of data from 47 locations in 24 states in the Central and Eastern United States. It may be expressed as:

$$A = RKLSCP \quad 3-1$$

where: A = average annual soil erosion in mass/area (tons/acre/year) for a slope length,
 R = erosivity factor (rainfall),
 K = soil erodibility factor,
 L = slope length factor,
 S = slope steepness factor,
 C = cover-management factor, and
 P = erosion-control practice factor.

In the above equation, $RK (=A_u)$ represents the average annual soil erosion on a unit plot which is defined on a 72.6 ft length and 9% slope with the baseline C and P . The terms $LSCP$ are normalized with respect to the unit plot and, therefore, are dimensionless and have a value of 1 for unit plot conditions.

There is a large body of literature that provide methods to obtain the above parameters. Some discussion is provided below which is based on: (a) reports and other model documentation provided by Foster (2005), (b) a book published by Yang (1996), and (c) a set of class notes from the web site: http://www.5counties.org/docs/roaedu/2012_5c_roads/rusle.pdf.

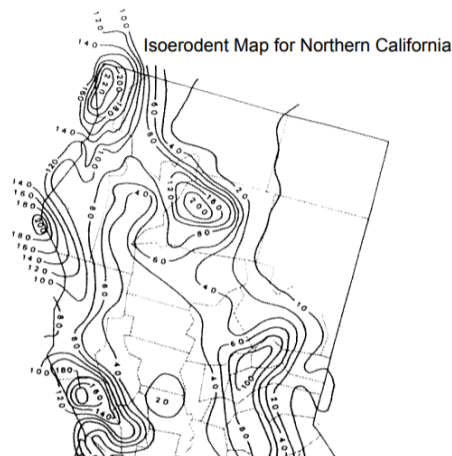
Rainfall erosivity (R) accounts for differences in rainfall intensity, duration and frequency at different locations. The annual erosivity (R_u) is the temporal integration (sum) of the unit plot erosivity for individual storms and is expressed as follows:

$$R_u = \sum_{Storm} (EI_{30}) \quad 3-2$$

where the storm event erosivity is EI_{30} - E is the total kinetic energy of the storm, and I_{30} is the average intensity over the continuous 30 minutes with the highest rainfall total during the storm. The summation of all storm erosivity over m years, when divided by m , yields the annual R factor. Only storms greater than 0.5 inch (12 mm) are taken into account. The rainfall erosivity equation applies to a unit plot of land – hence the USLE can be used to estimate the erosion from a single storm by extrapolating $(EI_{30})K$ (mass/area) over larger areas to estimate total soil erosion following a storm.

The R factor may be determined from isoerodent maps that depict yearly average soil erosivity, or from tables, nomographs and charts that distribute estimated annual soil erosivity by other periods such as by month. Figure 3-1, for example, shows an example of a map and table that can be used to estimate the R factor for northern California.

MONTH BASIS.



Adjustment factor for estimating monthly and periodic portions of annual soil loss. Ukiah (R=59)

Month	Percent
January	11
February	16
March	11
April	6
May	3
June	5
July	4
August	3
September	4
October	5
November	15
December	17
TOTAL	100

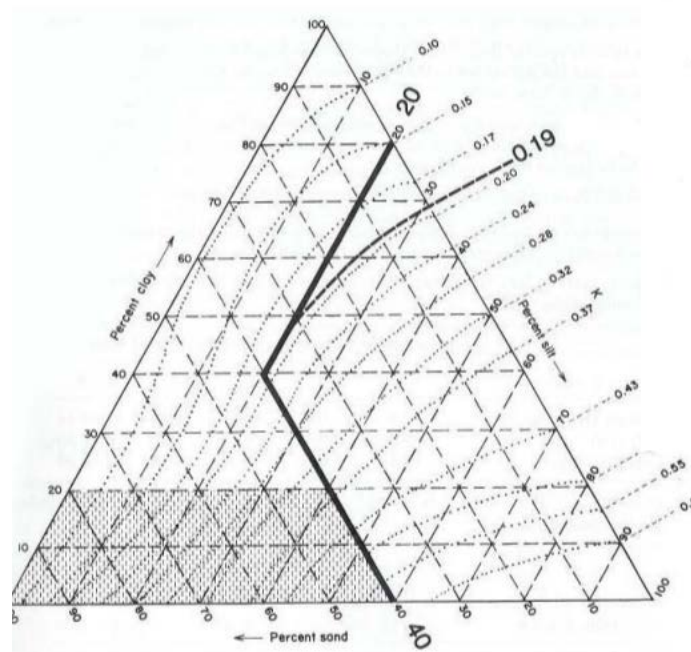
**Source: Internet- USEPA Rainfall Erosivity Factor Calculator

Figure 3-1. R factor map for northern California (Yang, 1996)

The soil-erodibility factor K is a measure of the intrinsic susceptibility of a given soil to erosion. Soil texture (size gradation) is the primary factor affecting K , but soil structure (how soil particles are bound together), organic matter and permeability also contribute. The soil erodibility factor is defined as the erosion rate per unit erosion-index for a specific soil in cultivated, continuous fallow, on a plot that is 72.6 feet long with a 9-percent slope. These were the dimensions of the plots first used to establish the USLE. The K -factor value ranges from 0.7 for highly erodible loams and silt loams to less than 0.1 for sandy and gravelly soils with a high infiltration rate.

According to source (c), the K value may also be determined from the figure or the table shown in Figure 3-2.

Soil K Value Nomograph



Generalized Soil Characteristic	K	
High clay content	0.05 – 0.15	resistance to detachment decreases erodibility
Course textured sandy soils	0.05 – 0.2	even though these soils are easily detached they produce low runoff
Medium textured silt loam soils	0.25 – 0.4	moderately susceptible to detachment and produce moderate runoff
High silt content	> 0.4	most erodible of all soils because they are easily detached; tend to crust and produce high rates of runoff

K values range from 0.02 to 0.69

Figure 3-2. Figure and table that may be used to estimate the K value (Wischmeier and Smith, 1978)

The slope-length factor L accounts for the increased quantity of runoff that occurs as distance from the top of the slope increases. It is the ratio of the soil loss from a given slope length to that from a 72.6-foot length, with all other conditions remaining the same. The slope-steepness factor S accounts for the increased velocity of runoff with slope steepness. It is the ratio of soil loss from a given slope steepness to that from a 9-percent slope. The effects of slope length and steepness are usually combined into one single factor, that is, the LS factor, which can be computed according to the equation (Yang, 1996):

$$LS = (\lambda/72.6)^m (65.41 \sin^2 \theta + 4.56 \sin \theta + 0.065)$$

3-3

where: λ = actual slope length in feet,
 θ = angles of slope, and
 m = an exponent with value ranging from 0.5 for slope equal to or greater than 5 percent to 0.2 for slope equal or less than 1 percent.

The LS factors for different slope angles and lengths are summarized in the table below (Figure 3-3) for a disturbed soil with little or no crop cover.

Slope %	Slope length in feet																
	<3	6	9	12	15	25	50	75	100	150	200	250	300	400	600	800	1000
0.2	0.05	0.05	0.05	0.05	0.05	0.05	0.05	0.05	0.05	0.05	0.06	0.06	0.06	0.06	0.06	0.06	0.06
0.5	0.07	0.07	0.07	0.07	0.07	0.07	0.08	0.08	0.09	0.09	0.10	0.10	0.10	0.11	0.12	0.12	0.13
1.0	0.09	0.09	0.09	0.09	0.09	0.10	0.13	0.14	0.15	0.17	0.18	0.19	0.20	0.22	0.24	0.26	0.27
2.0	0.13	0.13	0.13	0.13	0.13	0.16	0.21	0.25	0.28	0.33	0.37	0.40	0.43	0.48	0.56	0.63	0.69
3.0	0.17	0.17	0.17	0.17	0.17	0.21	0.30	0.36	0.41	0.50	0.57	0.64	0.69	0.80	0.96	1.10	1.23
4.0	0.20	0.20	0.20	0.20	0.20	0.26	0.38	0.47	0.55	0.68	0.79	0.89	0.98	1.14	1.42	1.65	1.86
5.0	0.23	0.23	0.23	0.23	0.23	0.31	0.46	0.58	0.68	0.86	1.02	1.16	1.28	1.51	1.91	2.25	2.55
6.0	0.26	0.26	0.26	0.26	0.26	0.36	0.54	0.69	0.82	1.05	1.25	1.43	1.60	1.90	2.43	2.89	3.30
8.0	0.32	0.32	0.32	0.32	0.32	0.45	0.70	0.91	1.10	1.43	1.72	1.99	2.24	2.70	3.52	4.24	4.91
10.0	0.35	0.37	0.38	0.39	0.40	0.57	0.91	1.20	1.46	1.92	2.34	2.72	3.09	3.75	4.95	6.03	7.02
12.0	0.36	0.41	0.45	0.47	0.49	0.71	1.15	1.54	1.88	2.51	3.07	3.60	4.09	5.01	6.67	8.17	9.57
14.0	0.38	0.45	0.51	0.55	0.58	0.85	1.40	1.87	2.31	3.09	3.81	4.48	5.11	6.30	8.45	10.40	12.23
16.0	0.39	0.49	0.56	0.62	0.67	0.98	1.64	2.21	2.73	3.68	4.56	5.37	6.15	7.60	10.26	12.69	14.96
20.0	0.41	0.56	0.67	0.76	0.84	1.24	2.10	2.86	3.57	4.85	6.04	7.16	8.23	10.24	13.94	17.35	20.57
25.0	0.45	0.64	0.80	0.93	1.04	1.56	2.67	3.67	4.59	6.30	7.88	9.38	10.81	13.53	18.57	23.24	27.66
30.0	0.48	0.72	0.91	1.08	1.24	1.86	3.22	4.44	5.58	7.70	9.67	11.55	13.35	16.77	23.14	29.07	34.71
40.0	0.53	0.85	1.13	1.37	1.59	2.41	4.24	5.89	7.44	10.35	13.07	15.67	18.17	22.95	31.89	40.29	48.29
50.0	0.58	0.97	1.31	1.62	1.91	2.91	5.16	7.20	9.13	12.75	16.16	19.42	22.57	28.60	39.95	50.63	60.84
60.0	0.63	1.07	1.47	1.84	2.19	3.36	5.97	8.37	10.63	14.89	18.92	22.78	26.51	33.67	47.18	59.93	72.15

NRCS Unit Plot, LS=1
 Figure 3-3. LS values for freshly prepared construction and other highly disturbed soil, with little, or no cover (crop canopy factor, C = 0) (Wischmeier and Smith, 1978).

The cover-management factor C was originally introduced to account for the crop rotation used, tillage method, crop residue treatment, productivity level, and other agricultural practice variables. It is the ratio of soil loss from a field with given cropping and management practices to the loss from the tilled, bare soil conditions used to evaluate the K-factor. The seasonal distribution of rainstorms in different locations influences the amount of soil erosion over the course of a year. The fraction of average annual erosion that occurs up to any point in the year varies according to the geographical location.

The crop cover factor changes in time with the crop stage changes. First, the crop cover factor at the site is estimated for the k-th crop stage (c_k). Then, the annual C is computed according to:

$$C = (\sum_{k=1}^n r_k c_k) / m \quad 3-4$$

where n is the total number of crop stages over a period of m years for which the simulation is performed (such as years in a crop rotation or years after disturbance of a construction site), and r_k is the portion of the average annual rainfall erosivity that occurs during the kth crop stage.

Source (c) states that the C factor reduces the soil loss estimate according to the effectiveness of vegetation and mulch at preventing detachment and transport of soil particles. Typical C values for construction sites are listed in Figure 3-4. The C factor can be an important calibration parameter in estimating the soil erosion.

Cover Management Factors for Construction Sites		
Vegetative Cover	C factor	Percent Reduction of soil loss
None (fallow ground)	1.0	0
Native vegetation (undisturbed)	0.01	99
Temporary Ryegrass, 90% (perennial)	0.05	95
Temporary Ryegrass, 90% (annuals)	0.1	90
Permanent Seedlings (90%)	0.01	99
Sod (laid immediately)	0.01	99
Mulching (for slopes 2:1 or less)		
Hay (0.5 tons/acre)	0.25	75
Hay (1.0 tons/acre)	0.13	87
Hay (1.5 tons/acre)	0.07	93
Hay (2.0 tons/acre)	0.02	98
Wood chips (6 tons/acre)	0.06	94
Wood cellulose (1.75 tons per acre)	0.10	90
Other		
Competent gravel layer	0.05	95
Rolled erosion control fabrics	(for slopes greater than 2:1)	variable C value by type

Figure 3-4. Typical C factor values for construction sites (Wischmeier and Smith, 1978).

The erosion-control practice factor P accounts for the effects of conservation practices, such as contouring, strip-cropping, and terracing, on the erosion process. It is the ratio of soil loss with a given practice to soil loss with straight-row farming parallel to the slope. For example, soil loss may be reduced by 50 percent on a 2- to 7-percent slope as a result of contouring. However, contouring becomes less effective with increasing slope. For steep slopes, terracing is a more effective conservation practice. The P factor is most relevant to practices undertaken to reduce runoff velocity and can be ignored for non-cultivated and native land use.

3.3 Specific Models for Cache Creek Modeling

For this study, a specific sediment erosion and delivery approach, adopted by the GWLF - Generalized Watershed Loading Function (Haith and Shoemaker, 1987; Haith et al., 1992), was selected to create a water quality model, PFHydro-WQ, to simulate sediment loads produced by the Cache Creek Watershed. The pre- and post-fire runoff, as well as the precipitation was input

into the model so that time series daily sediment load under pre- and post-fire conditions could be simulated.

The GWLF method may be considered as a variant of the USLE method; it computes the daily sediment erosion, E , from a source area using the following equation:

$$E = 0.132 RE * K * (LS) * C * P * AR \quad 3-5$$

where RE is the daily rainfall erosivity, K is the soil erodibility factor, L is the slope length factor, S is the slope steepness factor, C is the cover-management factor, P is the practice supporting factor, and AR is the source area. Most parameters in the equation may be estimated using any of the USLE/RUSLE methodologies. The constant 0.132 is a dimensional conversion factor used by the GWLF.

The parameter RE is the daily rainfall erosivity ($MJ\text{-}mm/ha\text{-}h$) and is computed using the equation:

$$RE = 64.6 \alpha R^{1.81} \quad 3-6$$

where α is a coefficient that varies with season and the geographical location, and R is the daily rainfall (mm/day).

The annual average sediment yield from a source area, E_{ann} , is normally obtained over a long period (multiple years). In this study, it is computed from the daily data as follows:

$$E_{ann} = \sum_{i=1}^{365} E / 365 \quad 3-7$$

The daily unit-area sediment supply (Y) from a source area (tons/day/ha) is then computed from the value of E_{ann} using the following equation (Schneiderman et al., 2002):

$$Y = E_{ann} * SDR * TC / TC_{ann} \quad 3-8$$

Where SDR is the sediment delivery ratio, TC is the daily transport capacity, and TC_{ann} is the annual average sediment transport capacity.

The daily total sediment supply (S) from the source (tons/day) having an area of A_{rea} (ha) is computed as:

$$S = E_{ann} * SDR * TC / TC_{ann} * Area \quad 3-9$$

The sediment delivery ratio (SDR) is defined as “the ratio of the erosion upslope of a point in the landscape to the sediment delivered from that point” (Kinnell, 2004). It accounts for soil losses due to sediment redeposition during the transport process. In the GWLF model, the ratio is used to determine the sediment supply or delivery to a gauge point by multiplying it with the estimated sediment yield. In GWLF, SDR was determined through the use of a logarithmic graph relating the SDR to the catchment area, which was originally developed by Vanoni (1975). This graph appeared in Figure B-2 of the GWLF user’s manual (Haith et al., 1992). For the present pre-fire modeling of the Cache Creek Watershed, the source area is 282 km², and the sediment delivery ratio of 0.082 was adopted.

The daily transport capacity may be correlated to the streamflow discharge Q (cm/day) as follows:

$$TC = Q^{tcp} \quad 3-10$$

The exponent tcp is the transport capacity power coefficient and has a default value of 1.67 according to Haith (1985) which is attributable to Vanoni (1975). In the pre-fire erosion simulation of the Cache Creek, tcp was calibrated to be 1.5.

3.4 Wildfire Impact

The impact of wildfire on soil erosion was simulated. Severe wildfires and subsequent precipitation and runoff can have a significant impact on soil erosion and sedimentation, as a result of the following factors:

- higher rainfall erosivity due to vegetation canopy loss (R)
- greater energy of impact on the litter layer and soil cover (C)
- loss of soil aggregate stability due to physicochemical changes (K)

Catchment sediment yields are known to increase significantly following intense wildfires. In general, high severity wildfires increase runoff and erosion rates by two or more orders of magnitude, while low and moderate severity burns have much smaller effects on runoff and sediment yields.

The following is a list of factors that may be used to represent changes due to fire:

- According to Diaz-Fierros et al. (1987), the factors LS and K need to be modified to adapt them to the conditions of burned forest soils. In their study, it was noted that serious erosion was observed during the first year after burning but the intensity of the process decayed exponentially and was negligible after the first 12 months.
- A study by Rulli et al. (2013) showed that in burned areas, fire effects on soil characteristics could be simulated by changing the C factor (increased C for higher burn severity area), by decreasing soil drainage capacity and by decreasing soil organic matter content. Post-fire organic matter reduction has been simulated by considering burned areas having fertility

class one level lower than in natural conditions, and soil water repellency layer formation has been accounted for by reducing soil drainage capacity, which was set to drainage class “very slow.”

3.5 Using HSPF results as sediment load boundary conditions

The current watershed model boundary has locations where runoff and sediment fluxes occur, so boundary conditions are needed. The suspended sediment load boundary conditions were obtained from a previous HSPF modeling study conducted for the Cache Creek watershed by Stern et al. (2016) (in Section 1.10). Hourly sediment loads were calculated for each sub basin and then summed to the daily values at two input locations as the boundary conditions for PFHydro-WQ modeling (Figure 1-7). HSPF calculates erosion and sediment transport as wash-off of detached sediment in storage and the scour of the soil matrix. The sediment outflow from the land surface is classified into sand, silt, and clay based on the soil texture of each land surface. The river module routes runoff and water quality constituents through a single reach assumed to be unidirectional, using the kinematic wave equation. The migration of each sediment fraction between suspension in water and the bed is modeled by balancing deposition and scour of sediment along with bed material.

The daily observed (regressed) calibration time series were downloaded from NWIS (National Water Information System, <https://waterdata.usgs.gov/nwis>) for comparison to daily modeled sediment loads at the Rumsey location (Gage number 4, Figure 1-7); these were calculated using a regression model (GCLAS, Koltun et al. 2006) that used a combination of sediment rating curves and 15-minute streamflow data.

Initial sediment parameters from the existing model were changed iteratively during the calibration process. Initially, one set of parameters were used for the full simulation period; this set of parameters for both the pre- and post-fire scenarios, however, resulted in an underestimation of suspended sediment concentrations in water year 2016, the first year following the fire. Sediment parameters were changed for sub-basins that were burned in the wildfires in the summer of 2015. For water year 2016, vegetation cover was reduced to zero and soil detachment and wash-off parameters were increased in affected sub basins until a satisfactory fit to observed (regressed) data was determined. In water year 2017, parameters were set back to pre-fire conditions for the affected sub basins, as it was expected that effects of the fire would be minimal by that time, due to the regrowth of vegetation and the breaking up of the SWR layer (Ch. 2). Daily sediment loads were compared to observed (regressed) (Figure 3-5) at the main calibration location (Rumsey outlet). The calculated NSE was 0.73 and the R^2 value was 0.75 for water years 2015-2017.

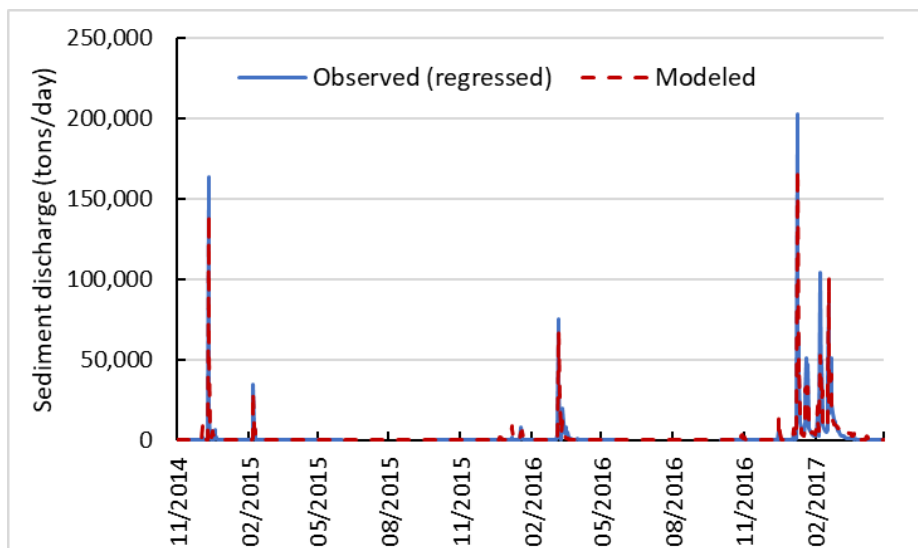


Figure 3-5. Daily time series of sediment load at Cache Creek Watershed (Rumsey outlet) for WY 2015-2017.

3.6 Pre- and post-fire modeling results

The pre-fire modeling results are shown at Figures 3-6, 3-7. The NSE criteria is 0.96 for time-series daily sediment load simulation in WY 2015, due mainly to the accurate reproduction of observed data for the two largest storm events.

The post-fire sediment model was firstly applied and calibrated in WY 2017 (2nd year post-fire) for daily sediment load simulation (Figures 3-8, 3-9); an NSE of 0.79 was obtained. The calibrated model was then applied to simulate daily sediment load in WY 2016 with minor adjustments of related parameters and obtained an NSE of 0.60 (Figures 3-10, 3-11).

It can be seen from Figures 3-10, 3-11 that the modeling results fail to replicate observations for the two biggest storm events in March of 2016. A probable cause is the model assumption that there are unlimited soil erosion sources to generate the sediment load. The observed data suggested that there was a first-flush phenomenon for the first large storm event, leading to a decreased sediment load for the subsequent storms.

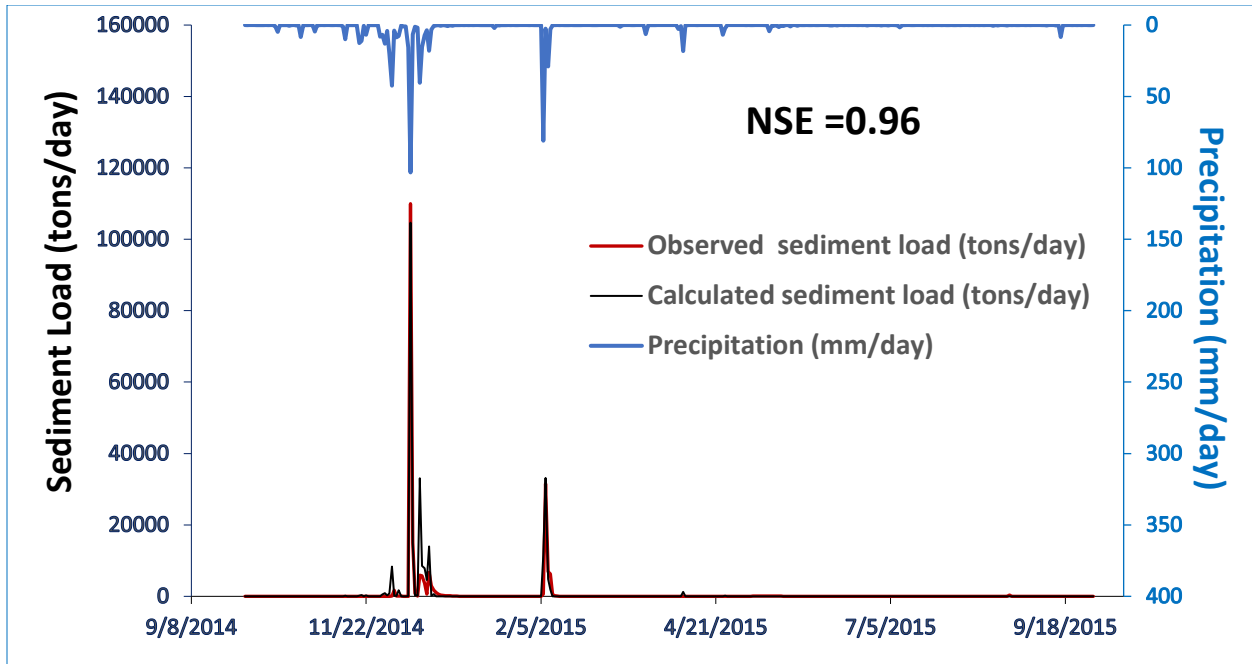


Figure 3-6. Daily time series sediment load at Cache Creek Watershed (Rumsey outlet) in WY 2015

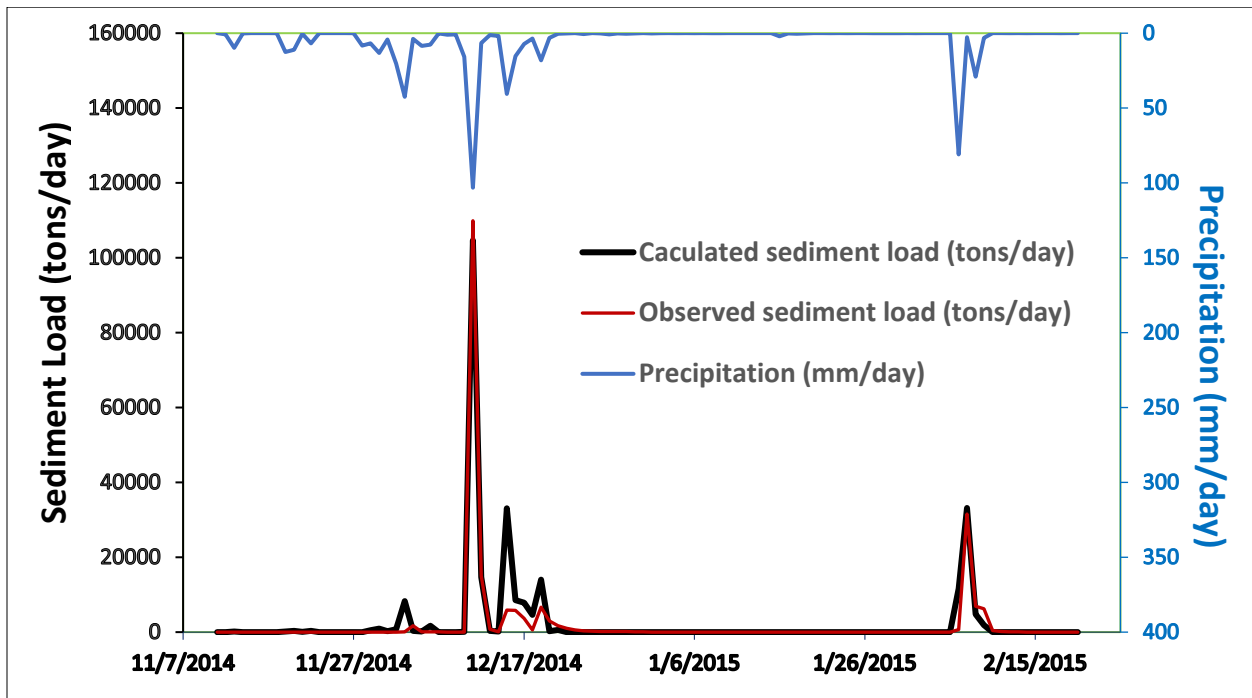


Figure 3-7. Daily time series sediment load at Cache Creek Watershed (Rumsey outlet) for major storm events in WY 2015

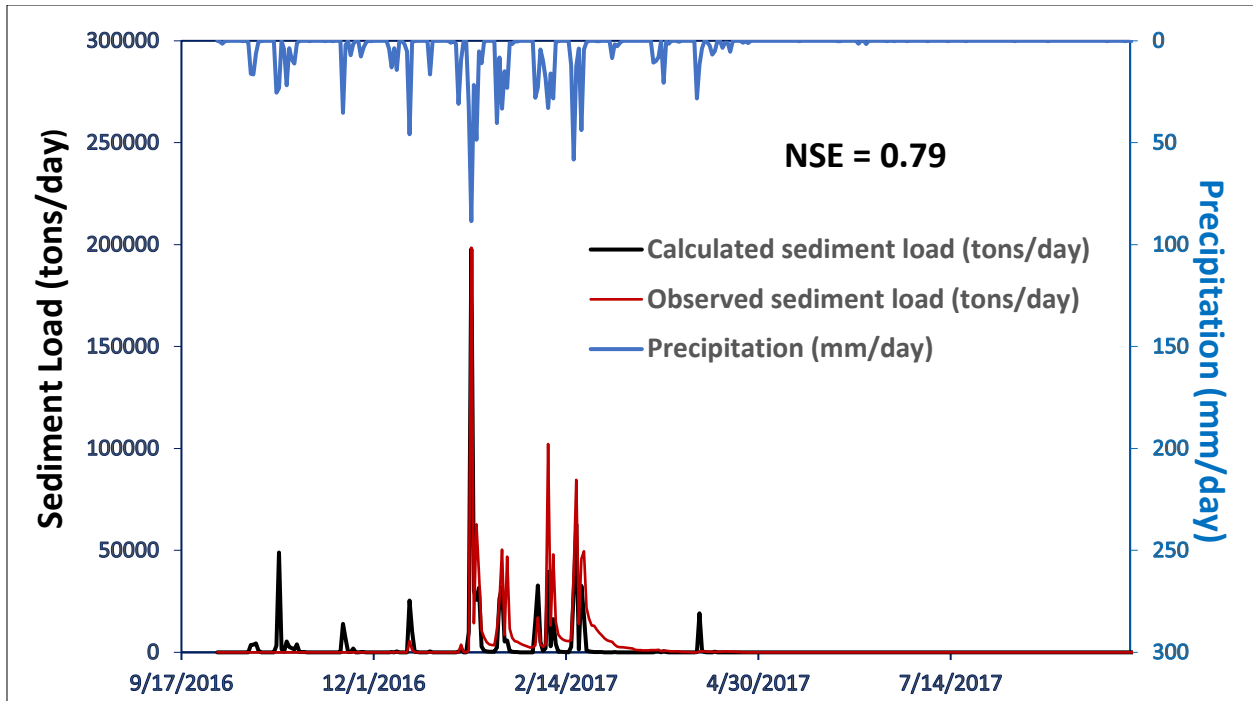


Figure 3-8. Daily time series sediment load at Cache Creek Watershed (Rumsey outlet) in WY 2017

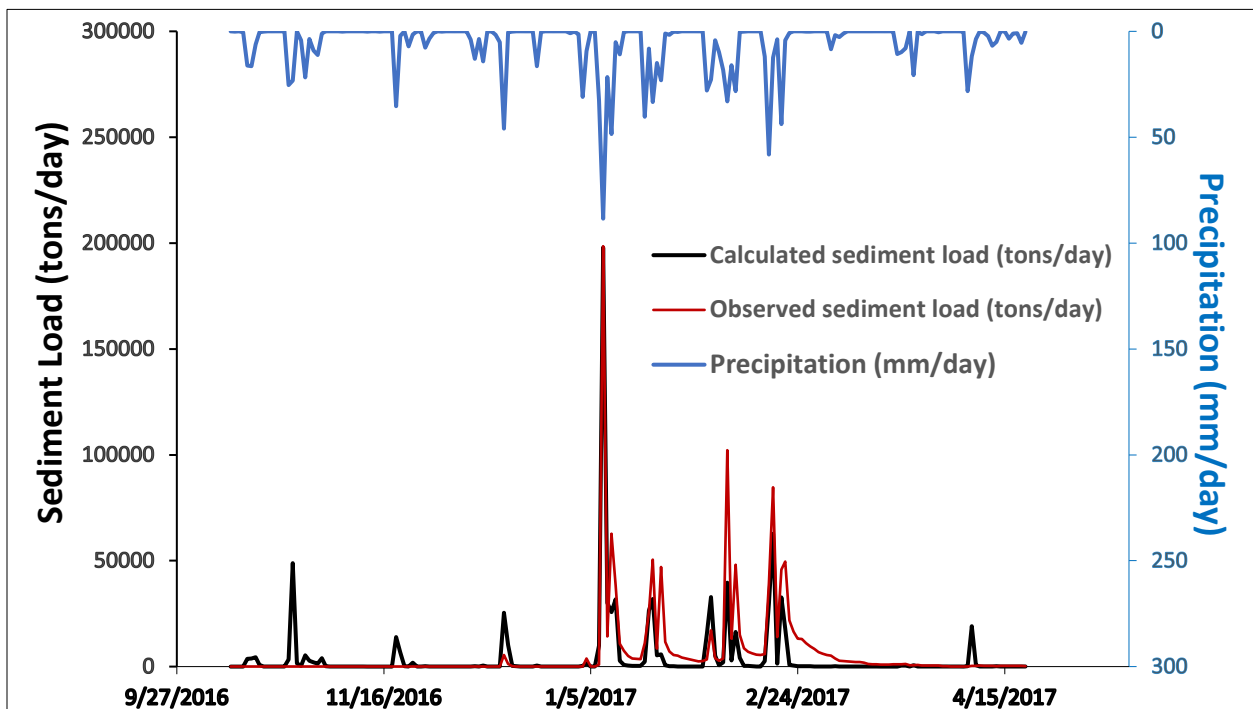


Figure 3-9. Daily time series sediment load at Cache Creek Watershed (Rumsey outlet) for the period surrounding for major storm events in WY 2017

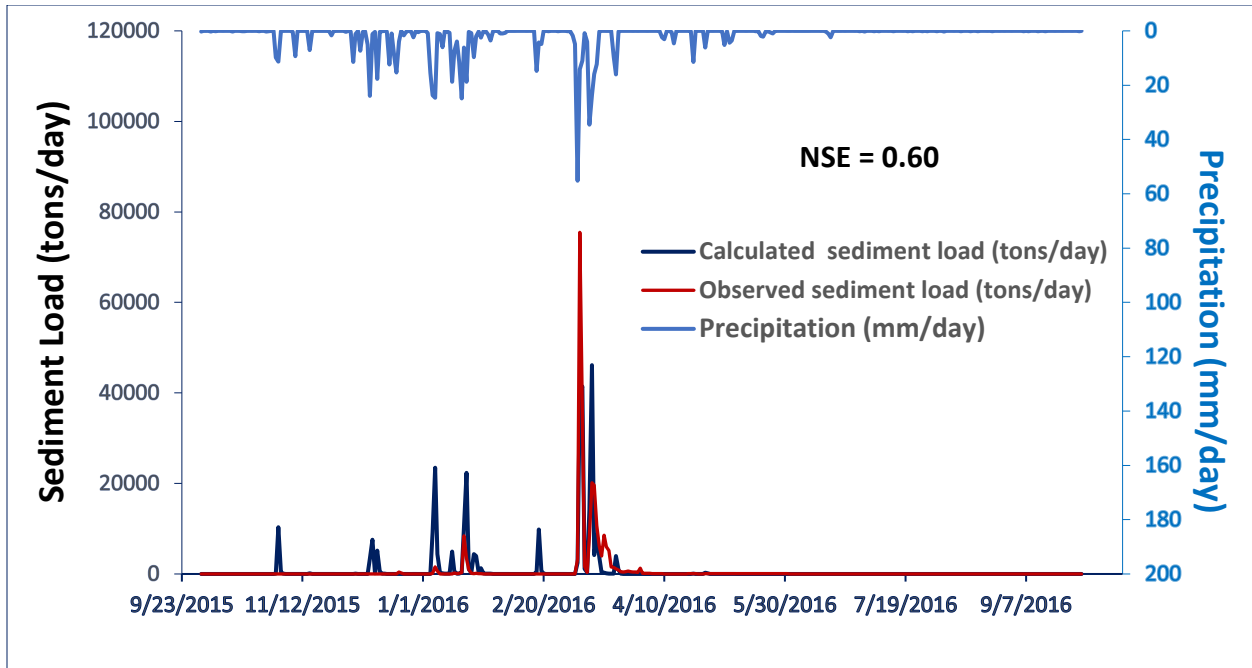


Figure 3-10. Daily time series sediment load at Cache Creek Watershed (Rumsey outlet) in WY 2016

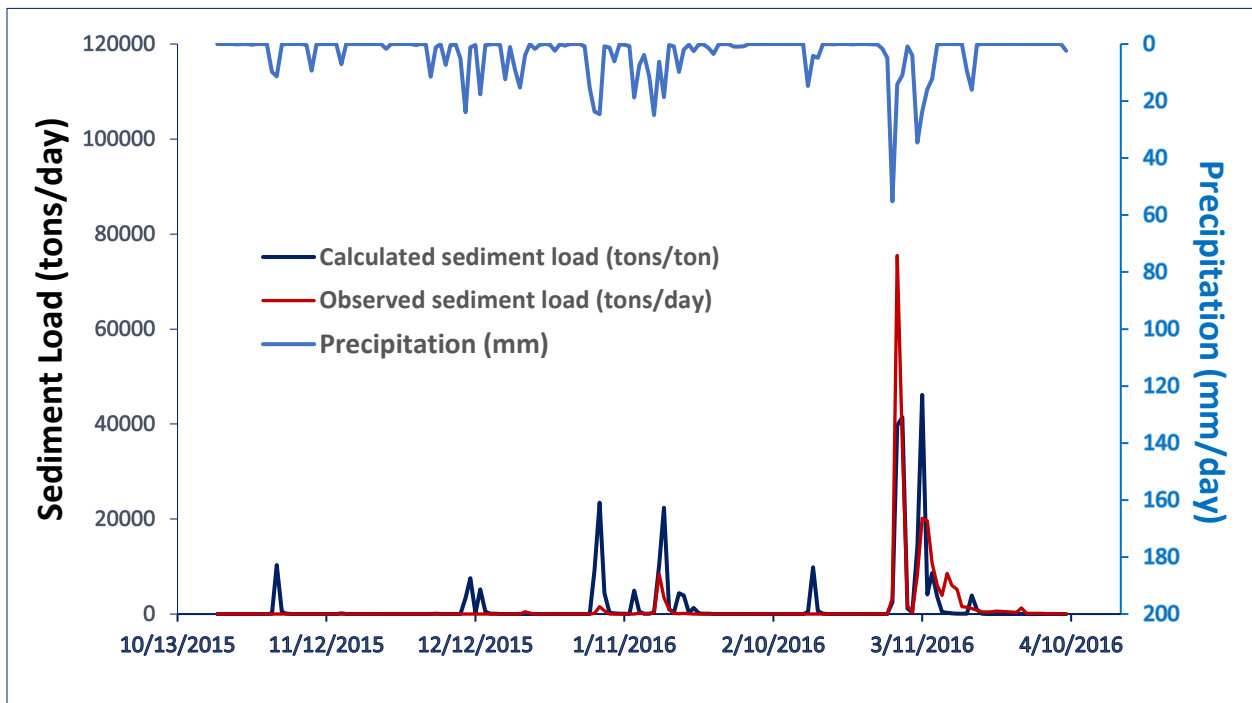


Figure 3-11. Daily time series sediment load at Cache Creek Watershed (Rumsey outlet) for the period surrounding major storm events in WY 2016

Two of the largest storm events, one in WY 2015 (1st year pre-fire) and the other in WY 2017 (2nd year post-fire), had similar precipitation intensity and total precipitation and were selected to investigate wildfire effects on soil erosion. The results are shown in Figure 3-12 and Table 3-1. It can be seen that simulated time series daily sediment load matches the observations well, especially peak sediment loads, for both pre- and post-fire storm events.

Table 3-1. Comparison of model results for the pre-fire and post-fire storm events

Precipitation Start and End Time (Duration: 4 days)	Total precipitation (mm)	Total simulated surface runoff (cfs)	Total simulated sediment load (tons)	Total observed sediment load (tons)
12/10/14 --12/13/14 (Pre-fire)	127 (5.0 in)	71,049	119,737	125,776
01/06/17– 01/09/17 (Post-fire)	143 (5.6 in)	115,940	235,632	213,702
Post-fire / Pre-fire	1.1	1.6	2.0	1.7

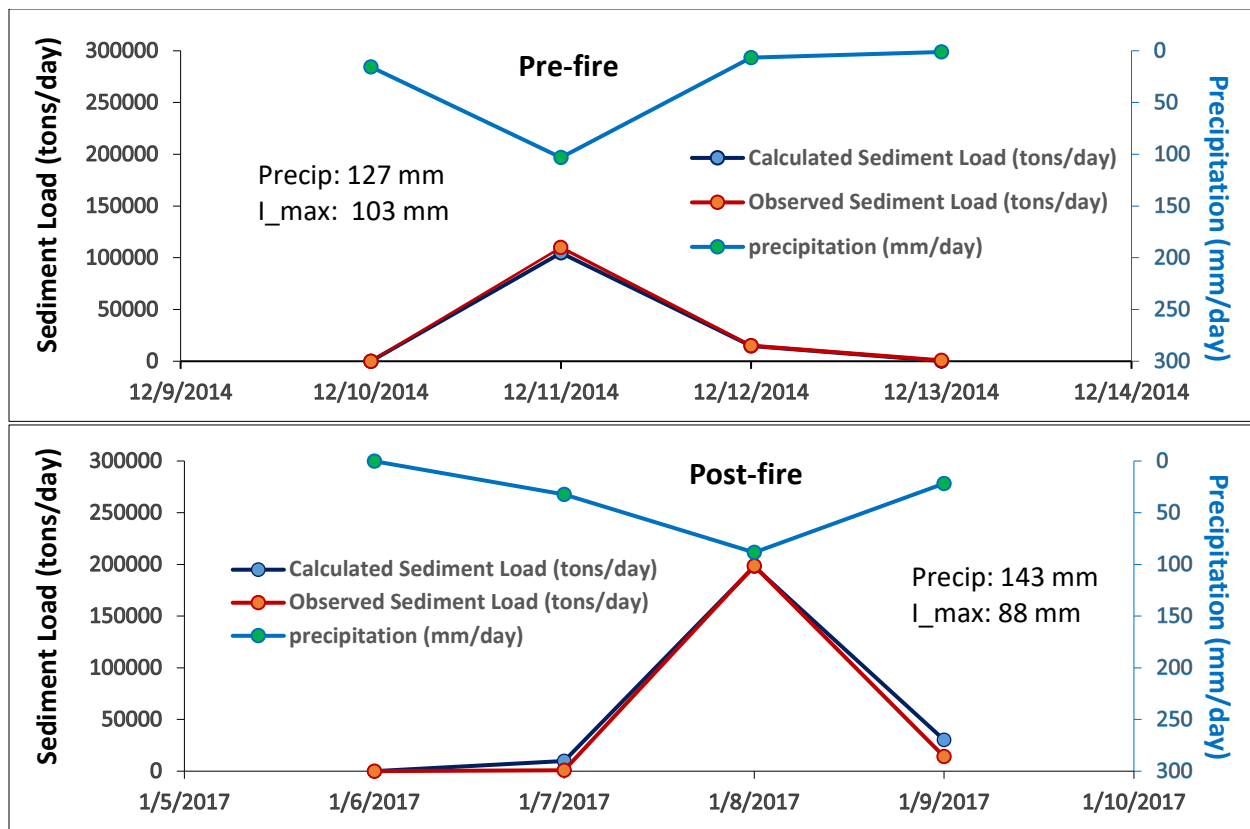


Figure 3-12. Comparison of model sediment simulations for similar pre-fire and post-fire storm events. “Precip” is total storm event precipitation, “I_max” is the maximum precipitation intensity.

The total observed sediment load for the three-day largest storm event in WY 2017 is around 1.7 times of that in WY 2015 with a slightly higher total precipitation (11% higher), but lower peak precipitation (15% lower). Therefore, the wildfire effect on soil erosion is still significant in the upper Cache Creek Watershed roughly sixteen months post-fire (Aug. 2015).

The total simulated surface runoff (Table 3-1) post-fire is approximately 1.6 times higher than that of pre-fire because of residual SWR effects as discussed in the previous chapter. Higher surface runoff caused by SWR was a major factor in increased soil erosion post-fire. Loss of pre-fire vegetation in burned areas also reduced protection against soil erosion post-fire.

Annual sediment loads for WYs 2015, 2016, and 2017 are listed in Table 3-2. The annual observed sediment loads of post-fire WYs 2016 and 2017 are elevated compared to the pre-fire WY 2015 load. This is predominately a result of higher surface runoff in post-fire WYs than in the pre-fire WY. The simulated annual surface runoff in WY 2016 is roughly 60% higher than in WY 2015, resulting in a WY 2016 annual sediment load that is 15% higher than in WY 2015. Note that annual total runoff (i.e. surface and shallow groundwater flow) in WY 2016 was only about 49% of that in WY 2015, despite a higher annual precipitation in WY 2015 (580 mm, compared to 630 mm in WY 2016). Precipitation in WY 2015 was concentrated primarily in two major storms resulting in more annual total runoff in WY 2015 than in WY 2016. The observed annual sediment load in WY 2017 is about six times higher than that in WY 2015, which may be explained by: 1) an almost doubled annual precipitation in WY 2017 over that in WY 2015 and 2) an almost tripled annual surface runoff in WY 2017 over that in WY 2015 (resulting primarily from SWR effects).

Table 3-2. Annual sediment load for WYs 2015, 2016 and 2017

Water Year	Annual Precipitation (mm)	Simulated Annual runoff (cfs)	Simulated Annual Surface runoff (cfs)	Simulated Annual Sediment Load (tons/day)	Observed Annual Sediment Load (tons/day)
WY2015 (pre-fire)	580 (22.9 in)	1,450,397	221,205	255,398	206,066
WY2016 (post-fire)	630 (24.8 in)	711,308	354,080	295,719	236,961
WY2017 (post-fire)	1118 (44.0 in)	2,664,382	652,991	810,907	1,194,000

3.7 Discussion and break-down of KLSCP under pre- and post-fire conditions

For the erosion simulation of the Upper Cache Creek Watershed, the calibrated coefficient for the combined KLSCP is 0.0034, 0.0062, 0.0061 for the pre-fire WY 2015, the post-fire WY 2016, and the post-fire WY 2017, respectively. The coefficient α , based on the GWLF user's manual (Haith et al., 1992), was calibrated to be 0.34 and 0.39 for the pre- and post-fire WYs, respectively. SDR (sediment delivery ratio) adopted the value of 0.082 as discussed in section 3-2. TCP (daily transport capacity) is calibrated to be 1.5. We assume that wildfire does not affect the sediment delivery ratio and the daily transport capacity in the Cache Creek Watershed. Accordingly, the two

parameters of SDR and TCP are the same for both the pre- and post-fire conditions. Calibrated parameters for pre- and post-fire sediment load simulation are listed in Table 3-3.

Table 3-3. Parameters for sediment load simulation pre-fire and post-fire.

Water Year	KLSCP	α	SDR	TCP
WY 2015 (Pre-fire)	0.0034	0.34	0.082	1.5
WY 2016 (Post-fire)	0.0062	0.39	0.082	1.5
WY 2017 (Post-fire)	0.0061	0.39	0.082	1.5
Post-fire/pre-fire	1.8	1.2	1	1

KLSCP is defined as follows:

- K = soil erodibility factor,
- L = slope length factor,
- S = slope steepness factor,
- C = cover-management factor, and
- P = erosion-control practice factor.

This research assumes that K and C increased post-fire, while L , S and P remained the same. The calibrated KLSCP for post-fire WYs is 1.8 times higher than that of the pre-fire WY; the rainfall erosivity (α) of the post-fire WYs is 1.2 times higher than that of the pre-fire WY. The resultant daily sediment erosion of the post-fire events from the modeling area is more than double ($1.8 \times 1.2 = 2.2$) that of the pre-fire period (Eq. 3-5).

Table 3-3 shows that: 1) the calibrated KLSCP in the post-fire WY 2016 is only slightly higher than in WY 2017 and 2) the rainfall erosivity parameter (α) is the same for the two post-fire WYs. A probable explanation is that soil erodibility, cover-management and rainfall erosivity have not changed significantly for the 1st and 2nd post-fire years. Another reason may be that the first flush phenomena in March of 2016 had limited the calibration and caused the lower NSE value of WY 2016.

3.7.1 A break-down of the combined coefficient KLSCP

The range of the pre-fire K factor for the present study was determined from Figure 3.2 to be 0.15 – 0.3, which corresponds to the soil types of clay loam and loam. The range of the pre-fire C factor was determined from Figure 3.4 to be 0.03 – 0.08, as this area has limited development and about 97% of the modeling area is covered by trees and vegetation. The P factor was assumed to be 1, because the area is primarily covered by natural vegetation and there is little to no influence from erosion control practices.

The L and S factors are typically calculated together, as the slope length and steepness factor LS. The slope length was calculated in ArcGIS 10.4, using the Unit Stream Power Erosion and Deposition (USPED) method (Moore and Wilson, 1992) as applied by Pelton et al. (2014). This method involves filling in a digital elevation model (DEM) to create a depressionless DEM, calculating the flow accumulation and slope using the ArcGIS spatial analyst extension, and finally calculating the LS factor using the following formula:

$$LS = (m + 1) * \left(\frac{F * l}{22.1} \right)^m * \frac{\sin(\theta * 0.01745)^n}{0.09} \quad (1)$$

where F is the flow accumulation, l is the DEM cell size in meters, θ is the slope in degrees, and m and n are adjustable parameters corresponding to the soil susceptibility to erosion. Values of 0.4 and 1.4 were chosen for m and n in this study, following Pelton et al. (2014). A DEM with a resolution of 1/3 arc-second (~9 meters) was used (USGS, 2017). Applying the above method resulted in a mean LS factor of 13.8.

The parameter ranges above for each component of KLSCP leads to a range of the pre-fire KLSCP value range of 0.021 to 0.083, which is approximately an order of magnitude larger than the final calibrated KLSCP value of 0.0034.

While there are other methods for calculating LS factor in the literature, all of the identified methods tried in this study yielded a LS value substantially greater than 1. The authors also tried adjusting the parameters of m and n in equation 1 within the range of reasonable values as defined by Moore and Wilson (1992) and Oliveira et al. (2013), which also yielded LS values substantially greater than 1. Additionally, the LS factor estimated in this research is comparable to the LS value calculated by the California State Water Resources Control Board (n.d.), which varied with the area of interest (AOI) from 1.23 to 15.9 and with a mean of 10.1. Their analysis followed the method of Lim et al. (2005) and utilized a DEM with 30-meter resolution.

The calculated sediment load matches well observed sediment loads for WY 2015 (pre-fire) and WY2017 (2nd year post-fire) in the modeled area of the Upper Cache Creek Watershed. The sediment calculation method is considered successful, and reliable within the study area (Cache Creek Watershed). K and C value ranges are invariant for the soil and vegetation type in the modeling area. These suggest that LS values published by the California State Water Resources Control Board and calculated above may be overestimated for the Cache Creek Watershed.

3.8 References

- Bicknell, B.R., Imhoff, J.C., Kittle, J.L., Donigian, A.S., and Johanson, R.C., Hydrological Simulation Program – FORTRAN User’s Manual, v. 11. U.S. Environmental Protection Agency, Athens, GA, 1996.
- California State Water Resources Control Board, n.d. RUSLE LS Factor Watershed Map Methodology. <https://ftp.waterboards.ca.gov/#/swrcb/dwq/cgp/Risk/RUSLE/>. Retrieved 7/7/2019.
- Diaz-Fierros, F., Benito Rueda, V.E., Perez Moreira, R. (1987). Evaluation of the U.S.L.E. for the prediction of erosion in burnt forest areas in Galicia (N.W. Spain), CATENA, Vol.14 (Issues 1–3),189-199
- Foster, G.R. (2005). Science Documentation: Revised Universal Soil Loss Equation Version 2 (RUSLE2). National Sedimentation Laboratory, USDA-Agricultural Research Service, Oxford, Mississippi.
- Haith, D. A. (1985). An Event-Based Procedure for Estimating Monthly Sediment Yields. Transactions of the American Society of Agricultural Engineers 28(6):1916-1920.
- Haith, D. A. and L. L. Shoemaker (1987). Generalized Watershed Loading Functions for Stream Flow Nutrients. Water Resources Bulletin 23(3):471-478.
- Haith, D. A., R. Mandel, and R. S. Wu (1992). Generalized Watershed Loading Functions Version 2.0 User’s Manual, Cornell University, Ithaca, New York.
- Kinnell, P.I.A. (2004). Sediment Delivery Ratios: A misaligned approach to determining sediment delivery from hill slopes. Hydrological Processes Today.
- Koltun GF, Eberle M, Gray JR, and Glysson GD (2006) User's manual for the Graphical Constituent Loading Analysis System (GCLAS): U.S. Geological Survey Techniques and Methods, book 4, chap. C1, 51p, <https://pubs.usgs.gov/tm/2006/tm4C1/pdf/tm4C1.pdf>
- Lim, K.J, Sagong, M., Engel, B.A., Tang, Z., Choi, J., and Kim, K.-S., 2005. GIS-based sediment assessment tool. Catena 64, 61-80.
- Oliveira, A.H., Aparecida da Silva, M., Silva, M.L.N., Curi, N., Neta, G.K., and França de Freitas, D.A., 2013. Development of Topographic Factor Modeling for Application in Soil Erosion Models, in *Soil Processes and Current Trends in Quality Assessment*, M. C. H. Soriano, Ed., InTech, pp. 111-138.
- Moore, I.D., and Wilson, J.P., 1992. Length-slope factors for the Revised Universal Soil Loss Equation: Simplified method of estimation. Journal of Soil and Water Conservation 47(5), 423-428.
- Pelton, J., Frazier, E., and Pickilngis, E., 2014. Calculating Slope Length Factor (LS) in the Revised Universal Soil Loss Equation (RUSLE).
- Rulli, M.C., L. Offeddu, and M. Santini (2013). Modeling post-fire water erosion mitigation strategies, Hydrol. Earth Syst. Sci., 17, 2323–2337.

- U.S. Geological Survey, 2017. 1/3rd arc-second Digital Elevation Models (DEMS) – USGS National Map 3DEP Downloadable Data Collection: U.S. Geological Survey.
- Vanoni, V. A. (Editor) (1975). *Sedimentation Engineering*. American Society of Civil Engineers. New York, New York.
- Wischmeier, W. H., and Smith, D. D. (1978). *Predicting Rainfall Erosion Losses: A Guide to Conservation Planning*, Agricultural Handbook np.537, USDA, Science and Education Administration.
- Yang, C.T. (1996). *Sediment Transport: Theory and Practice*, McGraw-Hill Book Company, New York.

4 Modeling Pre- and Post-fire Mercury Load Using PFHydro-WQ

4.1 Overview of mercury in the Cache Creek watershed

The mercury story in the Cache Creek watershed is complex. The watershed is highly contaminated with mercury due primarily to historical mining activities. Mercury mining and processing was conducted throughout the watershed and these mines continue to be point sources to the watershed mercury loading (Domagalski et al., 2004a; Holloway et al., 2009). In addition, historical mineral processing activities caused atmospheric emissions and subsequent localized deposition and contamination of surface soils near the mines (Holloway et al., 2009a). Beyond the mining legacy, the region receives mercury from global atmospheric deposition that is elevated throughout the coastal range of California due to precipitation patterns and biomass growth (Obrist et al., 2016). Furthermore, natural sources of mercury such as geothermal venting, erosion of mercury-bearing mineral bedrock and weathered soils associated with the bedrock, and remobilization of streambed and floodplain sediments all contribute to mercury loading from the watershed (Domagalski et al., 2004b).

4.1.1 Forms of mercury

The modeling domain in the Cache Creek watershed upstream of Rumsey contains hydrothermally altered rocks that contain the mineral cinnabar ($\text{HgS-}\alpha$), the target of many of the historical mining operations. Host rocks subject to mercury mineralization include serpentinites and other lithologies of the Franciscan Complex, marine sedimentary rocks of the Great Valley sequence, and Neogene volcanic rocks (Rytuba, 2000). The weathering of cinnabar-containing rocks and metacinnabar ($\text{HgS-}\beta$)-containing mine wastes contributes mercury to both streambed sediments and suspended particulate matter in Cache Creek. Weathered cinnabar-bearing rock and mercury mine wastes can produce particulates with total mercury (THg) concentrations greatly exceeding background concentrations in unmineralized areas. These particulates are transported as suspended and bedload sediments.

Geothermal sources contribute mercury to the Cache Creek watershed, and it is likely that sulfidic geothermal waters form colloidal $\text{HgS-}\beta$ that is then transported downstream. Colloidal $\text{HgS-}\beta$ is methylatable, and its grain size and transport behavior may also be governed by interactions with dissolved organic matter (Zhang et al., 2014; Aiken et al., 2011).

The upland soils throughout the watershed have received elevated atmospheric deposition of mercury due to the historic mining and mercury extraction activity (retorting) as well as deposition from globally distributed atmospheric sources and local geothermal and volcanic sources. The mercury deposited by wet and dry atmospheric deposition preferentially binds with organic matter in surficial soils. Specifically, mercury in surface soil is predominantly bound by reduced sulfur-bearing (thiol) functional groups in soil organic matter. The complexation reaction between mercury and reduced sulfur is strong, and soils retain mercury efficiently (Xia et al., 1999). During precipitation events, soluble soil organic matter can be leached from the soil as dissolved organic matter, which transports mercury associated with this fraction as a mercury-dissolved organic matter (Hg-DOM) complex (Mierle and Ingram, 1991). However, mercury

transport in Cache Creek is dominated by particulate-bound total mercury (p-THg), which typically accounts for more than 90% of mercury loading from the watershed (Alpers et al., in revision; Alpers et al., in review-a, -b).

4.1.2 Mercury in soils

According to Holloway et al. (2009a), mercury concentrations in the upland Millsholm are around 0.25 µg/g in the top 0 to 5 cm of the soils column and do not exceed 0.5 µg/g (graphically reported). In addition to the upland soils collected by Holloway et al., mercury concentrations in soils originating from serpentinite bedrock were also reported. Some of the mineralized serpentine soils were reported to contain nearly 300 µg/g THg, highlighting the presence of mercury-bearing minerals (cinnabar) in some of the region's bedrock. Similar concentrations ranging from 1 to 300 µg/g THg have been reported by Churchill and Clinkenbeard (2003) near mine locations along Sulphur Creek, a tributary to Bear Creek, which flows into Cache Creek.

The elevated concentrations are likely due to mining wastes containing high amounts of mercury: these include calcined tailings (10 – 1,530 µg/g THg), waste rock (5 – 990 µg/g THg), and ores (1,370 – 1,720 µg/g THg) (Churchill and Clinkenbeard, 2003). Holloway et al. (2009a) reported soil derived from serpentinite bedrock with mercury concentrations of 0.2 to 3.7 µg/g THg, though only one point was measured above 1 µg/g. Note that the reported soil-mercury values are mine-centric and tend to report very high concentrations compared to the national average of 0.06 µg/g THg (Smith et al., 2013). Considering that mercury samples taken from upland soils appear to have been collected near mines, these sites may have been influenced by localized atmospheric deposition associated with mercury retorting, as samples collected below 5 cm depth were significantly lower in mercury than the surficial soil (Holloway et al., 2009a). The regional background mercury concentration in soils is reported to be 0.08 to 0.31 µg/g THg. An average soil THg concentration of 0.17 µg/g from published sources was used for modeling purposes in this study.

4.1.3 Mercury in sediment

There are many cinnabar deposits in the watershed, many of which were mined heavily through the late 1800s (Domagalski et al., 2004a). Sediments originating from mine activities continue to be a significant source of mercury to Cache Creek. The largest increase in sediment transport and delivery to Cache Creek followed rain events that initiated mobilization. There are also geothermal sources of mercury to the waterway but a source loading comparison suggests that they are minor compared to mining waste sources (Churchill and Clinkenbeard, 2003). Stream-bed sediments were found to contain 0.1 to 1 µg/g dry weight (DW) THg in Cache Creek, with sediment concentrations being higher in tributaries with historical mining (Domagalski et al., 2004b).

Mercury concentrations in sediment along the main stem of Cache Creek increase within the watershed due to mine waste inputs. For instance, in Cache Creek at Lower Lake, downstream of the Sulphur Bank mercury mine on the shore of Clear Lake, stream sediments are reported to be 0.1 µg/g THg, whereas in Cache Creek at Rumsey the sediment concentrations are somewhat higher, 0.15 to 0.35 µg/g THg (Alpers et al., in review-a). Along the Cache Creek main-stem, sediment concentrations of total mercury increase greatly below confluences with streams that drain local watersheds containing mine sites. For example, the average total mercury in sediment

between Harley Gulch and Bear Creek was found to be 1 $\mu\text{g/g}$ THg, nearly 10-times higher than the sediment concentration above this confluence (Foe and Bosworth, 2008). A more detailed analysis of average mercury concentration in sediments between each tributary input reveals even higher local mercury concentrations that generally increase moving downstream along Cache Creek (Foe and Bosworth, 2008). Holloway et al. (2009a) reported that the parent alluvial mercury concentration ranged from 0.08 to 0.46 $\mu\text{g/g}$ THg along Cache Creek. The mercury concentration of parent alluvial soils naturally decreases with travel distance downstream, with the lowest flood-plain concentrations in the range of 0.13 to 0.2 $\mu\text{g/g}$ THg, levels much closer to the Great Valley Sequence mercury concentrations. This disparity between the parent alluvial material and bed sediment highlights the contamination in the stream.

The highest mercury concentrations in sediment in the Cache Creek watershed are found in historic mercury mining areas. At Harley Gulch, downstream of the Abbott and Turkey Run mines, reported mercury concentrations in streambed sediment range from 48 to 78 $\mu\text{g/g}$ THg (Rytuba et al., 2011). These numbers appear to reflect a large percentage of mine waste whereas downstream near the confluence of Cache Creek mercury concentrations have been reported to be 4.8 and 4.2 $\mu\text{g/g}$ THg in silt and sand respectively (Foe and Bosworth, 2008). For Sulfur Creek, host to numerous geothermal springs, as well as historical mercury and gold mines, the sediment mercury ranges from 1 to 141 $\mu\text{g/g}$ THg, with three of five samples around 20 $\mu\text{g/g}$ THg (Goff et al., 2001). Near the confluence of Sulphur Creek and Bear Creek, Rytuba et al. (2015) reported sediment mercury levels near 33 $\mu\text{g/g}$ THg. In the Bear Creek drainage, which includes the past-producing Rathburn and Petray mercury mines, the sediment mercury concentration is near 2 $\mu\text{g/g}$ THg (Churchill and Clinkenbeard, 2003; Rytuba et al., 2015). Rytuba et al. (2015) collected sediment samples from Bear Creek upstream and downstream of the Sulfur Creek confluence at different dates in the summer of 2010 and reported concentrations varying from 0.2 to 2 $\mu\text{g/g}$ THg in the same areas, suggesting either high spatial variability or seasonal shifts in sediment mercury content. In Davis Creek, downstream of the historic Reed mercury mine, the sediment mercury concentration reported by Foe and Bosworth (2008) ranged from 0.14 to 1.7 $\mu\text{g/g}$ THg, whereas Holloway et al. (2009a) reported that THg concentrations ranging from 0.5 to 70 $\mu\text{g/g}$.

4.1.4 Mercury in water

According to Domagalski et al. (2004a,b), total mercury concentrations in Cache Creek vary widely. They reported unfiltered mercury concentrations as high as 270 ng/L THg at Rumsey (1/31/2000) and frequently measured mercury concentrations below 10 ng/L THg at the same location. In this study, high particulate mercury concentrations were typically associated with considerably lower concentrations of filter-passing mercury, demonstrating that large mercury mobilization events are due to erosional transport. In general, mercury concentration in drainage close to or originating from mine sites is high; the mercury concentration at other watershed sites is lower and apparently diluted throughout the watershed.

Domagalski et al. (2004a) estimated that Sulfur Creek and Bear Creek could account for most of the mercury loading to lower Cache Creek (Rumsey) even though these tributaries account for a relatively small portion (10 to 25%) of the total watershed discharge. Harley Gulch may also contribute to mercury loading at Rumsey, but mercury loading is storm-dependent, as discharge from Harley Gulch was comparatively low for the years reported. Similar findings were reported by Rytuba et al. (2011), who reported that during high-flow conditions the THg concentration in

Harley Gulch was close to 43 $\mu\text{g/L}$ but fell to between 0.3 and 0.8 $\mu\text{g/L}$ during low-flow conditions.

Sediment deposition and remobilization downstream of the historic mercury mines plays a large part in total mercury loading. For example, the sum of mercury loads from tributary drainages in the Cache Creek Basin for discrete storm events in 2000 and 2001 exceeded the estimated mercury loading at Rumsey, suggesting significant deposition of mercury in this portion of the watershed (Domagalski et al., 2004a). Similarly, loading at the Cache Creek Settling Basin can exceed estimated loads from upstream point-sources, suggesting remobilization of streambed sediments, which are a potential long-term source of mine-derived mercury-contaminated sediment that was transported and deposited during past storm events.

Alpers et al. (in review-a) reported a single large storm event (Dec. 2014) in Cache Creek at Rumsey where discharge increased from 0 to more than 20,000 cubic feet per second (cfs). During this event, suspended sediment increased to a peak concentration of greater than 10,000 mg/L TSS. After peaking, the falling limb of the hydrograph was associated with lower concentrations of sediment for a given flow compared to the rising limb — a hysteresis effect — however the suspended sediment contained higher p-THg levels in the falling limb of the hydrograph. The rising limb of the hydrograph had a gravimetric concentration around 0.1 $\mu\text{g/g}$ total p-THg whereas the falling limb had a concentration of between 0.2 and 0.5 $\mu\text{g/g}$ p-THg. These data illustrate some of the complexities of mercury transport dynamics in the Cache Creek watershed.

4.1.5 Methylmercury in soils, sediment, and water

Methylmercury (MeHg) distribution is typically much more variable in space and in time than total mercury, in soils, stream sediment, and water. Methylmercury is typically higher during wet periods in soils, such as in the Davis Creek drainage (Holloway et al., 2009b) and in floodplain sediment, such as the Cache Creek Settling Basin (Alpers et al., in review-a). For the purpose of modeling methylmercury in this study, the ratio of MeHg to THg observed in Cache Creek at Rumsey was used, as discussed below in section 4.2.2.

4.2 Observed changes in post-fire in-stream mercury and conceptual model for transport

4.2.1 Total mercury

Following the 2015 fires, particulate total mercury (p-THg) in water samples collected from Cache Creek at Rumsey decreased by more than half, from a median concentration of 0.33 $\mu\text{g/g}$ during Water Year 2015 ($n = 12$) to 0.14 $\mu\text{g/g}$ during Water Year 2016 ($n = 29$) (Alpers et al., in review-a). These data are somewhat variable; many of the p-THg concentrations during Water Year 2016 were near 0.10 $\mu\text{g/g}$ with a few high measured values. The variability in these data is consistent with typical upland sediments and soil that show relatively low Hg concentrations, and a small fraction of sediment and soil measurements with higher total mercury concentrations, likely representing HgS-bearing mineral particles (a “nugget effect”).

The decrease in the measured gravimetric p-THg concentrations on suspended particles at Rumsey aligns with the mercury loss predicted and observed for upland soils following fire. The soil heating model simulation results suggest that fire-affected surface soils heated above a

threshold temperature of 150°C will lose significant mercury mass during heating, particularly the surficial layer which is most likely to be transported post-fire by the mechanism of soil erosion. Although much of the model project area is shrub land with little expected soil heating and consequent mercury loss, wooded areas in closer proximity to waterways are likely to have greater hydraulic connectivity and are predicted to experience greater mercury losses than shrub land.

Rocky Fire Soil & Ash Samples - Sept. 2015

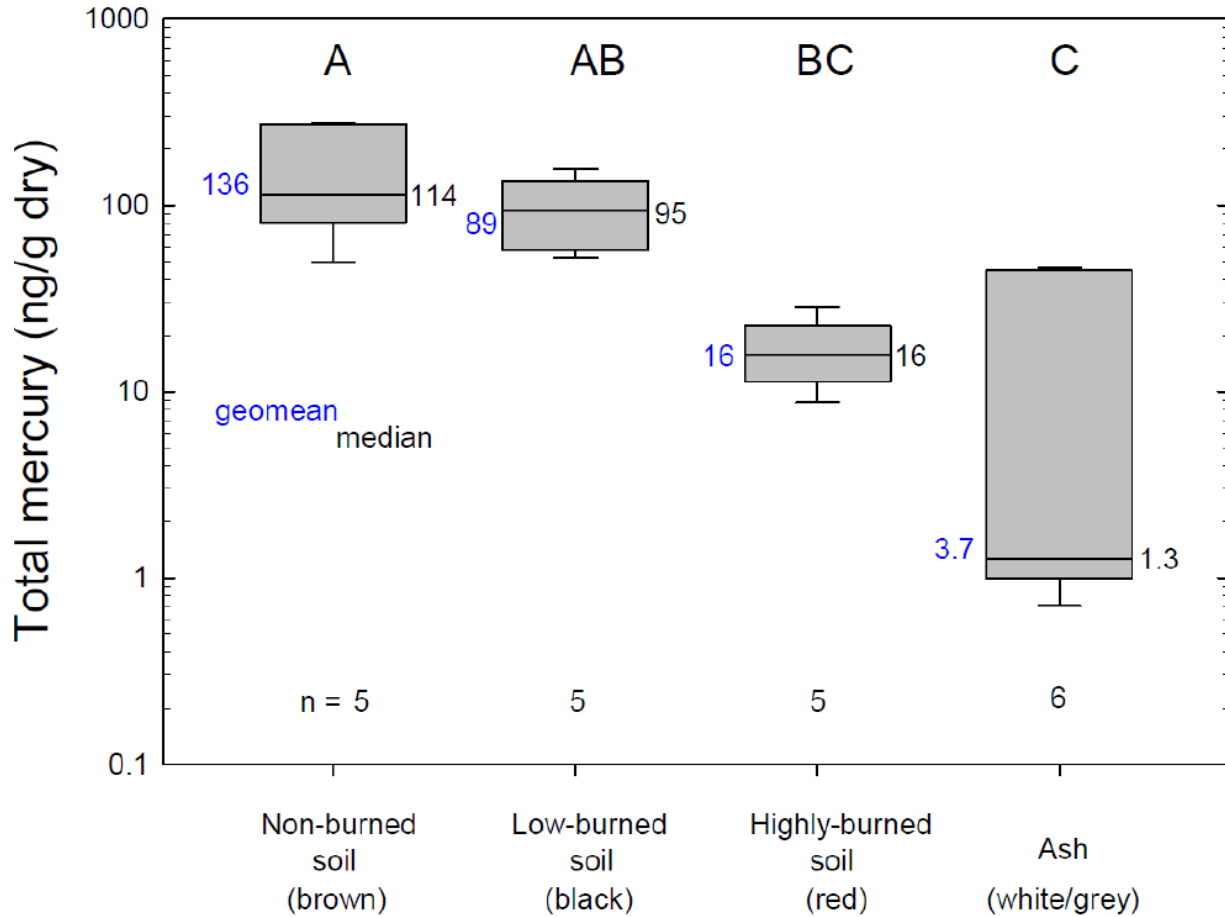


Figure 4-1. Box plots showing data for total mercury in soils and ash in the area affected by the Rocky Fire in summer 2015. Geomean and median values are indicated for each type of material. Boxes indicate interquartile range (25th to 75th percentile; whiskers indicate 10th and 90th percentile; n = number of observations.

USGS data for mercury in soils affected by the 2015 Rocky fire indicate loss of up to 85% of THg from heating. Figure 4-1 shows THg data for non-burned soils, low-burned soils, highly burned soils, and ash; the top two centimeters were sampled during Sept. 2015 from BLM-administered lands near Highway 20. The median value of THg in five non-burned soils, brown in color, was 136 ng/g; five highly burned soils, red in color, had a median THg concentration of

16 ng/g, an 85% reduction compared with the non-burned soils. Five low-burned soils (black in color) were intermediate in composition between the non-burned and highly burned soils (median of 89 ng/g) and were not statistically distinct from either. Five ash samples, white to grey in color, had a median THg concentration of 3.7 ng/g, statistically lower than the non-burned and lightly burned soils but not significantly lower than the highly burned soil (Figure 4-1).

The median p-THg concentration at Rumsey increased from 0.14 µg/g in Water Year 2016 (first year post-fire) to 0.26 µg/g in Water Year 2017 (second year post-fire). This increase in total particulate mercury is thought to reflect partial recovery of the system, that has a reduced mercury content in soil caused by fire-related mercury losses from heating above the 150°C threshold.

Some studies have reported the opposite effect to that observed at Rumsey in response to the summer 2015 fires in the Cache Creek watershed -- increased soil-mercury following burning and precipitation (Engle et al., 2006; Burke et al., 2010). The exact mechanism for this is unclear; it has been hypothesized that soil heating creates increasingly surface-active carbon-bearing material (charcoals) that increases mercury retention (Olson et al., 2000). Others have suggested loss of depositional mercury from the canopy to the ground surface during precipitation (Witt et al., 2009). A recent study by Jensen et al. (2017) seems to support the findings of the study by Olson et al. (2000), reporting that suspended particulate total mercury doubled following a burn. In this study, a comparison of pre- and post-fire suspended-sediment mercury concentrations and loads at Rumsey suggests that particulate mercury concentrations of suspended particles (p-THg) (in µg/g) decreased immediately post-fire, and that the amount of suspended sediment carried by a given discharge (in mg/L) increased greatly post-fire.

Comparing two large storm events, one pre-fire (December 10-13, 2014) and one post-fire (January 6-9, 2017) we observed that these two effects approximately cancelled each other out, such that loads of p-THg were very similar for these two 4-day storm events. During the 4-day December 2014 storm event, observed particulate THg loads for Cache Creek at Rumsey at were 53 kg, compared with 51 kg for the 4-day January 2017 storm event. The observed sediment load at Rumsey during the 2014 event was 169×10^6 kg compared with 206×10^6 kg in the 2017 event, and the average THg concentration on suspended sediment was 311 ng/g during 2014 event and 249 ng/g during the 2017 event.

4.2.2 Methylmercury

Following the Rocky and Jerusalem fires in summer 2015, there was an increase in concentrations of MeHg in water and suspended sediment in Cache Creek at Rumsey, and in the MeHg/THg ratio of concentrations and loads. The concentration of particulate-associated methylmercury (p-MeHg) in suspended sediment at Rumsey increased from a geometric mean value of 0.62 ng/g in Water Year 2015 (pre-fire) to 1.05 ng/g in Water Year 2016 (first year post-fire). During Water Year 2017 (second year post-fire), the geometric mean concentration of p-MeHg was 1.02 ng/g. The ratio MeHg/THg for suspended sediment (using geometric mean values) varied from 0.22% in WY 2015, to 0.70% in WY 2016, and to 0.37% in WY 2017.

Based on the previous findings by Jensen et al. (2017), it is hypothesized that the thermal changes to the carbon-bearing particles and formation of sorption-active surfaces during heating enhances methylmercury binding to particulates. This likely contributed to the observed

increases in gravimetric methylmercury concentrations on suspended particulates. Methylmercury formation can be stimulated with addition of sulfate and labile carbon, both of which are generated during soil heating (Krabbenhoft and Fink, 2001). Previous studies have reported increases in methylmercury accumulation in sediment and biomass following burning (Caldwell et al., 2000; Kelly et al., 2006) and this mechanism may explain why methylmercury production often increases in soils following burning. Future field and laboratory studies that would shed light on mechanisms for MeHg changes after wildfire are described in Chapter 5 of this report (Future Work).

During Water Year 2015 (pre-fire), the ratio of MeHg/THg in whole water and suspended particulates in Cache Creek at Rumsey was 0.002 (0.2%). During WY 2016 (first year post-fire), the ratio MeHg/THg rose to 0.006 (0.6%) at Rumsey. During WY 2017, the second post-fire year, the ratio MeHg/THg was 0.0033 (0.33%). Because there is little other information on the distribution of MeHg in water, soil, and streambed sediment in the upper Cache Creek watershed, these percentages were used for modeling purposes.

4.3 Characterizing Cache Creek soils for post-fire mercury transport modeling

To evaluate the effects of wildfire on mercury transport throughout the Cache Creek watershed, a model that simulates mercury remaining in the upland soils following fire-related heating was developed based on estimated pre-fire soil-mercury concentrations and soil heating losses. Pre-fire mercury concentrations in upland soils were estimated using the USGS's national geochemical database (Smith et al., 2013). ArcGIS (ESRI, USA) Spatial Analyst was used with an inverse distance weighting to interpolate between proximal data points. An average THg soil concentration of 0.17 $\mu\text{g/g}$ was used for modeling purposes.

Mercury losses due to soil heating were estimated using a soil-heating model (FOFEM6; Lutes et al., 2012) which uses factors such as vegetation type, soil type, and moisture inputs to estimate the depth of soil heating during wildfire. Mercury losses in the 0–5 cm soil increment was estimated based on a temperature threshold of 150°C, which equates to the heating required to initiate mercury loss from weak ligands in soils (Biester and Scholz, 1996). The resulting post-fire soil concentration can be used to approximate the concentration of p-THg resulting from the burned soils of the watershed.

4.3.1 Vegetation

The Cache Creek drainage represents an area of about 3,000 km² in the Coastal Range of California. The relative elevations of drainage monitoring sites in the model project area are 125 m at Rumsey, a frequent sampling location for USGS mercury studies (Alpers et al., in review-a), and the top of Pine Mountain at 1,250 m. The vegetation composition within the watershed boundary is a combination of shrub, conifer and hardwood forest, grassland, and oak-grassland (**Figure 4-2**). Conifer species including Douglas fir (*Pseudotsuga menziesii*) and Ponderosa pine (*Pinus ponderosa*) tend to be found at the higher elevations of the watershed, whereas lower elevations support grey pine (*Pinus sabiniana*) and knobcone pine (*Pinus attenuata*). Blue oak

(*Quercus douglasii*) is the dominant hardwood in the oak-grassland land-cover type, preferring north-facing slopes; black oak (*Quercus kelloggii*), and canyon live oak (*Quercus chrysolepis*), can be found throughout watershed. Examination of the model domain suggests that most of the landscape is primarily shrub-covered with interspersed hardwood and conifer woodland. Three species were used to simulate wildfire soil heating: “oak shrubland,” “mixed gray pine and oak,” and “oak woodland.” Knobcone pine was also considered, but it was not possible to distinguish conifer types after an analysis of available imagery of vegetation within the model boundary.

4.3.2 Modeling soil mercury concentrations

A general soil-texture classification was used for predicting heat conduction and temperature response in the soil. A study of mercury concentration in local soils was conducted by Holloway et al. (2009a) that characterized upland soils as sedimentary Millsholm. The Millsholm soil series is a light clay loam with up to 35% rock fragments originating from shales. This soil classification was used for assigning input parameters for all upland soils in the model.

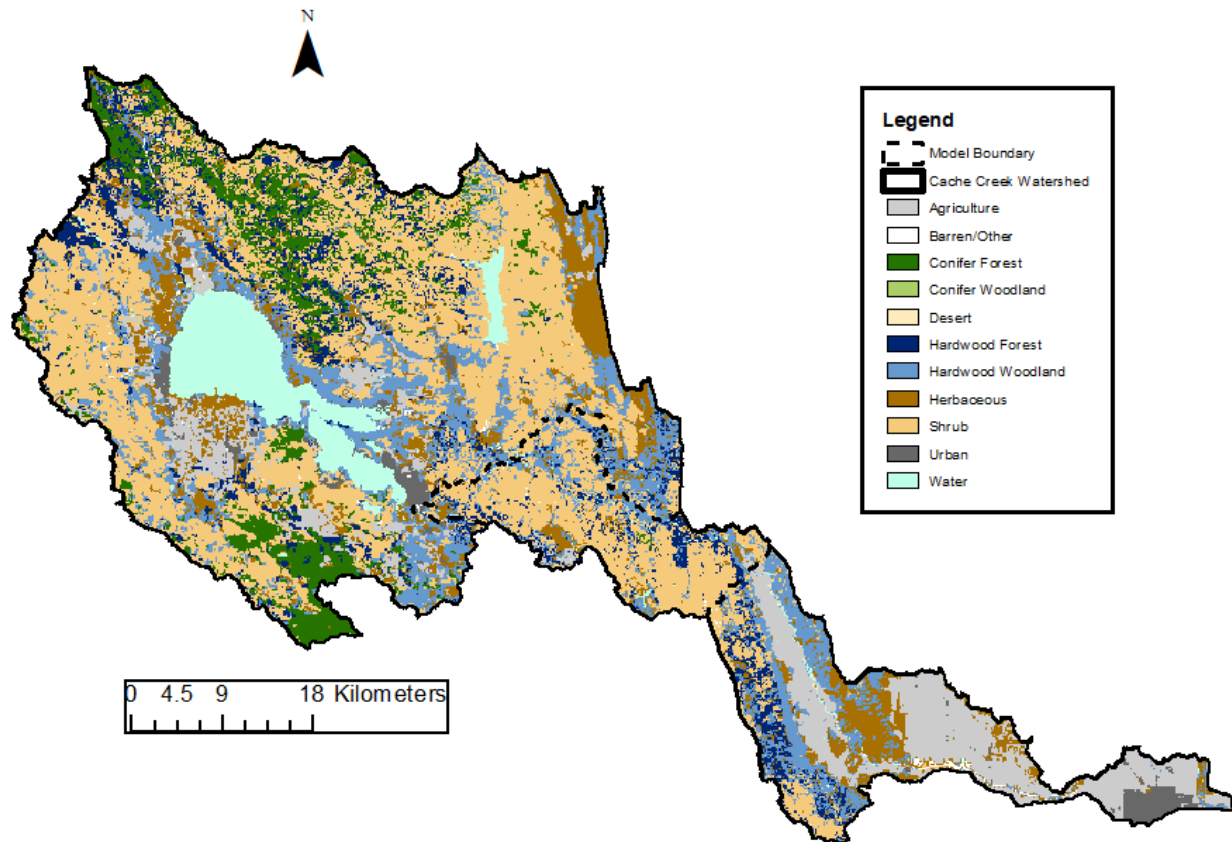


Figure 4-2: Vegetation types used in modeling.

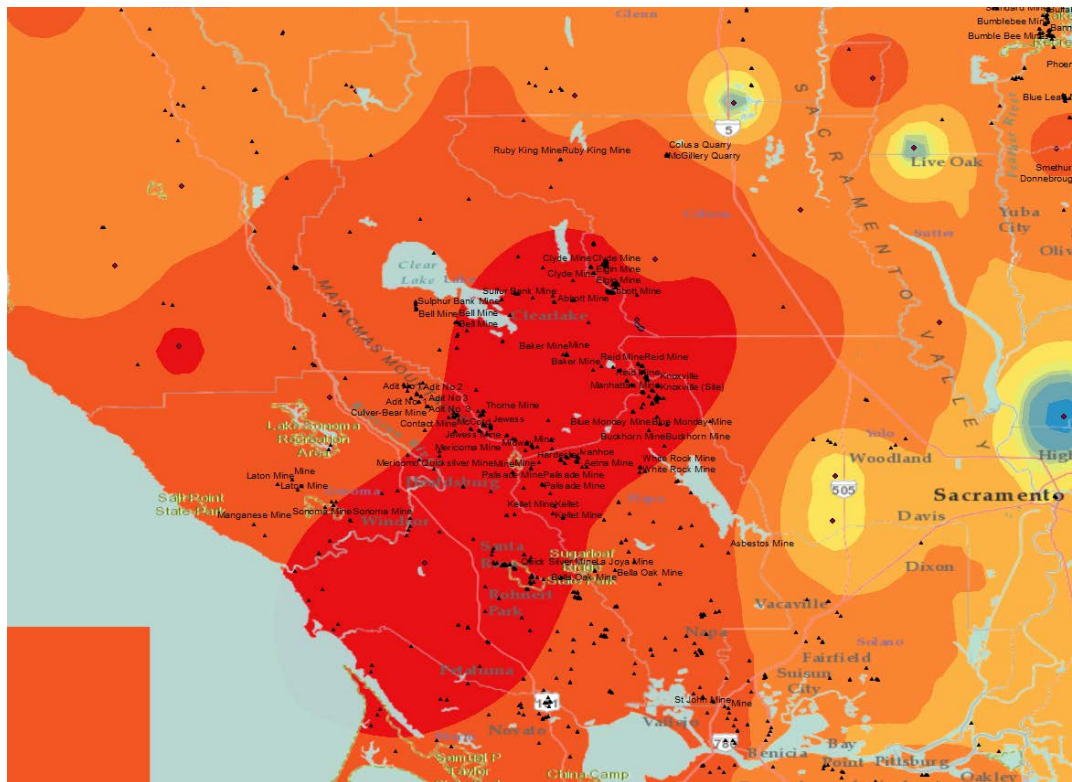


Figure 4-3: A map of regional soil-mercury concentrations developed using the national geochemical database and a local data set which was generated using an inverse distance weighting algorithm applied to local points.

Northern California soil mercury concentrations in the depth range 0-5 cm from the U.S. Geological Survey’s geochemical inventory database (Smith et al., 2013) were interpolated spatially (**Figure 4-3**). Interpolation of the data was performed using an inverse distance-weighting algorithm and a maximum number of 15 surrounding points. In California, mercury concentrations in soils show great variability based on the geological origin of the soil, mining activities, and exposure to atmospheric deposition. Points in the database located in California’s Central Valley, east of the model domain, have been assigned low values. These values are low compared to national averages and are particularly low with respect to the soils included within the model boundary. Some of the reported Coastal Range soil-mercury concentration data in the

geochemical database are high compared to the national average but are not as high as some values reported for Coastal Range soils (e.g. Holloway et al., 2009a). The closest point to the model domain within the Coastal Range was collected in the vicinity of Santa Rosa, CA. These Sonoma County data points averaging $0.17 \mu\text{g/g}$ THg are within the range of the simulated soil-mercury concentrations (0.03 to $0.22 \mu\text{g/g}$) collected within the Cache Creek watershed boundary. The estimated average watershed soil Hg concentrations are shown on **Figure 4-4**.

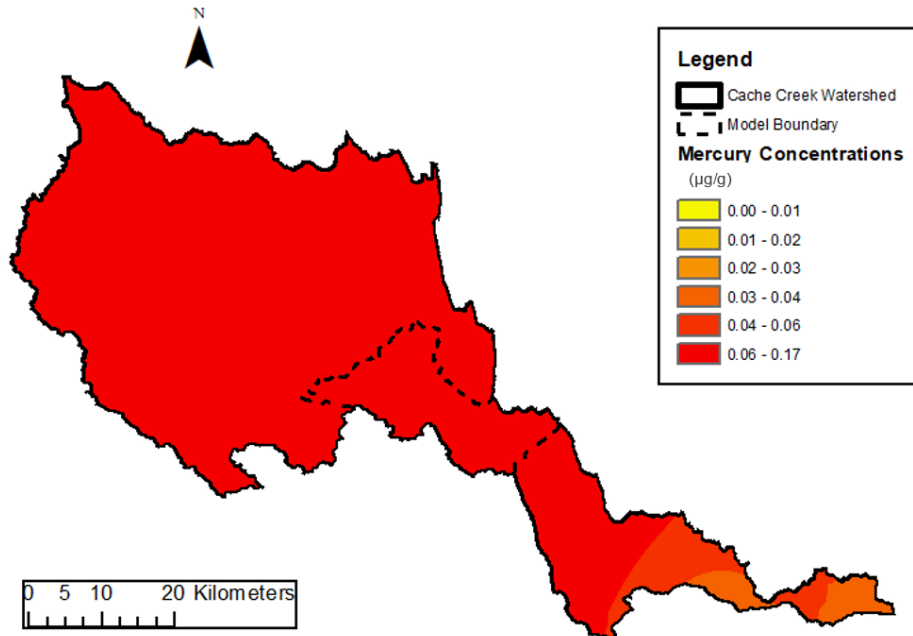


Figure 4-4. Background Hg concentrations for the Cache Creek watershed located within the model boundary were estimated based on regional soil-mercury concentrations.

A single data set including five surface soil samples from non-burned locations within the area of interest was made available by the USGS (**Figure 4-1**). The locations of sampling sites were set relatively close together relative to the model boundary – combined they provide a local point that can be recognized on the national soil mercury concentration map. This action also has utility in weighting the watershed background mercury concentration for the spatial model. The net effect of arrangement of the sample points and the interpolation is to increase the estimated soil-mercury regional background concentration and to account for the “belt” of mines and mine spoil locations that most likely have high soil mercury content. Reported THg concentrations in soils ranged from 0.05 to $0.28 \mu\text{g/g}$ over the Cache Creek watershed.

The estimation of mercury loss from upland soils is based on the temperature that initiates the destruction of the ligands that bind mercury to organic matter. Biester and Scholz (1996) reported that this process develops at a temperature just below 200°C. Some mercury species such as Hg^0 and HgCl_2 , although not major components of the mercury budget, have been reported to start evading soil at temperatures around 70°C. Other minor mercury species can be lost from soil at relatively low temperatures. It is commonly assumed that all mercury at the soil surface is lost in a burned zone, regardless of burn severity, and that very little mercury is lost at depths where the temperature does not exceed 150°C.

For the purposes of the spatial model developed as part of this study, and for consistency with the national data base, soil-mercury losses are considered only in the first 3 cm of depth. This assumption is important because samples that are taken within a smaller depth interval, closer to the surface, will produce estimates of greater loss of mercury and samples collected from a larger depth interval will produce a lower estimate of losses (**Figure 4-5**). Similarly, if only the shallowest soil depth interval is mobilized during storm events, the mobilized particles will have lower mercury concentrations than erosion of soil from deeper intervals.

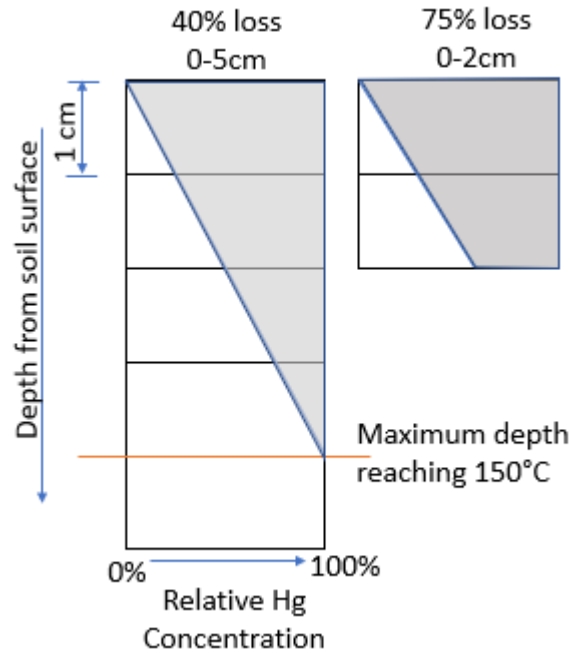


Figure 4-5: Conceptual model for Hg_T loss from 0-5 cm and 0-2 cm depth intervals during heating to a temperature of 150°C at 4 cm depth. Losses are illustrated in grey.

Soil heating was evaluated for the dominant vegetation cover types identified in the watershed. The cover types included oak woodland, gray pine with oak woodland, knobcone pine, and shrub oak. Soil moisture was varied in the model to simulate varying temperatures representing heating severity. The resulting heat penetration into the soil column was simulated using FOFEM6, a model which uses the average fuel loading for each cover type selected to evaluate mercury loss due to heating. A summary of the post-fire mercury concentration predictions is provided in **Table 4-1**.

Table 4-1. Predicted post-fire mercury concentration in the 0-5 cm depth increment of upland soils by cover type and fire severity

Cover type	Unburned ($\mu\text{g/g}$)	Low Severity ($\mu\text{g/g}$)	Moderate Severity ($\mu\text{g/g}$)	High Severity ($\mu\text{g/g}$)
Oak Woodland	0.17	0.17	0.14	0.10
Knobcone Pine	0.17	0.17	0.15	0.12
Grey Pine & Oak	0.17	0.17	0.14	0.10

Oak Shrub	0.17	0.17	0.17	0.17
-----------	------	------	------	------

Upland soils heated during the 2015 wildfires in the Cache Creek watershed likely lost Hg to the atmosphere, thereby decreasing the soil Hg burden, particularly in severely burned areas. The extent of Hg loss is estimated based on predicted soil heating. Elemental mercury is released from soil at temperatures as low as 100°C, whereas mercury associated with soil organic matter is released from soil beginning around 150°C. Soil temperature can be much higher than this at the soil surface, approaching 700°C. To establish the boundary conditions for mercury losses in the soil, it was assumed that 100% of Hg is lost at the surface, and that no Hg is lost from below the soil-column depth that reaches 150°C.

To determine the depth of soil heating to 150°C, vegetation classes for the region were identified for use in the FOFEM soil heating model. Using a landcover GIS layer, five dominant classes were identified: shrub/scrub, evergreen, mixed forest, herbaceous, and deciduous. From these general classes, vegetation types present in the area matching these covers were identified for use in the soil heating model (FOFEM 6.5). The “shrub/scrub” was identified as scrub oak and mixed shrub (SRM207), “mixed forest” was identified as mixed Blue Oak and Grey Pine (SRM 250), “deciduous” was identified as Blue Oak (SRM 201), “herbaceous” was modeled as annual grassland (SRM215) and “evergreen” was modeled as Knobcone Pine (SAF 248). Each specific forest type has an assigned average fuel load that is used to calculate soil heating depth within the model.

Considering high severity burning, the fraction of Hg remaining in the soil by depth was calculated by vegetation type for depths up to 3 cm, a depth which was below the deepest significant heat penetration for all vegetation types considered (**Table 4-2**). Mercury losses by vegetation type and depth considered were generated for the dominant land cover types using the 150°C threshold for Hg loss (**Table 4-3**). These estimates are presented by depth so that erosion depth can be converted into particulate Hg concentrations.

Table 4-2. Temperature of soil during high severity burning by cover type and depth

Depth	Scrub/Shrub	Knobcone	Mixed Oak/Grey Pine	Annual Grassland	Blue Oak
	Max Temp (°C)				
Surface	291	206	174	70	20
1 cm	171	144	103	24	20
2 cm	100	97	63	23	20
3 cm	68	68	51	22	20

Table 4-3. Percent of Hg remaining in soil following heating by cover type and depth.

Depth	Scrub/ Shrub	Knobcone	Mixed Oak/Grey Pine	Annual Grassland	Blue Oak
	Percent Hg Remaining (%)				
0 - 0.5 cm	6	13	50	100	100
0 - 1 cm	22	50	75	100	100
0 - 1.5 cm	50	67	83	100	100
0 - 2 cm	63	75	88	100	100
0 - 2.5 cm	70	80	90	100	100
0 - 3 cm	75	83	92	100	100

Using the predicted losses based on vegetation, the estimated average amount of mercury remaining in the soil throughout the model domain was determined. For this estimate, the fraction of Hg remaining was determined for each land cover class and then weighted by total area within the sub-basin to obtain an average total loss. This was repeated for depth increments of 0 - 0.5 cm, 0 - 1 cm, and 0 - 3 cm (**Figure 4-6**).

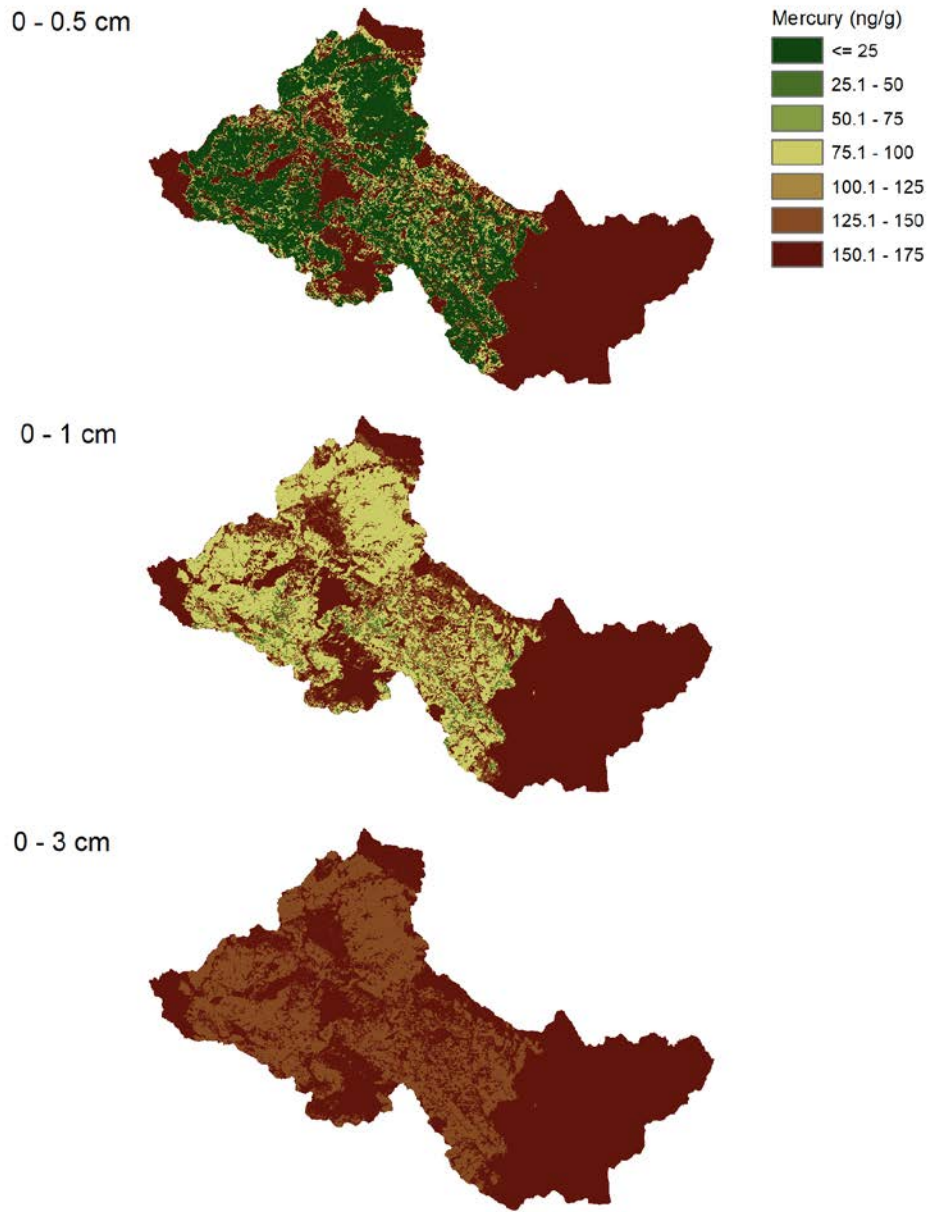


Figure 4-6: Post-fire soil mercury concentrations within the model space

4.4 Modeling of Mercury and methyl mercury using HSPF

4.4.1 Development of HSPF Mercury boundary conditions

Total mercury (Hg) and Methyl-mercury (MeHg) time-series boundary conditions to the PFHydro-WQ model were provided from the HSPF model (described in Section 1.1). Hourly total mercury loads were calculated in Hydrological Simulation Program – FORTRAN (HSPF) by adding a generalized quality constituent (sediment associated) module to the existing calibrated model, following the approach of Eggleston (2009). Mercury as a sediment-associated

quantity in HSPF is considered as wash off and erosion from pervious and impervious land surfaces, additions from point sources, and mercury contaminated sediments suspended in the stream and in the stream bed. Mercury in the stream is modeled in suspension associated with suspended sediment and can be deposited or scoured from the river bed within each modeled river segment. Initial concentrations of mercury in each reach were determined by proximity to legacy mercury and gold mines in the watershed (**Figure 4.7**).

To estimate particulate mercury in the model space it is assumed that there are three sources that could be contributing to total loads: re-suspension of bed sediment, erosion of soil particles from the contributing watershed, and geothermal inputs. The rankings were based on mapped mining activity, estimated geothermal inputs, and previously reported soil and sediment data where available.

4.4.2 Soils

Mining history and previously reported mercury concentrations were used to assign mercury concentrations of soils within each of the 25 sub-basins in the HSPF modeling domain. Areas that are near historical mines typically have elevated mercury in soils from the retort process and associated atmospheric mercury deposition. Although mercury locations at the historical mine sites are known to be very high (Churchill and Clinkenbeard, 2003), average soil concentrations within an entire mining-affected sub-basin reduced the overall concentration. We estimated that sub-basins with historical mercury mines had soil THg concentrations of 1.0 $\mu\text{g/g}$, whereas sub-basins without mines had mercury concentrations averaging 0.1 $\mu\text{g/g}$.

Initial soil storages of mercury were also set by proximity to contamination point sources of mines or hot springs. Initial soil storage of land segments were set to either 0.2 or 2.0 grams per acre, depending on nearby mines. Model land segments 5, 6, 17, and 22 were assigned the higher value of 2.0 grams per acre based on proximity to historical mercury mines (**Figure 4-7**).

4.4.3 Streambed Sediment

Legacy mining in the Cache Creek watershed has resulted in elevated mercury concentrations in streambed sediment throughout the drainages downstream of the mines. We estimated that sediments in reaches with no mining activity had low Hg concentrations (0.1 $\mu\text{g/g}$) and reaches immediately downstream of mines had high mercury concentrations (10 $\mu\text{g/g}$). Reaches below sub-basins with mining activity were estimated to have medium Hg levels (1.0 $\mu\text{g/g}$). The distribution of Hg concentrations assigned to the HSPF model sub-basins is shown in **Figure 4-7**.

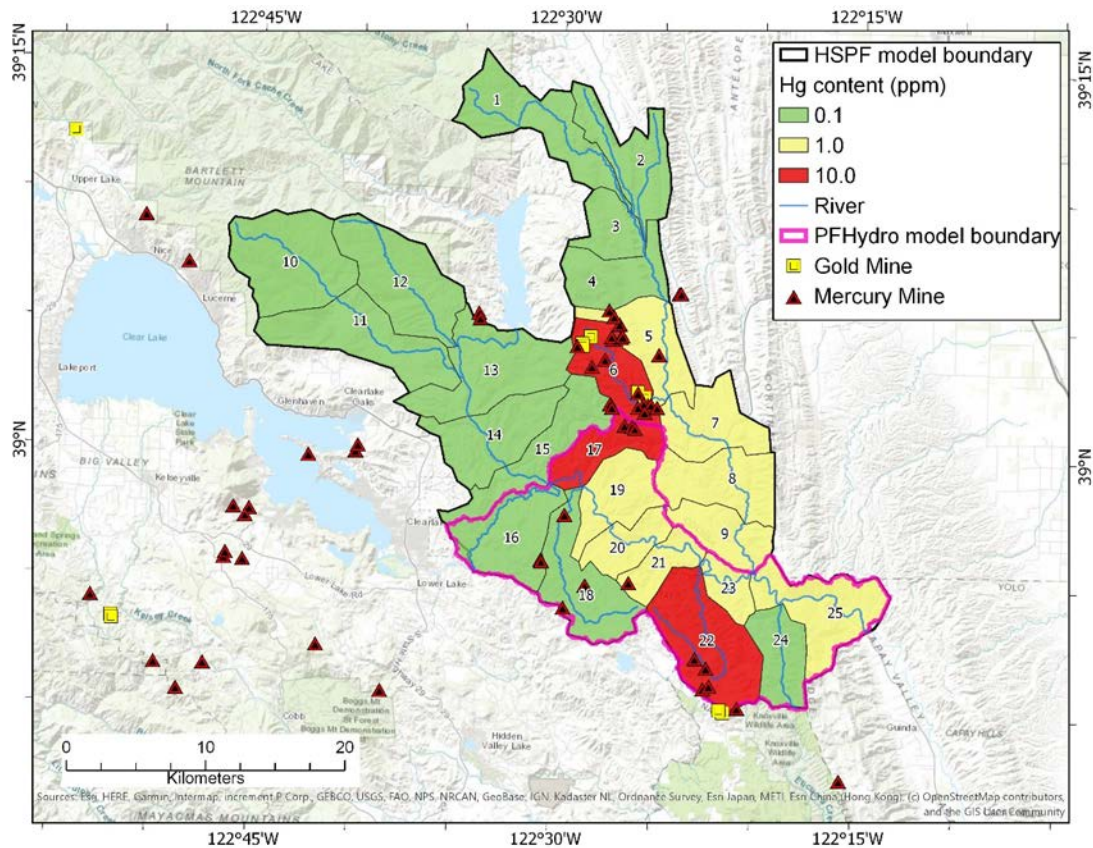


Figure 4.7: Initial mercury (Hg) content for each model reach in the HSPF model domain. Units are ppm (equal to $\mu\text{g/g}$). PFHydro-WQ model domain and locations of historical mercury and gold mines are also shown.

4.4.4 Geothermal inputs

Inflows of hot springs in the area were considered point source contamination, and a constant time series was applied to the stream segments affected by the hot spring. Hot springs in the Sulphur Creek watershed (model segment 6) and Harley Gulch watershed (model segment 17) were assigned constant mercury inflows of 0.218 kg/year and 0.0056 kg/year, respectively (Goff et al., 2001). Streambed sediment in model segment 6 was assigned a medium ranking (Hg concentration of 1.0 $\mu\text{g/g}$).

4.4.5 Modeling effects of wildfire in HSPF

Land surface storage of Hg was reduced by half in the first year following the summer 2015 wild fires (Water Year 2016) for land segments that were burned and returned to pre-fire conditions the following year (Water Year 2017). Hourly time series of Hg and MeHg loads were summed to daily and the time series were used as inputs to PFHydro-WQ.

4.5 Mercury simulation method in PFHydro-WQ

4.5.1 Mercury load calculation method and soil mercury concentrations

The simulation of total mercury (Hg) load in the Cache Creek Watershed modeling domain (**Figure 1 in Appendix 1**) assumes that mercury (Hg) load is associated with sediment from the soil:

$$\text{Hg} = S \times C_{\text{Hg}} \times 10^{-3} \quad (4-1)$$

where Hg is mercury load (g/day), S is sediment Load (tons/day), C_{Hg} is the average mercury concentration in soil (ng/g).

The assumed mercury concentration of soil pre-fire is 175 ng/g (see Section 4). The mercury concentration of soil post-fire depends on the burn severity, and soil erosion depth. The average mercury concentration (C_{Hg} , ng/g) in the modeling domain for each soil erosion depth is calculated based on burn severity and its burned area percentage in the modeling domain (see **Table 4-4**).

Table 4-4. Mercury concentration (ng/g) of four burn severities with various soil erosion depth

Soil erosion depth (cm)	Mercury concentration (ng/g) (burned area percentage)				
	High burn (6.9%)	Moderate burn (38.5%)	Low burn (12.5%)	No burn (42.1%)	Average mercury concentration C_{Hg}
0.5	35.6	45.7	114.8	175.0	108.1
1.0	79.8	101.1	144.9	175.0	136.2
1.5	112.5	126.1	153.4	175.0	149.2
2.0	129.0	138.1	160.6	175.0	155.8
2.5	137.7	145.4	163.0	175.0	160.0
3.0	143.9	149.9	165.4	175.0	162.0

The simulation of pre-fire total mercury load (Hg) is calculated using Eq. 4-1 with the average mercury concentration C_{Hg} of 175 ng/g. The simulation of post-fire total mercury load (Hg) is calculated using Eq. 4-1 with the calibrated parameter of average soil erosion depth.

4.5.2 Pre- and post-fire total mercury (Hg) load simulations

The simulated daily time series total mercury (Hg) load of WY 2015 (pre-fire) are shown in **Figures 4-8 and 4-9**. The simulation matches the observation very well with an NSE of 0.90. **Figure 4-9** shows results of major storms in WY 2015.

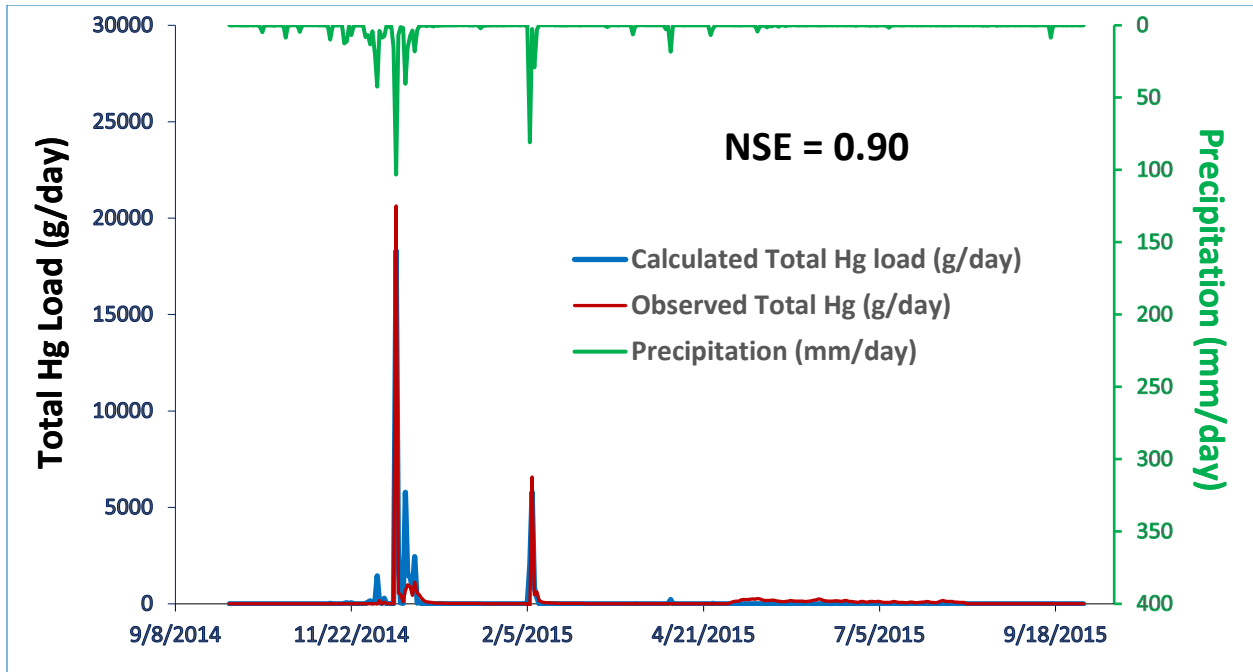


Figure 4-8. Daily time series total Hg load of simulation and observation in the Upper Cache Creek Watershed (Rumsey outlet) for WY 2015

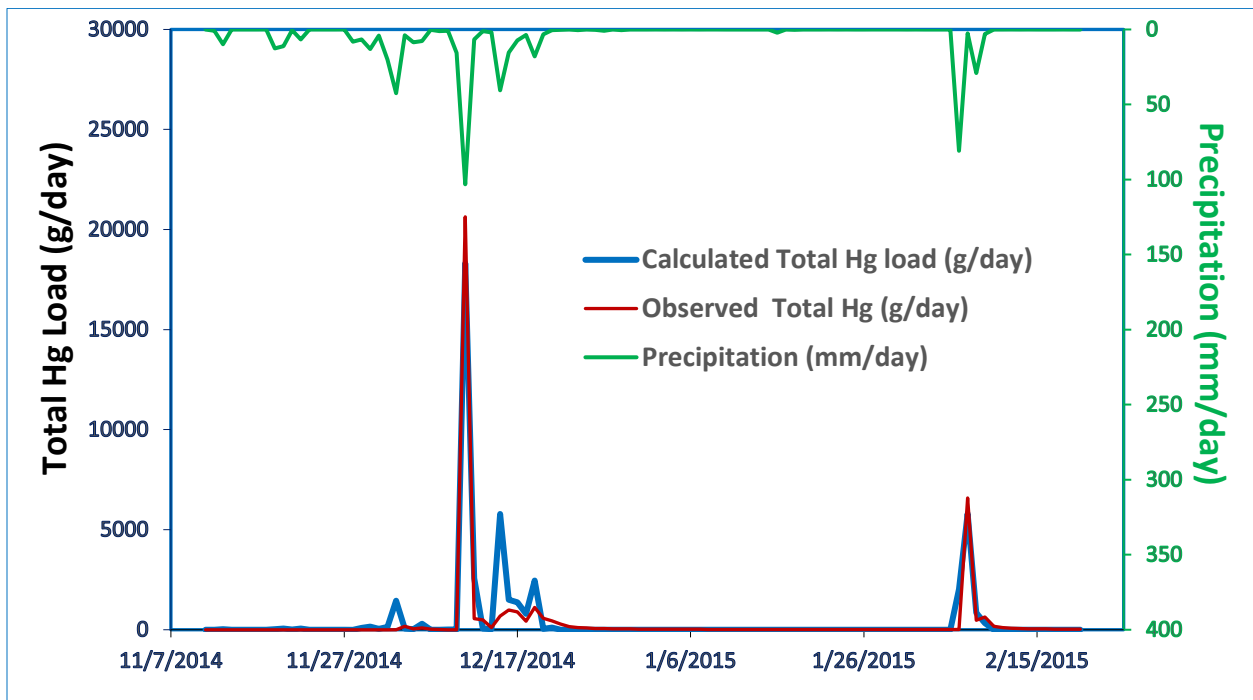


Figure 4-9. Daily time series total Hg load of simulation and observation in the Upper Cache Creek Watershed (Rumsey outlet) showing major storms for WY 2015

The simulated daily time series total mercury (Hg) load of WY 2016 (1st year post-fire) are shown in **Figures 4-10 and 4-11**. The simulation has difficulty reproducing observed mercury loads with an NSE of 0.29. **Figure 4-11** shows results of major storms in WY 2016. The calibrated soil erosion depth is 1.0 cm.

The simulated daily time series total mercury (Hg) load of WY 2017 (2nd year post-fire) are shown in **Figures 4-12 and 4-13**. The model generally underestimates mercury loading during storm events (NSE of 0.36) for the entire WY 2017, but the model does faithfully reproduce mercury loading for the biggest storm event in WY 2017. **Figure 4-13** shows results of major storms in WY 2017. The calibrated soil erosion depth is 0.5 cm.

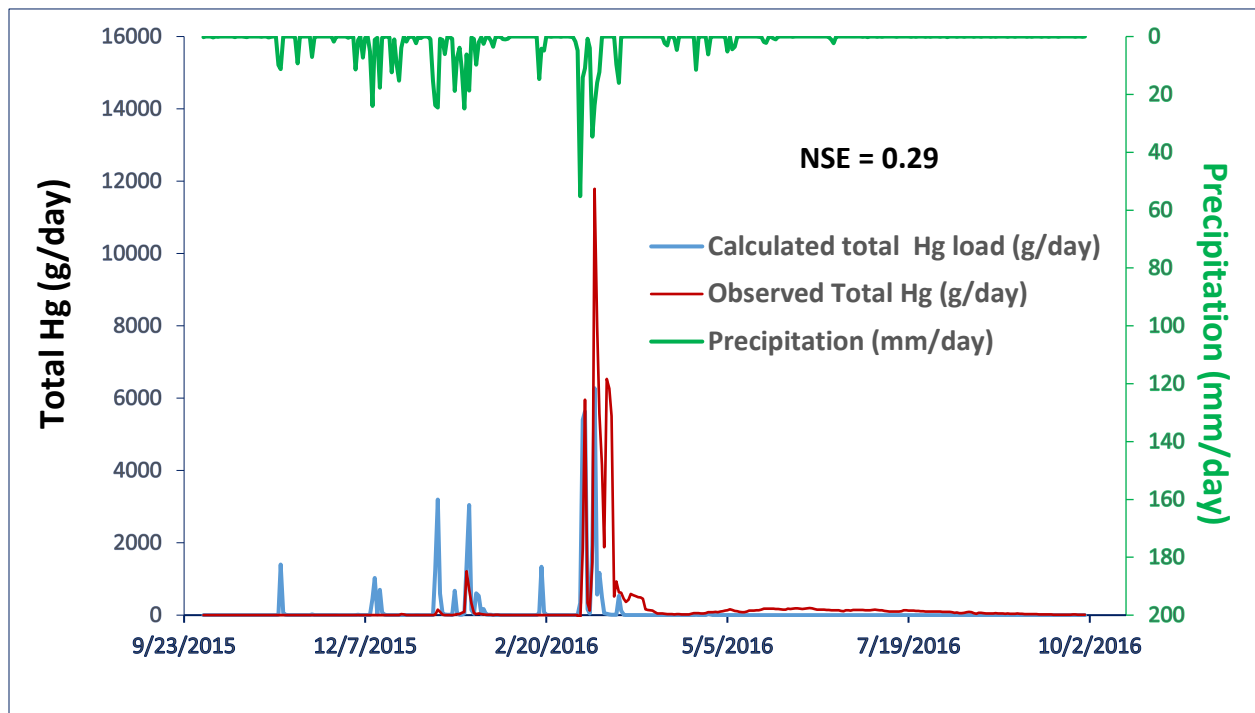


Figure 4-10. Daily time series total Hg load of simulation and observation in the Upper Cache Creek Watershed (Rumsey outlet) for WY 2016

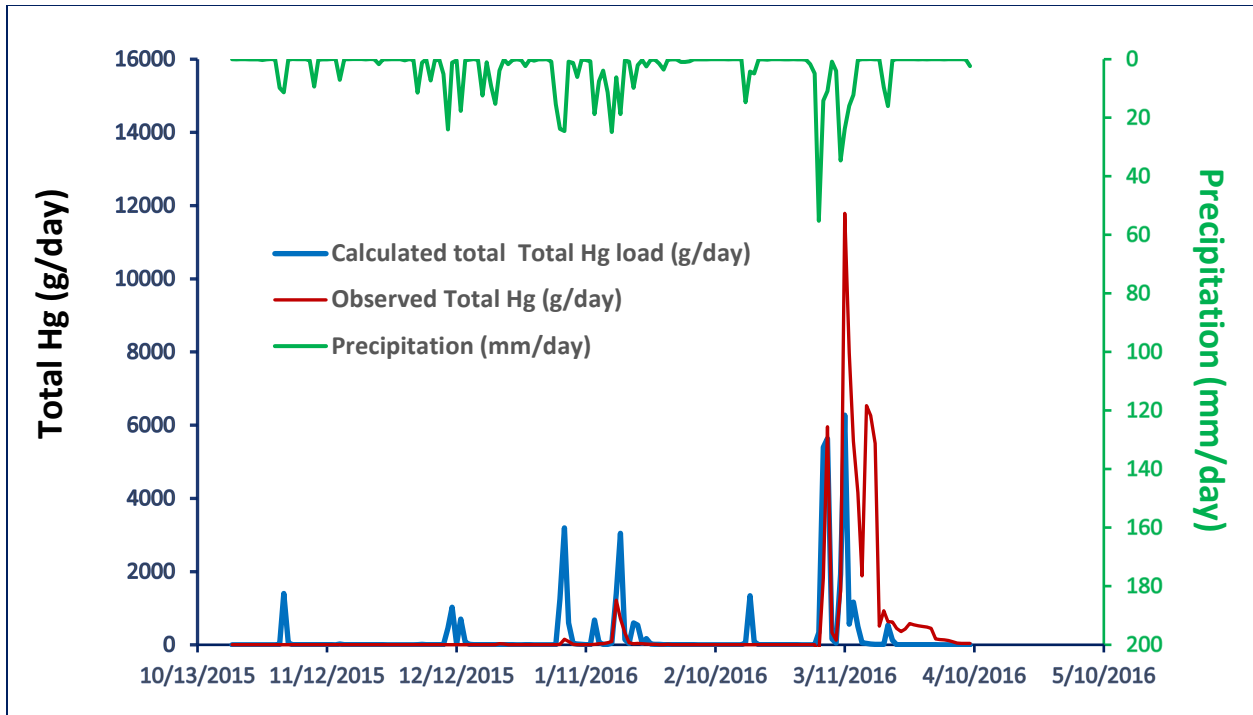


Figure 4-11. Daily time series total Hg load of simulation and observation in the Upper Cache Creek Watershed (Rumsey outlet) - major storms for WY 2016

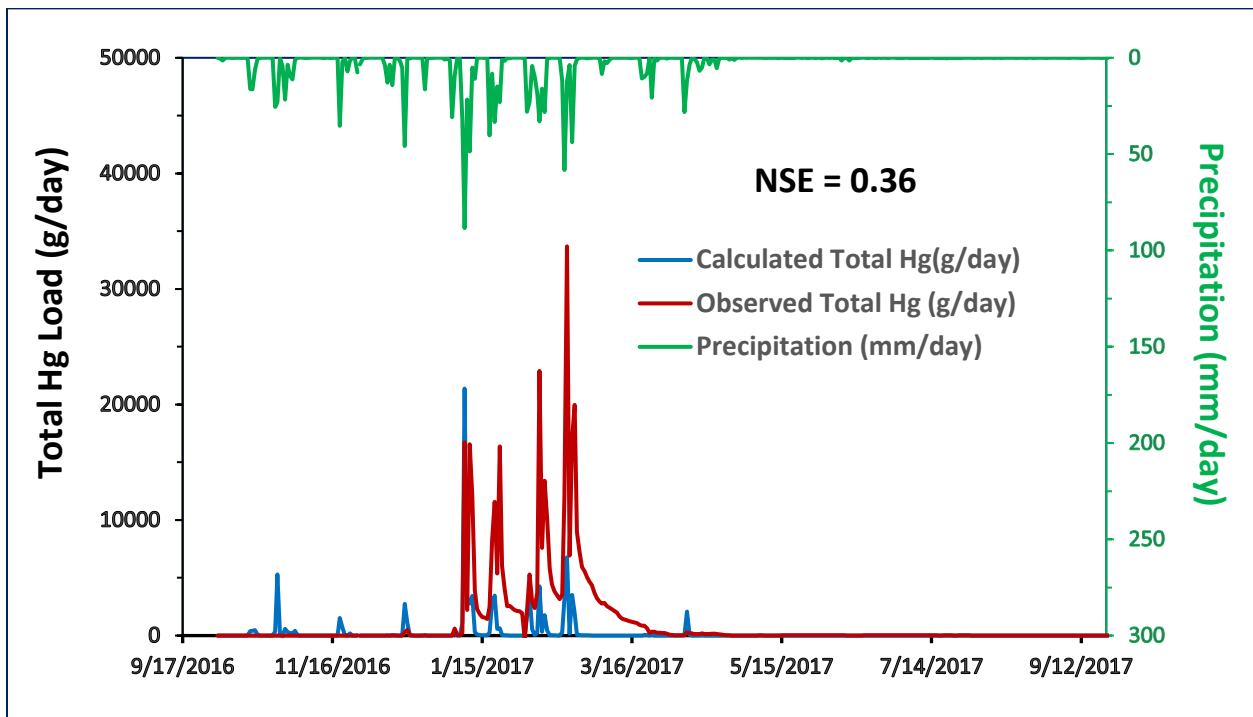


Figure 4-12. Daily time series total Hg load of simulation and observation in the Upper Cache Creek Watershed (Rumsey outlet) for WY 2017

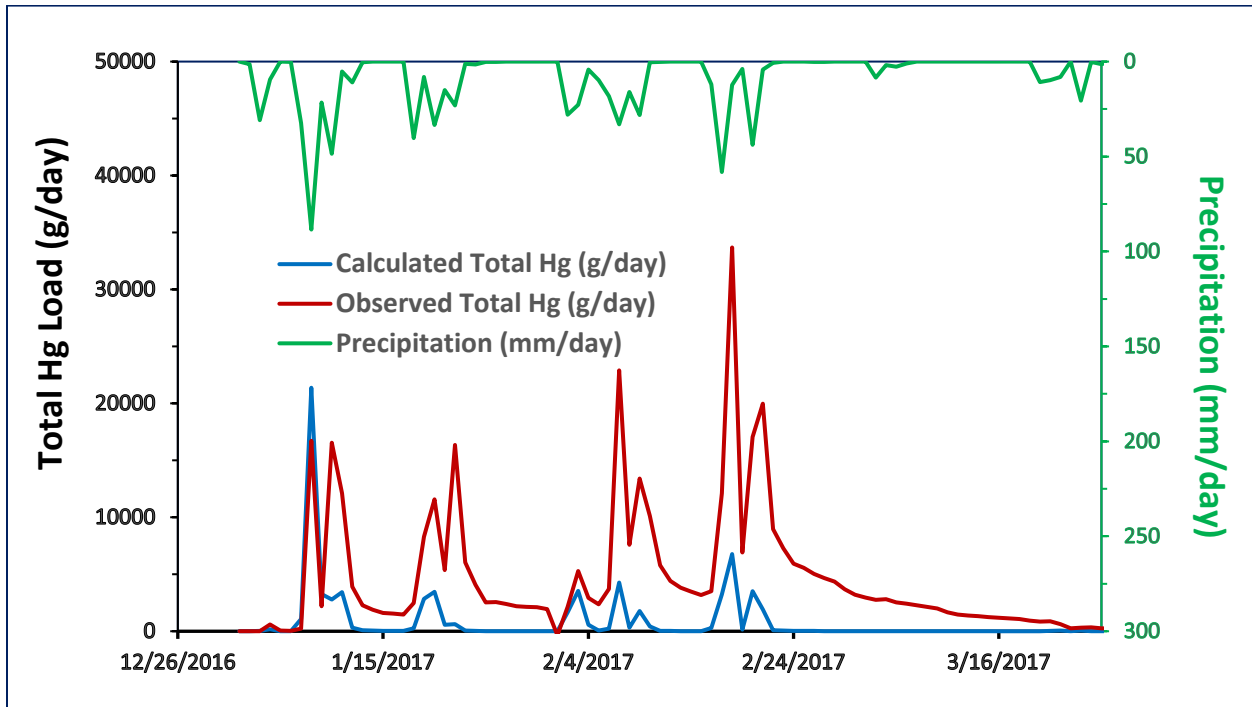


Figure 4-13. Daily time series total Hg load of simulation and observation in the Upper Cache Creek Watershed (Rumsey outlet) - major storms for WY 2017

The modeling results of the two similar biggest storm events in WY 2015 and WY 2017 were compared to demonstrate post-fire effects on runoff and sediment erosion in Chapter 2 and 3, respectively. The two storm events were also selected to compare post-fire effects on total mercury in the modeling area. The results are shown in **Figure 4-14** and **Table 4-5**.

Table 4-5. Comparison of model results for the pre-fire and post-fire storm events

Precipitation Start and End Time (Duration: 4 days)	Total precipitation (mm)	Total simulated sediment load (tons)	Total simulated Hg load (g)	Total observed Hg load (g)
12/10/14 --12/13/14 (Pre-fire)	127 (5.0 in)	119,737	20,954	21,682
01/06/17– 01/09/17 (Post-fire)	143 (5.6 in)	235,632	25,697	19,525
Post-fire / Pre-fire	1.1	2.0	1.2	0.9

The simulated total sediment load of post-fire is about double compared to that of pre-fire. However, the mercury (Hg) concentration of soil post-fire (108 ng/g) is much lower than that of

pre-fire (175 ng/g). So, the total mercury load for the storm event is about the same pre-fire and post-fire.

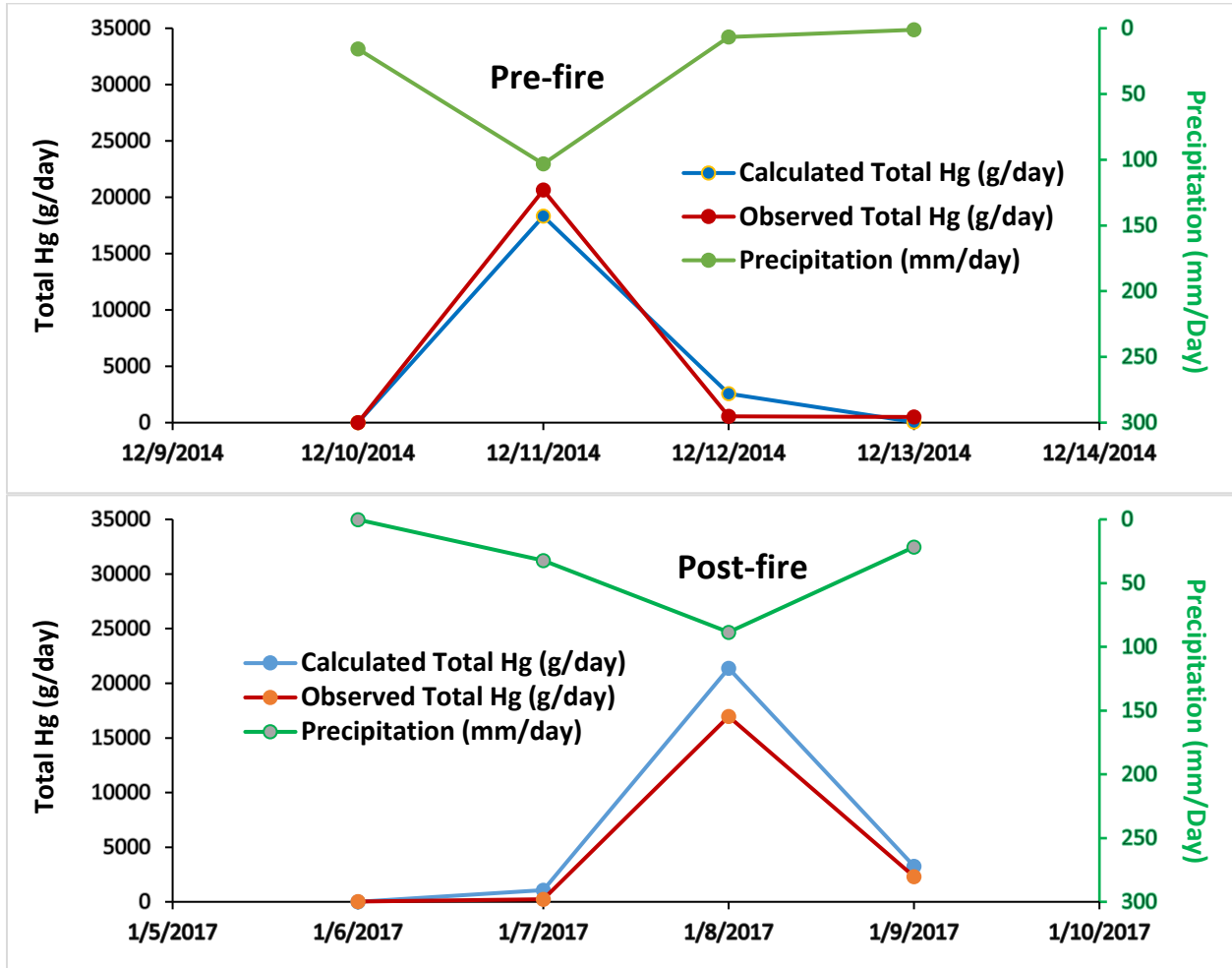


Figure 4-14. Comparison of model Hg simulation for similar pre-fire and post-fire storm events

4.5.3 Pre- and post-fire total methylmercury (MeHg) load simulations

For modeling purposes, the ratio MeHg/THg was assumed to be as follows (as explained in Section 4):

- WY 2015 - 0.20%
- WY 2016 - 0.60%
- WY 2017 - 0.33%

The simulated daily time series total methyl mercury (MeHg) load for WY 2015 (pre-fire) are shown in **Figures 4-15 and 4-16**. The simulation matches the observation very well with an NSE of 0.90. **Figure 4-16** shows results of major storms in WY 2015.

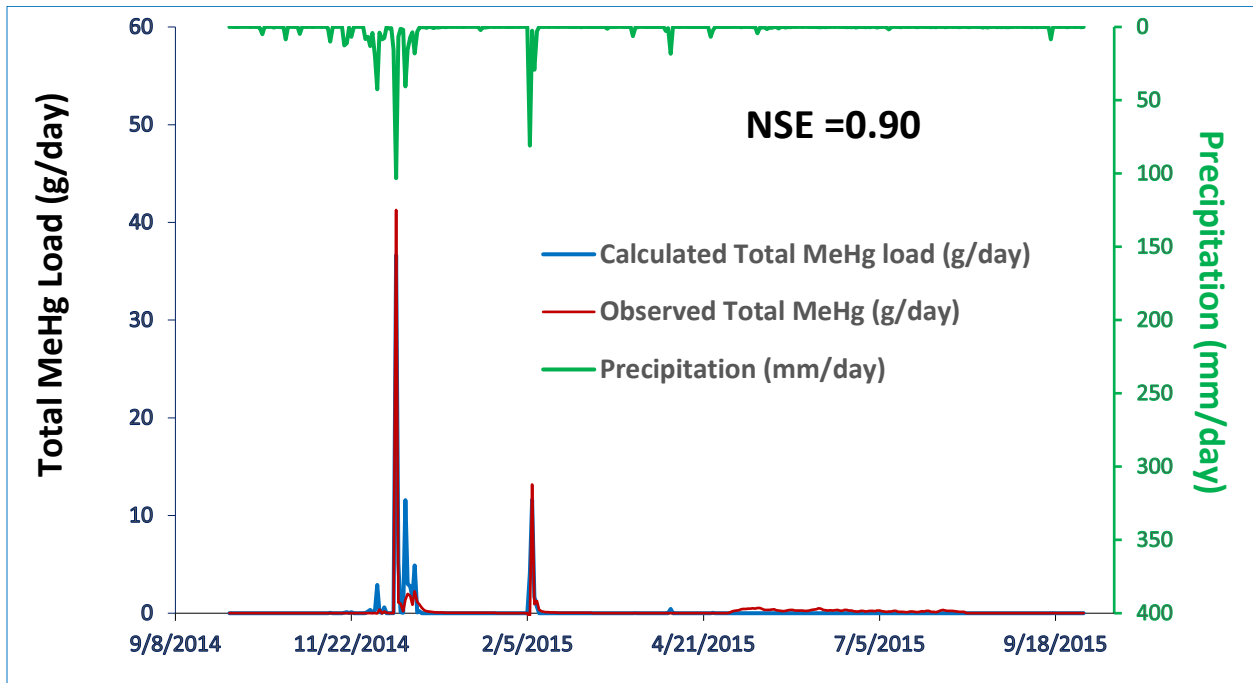


Figure 4-15. Daily time series total MeHg load of simulation and observation in the Upper Cache Creek Watershed (Rumsey outlet) for WY 2015

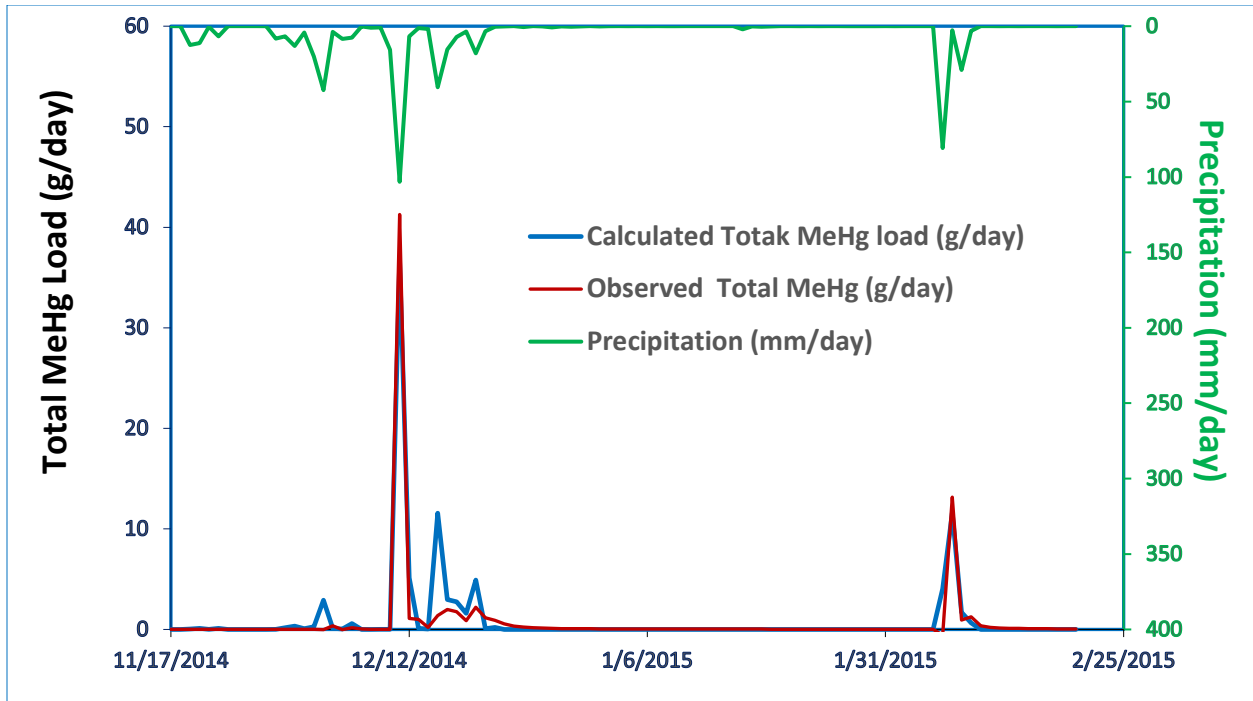


Figure 4-16. Daily time series total MeHg load of simulation and observation in the Upper Cache Creek Watershed (Rumsey outlet) - major storms for WY 2015

The simulated daily time series total methyl mercury (MeHg) load of WY 2016 (first year post-fire) are showed in **Figures 4-17 and 4-18**. The simulation doesn't match the observation well with an NSE of 0.29. **Figure 4-18** shows results of major storms in WY 2016. The calibrated soil erosion depth is 1.0 cm.

The simulated daily time series total methyl mercury (MeHg) load of WY 2017 (second year post-fire) are showed in **Figures 4-19 and 4-20**. Agreement between simulated and observed MeHg is generally poor (NSE of 0.36) for the entire WY 2017, but modeled and observed MeHg match quite well for the biggest storm event in WY 2017. **Figure 4-20** shows results of major storms in WY 2017. The calibrated soil erosion depth is 0.5 cm.

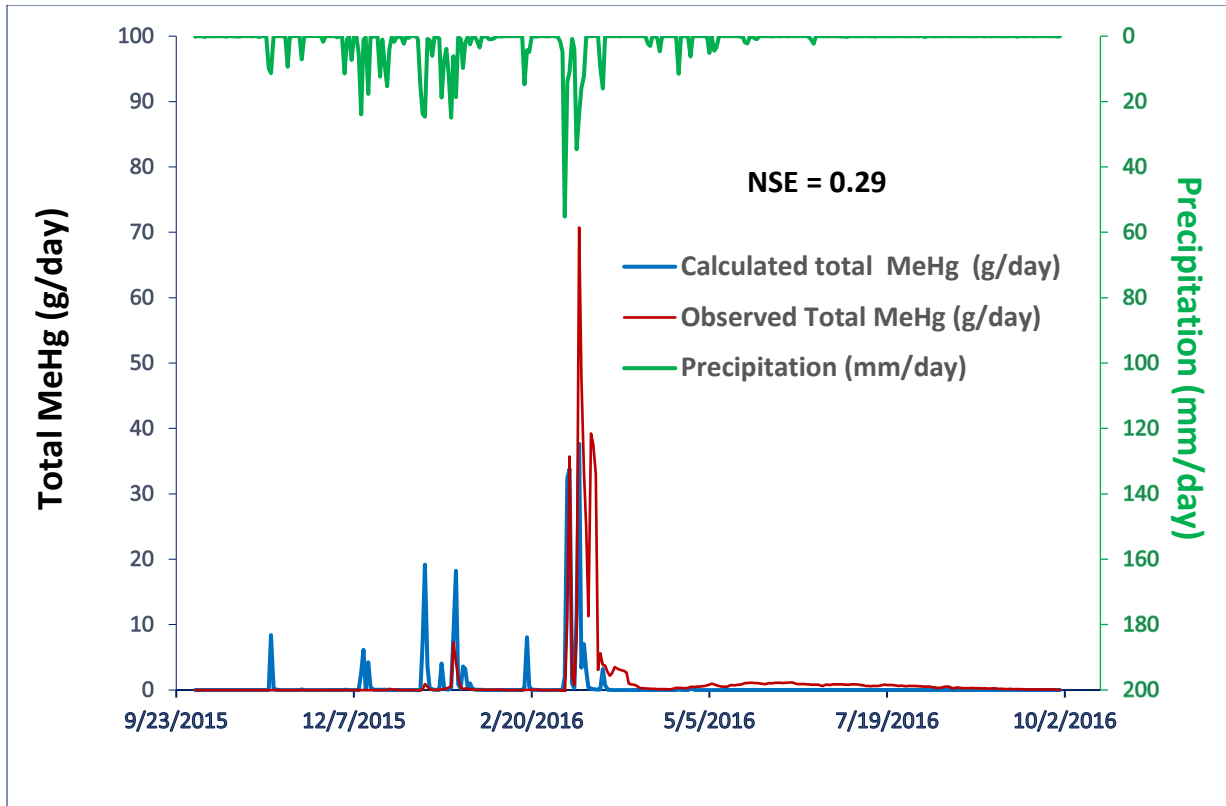


Figure 4-17. Daily time series total MeHg load of simulation and observation in the Upper Cache Creek Watershed (Rumsey outlet) for WY 2016

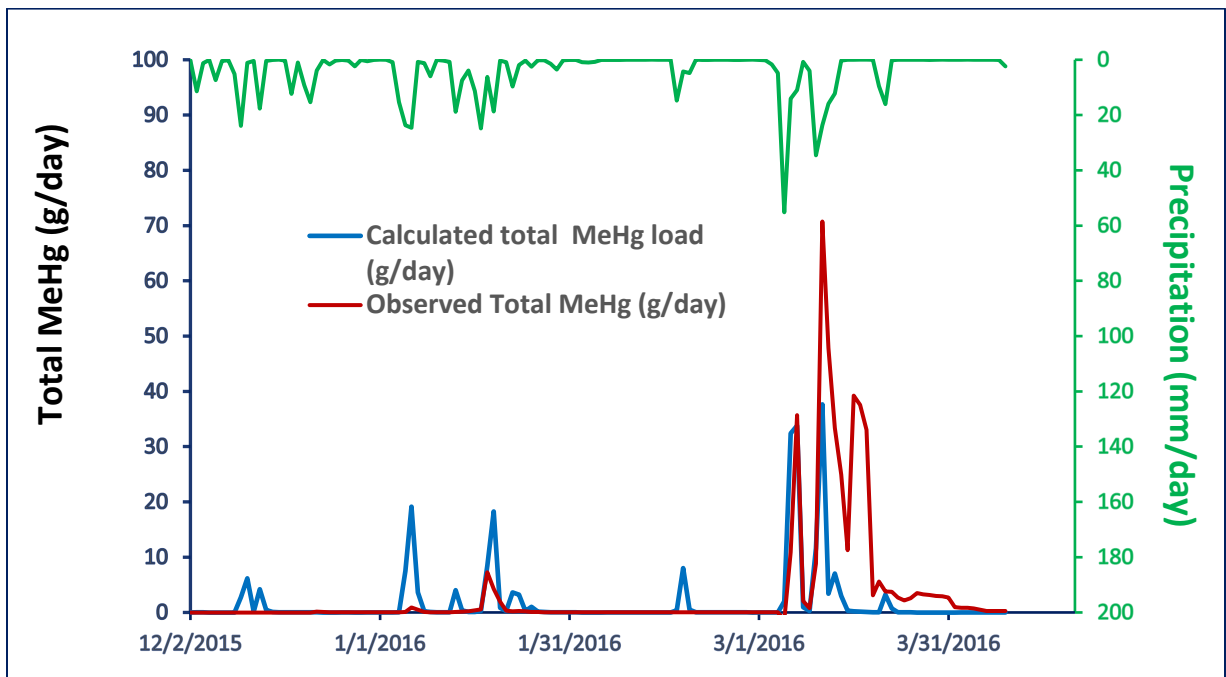


Figure 4-18. Daily time series total MeHg load of simulation and observation in the Upper Cache Creek Watershed (Rumsey outlet) - major storms for WY 2016

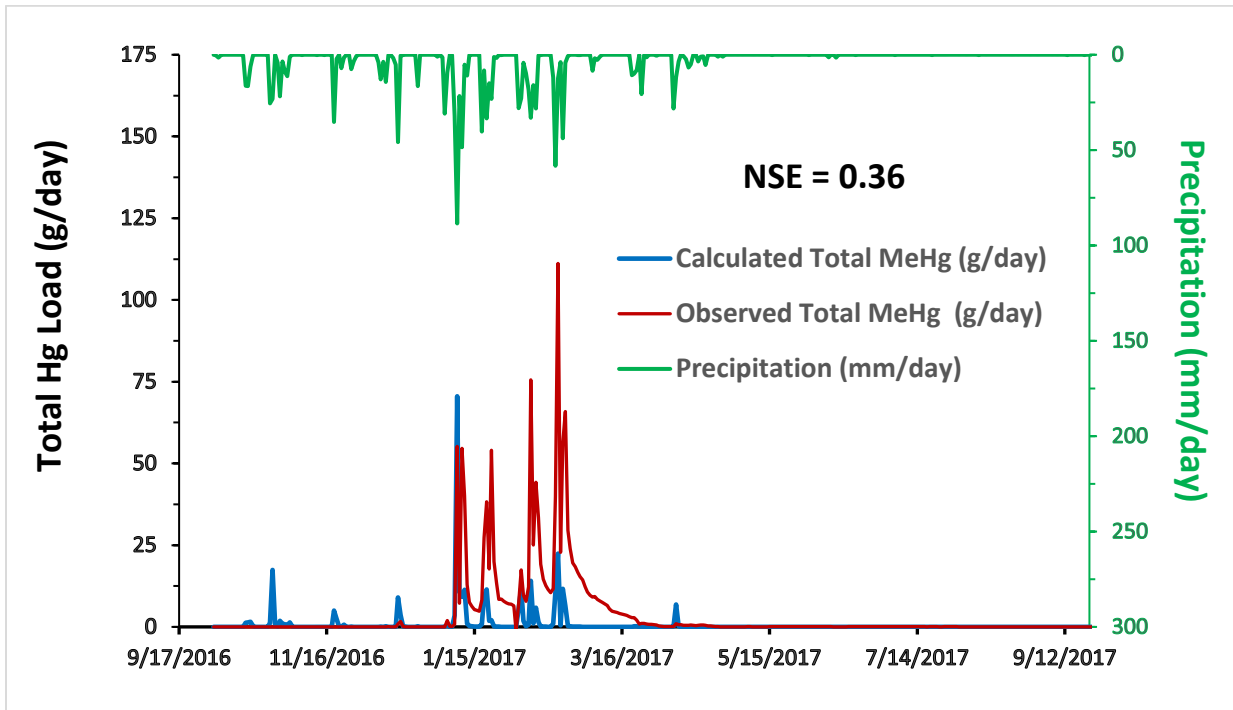


Figure 4-19. Daily time series total MeHg load of simulation and observation in the Upper Cache Creek Watershed (Rumsey outlet) for WY 2017

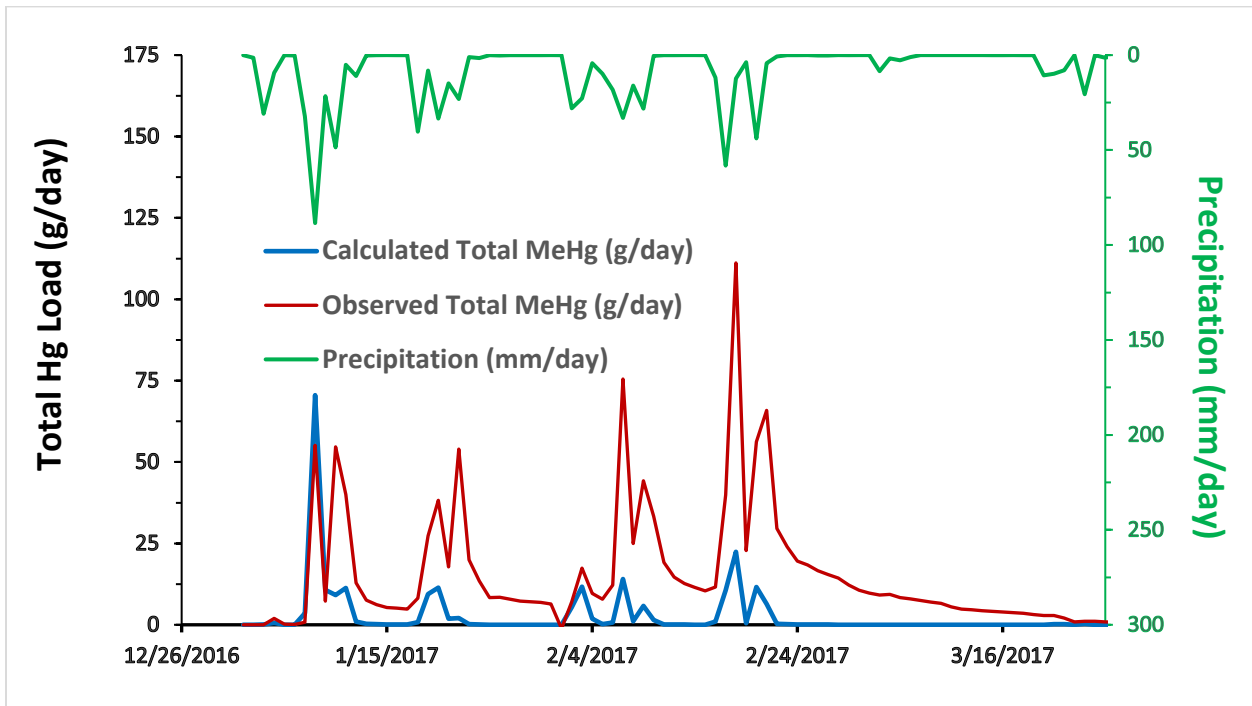


Figure 4-20. Daily time series total MeHg load of simulation and observation in the Upper Cache Creek Watershed (Rumsey outlet) - major storms for WY 2017

The modeling results of the two similar biggest storm events in WY 2015 and WY 2017 were compared to demonstrate post-fire effects on total methylmercury in the modeling area. The results are shown in **Figure 4-21** and **Table 4-6**.

Table 4-6. Comparison of model results for the pre-fire and post-fire storm events

Precipitation Start and End Time (Duration: 4 days)	Total precipitation (mm)	Total simulated sediment load (tons)	Total simulated MeHg load (g)	Total observed MeHg load (g)
12/10/14 --12/13/14 (Pre-fire)	127 (5.0 in)	119,737	41.9	43.4
01/06/17– 01/09/17 (Post-fire)	143 (5.6 in)	235,632	84.8	63.2
Post-fire / Pre-fire	1.1	2.0	2.0	1.5

The simulated total methylmercury (MeHg) load of post-fire is about double the pre-fire MeHg load. The observed total MeHg load of post-fire is roughly 1.5 times that of the pre-fire load. The model is therefore consistent with wildfire events resulting in increased methylmercury load.

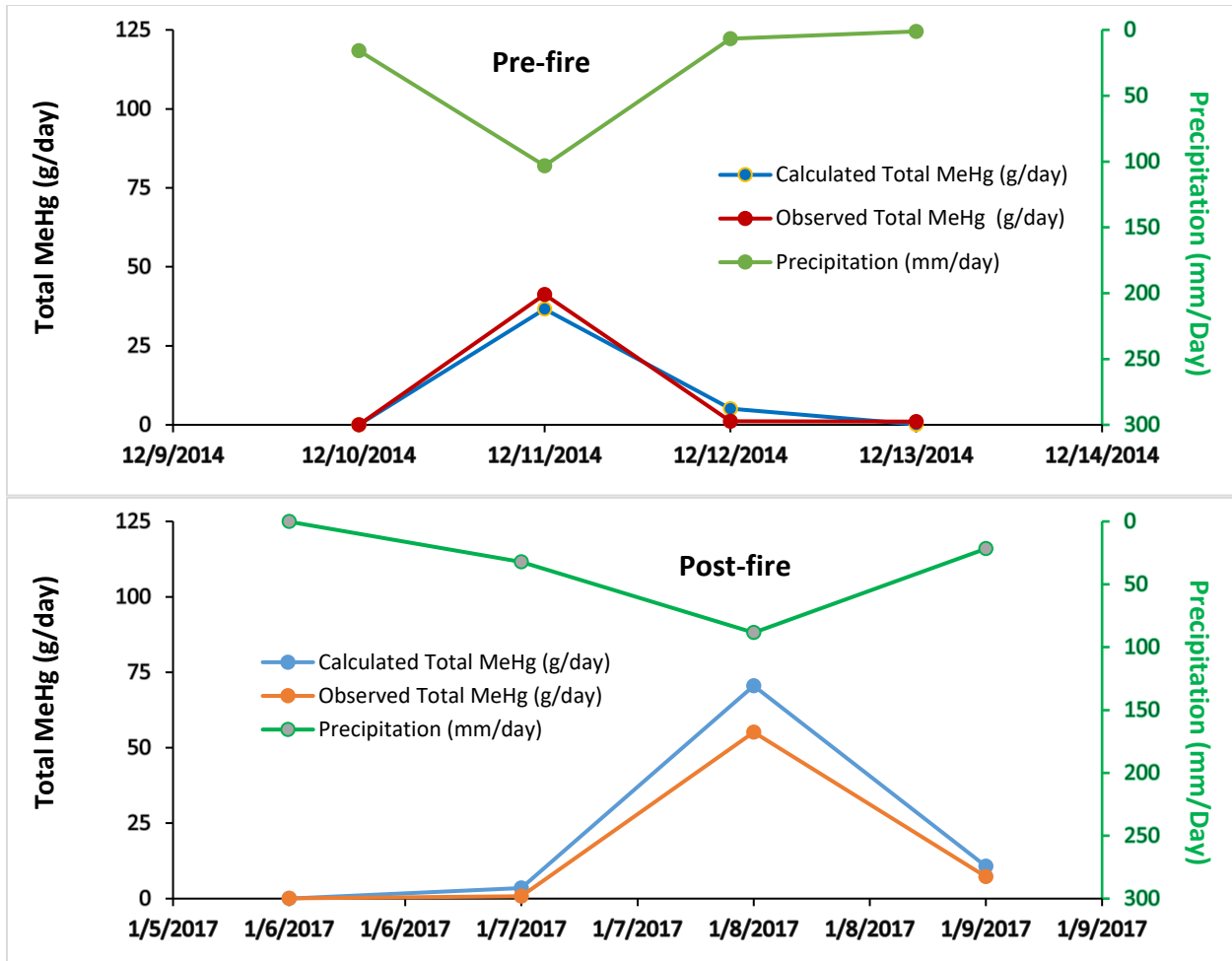


Figure 4-21. Comparison of model MeHg simulation for similar pre-fire and post-fire storm events.

4.5.4 Summary of PFHydro modeling results

A summary of PFHydro and PFHydro-WQ modeling results of total runoff, surface runoff, sediment load, mercury and methylmercury load for pre-, and post-fire conditions is shown in **Table 4-7**. It can be seen from the table that surface runoff of post-fire WYs (WY 2016, WY 2017) is significantly increased compared to that of pre-fire (WY 2015). The increased surface runoff post-fire caused more soil erosion and thus more sediment load. Total mercury load decreased the first year post-fire (WY 2016) because the wildfire decreased mercury concentration from 175 ng/g to 108 ng/g in the soil. The total mercury load almost doubled in the second year post-fire (WY 2017) compared to that of the WY 2015 (pre-fire) because of an increased soil mercury concentration (136 ng/g) and more precipitation that caused more surface runoff, thus more sediment erosion. The total methylmercury load of post-fire WYs 2016, 2017 increased significantly compared to that of pre-fire WY 2015.

Table 4-7. Summary of PFHydro and PFHydro-WQ modeling results. [Note: These results pertain to the PFHydro model domain, computed by taking simulated values at Rumsey and

subtracting boundary condition values (computed using HSPF) flowing into the PFHydro modeling domain.]

	PFHydro /Observed	PFHydro	PFHydro- WQ	PFHydro- WQ /Observed	PFHydro- WQ	PFHydro- WQ / Observed	PFHydro -WQ
	Total Discharge	Total Surface Flow	Sediment load	Total Hg load	THg on SS	Total MeHg load	MeHg on SS
	10⁹ L	10⁹ L	10⁶ kg	kg	ng/g (ppb)	g	ng/g (ppb)
Annual							
WY 2015	148/176	22	255	44.7 /50.9	175	89.4 /102	0.35
WY 2016	55/72	36	296	40.2 /86.1	136	241 /517	0.82
WY 2017	272/211	66	811	87.6 /405	108	289 /1337	0.36
4-Day Storm Event							
pre-fire storm (12/10/14- 12/13/14)	10.2/12.1	7.3	120	21.0 /21.7	175	42.0 /43.4	0.35
post-fire storm (1/6/17 - 1/9/17)	15.7/16.3	12.6	238	25.7 /19.5	108	84.8 /63.3	0.36

4.6 Summary of mercury modeling approach and results

The project goals were achieved by constructing a relatively simple watershed-scale model (PFHydro) that demonstrates the effect of wildfire on surface run-off and sediment transport, and a related model (PFHydro-WQ) that simulates pre- and post-wildfire transport of mercury and methylmercury. To achieve these goals, we used another watershed-based model (HSPF, Donigian et al., 1995) to provide boundary conditions to PFHydro and PFHydro-WQ. A soil-heating model (FOFEM2, Lutes et al., 2012) was used to estimate mercury losses as a function of soil depth for different vegetation types.

The HSPF modeling approach considered a larger modeling domain than PFHydro. The HSPF modeling domain was divided into 25 sub-basins. Each sub-basin was assigned an initial concentration of soil THg (0.1 or 1.0 µg/g) and streambed sediment Hg (0.1, 1.0 or 10.0 µg/g) based on published information and the distribution of historical mercury and gold mines.

Information on mercury fluxes from active hot springs (Goff et al., 2001) were included in the HSPF modeling, although these turned out to be a small component of overall mercury loads.

The modeling was successful in simulating fire-related decreases in the total mercury (THg) concentration of suspended particles. Post-fire conditions led to increased erosion and higher sediment loads for a given amount of precipitation and streamflow. The increase in suspended particulates during post-fire conditions was balanced off by lower concentrations of mercury on the suspended particles, such that mercury loads were similar when comparing a large pre-fire storm event (Dec. 10-13, 2014) to a post-fire storm event (Jan. 6-9, 2017) of similar magnitude.

Because of limited data on the distribution of methylmercury (MeHg) in the watershed, available monitoring data for Cache Creek at Rumsey and related load data (Alpers et al., in review-a,b) were used to calibrate the HSPF and PFHydro-WQ models. Ratios of MeHg/THg based on the available data at Rumsey were assigned to each of the water years considered. Estimated concentrations and loads of THg for boundary conditions to the PFHydro-WQ model were multiplied by the corresponding MeHg/THg ratio for each water year. This resulted in a reasonable simulation of the observed increase in MeHg/THg during the post-fire years (WY 2016 and 2017) compared to the pre-fire year (WY 2015).

The modeling approach used in this study should be considered as a proof of concept. There are strengths and limitations to the approach that must be considered in any attempts to apply the approach elsewhere. The approach used for modeling total mercury (THg) is relatively robust regarding particulate transport. A process-based understanding of mercury losses from heating of soils was used, and there was a considerable amount of published data on the distribution of THg in soils and streambed sediment throughout the modeling domains that give confidence in the assumptions that were made. In the model domain considered, particulate THg (as defined by 0.3 μm filtration) made up more than 95% of whole-water THg transport at Rumsey (Alpers et al., in review-a, -b), so no effort was made to quantify dissolved (filter-passing) THg transport. In other settings, filter-passing THg may constitute a much larger proportion of whole-water THg loads, so a more comprehensive modeling approach considering complexation of THg with dissolved organic matter would be needed.

The modeling of methylmercury (MeHg) in this study was relatively crude and was not process-based; rather, it was based on empirical data from a single monitoring location. The biogeochemical processes controlling methylmercury concentration in soils and streambed sediment remain poorly understood, and there are relatively few data available compared with THg. In Section 5 of this report, future work is described that would result in improvements to THg and MeHg modeling.

4.7 References

- Aiken, G.R., Hsu-Kim, H., and Ryan, J.N., 2011, Influence of dissolved organic matter on the environmental fate of metals, nanoparticles, and colloids: *Environmental Science and Technology*, v. 45, p. 3196–3201. Doi: 10.1021/es103992s
- Alpers, C.N., Marvin-DiPasquale, M., Ackerman, J.A., Fleck, J.A., Windham-Myers, L, Fuller, C.C., Arias, M., Agee, J., Hartman, C.A., Herzog., M.P., & Eagles-Smith, C.A., in revision, Mercury studies in the Cache Creek Settling Basin, Yolo County California, Preliminary Results, 2010-14: USGS Scientific Investigations Report.
- Alpers, C.N., Marvin-DiPasquale, M., Fleck, J.A., Ackerman, J.T., & Stricker, C.A., in review-a, Mercury studies in the Cache Creek Settling Basin, Yolo County California: Updated Results, 2010–16: USGS Open-File Report.
- Alpers, C.N., Rose, S.L., Schmidt, E.R., Fleck, J.A., Agee, J.L., Marvin-DiPasquale, M.C., & Ward, A.J., in review-b, Water quality including mercury and methylmercury at selected sites in the Cache Creek Watershed, Yolo County, California, 2010–16, USGS Data Release.
- Arias, M.R., Alpers, C.N., Marvin-DiPasquale, M., Fuller, C.C., Agee, J.L., Sneed, M., Morita, A.Y., & Salas, A.J., 2017, Sediment mercury, iron, sulfur, cesium-137, grain-size, and loss-on-ignition analyses from 2011 and 2012 coring campaigns, Cache Creek Settling Basin, Yolo County, California. U.S. Geological Survey Data Series 1061, 150 p.
<https://pubs.er.usgs.gov/publication/ds1061> doi: 10.3133/ds1061
- Benedict, S.T., Conrads, P.A., Feaster, T.D., Journey, C.A., Golden, H.E., Knightes, C.D., Davis, G.M., & Bradley, P.M., 2012, Data visualization, time-series analysis, and mass-balance modeling of hydrologic and water-quality data for the McTier Creek watershed, South Carolina, 2007–2009: U.S. Geological Survey Open-File Report 2011–1209, 21 p.
<https://pubs.usgs.gov/of/2011/1209/>
- Biester, H., and Scholz, C., (1996, Determination of mercury binding forms in contaminated soils: mercury pyrolysis versus sequential extractions: *Environmental Science and Technology*, v. 31(1), p. 233-239.
- Burke, M.P., Hogue, T.S., Ferreira, M., Mendez, C.B., Navarro, B., Lopez, S., and Jay, J.A., 2010, The effect of wildfire on soil mercury concentrations in Southern California watersheds: *Water, Air, & Soil Pollution*, v. 212(1-4), p. 369-385.
- Caldwell, C.A., Canavan, C.M., and Bloom, N.S., 2000, Potential effects of forest fire and storm flow on total mercury and methylmercury in sediments of an arid-lands reservoir: *Science of the Total Environment*, v. 260(1-3), p. 125-133.
- Churchill, R., and Clinkenbeard, J., 2003, Assessment of the feasibility of remediation of mercury mine sources in the Cache Creek watershed. Final Report, Task 5C1, An Assessment of

Ecological and Human Health Impacts of Mercury in the Bay-Delta Watershed, CALFED Bay-Delta Mercury Project. California Department of Conservation, California Geological Survey, 58 p., plus 18 appendices.

Domagalski, J.L., Alpers, C.N., Slotton, D.G., Suchanek, T.H., and Ayers, S.M., 2004a, Mercury and methylmercury concentrations and loads in the Cache Creek Watershed, California: *Science of the Total Environment*. v. 327, p. 215–237.

<http://www.sciencedirect.com/science/article/pii/S0048969704000543> doi:

10.1016/j.scitotenv.2004.01.013

Domagalski, J.L., Slotton, D.G., Alpers, C.N., Suchanek, T.H., Churchill, R., Bloom, N., Ayers, S.M., and Clinkenbeard, J., 2004b, Summary and Synthesis of Mercury Studies in the Cache Creek Watershed, California, 2000–01: U.S. Geological Survey Water-Resources Investigations Report 03-4335, 30 p. <https://pubs.usgs.gov/wri/wri034335/>

Donigian, A.S., Bicknell, B.R. and Imhoff, J.C., 1995. Hydrological simulation program—Fortran (HSPF). *Computer Models of Watershed Hydrology*, v. 12, p. 395-442.

Eggleston, J., 2009, Mercury loads in the South River and simulation of mercury total maximum daily loads (TMDLs) for the South River, South Fork Shenandoah River, and Shenandoah River—Shenandoah Valley, Virginia: U.S. Geological Survey Scientific Investigations Report 2009–5076, 80 p. <http://pubs.usgs.gov/sir/2009/5076/>

Engle, M.A., Gustin, M.S., Johnson, D.W., Murphy, J.F., Miller, W.W., Walker, R.F., Wright, J., and Markee, M., 2006, Mercury distribution in two Sierran forest and one desert sagebrush steppe ecosystems and the effects of fire: *Science of the Total Environment*, v. 367, p. 222-233.

Foe, C., and Bosworth, D., 2008, Mercury Inventory in the Cache Creek Canyon. Staff Report. Regional Water Quality Control Board Central Valley Region, Rancho Cordova, Calif.

Foe, C., and Croyle, W., 1998, Mercury Concentrations and Loads from the Sacramento River and from Cache Creek to the Sacramento-San Joaquin Delta Estuary. California Regional Water Quality Control Board Central Valley Region, Rancho Cordova, Calif.

Goff, F., Bergfeld, D., Janik, C.J., Counce, D., and Stimac, J.A., 2001, Geochemical Data on Waters, Gases, Rocks, and Sediments from The Geysers-Clear Lake Region, California (1991-2000), Los Alamos National Laboratory, LA-13882-MS, 50 p.

Golden, H.E., and Knightes, C.D., 2011, Simulated watershed mercury and nitrate flux responses to multiple land cover conversion scenarios: *Environmental Toxicology and Chemistry*, v. 30 (4), p. 773-786.

Golden, H.E., Knightes, C.D., Conrads, P.A., Davis, G.M., Feaster, T.D., Jouney, C.A., Benedict, S. T., Brigham, M.E., and Bradley, P.M., 2012, Characterizing mercury concentrations

and fluxes in a Coastal Plain watershed: Insights from dynamic modeling and data: *Journal of Geophysical Research*, v. 117, G01006. doi:10.1029/2011JG001806

Holloway, J.M., Goldhaber, M.B., and Morrison, J.M., 2009a, Geomorphic controls on mercury accumulation in soils from a historically mined watershed, Central California Coast Range, USA: *Applied Geochemistry*, v. 24(8), p. 1538-1548.

Holloway, J.M., Goldhaber, M.B., Scow, K.M., and Drenovsky, R.E., 2009b, Spatial and seasonal variations in mercury methylation and microbial community structure in a historic mercury mining area, Yolo County, California: *Chemical Geology*, v. 267, p. 85-95.

Jensen, A.M., Scanlon, T.M., and Riscassi, A.L., 2017, Emerging investigator series: the effect of wildfire on streamwater mercury and organic carbon in a forested watershed in the southeastern United States: *Environmental Science: Processes and Impacts*, v. 19(12), p. 1505-1517.

Kelly, E.N., Schindler, D.W., Louis, V.L.S., Donald, D.B., and Vladicka, K.E., 2006, Forest fire increases mercury accumulation by fishes via food web restructuring and increased mercury inputs: *Proceedings of the National Academy of Sciences*, v. 103(51), p.19380-19385.

Krabbenhoft, D.P., and Fink, L.E., 2001, Appendix 7-8: The effects of dry down and natural fires on mercury methylation in the Florida Everglades. Everglades Consolidated Report. South Florida Water Management District. A7-8-1 to A7-8-14.

Lutes, D.C., Keane, R., and Reinhardt, E., 2012, FOFEM 6.0 user guide. USDA Forest Service, Rocky Mountain Research Station: Fort Collins, CO). Available at http://www.firelab.org/ScienceApps_Files/downloads/FOFEM/FOFEM6_Help.Pdf

Mierle, G., and Ingram, R., 1991, The role of humic substances in the mobilization of mercury from watersheds: *Water Air & Soil Pollution*, v. 56(1), p. 349-357.

Obrist, D., Pearson, C., Webster, J., Kane, T., Lin, C.-J., Aiken, G.R., and Alpers, C.N., 2016, Terrestrial mercury in the western United States: spatial distribution defined by land cover and plant productivity: *Science of the Total Environment*, v. 568, p. 522–535.
<http://www.sciencedirect.com/science/article/pii/S0048969715310858> doi: 10.1016/j.scitotenv.2015.11.104

Olson, E.S., Miller, S.J., Sharma, R.K., Dunham, G.E., and Benson, S.A., 2000, Catalytic effects of carbon sorbents for mercury capture: *Journal of Hazardous Materials*, v. 74(1-2), p. 61-79.

Rytuba, J.J., 2000, Mercury mine drainage and processes that control its environmental impact: *Science of the Total Environment*, v. 260, p. 57-71.

Rytuba, J.J., Hothem, R.L., Brussee, B.E., and Goldstein, D.N., 2011, Impact of mine and natural sources of mercury on water, sediment, and biota in Harley Gulch adjacent to the Abbott-Turkey

Run mine, Lake County, California: U.S. Geological Survey Open File Report 2011–1265, 105 p. <http://pubs.usgs.gov/of/2011/1265/>

Rytuba, J.J., Hothem, R.L., Brussee, B.E., Goldstein, D.N., and May, J.T., 2015, Environmental assessment of water, sediment, and biota collected from the Bear Creek watershed, Colusa County, California: U.S. Geological Survey Open-File Report 2013–1070, 83 p., <http://dx.doi.org/10.3133/ofr20131070>

Smith, D. B., Cannon, W. F., Woodruff, L. G., Solano, F., Kilburn, J. E., and Fey, D. L., 2013, Geochemical and mineralogical data for soils of the conterminous United States. U.S. Geological Survey Data Series 801, 19 p., <https://pubs.usgs.gov/ds/801/>

Witt, E.L., Kolka, R.K., Nater, E.A., and Wickman, T.R., 2009, Forest fire effects on mercury deposition in the boreal forest: *Environmental Science and Technology*, v. 43(6), p. 1776-1178.

Writer, J.H., and Murphy, S.F., 2012, Wildfire Effects on Source-water Quality: Lessons from Fourmile Canyon Fire, Colorado, and Implications for Drinking-water Treatment. U.S. Geological Survey Fact Sheet 2012–3095, 4 p. <https://pubs.usgs.gov/fs/2012/3095/>

Xia, K., Skyllberg, U.L., Bleam, W.F., Bloom, P.R., Nater, E.A., and Helmke, P.A., 1999, X-ray absorption spectroscopic evidence for the complexation of Hg(II) by reduced sulfur in soil humic substances: *Environmental Science and Technology*, v. 33, p. 257-261. doi: 10.1021/es980433q

Zhang, T., Kucharzyk, K.H., Kim, B., Deshusses, M.A., and Hsu-Kim, H., 2014, Net methylation of mercury in estuarine sediment microcosms amended with dissolved, nanoparticulate, and microparticulate mercuric sulfides: *Environmental Science and Technology*, v. 48, p. 9133–9141. doi: 10.1021/es500336j

5 Future Work

The work accomplished during the current project represents substantial progress toward the goal of providing land and water managers at Reclamation and elsewhere with a decision-support tool for evaluating the effects of wildfire on surface water flow and transport of sediment, total mercury (THg), and methylmercury (MeHg). The results detailed in Chs. 2-4 of this report indicate that the models PFHydro and PFHydro-WQ did a fairly good job in simulating fire effects on the Cache Creek watershed in relation to the fires that affected the area in summer 2015.

There are several types of follow-up work that would bring Reclamation closer to the goal of having a reliable decision-support tool. Four categories of suggested follow-up studies are described briefly in this section:

- 1) Extend modeling of Cache Creek watershed through Water Year 2020 to characterize effects of 2018 fires;
- 2) Gather hydrologic and soils data to support modeling;
- 3) Perform process-oriented studies to improve knowledge of fire effects on Hg methylation and transport;
- 4) Initiate or expand data collection for water flow, suspended sediment, total mercury, and methylmercury in watersheds of interest to Reclamation, especially in the context of the pending state-wide mercury control program on reservoirs (SWRCB, 2019); and
- 5) Update PFHydro and PFHydro-WQ algorithms for the model to be applied in a heterogeneous watershed and simulate SWR effects and Hg/MeHg load more effectively
- 6) Construct a user-friendly interface for PFHydro and PFHydro-WQ and publish documentation so that these models may be readily used by land and water managers and their staff.

5.1 Extend modeling of Cache Creek watershed through Water Year 2020 to include effects of 2018 fires

An additional cycle of wildfire greatly affected the upper Cache Creek watershed during summer 2018. The Mendocino Complex Fire, consisting of the River and Ranch fires (Figure 5-1) was the largest fire in California history, measured by aerial extent. It covered 459,123 acres and

burned from July 27, 2018 through January 4, 2019 (CalFire, 2019a). In addition, the Pawnee Fire affected an adjacent 13,185 acres (Figure 5-1) during the same period (CalFire, 2019a).

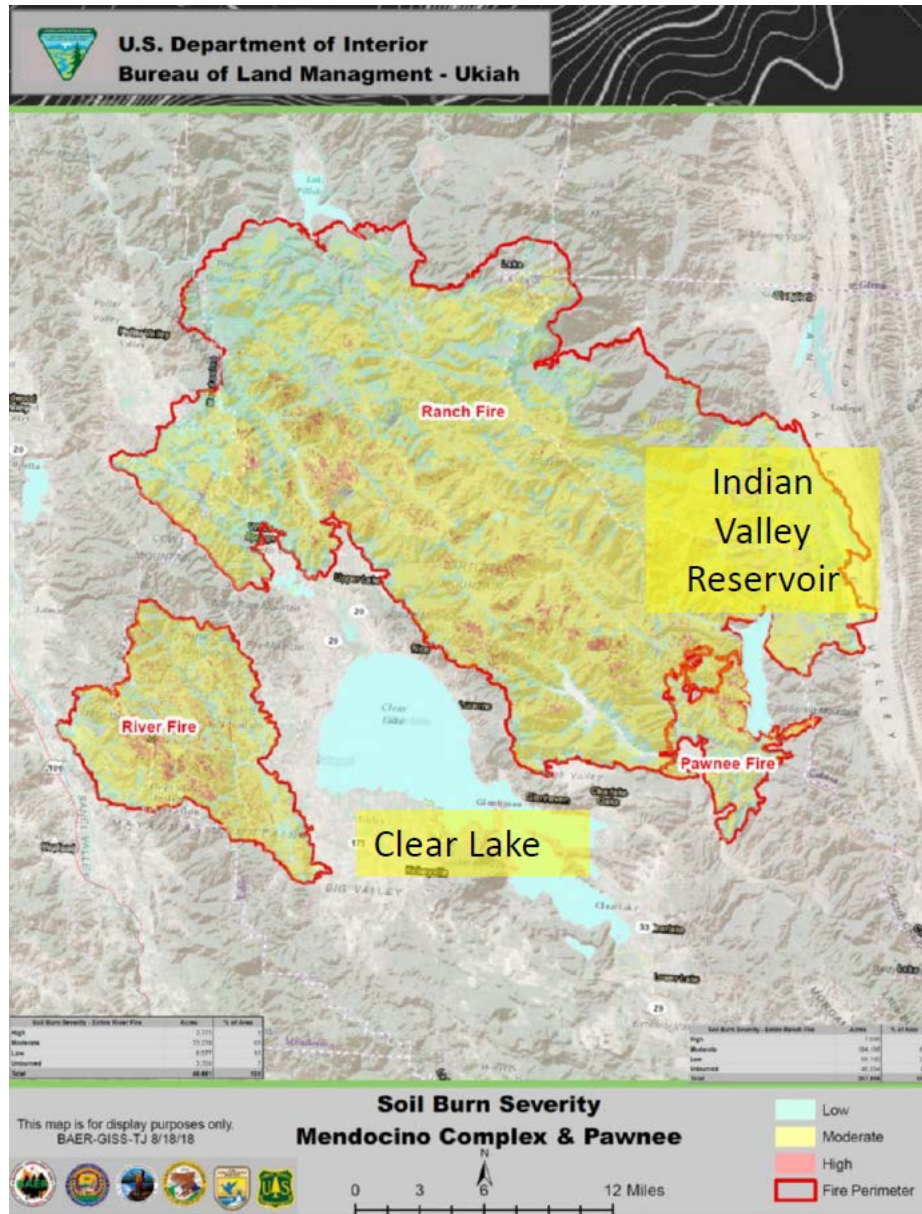


Figure 5-1. Burn perimeter and severity of River and Ranch Fires (Mendocino Complex) and Pawnee Fire, 2018-19.

The area affected by the River Fire drains mostly into Clear Lake, as does some of the area affected by the Ranch Fire. In addition, much of the area affected by the Ranch Fire drains into Indian Valley Reservoir (Figure 5-1). However, portions of the area burned by the Ranch Fire and most of the area affected by the Pawnee Fire drain into tributaries of Cache Creek (including North Fork Cache Creek) that do not flow into lakes or reservoirs. These unregulated parts of the Cache Creek watershed are more likely to have generated suspended sediment from post-fire

erosion that would have impacted Cache Creek at Rumsey, the modeling point for the current study.

The U.S. Geological Survey has an agreement in place with the California Dept. of Water Resources that includes continued monitoring of discharge and water quality at Cache Creek at Rumsey through Water Year 2020 (September, 2020). The current report documents modeling of sediment and mercury transport for one pre-fire year (WY 2015) and two post-fire years (WYs 2016-17) based on the 2015 fires in the area. The additional monitoring by USGS during WY's 2018-20 will include data for another fire cycle, with two additional post-fire years (WY's 2019-20). The availability of detailed monitoring data for suspended sediment, THg, and MeHg in the same area as the previous monitoring provides an excellent opportunity to test (i.e. validate) the PFHydro and PFHydro-WQ models and modify them, if needed.

In addition to data for suspended sediment, THg, and MeHg, the USGS monitoring effort for Cache Creek at Rumsey during WY's 2018-20 also includes nutrients and dissolved organic carbon. Reclamation has expressed interest in understanding the effects of wildfire on nutrients, especially particulate forms of nitrogen and phosphorus, and possible effects of fire retardants, which are the subject of a pending R&D proposal (to start in FY 2020) by J. Wang.

Given the spatial extent of the 2018 fires (**Figure 5-1**) compared with the 2015 fires (**Appendix 1, Figure 2**) it would likely be necessary to extend the model domain of PFHydro and PFHydro-WQ to the entire Cache Creek watershed for the follow-up modeling effort. It would be logical to take a similar approach as the current study in terms of interpolating and downscaling precipitation and air temperature data for input to PFHydro and modeling the same domain with HSPF for comparison.

5.2 Gather hydrologic and soils data to support modeling

One limitation of the modeling described in this report is that very few data were available for soil properties, both physical and chemical, in the study area. The main exception to this was data for THg in soil and streambed sediment, but more data for those parameters would have also improved model certainty. Sampling and analysis of THg and MeHg in a suite of soil samples throughout the Cache Creek watershed upstream of Rumsey would provide a useful ground-truthing for the assumptions made in the current modeling effort.

Useful studies would (1) examine the mercury leaching potential of soils and charcoals collected from recently burned landscapes; (2) evaluate the effects of burn severity on mercury leaching from soil and charred material; and (3) evaluate the changes in fractional distribution between dissolved and sediment associated mercury as a function of burn severity.

Measuring physical properties of soils affected and unaffected by wildfire would also provide important information that could be used to confirm assumptions made in the current modeling. In regard to soil-water repellence and hydrophobicity, it would be useful to develop a quantitative understanding of the variability of soil infiltration properties as a function of soil type, burn severity, vegetation type, soil organic matter content, and other factors. Getting data

on soil physical properties including hydraulic conductivity and permeability from other watersheds would be useful as well (see section 5.4).

5.3 Perform process-oriented studies to improve knowledge of fire effects on Hg methylation and transport

An important scientific information gap identified in this project is that the biogeochemical processes affecting post-fire methylmercury formation and transport remain poorly understood. It is not currently known why MeHg concentrations increased in the study area post-fire. In the scientific literature, there are some areas that had similar observations, and other areas where MeHg concentrations decreased post-fire.

Some hypotheses regarding biogeochemical processes affecting MeHg include:

- 1) Burning produces bio-char or activated carbon surfaces that are very effective at adsorbing aqueous MeHg that was produced pre-fire and survived in unburned niches. Post-fire, including during the first flush, the concentration of MeHg on suspended particles was higher than pre-fire levels primarily because of changes in the nature of the solid substrate.
- 2) Residual mercury that is not vaporized during fire becomes more oxidized and therefore more reactive and subject to later methylation. Fire is fundamentally an oxidative process, so one would expect the partial conversion of HgS and Hg⁰ to Hg(II)-bearing species. It is well established that Hg(II) is the main precursor to MeHg.
- 3) Fire may affect nutrient cycling in a way that results in stimulation of microbial ecosystems that methylate Hg(II).

To evaluate these competing hypotheses, field and laboratory studies are needed. Field work should include sampling at narrow time intervals during the first flush in a fire-affected area such as the recent Ridge, Pawnee, or County fires in the Cache Creek and Putah Creek watersheds. Laboratory studies could investigate this phenomenon by adding water to dry soils from burned areas of variable burn severity to determine if methylmercury is liberated on first wetting. Confirmation of this finding would indicate that methylmercury was formed previously and was preserved during dry conditions, rather than newly formed by microbial reactions after the first wetting.

Multiple experiments could be carried out to guide modeling efforts. One of the greatest challenges for doing this work is obtaining samples immediately following fire; the use of prescribed fire settings (i.e., controlled burns, which are commonly conducted by various state and federal agencies in California) could decrease the difficulty of sampling a recently burned site and provide opportunities for pre-fire sampling. On freshly burned lands, careful collection of soil, ash, and charcoal should be made initially and then at multiple time intervals to assess the effects of weathering on mercury concentrations and MeHg/THg ratios. Further, use of laboratory techniques such as competitive ligand exchange could be used to quantify MeHg sorption capacity in burned material.

Following burning, watershed export of dissolved organic matter (DOM; measured as dissolved organic carbon, DOC) can increase markedly, at least temporarily (Writer and Murphy, 2012). There is very little information available regarding post-fire relationships between mercury and DOM, though one study by Jensen et al. (2017) measured the relationship between Hg and DOC following burning and found that the slope of the THg:DOC regression line did not vary significantly following burning. Studies of THg:DOC and MeHg:DOC relationships pre- and post-fire in would be helpful in future modeling, and are especially critical for adding filtered THg and MeHg to the PFHydro-WQ model and for applying other watershed models that account for changes in nutrients, mercury and DOC, such as VELMA-Hg model (Golden et al., 2012). These measurements should be confirmed across gradients of burn severities and vegetations types to evaluate whether the relationship remains consistent. Controlled burns and laboratory experiments would be useful settings for this type of work so that pre-fire and post-fire data can be collected with identical protocols and data density, which is necessary for sound statistical analysis.

5.4 Collect data for water flow, suspended sediment, total mercury, and methylmercury in watersheds of interest

The approach developed in this study to modeling the effects of wildfire on surface-water flow and transport of sediment, Hg, and MeHg was intended to be applicable to any watershed. The decision to base model development and initial calibration of the PFHydro and PFHydro-WQ models in the Cache Creek, watershed was based largely on data availability. A logical next step would be to apply the model to other watersheds in California. To do that, suitable data must be identified or collected. Preferably, there would be pre-fire and post-fire data for key parameters including continuous water flow (i.e., a gaging station) and concentrations of suspended sediment and various Hg and MeHg constituents over a wide range of hydrologic conditions.

5.4.1. Prioritizing watersheds: Mercury impairment in Reclamation reservoirs

Currently, the California State Water Resources Control Board is implementing the “Statewide Mercury Control Program for Reservoirs” which will create total maximum daily loads (TMDLs) for mercury in California’s reservoirs (Austin and Smitherman, 2017; SWRCB, 2019). A total of 131 reservoirs that were listed by the State of California as mercury-impaired as of January, 2018 are being considered in the state-wide TMDL process. Seventeen reservoirs that are owned by Reclamation are on the Hg-impaired list; of these, eight are operated by Reclamation and nine are operated by other agencies (**Table 5-1**).

Table 5-1. Reclamation reservoirs in California that are listed by the State of California as impaired by mercury (SWRCB, 2019).

List of Mercury-Impaired Reservoirs Included in the Statewide Mercury Control Program for Reservoirs as of January 2018

Reservoir	Water Board Region	County(ies)	Owner	Operator (if different from owner)
Berryessa, Lake	5	Napa, Yolo	U.S. Bureau of Reclamation	Solano County Water Agency/Solano Irrigation District
Cachuma, Lake	3	Santa Barbara	U.S. Bureau of Reclamation	
Casitas, Lake	4	Ventura	U.S. Bureau of Reclamation	Casitas Municipal Water District
Contra Loma Reservoir	5	Contra Costa	U.S. Bureau of Reclamation	Contra Costa Water District
East Park Reservoir	5	Colusa	U.S. Bureau of Reclamation	Orland Unit Water Users' Association
Folsom Reservoir	5	El Dorado, Placer, Sacramento	U.S. Bureau of Reclamation	
Los Banos Reservoir	5	Merced	U.S. Bureau of Reclamation	California Department of Water Resources
Millerton Lake	5	Fresno, Madera	U.S. Bureau of Reclamation	
Natoma, Lake	5	Sacramento	U.S. Bureau of Reclamation	
New Melones Lake	5	Calaveras, Tuolumne	U.S. Bureau of Reclamation	
O'Neill Forebay	5	Merced	U.S. Bureau of Reclamation	California Department of Water Resources
San Luis Reservoir	5	Merced	U.S. Bureau of Reclamation	California Department of Water Resources
Shasta Lake	5	Shasta	U.S. Bureau of Reclamation	
Solano, Lake	5	Yolo	U.S. Bureau of Reclamation	Solano County Water Agency/Solano Irrigation District
Stony Gorge Reservoir	5	Glenn	U.S. Bureau of Reclamation	Orland Unit Water Users' Association
Trinity Lake	1	Trinity	U.S. Bureau of Reclamation	
Whiskeytown Lake	5	Shasta	U.S. Bureau of Reclamation	

The goals of the state-wide TMDL program are to: “(1) Reduce fish methylmercury concentrations in reservoirs that have already been determined to be mercury-impaired; (2) Have a control program in place that will apply to additional reservoirs when they are determined in the future to be mercury-impaired; and (3) Protect additional reservoirs from becoming mercury-impaired” (Austin and Smitherman, 2017). Notably, one of the strategies for reducing mercury inputs to reservoirs is to control upstream mercury sources.

The pending regulatory framework underscore the need for monitoring and modeling mercury transport in post-wildfire runoff. Hotter and drier climate conditions are leading to increasing fire occurrence in the State (Miller et al., 2009; Westerling et al., 2014) and it is known that wildfires contribute to mercury mobilization and bioaccumulation in streams, lakes, and reservoirs (Caldwell et al., 2000; Kelly et al., 2006). To meet Hg and MeHg loading objectives required under the new TMDLs, managers will need to determine post-fire Hg and MeHg loads using modeling tools. These tools will need to be versatile for a number of different watersheds that may have very different Hg and MeHg sources and loading rates.

Although many of the fish-consumption advisories in California have been linked to legacy mining activities such as mercury mining in the coastal range (e.g., Clear Lake and Cache Creek) and gold-mining areas (Sierra foothills and downstream waterbodies), two of the largest waterbodies in Northern California (Shasta Lake and Lake Almanor) have recently received

mercury consumption advisories and both have minimal legacy mining activity upstream (OEEHA, 2017a,b). The relatively low levels of mining-related contamination in these watersheds suggests watershed contamination from atmospheric deposition, a ubiquitous problem. Future modeling effort should be calibrated across several different watersheds to assess model effectiveness in watersheds with different land use histories.

The State of California’s draft TDML report (Austin and Smitherman, 2017) lists available data for Hg in fish and sediment, and MeHg in water, for the Hg-impaired reservoirs. For the 17 Reclamation-owned reservoirs on the Hg-impaired list, a summary of available data is shown in **Table 5-2**. As of 2017, no Hg data were available for fish in 2 of 17 the reservoirs; no MeHg data were available for water in 9 of the 17 reservoirs; and no Hg data were available for sediment in 6 of the 17 reservoirs.

It would be worthwhile for Reclamation to fill the data gaps indicated in **Table 5-2** so that priorities can be established regarding which watersheds should be targeted for additional data collection and modeling of fire effects, as an extension of the work described in this project. Such monitoring would establish baseline conditions. In a situation where wildfire affects one of these reservoirs, post-fire sampling can then be compared to the baseline data to provide information on fire effects.

Table 5-2. Data for mercury in fish and sediment and methylmercury in water at 17 mercury-impaired Reclamation-owned reservoirs in California (data from Austin and Smitherman, 2017)

	Hg in fish	MeHg in water	THg in Sediment
Lake Berryessa	0.55	na	1.1
Lake Cachuma	na	na	na
Lake Casitas	0.34	na	na
Contra Loma Reservoir	na	na	na
East Park Reservoir	0.39	na	na
Folsom Lake	0.52	0.03	0.073
Los Banos Reservoir	0.55	0.079	0.64
Millerton Lake	0.36	na	0.12
Lake Natoma	0.49	0.026	0.055
New Melones Lake	0.39	0.013	0.21
O’Neill Forebay	0.20	0.048	0.11
San Luis Reservoir	0.61	0.028	0.071
Shasta Lake	0.29	0.014	0.11
Lake Solano	0.43	na	na
Stony Gorge Reservoir	0.32	na	0.11
Trinity Lake	0.43	0.015	0.093
Whiskeytown Lake	0.18	na	na
Total = 17	15	8	11

The Carr Fire (July-August, 2018) affected 229, 651 acres in Shasta and Trinity Counties, California during July-August, 2018 (CalFire, 2019b) including drainages affecting Whiskeytown Lake, Shasta Lake, and Trinity Lake (**Figure 5-2**). The drainages affecting

Whiskeytown Lake were most severely affected, however, the lack of pre-fire data for MeHg in water or THg in sediment at Whiskeytown Lake makes it difficult to quantify fire effects from additional in-reservoir sampling. Nevertheless, collection of post-fire data in these three reservoirs and their tributaries affected by the Carr Fire would provide useful information regarding fire effects on mercury-impaired Reclamation reservoirs. An effort could be made to compile data collected by Reclamation and other agencies in the areas affected by the Carr Fire, including any pre-fire data that may exist.

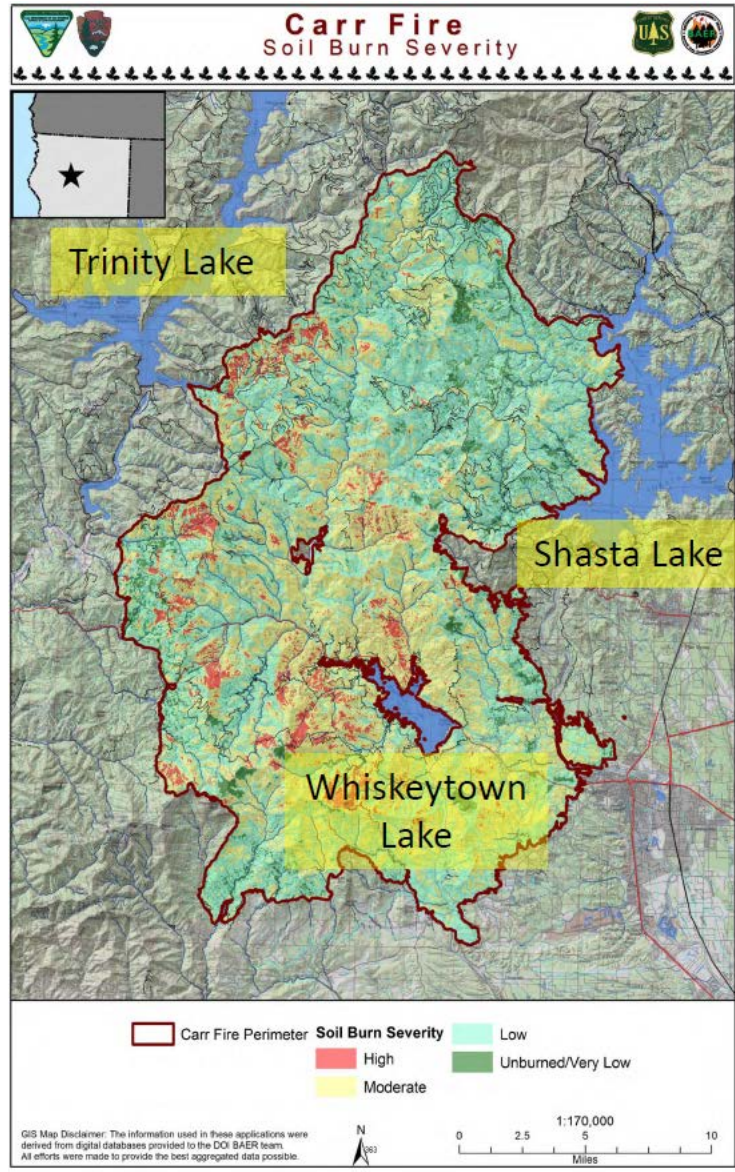


Figure 5-2. Burn severity map for Carr Fire (July-August, 2018) affecting Whiskeytown Lake, Shasta Lake, and Trinity Lake.

5.4.2 Quantifying mercury and methylmercury loads into Reclamation reservoirs

It would be useful to have baseline data on loads of THg and MeHg for inflows and outflows of some or all of Reclamation's 17 Hg-impaired reservoir in California. In particular, loading data for MeHg for reservoir inflows and outflows is critical for establishing a mass balance relationship to evaluate the dominant source(s) of MeHg so that pilot studies can be designed and implemented as part of the TMDL process. The three main sources of MeHg to reservoirs are: (1) upstream tributaries, (2) in-reservoir production in sediment, and (3) in-reservoir production in the water column (Fleck et al., 2018). Data for MeHg loads for reservoir inflows and outflows provide an important data component; together with in-reservoir data on sediment, pore water, and the water column, an evaluation can then be made of MeHg sources (Fleck et al., 2018).

5.5 Update PFHydro and PFHydro-WQ algorithms for the model to be applied in a heterogeneous watershed and simulate SWR effects, simulate Hg/MeHg load more effectively

The current PFHydro model was applied to the Upper Cache Creek Watershed, which was assumed to be homogenous. The model could be updated so that it can be applied to a heterogeneous watershed. In the natural environment soil water repellency (SWR) significantly decreases with increasing soil moisture. For simplicity, the current model assumes SWR remains for the first two years post-fire and remains constant within a single year. An algorithm could be developed to simulate the soil moisture content dynamically year-round to simulate post-fire SWR effects more accurately. The current model implemented a simple approach to simulate Hg/MeHg load. New algorithms could be added to simulate Hg/MeHg fate and transport in the watershed scale.

5.6 Construct a user-friendly interface for PFHydro and PFHydro-WQ and publish documentation

The scope of the current project did not include resources for developing a user-friendly interface for the PFHydro and PFHydro-WQ programs. Such an interface is necessary so that land and water managers and their staff can apply the program to its intended goals of estimating the effects of fire on water flow and transport of sediment, Hg and MeHg on a watershed scale.

It is also necessary to publish documentation of these programs (user's guides) to assist users. If there is sufficient interest, then a training class regarding the use of these program could be provided.

5.7 References

- Austin, C., and Smitherman, L., 2017, Draft Staff Report for Scientific Peer Review for the Amendment to the Water Quality Control Plan for Inland Surface Waters, Enclosed Bays, and Estuaries of California, Mercury Reservoir Provisions - Mercury TMDL and Implementation Program for Reservoirs. April 2017, 401 p., plus figure, tables, and appendices. https://www.waterboards.ca.gov/water_issues/programs/mercury/reservoirs/ accessed Sept. 30, 2019.
- Caldwell, C. A., Canavan, C. M., Bloom, N. S., 2000. Potential effects of forest fire and storm flow on total mercury and methylmercury in sediments of an arid-lands reservoir. *Science of the Total Environment* 260, 125-133.
- CalFire (California Department of Forestry & Fire Protection), 2019a, Ranch Fire (Mendocino Complex). <https://www.fire.ca.gov/incidents/2018/7/27/ranch-fire-mendocino-complex/> Accessed Sept. 30, 2019.
- CalFire (California Department of Forestry & Fire Protection), 2019b, Carr Fire. <https://fire.ca.gov/incidents/2018/7/23/carr-fire/> Accessed Sept. 30, 2019.
- Fleck, J.A., Marvin-DiPasquale, M., Eagles-Smith, C.A., Stewart, A.R., Alpers, C.N., Harris, R., and Krabbenhoft, D.P., 2018, Synthesis of mercury case studies in reservoirs — matching study design to research and management questions. Webinar presentation, May 2, 2018, available at: <https://www.usgs.gov/center-news/webinar-series-mercury-reservoirs>
- Golden, H.E., Knightes, C.D., Conrads, P.A., Davis, G.M., Feaster, T.D., Journey, C.A., Benedict, S.T., Brigham, M.E., and Bradley, P. M., 2012, Characterizing mercury concentrations and fluxes in a Coastal Plain watershed: Insights from dynamic modeling and data: *Journal of Geophysical Research: Biogeosciences*. <https://doi.org/10.1029/2011JG001806>
- Jensen, A.M., Scanlon, T.M., and Riscassi, A.L., 2017, Emerging investigator series: the effect of wildfire on streamwater mercury and organic carbon in a forested watershed in the southeastern United States: *Environmental Science: Processes and Impacts*, v. 19(12), p. 1505-1517.
- Kelly, E.N., Schindler, D.W., St Louis, V.L., Donald, D.B., Vlaclicka, K.E., 2006, Forest fire increases mercury accumulation by fishes via food web restructuring and increased mercury inputs. *Proceedings of the National Academy of Sciences of the United States of America* 103, 19380-19385.
- Miller, J.D., Safford, H.D., Crimmins, M., Thode, A.E., 2009. Quantitative evidence for increasing forest fire severity in the Sierra Nevada and Southern Cascades Mountains, California and Nevada, USA: *Ecosystems*, v. 12, p. 16-32.
- OEHHA (Office of Environmental Health Hazard Assessment), 2017a, Information about Eating Fish from Shasta Lake. Fact sheet. Sacramento, CA. <https://oehha.ca.gov/advisories/shasta-lake>

Accessed Feb. 08, 2018.

OEHHA (Office of Environmental Health Hazard Assessment), 2017b, Information about Eating Fish from Lake Almanor. Fact sheet. Sacramento, CA. <https://oehha.ca.gov/advisories/lake-almanor> Accessed Feb. 8, 2018.

SWRCB (State Water Resources Control Board), 2019, Statewide Mercury Control Program for Reservoirs. California State Water Resources Control Board, Sacramento, CA. https://www.waterboards.ca.gov/water_issues/programs/mercury/reservoirs/ accessed Sept. 30, 2019.

Westerling, A., Brown, T., Schoennagel, T., Swetnam, T., Turner, M., and Veblen, T., 2014. Briefing: Climate and wildfire in western US forests, In: Sample, V.A., and Bixler, R.P. (eds.), Forest conservation and management in the Anthropocene: Conference proceedings. Proceedings. RMRS-P-71. Fort Collins, CO: US Department of Agriculture, Forest Service. Rocky Mountain Research Station. pp. 81-102.

Writer, J.H., and Murphy, S.F., 2012, Wildfire effects on source-water quality—Lessons from Fourmile Canyon fire, Colorado, and implications for drinking-water treatment: U.S. Geological Survey Fact Sheet 2012–3095, 4 p. <https://pubs.usgs.gov/fs/2012/3095/FS12-3095.pdf>

Appendix 1: Accepted Manuscript by Environmental Modeling and Software for Publication

PFHydro: A New Watershed-Scale Model for Post-Fire Runoff Simulation

Jun Wang, U.S. Bureau of Reclamation, Sacramento, CA
Michelle Stern, U.S. Geological Survey, Sacramento, CA
Vanessa M. King, U.S. Bureau of Reclamation, Sacramento, CA
Charles N. Alpers, U.S. Geological Survey, Sacramento, CA
Nigel W.T. Quinn, Berkeley National Laboratory, Berkeley, CA
Alan Flint, U.S. Geological Survey, Sacramento, CA
Lorraine Flint, U.S. Geological Survey, Sacramento, CA

Abstract

Runoff increases after wildfires that burn vegetation and create a condition of soil-water repellence (SWR). A new post-fire watershed hydrological model, PFHydro, was created to explicitly simulate vegetation interception and SWR effects for four burn severity categories: high, medium, low severity and unburned. The model was applied to simulate post-fire runoff from the Upper Cache Creek Watershed in California, USA. Nash–Sutcliffe modeling efficiency (NSE) was used to assess model performance. The NSE was 0.80 and 0.88 for pre-fire water years (WY) 2000 and 2015, respectively. NSE was 0.88 and 0.93 for WYs 2016 (first year post-fire) and 2017 respectively. The simulated percentage of surface runoff in total runoff of WY 2016 was about **six** times of that of pre-fire WY 2000 and **three** times that of WY 2015. The modeling results suggest that SWR is an important factor for post-fire runoff generation. The model was successful at simulating SWR behavior.

Key words: wildfire effects, post-fire runoff simulation, watershed model, soil water repellence

Highlights

- A new physically based model to simulate post-fire runoff at a watershed scale.
- Four burn severity categories considered: high, medium, low and unburned.
- Explicitly simulated vegetation interception and fire-induced, soil water repellence effects.
- Model incorporates both saturation-excess and infiltration-excess runoff generation mechanisms.
- Model calibrated and validated for a wildfire-prone watershed in California, USA.

1. Introduction

In addition to the immediate threat posed by wildfires, such events can also threaten natural resource sustainability by increasing runoff and erosion in the years following a fire. Increased post-fire surface runoff is directly associated with increased erosion and mud flow.

Experimental plot and hillslope-scale studies indicate that wildfires may increase rainfall-event-induced runoff and soil erosion by a factor of 2–40 on small-plot scales and by more than 100-fold on large-plot to hillslope scales (Williams et al., 2014). In burned areas, annual suspended sediment yields can increase by a factor of between 1 and 1,459 as compared with suspended sediment yields under unburned conditions (Smith et al., 2011). For example, sedimentation from flooding after the 1996 Buffalo Creek Fire in Colorado reduced Denver’s municipal reservoir capacity by roughly a third (Agnew *et al.* 1997). The Thomas Fire of southern California (December 4, 2017 – January 12, 2018), which burned 1141 square kilometers (km²), was followed by heavy rains that led to mudflows and 21 deaths in the unincorporated community of Montecito in Santa Barbara County, California (Dolan, 2018).

The runoff response from burned watersheds is a function of rainfall amount and intensity, burn severity, and properties of the impacted soils and vegetation cover (Moody and Martin, 2001; Benavides-Solorio and MacDonald, 2005; Spigel and Robichaud, 2007). The reduction of vegetation cover may reduce interception, thereby reducing moisture storage, increasing water yields, and creating greater runoff with smaller storms, while the elimination of transpiration increases soil moisture and streamflow (Neary et al., 2003). The first-order effect of fire on runoff and erosion is decreased interception. Unburned shrubs and conifers can intercept up to 35% of rainfall during high intensity storms and 80% of rainfall during low intensity storms (Rowe, 1948; Hamilton and Rowe, 1949; Skau, 1964; Tromble, 1983; Owens et al., 2006). Rainfall interception by rangeland plants can reduce erosivity of high-intensity rainfall by up to 50% (Wainwright et al., 1999; Martinez-Mena et al., 2000). Numerous studies in forested areas have found rainfall erosivity and its dissipation by vegetation cover to be the primary factors controlling post-fire erosion rates (Inbar et al., 1998; Moody and Martin, 2001; Benavides-Solorio and MacDonald, 2005; Spigel and Robichaud, 2007; Robichaud et al., 2008; Moody and Martin, 2009; Robichaud et al., 2013a, 2013b).

In addition to changes in rainfall interception, wildfire can cause the alteration of soil physical and chemical properties that can impact soil structure and increase soil-water repellence (SWR) for a significant period of time. Numerous watershed-scale studies considered fire-induced SWR to be a major factor controlling post-fire runoff and erosion rates (Morris and Moses, 1987; Imeson et al., 1992; Shakesby et al., 2000; Letey, 2001). Post-wildfire infiltration into the unsaturated zone is controlled by fire-induced changes in soil-water storage and soil hydraulic properties. After a fire, water repellency is typically found as a discrete layer of variable thickness and spatial continuity found on the soil surface or a few centimeters below and parallel to the mineral soil surface. Water repellency has been shown to be created and intensified by soil heating that occurred during a fire (DeBano, 1966; DeBano and Krammes, 1966). This soil condition dramatically reduces infiltration, increases overland flow, and

consequently amplifies the risk of severe erosion. Increased SWR and reduced vegetation interception/protection are major causes of increased post-fire overland flow and erosion. Under field conditions, the water-repellent soil layer is not typically continuous, so irregular wetting patterns are common (Bond, 1964; Meeuwig, 1971; DeBano, 1981; Dekker and Ritsema, 1995). An increase in bare ground post-fire increases the connectivity of water-repellent soil patches (Shakesby et al., 2000; Doerr and Moody, 2004; Cawson et al., 2010; Nyman et al., 2010). A possible threshold of 60–70% bare ground was found to be related to the connectivity of the bare patches (Johansen et al., 2001) and seemed to explain much of the post-wildfire erosion caused by increased runoff (Moody et al, 2013). Another commonly observed phenomenon is that SWR decreases with increasing soil moisture (MacDonald and Huffmann, 2004). Once wet, soils are no longer water repellent until they become desiccated (Doerr and Thomas, 2000). For unburned soils, soil moisture thresholds that mark the range of soil infiltration properties from hydrophobic to hydrophilic occur between 2 and 5% moisture for a dune sand (Dekker et al., 2001), 5 to 12% moisture for naturally hydrophobic soils (de Jonge et al., 1999), and 34 to 38% moisture for clayey peat soils (Dekker and Ritsema, 1995). There are very few data that can be used to suggest a soil moisture threshold for the elimination of SWR; however, Doerr and Thomas (2000) noted an absence of SWR once the soil moisture content exceeded 28% in a coarse-textured forest soil in Portugal. Huffman et al. (2001) reported that the soil moisture threshold ranged from about 12% in unburned areas to above 25% in severely burned areas in experiments conducted in the Colorado Front Range. A study by MacDonald and Huffmann (2004) suggested that the soil moisture threshold for the shift from hydrophobic to hydrophilic soil properties was about 10% for unburned sites, 13% for sites burned at low severity, and 28% for sites burned at moderate severity.

Depending on the post-fire response domain, hillslope-runoff-generating processes may be described by either of two conceptual models of runoff generation, or a combination of both: infiltration-excess or saturation-excess overland flow (Dunne, 1978; Wondzell and King, 2003; Keizer et al., 2005; Onda et al., 2008; Ebel et al., 2012). Under the former model, the runoff volume is limited by the infiltration capacity of the soil. Under the latter model, the saturation state of the soil limits any further infiltration. The relative weight of the two runoff-generating processes can vary on steep hillslopes between successive rainfall events (Schmidt et al., 2011). Post-fire, both runoff-generating mechanisms can occur within the same watershed. In humid areas, saturation-excess runoff processes typically dominate under pre-fire conditions, whereas infiltration-excess runoff processes are expected to dominate in burned areas during the first 1-2 years post-fire while SWR effects remain.

For the above reasons, a realistic post-fire, watershed-scale runoff model should simulate the following: (a) both infiltration-excess and saturation-excess overland flow; (b) vegetation precipitation interception for pre- and post-fire conditions; and (c) post-fire soil water repellent behavior. In this paper, we introduce PFHydro, a new watershed-scale post-fire runoff model that simulates those three phenomena and demonstrate its application to the Upper Cache Creek Watershed in northern California.

1.1. Review of post-fire rainfall-runoff simulation models

There are several existing public-domain and proprietary models that are used to simulate post-fire effects on rainfall-runoff generation. Much of the hydrological research literature has focused on predicting peak discharge of post-fire runoff by using the paleo-flood method (e.g. Jarrett and England, 2002), the curve number method (Hawkins and Greenberg, 1990; Cerrelli, 2005; Foltz et al., 2009), or direct measurements from burned basins (Moody and Martin, 2001; Moody et al., 2008; Foltz et al., 2009; Kean et al., 2011; Moody, 2012). Little research has covered predicting flood timing relative to rainfall (Elliot et al., 2010).

Early models utilized the rational method to compute total discharge ($Q=CIA$, where C is runoff coefficient, I is rainfall intensity, and A is contributing area), which was designed to calculate the flood peak flow under the assumption that the intensities of both rainfall and infiltration were uniformly distributed in time and space (Ponce, 1989). However, curve number methods had difficulties accounting for fire effects (Moody et al, 2013). For post-fire hydrology simulation, Moody et al. (2008) developed a new burn severity variable known as the hydraulic functional connectivity (Φ), which incorporates both the magnitude of the burn severity and the spatial sequence of the burn severity along hillslope flow paths. The runoff coefficient C became a linear function of the mean hydraulic functional connectivity of the subwatersheds. The dimensionless hydraulic functional connectivity Φ was computed as follows:

$$\phi_i = \frac{1}{\alpha} \sum_{i=1}^k \alpha_{ij} \Delta NBR_{ij} S_{ij}^{1/2} \quad (1)$$

where α_{ij} is a weighting factor equal to the uphill contributing area to pixel i in flow path j , S_{ij} is the local slope from pixel i to the next downstream pixel in flow path j , α is the total area of the flow path, and the differenced Normalized Burn Ratio (NBR), $\Delta NBR = NBR_{prefire} - NBR_{postfire}$. The total discharge per unit area from a subwatershed could then be represented by the sum of the Φ_i values for each flow path normalized by the number of flow paths.

Luce (2001) developed the Fire Enhanced Runoff and Gully Initiation (FERGI) model, a physically based mathematical description of hillslope hydrologic and geomorphic response for a given set of weather events. FERGI estimated the probability of post-fire rainfall excess, the quantity of runoff generated, and the initiation of gully erosion on hillslopes with and without mitigations using contour-felled logs or log erosion barriers.

A significant advance in physically based, numerical process models for simulating runoff and erosion from simple hillslopes or watersheds came with the introduction of the Water Erosion Prediction Project (WEPP) model (Flanagan et al., 1995). The GIS-based GeoWEPP version of the model (GeoWEPP ArcX 2003; Renschler, 2003), which utilizes ArcGIS software, combines the WEPP v2002.7 model (Flanagan et al., 1995) with Topography Parameterization software (TOPAZ) (Garbrecht and Martz, 1997) to predict runoff and erosion at the hillslope and watershed scale. GeoWEPP was developed to allow WEPP hillslope parameterization to be based on digital data sources, such as digital elevation models (DEMs), and for digital outputs to be viewed and analyzed in a GIS environment (Renschler, 2003). An online GIS interface for the WEPP watershed model was developed to help input spatial files for forested applications including the impacts of wildfire (Frankenberger et al., 2011). This simplifies downloading or pre-processing of topographic, soils, or land cover databases necessary for running the

GeoWEPP model (Miller et al., 2015). WEPP and GeoWEPP were also applied to simulate post-fire runoff and soil erosion (Elliot et al., 2006; Miller et al., 2016). The soil burn severity map was an input for WEPP and GeoWEPP simulations to help to quantify burn effects on soils runoff and erosion.

Kinoshita et al. (2014) reviewed five models for post-fire peak discharge predictions: the Rowe Countryman and Storey (RCS) (Rowe et al., 1949), United States Geological Survey (USGS) Linear Regression Equations (Foltz et al., 2009), USDA Windows Technical Release 55 (USDA, 2009), Wildcat5 (Hawkins and Munoz, 2011), and U.S. Army Corps of Engineers (USACE) Hydrologic Modeling System (HEC-HMS) (USACE, 2010). The TR_55, HEC-HMS and Wildcat5 were curve number-based models. These models were applied to eight diverse basins in the western United States affected by wildfires. According to Kinoshita et al. (2014), no one model performed sufficiently well for application to all study sites. The review results showed inconsistency between model predictions for events across the sites and poor results with larger return periods (25- and 50-year events) and when applied to post-fire watershed simulations.

Chen et al. (2013) evaluated the capability of four models representing empirical, semi-empirical, and process-oriented methods for simulation of post-fire hydrology using data from the San Dimas Experimental Forest (SDEF), San Dimas, California. The four models are: empirical-based Rule of Thumb by Kuyumjian (Foltz et al., 2008) and Rational Method (MODRAT) (LACDPW, 1991), semi-empirical HEC-HMS, and physical, process-oriented KINematic Runoff and EROSion Model 2 (KINEROS2) (Goodrich et al., 2005). These modeling studies showed that simple, empirical peak flow models may perform acceptably if calibrated correctly. However, these models may not be applicable for watersheds outside the area where they were calibrated when they do not incorporate pertinent hydrological mechanisms. Analysis by Chen et al. (2013) suggests that the runoff-generation mechanism in the watershed may have changed from a saturation-excess runoff to an infiltration-excess dominated runoff mechanism due to fire effects. Physically based, process-oriented models can be valuable for in-depth analysis of pre- and post-fire hydrographs and provide consistent and satisfactory predictions (Chen et al., 2013).

In summary, most hydrological models simulating post-fire runoff are event-based for peak discharge using curve-number or regression methods. The curve-number-based models are best applied to small watersheds where infiltration-excess mechanism dominates. Regression-method-based models are limited to use in watersheds with similar characteristics to the watershed for which the regression equations were developed. However, burn severity, which represents the post-fire impacts on vegetation and soil characteristics and subsequent rainfall runoff response, needs to be incorporated into this modeling approach. The physically based WEPP/GeoWEPP model that incorporates burn severity has been applied in some watersheds to simulate post-fire runoff and soil erosion in a hillslope and watershed scale. However, this and other models are limited in their capability to simulate post-fire runoff when vegetation cover and soil properties change, due to changes in factors such as vegetation interception, evapotranspiration, and water repellency. A physically based model is needed that can quantify post-fire changes in vegetation interception and water repellency and has both saturation-excess and infiltration-excess runoff generation mechanisms to improve simulation of wildfire effects on runoff generation and subsequent soil erosion on a watershed scale.

2. Methods to the development of a new post-fire hydrologic model

A new watershed scale post-fire hydrologic model, PFHydro, was created based on UFORE-Hydro (Wang et al., 2005, Wang et al., 2008) by integrating algorithms to quantify SWR effects and modifying the model structure to simulate rainfall runoff in both unburned areas and burned areas with four burn severity categories. UFORE-Hydro (now called i-tree hydro) which is based on TOPMODEL theory (Beven and Kirkby, 1979, Beven, 1997a, Beven, 1997b, Kirkby, 1997), can simulate rainfall runoff process in a watershed scale (snowmelt component is under development)

2.1 A summary of UFORE-Hydro and TOPMODEL theory

TOPMODEL has been used for numerous watershed hydrologic simulation applications. TOPMODEL is a semi-distributed hydrological model that assumes that watershed topography exerts control of flow routing through upland catchments. The model allows variable contributing area and catchment topography and allows for variable soil transmissivity with soil depth to improve the simulation of watershed runoff. The original TOPMODEL code was applied to catchments with shallow soils and moderate topography, which typically do not experience extended dry periods. Saturation-excess overland flow processes are likely to dominate in this type of catchment. A later version of TOPMODEL (Beven, 1984) used the exponential Green-Ampt model to calculate infiltration-excess runoff. A major advantage of TOPMODEL is its simplicity, which is exemplified by the use of the topographic index, $TI = \ln(a/\tan\beta)$, where a is the upslope contributing area per unit contour length and $\tan\beta$ represents the local slope. TI is used as an index of hydrological similarity. All points with the same index value are assumed to respond in a hydrologically similar way. Hence, it is only necessary to make calculations for points with different index values, spanning the index distribution function for a catchment.

Enhancements to the standard TOPMODEL code were made to create the UFORE-Hydro model (Wang et al., 2005, Wang et al., 2008), a more flexible tool for simulating pre-wildfire hydrologic events. The specific enhancements include: (a) a soil topographic index; (b) a power function for the decay of transmissivity with soil depth; and (c) a vegetation interception routine. The Topographic Index approach recognizes that the saturated surface transmissivity $T(z)$ of the soil varies widely over the area of the catchment. The topographic index $TI = \ln(a/\tan\beta)$, for each point in the catchment was replaced by a soil topographic index $STI = \ln(a/T_0 \tan\beta)$, where T_0 is the saturated surface soil transmissivity for each cell. This addition provides model flexibility and allows the model to deal with catchment heterogeneity more readily. Users are required to provide an initial T_0 value for each cell or provide T_0 for several blocks of cells representing different soil types.

To simulate the decline of transmissivity with soil depth, TOPMODEL uses an exponential function $T(z) = T_0 \text{Exp}(-S_i/m)$ that results in the indices TI and STI , as defined above. In this formula, T_0 is the transmissivity at saturation, S_i is the local saturation deficit, and m is a scaling parameter. Beven (1984) demonstrated that this profile signature was not universal, however it was appropriate for many soil profile hydraulic conductivity data sets. A generalized power function decay term, $T(z) = T_0(1 - S_i/m)^n$ (Ambroise et al., 1996, Iorgulescu and Musy, 1998), was incorporated into the UFORE-Hydro model to help represent the soil infiltration characteristics of different soil types. The user can select a value of n for a particular simulation,

which provides flexibility in modeling runoff hydrograph recession characteristics, particularly when soil transmissivity varies with depth and complicates soil infiltration estimation. For exponential decay of soil transmissivity and estimated infiltration, the Topographic and Soil Topographic indices take the following forms:

$$\text{Topographic index: } TI = \ln(a/\tan\beta); \text{ Soil topographic index: } STI = \ln(a/T_0 \tan\beta)$$

For those infiltration events that follow a generalized power function decay pattern for soil transmissivity and estimated infiltration, the index is modified as follows:

$$\text{Topographic index: } TI = (a/\tan\beta)^{1/n}; \text{ Soil topographic index: } STI = (a/T_0 \tan\beta)^{1/n}$$

2.1.1. Simulation of subsurface flow

An important next step in model development involves calculating subsurface flow based on estimates of soil infiltration. For homogenous watersheds using the topographic index where soil hydraulic conductivity decays with soil depth exponentially, the resultant equation for subsurface flow [L/T] is:

$$q_{\text{subsurface}} = T_0 e^{-\lambda} e^{-\frac{\bar{s}}{m}} \quad (2)$$

where $\lambda = 1/A \int \ln(a/\tan\beta) dA$ is the average topographic index, A is contributing area, and $\bar{s} = -m \ln(R/T_0) - m\lambda$ is the average soil moisture deficit under λ .

Watershed soils are rarely homogeneous, hence when using the soil topographic index for heterogenous conditions, the equation for subsurface flow becomes:

$$q_{\text{subsurface}} = e^{-\lambda} e^{-\frac{\bar{s}}{m}} \quad (3)$$

where $\lambda = 1/A \int \ln(a/T_0 \tan\beta) dA$ is the average soil topographic index, and $\bar{s} = -m \ln R - m\lambda$ is the average soil moisture deficit under λ .

The generalized power function decay of mean subsurface flow using the topographic index in the case where soil hydraulic conductivity decays with soil depth in a power function profile and where the watershed is homogenous is given as:

$$q_{\text{subsurface}} = T_0 \lambda^{-n} \left(1 - \frac{\bar{s}}{m}\right)^n \quad (4)$$

where $\lambda = 1/A \int (a/\tan\beta)^{\frac{1}{n}} dA$ is the average topographic index, and $\bar{s} = -m[1 - (R/T_0)^{1/n} \lambda]$ is the average soil moisture deficit under topographic index λ .

For a heterogeneous watershed using the same soil topographic index and assuming soil hydraulic conductivity decay with depth in a power function profile, the mean subsurface flow can be estimated using:

$$q_{\text{subsurface}} = \lambda^{-n} \left(1 - \frac{\bar{S}}{m}\right)^n \quad (5)$$

where $\lambda = 1/A \int (a/T_0 \tan \beta)^n dA$ is the average soil topographic index, and $\bar{S} = -m[1-R^{1/n} \lambda]$ is the average soil moisture deficit under λ .

2.1.2. Simulation of saturation excess and infiltration excess overland flow

A major conceptual model improvement in the simulation of rainfall-induced runoff has been the recognition of two main mechanisms of soil infiltration that affect overland flow. The saturation-excess overland flow algorithm considers the moisture status of the soil during a precipitation event. The overland flow rate, $q_{\text{overland}} [L/T]$, is calculated as a function of the rainfall throughfall and the moisture status (degree of saturation) of the hillslope area as follows:

$$q_{\text{overland}} = \frac{A_{\text{sat}}}{A} P \quad (6)$$

where (A_{sat}/A) is the fraction of the hillslope area that is saturated, and $P [L/T]$ is the throughfall. The infiltration-excess overland flow conceptual model, on the other hand, is represented by an infiltration rate, i , defined by Beven (1984) as follows:

$$i = \frac{dI}{dt} = \frac{\Delta\psi + Z}{\int_{z=0}^{z=Z} \frac{dz}{K_z}} \quad (7)$$

where I is the cumulative infiltration [L], K_z is the hydraulic conductivity at soil depth z , and $\Delta\psi$ is the effective wetting front suction. Two independent algorithms were developed to account for different decay rates of infiltration with depth in the soil profile:

$$\text{For exponential decay: } K_z = K_0 e^{-fz} \quad (8)$$

$$\text{For power function decay: } K_z = K_0 (1 - fz)^n \quad (9)$$

where f is a scaling parameter. In general, the saturation-excess overland flow mechanism is most often applied to forested areas where rapid infiltration into shallow forest soils produces vadose zone saturation that acts to initiate soil runoff. The infiltration-excess overland flow mechanism is more applicable to arid areas and post-fire applications where the top soil layers with SWR are the major limitation to infiltration of precipitation and typically leads to an earlier onset of overland flow.

2.1.3. Simulation of vegetation interception

In watersheds subject to wildfire, the presence of vegetation before a fire and the removal of vegetation as a result of the fire can have a significant effect on rainfall interception and erosivity. The UFORE-Hydro vegetation interception routine (Wang et al., 2008) maintains a continuous water balance of rainfall canopy interception and directs a portion of the intercepted flow along the vegetative stem (plant branches and trunk) in a similar manner to the algorithm developed by Rutter (Rutter et al., 1971, 1975). This algorithm also accounts for the effect of

precipitation intensity, duration and changing vegetation cover on both rainfall throughfall and canopy interception according to the expression:

$$\frac{\Delta C}{\Delta t} = P - R - E \quad (10)$$

where C (m) is the depth of water on the unit canopy at time t , P (m/s) is above-canopy precipitation rate, R (m/s) is the below-canopy throughfall precipitation rate that reaches the ground (reduced from total P by canopy interception), E (m/s) is the evaporation rate from the wet canopy, and Δt is the simulation time interval (s).

This model allows a small amount of precipitation to fall through the canopy as free throughfall (P_f) without contact with vegetation, and allows interception to increase to a threshold C_{max} , which is the maximum water retained on the canopy. In this case R is equal to P_f . In the UFORE-Hydro model the value of P_f was selected to be complementary to the canopy cover fraction, c , which is related to the canopy leaf area index (LAI) and is relative to the fraction of watershed with vegetation cover following van Dijk and Bruijnzeel (2001). Canopy leaf storage, S , is defined as the water retained on the canopy that would not drain to the ground under normal conditions. This results in the following set of equations:

$$P_f = P(1 - c) \quad (11)$$

$$c = 1 - e^{-\kappa LAI} \quad (12)$$

$$S = S_L LAI \quad (13)$$

where κ is an extinction coefficient and S_L (m) denotes specific leaf storage. The effective vegetation coverage of a watershed is reduced post-fire. The total amount of precipitation that reaches the ground is increased in direct proportion to the burn area and contributes to increased runoff and overland flow.

2.2. Simulating SWR effects in burned areas

As might be expected, the most severe fires typically have the greatest impact on the infiltration characteristics of forest, woodland, and grassland soils. Fire severity affects saturated hydraulic conductivity (K_{sat}) due to factors that change water repellency, including sealing of macropores and combustion of organic matter in near-surface soil layers within the profile (Neary, 2011). High water repellency can reduce K_{sat} to low values or even zero (DeBano et al. 1998; Neary et al., 2005). For a typical high-severity burn, hydrophobic or water-repellent soil conditions can cause a temporary 10–40% reduction in the K_{sat} values in comparison with a normal infiltrating soil (Robichaud, 2000). Blake et al. (2009) noted K_{sat} reductions of 88 to 92% with high severity wildfire. Saturated hydraulic conductivity reductions of 20 to 48% are commonly reported (Neary, 2011).

Hence, in the new PFHydro model, the saturated hydraulic conductivity of watershed soils is assigned based on burn severities (unburned, low severity burn, medium severity burn, and high severity burn). The saturated hydraulic conductivities of burned areas can be assigned relative to the unburned saturated hydraulic conductivity K_{sat} , as follows:

1. High severity: μK_{sat}
2. Medium severity: $1.2\mu K_{sat}$
3. Low severity: $1.4\mu K_{sat}$

where μ is a calibration parameter with values between 0.1 and 0.7 that assumes K_{sat} reductions of 30% to 90% with high severity burn. Here K_{sat} is equivalent to K_0 in equations 8 and 9. There is no known previous research on the relationship between K_{sat} of different burn severities.

For PFHydro, the saturated hydraulic conductivity of the low-severity burn area was set to $1.4\mu K_{sat}$ to ensure its value is lower than the saturated hydraulic conductivity of the unburned area for the range of μ between 0.1 and 0.7. The saturated hydraulic conductivity for the medium-severity burn area was then set to $1.2\mu K_{sat}$, the midpoint between the values for high- and low-severity areas.

The SWR connectivity Φ is a calibration parameter in the PFHydro model with a value between 0 and 1 that represents the fraction of runoff from the burned soils that can be routed to the channel network without further infiltration into the surrounding surface soil.

The SWR significantly decreases with increased surface soil moisture (MacDonald and Huffmann, 2004). Researchers have documented persistence of SWR effects from weeks to years (DeBano et al., 1967; Holzhey 1969). In general, SWR-induced hydrophobicity is broken up, or is sufficiently washed away, within one to two years after a fire (Ritsema and Dekker, 2003). The PFHydro post-fire runoff model makes a simplifying assumption that SWR effects decreased the 2nd year compared to 1st year post-fire, but the effects remain constant within each one-year period post-fire.

3. Modeling application area

One of the major challenges in developing watershed hydrologic and water quality models applicable to wildfire impacts is the difficulty in obtaining appropriate time-series data given the remoteness of the terrain being analyzed and the high cost of obtaining a comprehensive data set. Many watersheds in California have been affected by major wildfire events in recent years, and major fires appear to have become more severe and more costly in terms of lives lost and property damage over the recent decades (Westerling et al., 2014). The Upper Cache Creek Watershed covers portions of Lake County, Yolo County, and Colusa County in northern California (Figure 1). It has an area of 3,017 square kilometers (km^2), with elevations ranging from approximately 0 to 1800 meters and a total population of about 58,000 (Sacramento River Watershed Program, 2018). This region does not experience significant amounts of snowfall.

During July-August 2015, the Jerusalem and Rocky fires burned a combined 384 km^2 and about 214 km^2 within the Upper Cache Creek watershed downstream of Clear Lake (Figure 2). The fires varied in intensity across the watershed, resulting in spatially variable changes of soil properties and reductions in vegetation cover. A gauged sub area of the Upper Cache Creek Watershed was chosen for the model application area, comprising 282 km^2 in which 163 km^2 were burned. The Shuttle Radar Topography Mission (SRTM) 1-arcsecond digital elevation model (DEM) (USGS, 2014) was reprojected into the State Plane California II coordinate system using ArcGIS and then resampled to a grid size of 30 meters for input into the UFORE-Hydro model for pre-fire hydrological simulations and PFHydro model for post-fire hydrological simulations.

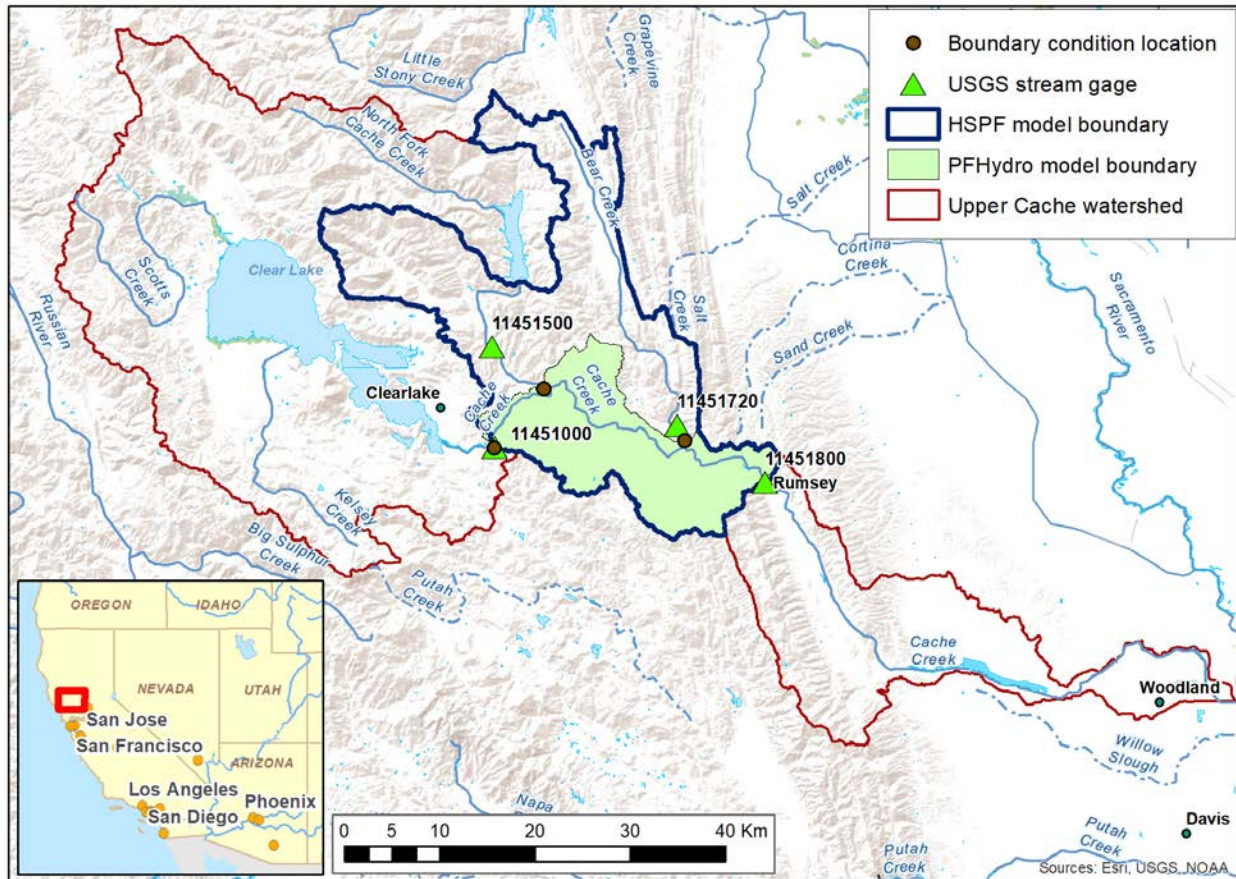


Figure 1: Location of Upper Cache Creek Watershed in northern California showing boundaries for the HSPF model and PFHydro model. The UFORE-Hydro model boundary is equivalent to the PFHydro model boundary. The map also shows flow monitoring stations located along Cache Creek with outflow from the study watershed at the Rumsey gauge (green triangles), along with locations for hourly time series flow from the HSPF model used as boundary conditions for the PFHydro model (see Section 4.4).

3.1 Model Vegetation Burn Estimation

The Rocky and Jerusalem Fire events occurred during the 2015 fire season. The Rocky Fire burned from July 29 to August 14, 2015 and the Jerusalem Fire burned from August 9 to August 25, 2015. The two fires merged on August 12, 2015. Burn severity data for the fires used the Burned Area Reflectance Classification (BARC), a satellite-derived layer of post-fire vegetation conditions. BARC classifies data into four burn severity classes: high, moderate, low, and unburned, based on the relationship between near- and mid-infrared reflectance values (USFS Geospatial Technology and Applications Center, 2018).

The Rocky and Jerusalem Fires were considered a single fire for modeling purposes and the burn severity classification areas were merged accordingly. Figure 2 shows the burn severity classifications for the combined Rocky and Jerusalem Fires, with the model boundary shown for reference. The areas and percentages of each burn severity class within the model boundary are shown in Table 1.

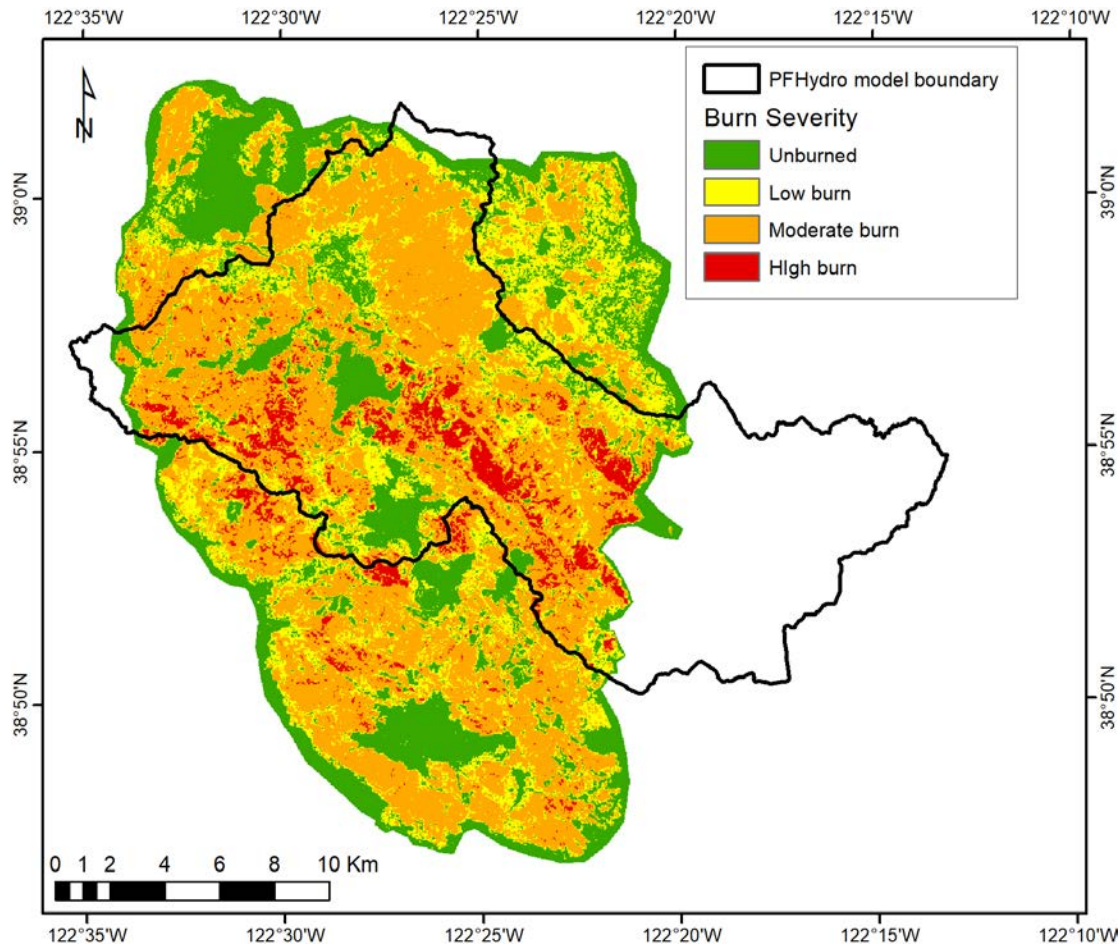


Figure 2: Burn severity classifications for combined Rocky and Jerusalem Fires. The model application area boundary is shown for reference on the map in the area outlined in black.

The percentages of trees and short vegetation pre- and post-fire are used as inputs to PFHydro, in order to calculate the effects of vegetation interception. Two Landsat 8 images were selected for land-cover classification, namely: a pre-fire image taken on July 27, 2015, and a post-fire image taken on September 4, 2015. These images were selected because of their temporal proximity to the start and end dates, respectively, of the Rocky and Jerusalem fires, and their lack of visible cloud cover.

Table 1: Area and percent area in each burn severity class within the model application area.

Burn severity	Area (km ²)	Percent
Unburned	118.7	42.1
Low Burn	35.3	12.5
Moderate Burn	108.6	38.5
Severe Burn	19.4	6.9

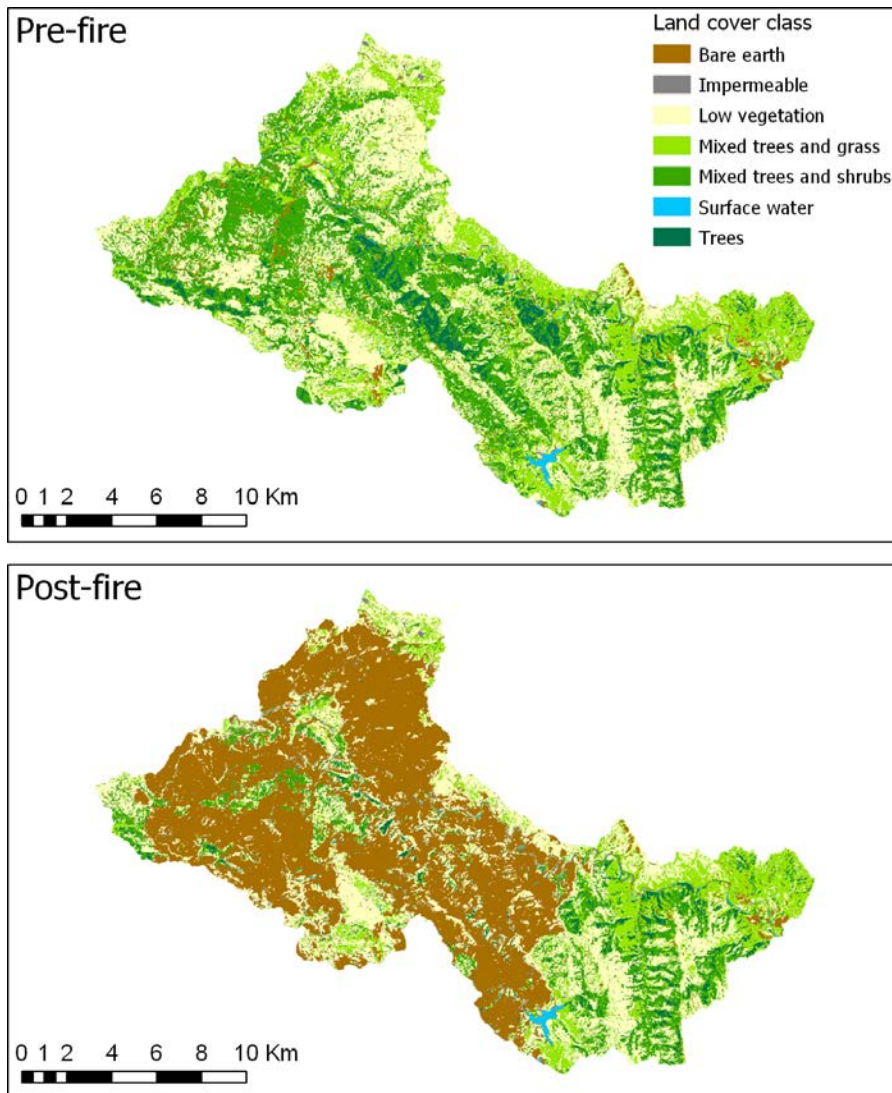


Figure 3: Pre- and post-fire land cover classifications for the model application area showing the major vegetation categories and the extent of the burn area in 2015.

Supervised land-cover classification was performed in ArcGIS Pro. The study area contains numerous areas where trees and short vegetation are mixed on scales smaller than the imagery's 30-meter pixel size. To account for this, two additional classes were created: one for mixed trees and shrubs, and one for mixed trees and grass. The mixed trees and shrubs class was estimated by visual inspection to contain approximately 50% trees and 50% short vegetation, while the mixed trees and grass class was estimated to contain approximately 30% trees and 70% short vegetation. After classification (Figure 3), the areas in these classes were split into trees and short vegetation using these percentages to obtain the areas in each of the final five classes listed above and for each burn severity classification (Table 2). The data in Table 2 was input to PFHydro model for post-fire runoff simulation.

Table 2: Areas and percentages of land use in each burn severity class and vegetation classification for the total modeling area showing a significant reduction in live vegetation post-fire.

Burn Severity	Class Name	Pre-fire		Post-fire	
		Area (km ²)	Percent	Area (km ²)	Percent
Total	Trees	87.4	30.9	37.1	13.2
	Low Vegetation	183.8	65.1	107.7	38.2
	Impermeable	0.6	0.2	2.6	0.9
	Surface water	1.5	0.5	1.6	0.6
	Bare earth	9.2	0.3	132.6	57.1
Unburned	Trees	33.0	27.8	32.9	27.8
	Low Vegetation	78.4	66.1	78.4	66.1
	Impermeable	0.6	0.5	0.6	0.5
	Surface water	1.1	0.9	1.1	0.9
	Bare earth	5.5	4.6	5.5	4.6
Low burn	Trees	10.2	29.0	2.6	7.4
	Low Vegetation	22.8	64.8	18.4	52.3
	Impermeable	0.0	0.1	1.1	3.1
	Surface water	0.3	0.8	0.2	0.7
	Bare earth	1.9	5.3	12.9	36.5
Moderate burn	Trees	33.1	30.5	1.5	1.4
	Low Vegetation	73.5	67.8	10.0	9.3
	Impermeable	0.0	0.0	0.8	0.7
	Surface water	0.1	0.1	0.2	0.2
	Bare earth	1.8	1.7	95.9	88.4
Severe burn	Trees	10.9	56.4	0.1	0.7
	Low Vegetation	8.5	43.6	0.8	4.3
	Impermeable	0.0	0.0	0.1	0.5
	Surface water	0.0	0.0	0.0	0.2
	Bare earth	0.0	0.1	18.3	94.3

3.2 Soil Permeability Data

Soil data were primarily from the U.S. Department of Agriculture (USDA) SSURGO database, which contains survey information collected by the National Cooperative Soil Survey over the course of the past century at scales ranging from 1:12,000 to 1:63,360. A total of 70 soil units were represented within the project model area. For each soil unit, a range of typical hydraulic conductivities was provided by the SSURGO database. The average of the range of minimum and maximum hydraulic conductivity values for each soil type was assumed to be representative of the hydraulic conductivity for that soil type. Given this assumption, the soil hydraulic conductivity is greater than 9.5 mm/hr for more than 95% of the project area, with the majority of the study area having a hydraulic conductivity of 26.2 mm/hr or above (Fig .4). The highest precipitation intensity in this area between 2000 and 2018 was 11.0 mm/hr, so saturation-excess overland flow is expected to be the dominant mechanism for initiating overland flow in the project watershed under pre-fire conditions.

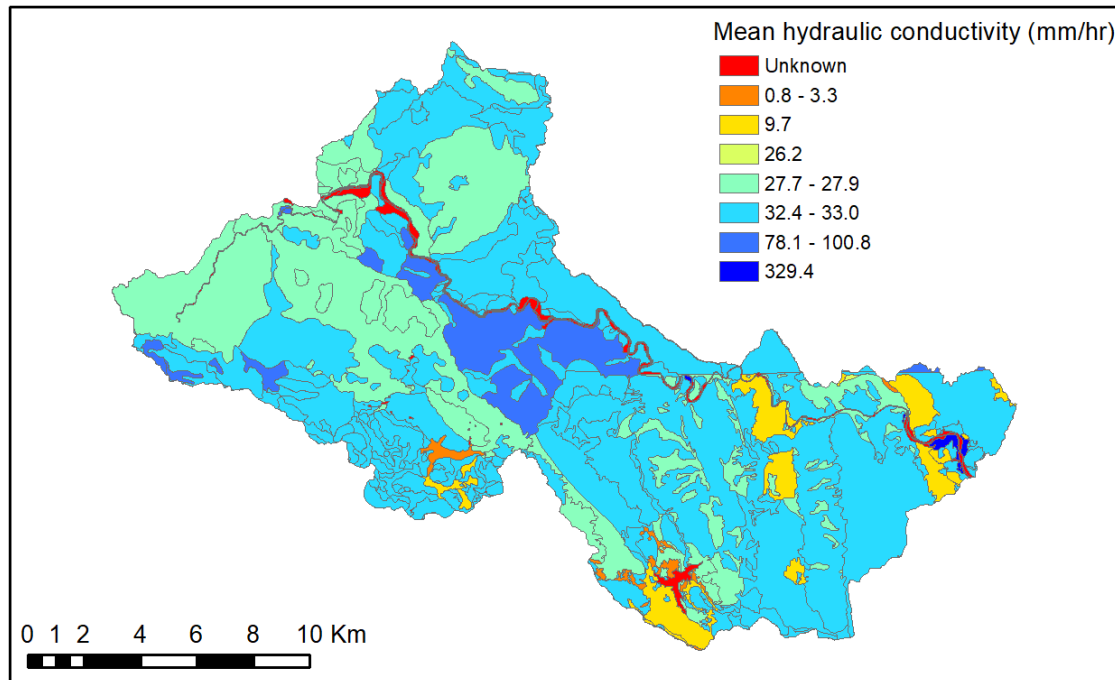


Figure 4: Hydraulic conductivities for major soil units over the project area.

3.3 Stream flow, climatology and weather data

Hourly Streamflow data at Rumsey for model calibration were downloaded from the U.S. Geological Survey (USGS) National Water Information System (NWIS)(station 11451800) (Figure 1). California Department of Water Resources (DWR) station RUM was used for discharge data during Water Years 2000 and 2015

(http://cdec.water.ca.gov/dynamicapp/staMeta?station_id=RUM). USGS took over operations of this station as USGS gage 11451800 from September 23rd, 2015.

The UFORE-Hydro and PFHydro models require hourly time series precipitation and potential evapotranspiration (PET) rates for the whole watershed. The models also require time series potential evaporation (PE) rates for trees and short vegetation, leaf area index (LAI) values, and the dates of leaf emergence and leaf fall for each year to quantify vegetation interception of precipitation.

Hourly climate station data are sparse in the area and cannot capture the variability of elevation and local climatology patterns. Hourly climate grids of precipitation and air temperature were developed using eleven local climate stations to represent the spatial heterogeneity of the watershed. An existing FORTRAN-based program was edited to input hourly station data and interpolate the data over the watershed using a geospatial algorithm and a knowledge-based climate product called Parameter-elevation Regressions on Independent Slopes Model (PRISM, <http://prism.oregonstate.edu/>).

Hourly PET was developed for the study area using hourly air temperature grids and the Priestley-Taylor evapotranspiration equation, which considers topographic shading, solar

radiation, atmospheric parameters, and cloudiness (Flint et al., 2013). Hourly PE for short vegetation (assumes average height of short vegetation is 2 meters) was calculated using the Priestley-Taylor equation, which assumes a wetted surface (Flint and Childs, 1991). Hourly PE for trees (assumes average height of trees is 10 meters) was calculated using the Penman-Monteith equation (Shuttleworth, 1993) and verified using Holmes (2015) equation and local hourly wind data.

Annual LAI values were developed from MODIS (Moderate Resolution Imaging Spectroradiometer; Myneni, 2015) remotely sensed data. Leaf on and leaf off dates were developed using eMODIS NDVI grids (Swets et al., 1999; Jenkerson, 2010; <https://phenology.cr.usgs.gov>). Hourly gridded climate (precipitation and potential evapotranspiration), LAI values, and leaf on/off dates were provided as inputs to the UFORE-Hydro and PFHydro model. The meteorological data were averaged over the model domain (Figure 1) to provide a time series input.

3.4 Use of USGS HSPF model to provide the UFORE-Hydro and PFHydro boundary conditions

The Hydrological Simulation Program – FORTRAN (HSPF) rainfall-runoff model (Bicknell et al., 2001) was used to provide time-series hourly flow at the three tributaries upstream of the UFORE-Hydro, PFHydro model domain as boundary conditions (Figure 1). An HSPF model of the Sacramento River Basin (Stern et al., 2016) was modified to include the model domain shown in Figure 1, and was calibrated using data from Water Years (WY: October 1-September 30) 2015–17. The HSPF modeling watershed outlet is Rumsey, which is the same as that of the UFORE-Hydro and PFHydro models, but the HSPF model domain includes a larger contributing area that overlaps the UFORE-Hydro, PFHydro model domain (Figure 1). The HSPF Nash-Sutcliffe modeling Efficiency (NSE) for hydrograph simulation at Rumsey was 0.87 for WY 2015 – WY 2017 (Stern et al., 2019). The NSE compares the model simulation to observations and tends to emphasize calibration with respect to higher flows (Nash and Sutcliffe, 1970).

4. Results of the models' application

The UFORE-Hydro and PFHydro models were applied to the sub area of the Upper Cache Creek Watershed discussed in the previous section for pre- and post-fire conditions, respectively. The simulation time step is one hour. A Dell laptop with a processor: Intel(R) Core (TM) i7-8850H CPU @ 2.6GHz, 2.59GHZ, and RAM of 32.0GB was used for the modeling work. The simulation time for one water year is several seconds for the two models.

Three objective functions were used to evaluate model performance for both UFORE-Hydro and PFHydro: The NSE (described above), CRF2 statistic (Equation 13), and CRF3 statistic (Equation 14). The CRF2 statistic puts more emphasis on simulation accuracy at every time step (Ye et al., 1997), whereas CRF3 is biased to place more importance on lower flows (Perrin et al., 2001). The value 1.0 of NSE, CRF2, CRF3 means 100% match between simulation and observation. The results of these comparisons are discussed in Sections 4.1 and 4.2.

$$CRF2 = 1 - \frac{\sum_{i=1}^n |Q_{obs,i} - Q_{cal,i}|}{\sum_{i=1}^n |Q_{obs,i} - Q_{aveobs}|} \quad (13)$$

$$CRF3 = 1 - \frac{\sum_{i=1}^n (\sqrt{Q_{obs,i}} - \sqrt{Q_{cal,i}})^2}{\sum_{i=1}^n (\sqrt{Q_{obs,i}} - \sqrt{Q_{aveobs}})^2} \quad (14)$$

where $Q_{obs,i}$ is the observed flow at time step i , $Q_{cal,i}$ is the model calculated flow at time step i , Q_{aveobs} is the average observed flow for the whole simulation period, and n is the number of time steps.

4.1 UFORE-Hydro pre-fire runoff model calibration and validation

The WY 2000 (10/1/1999 – 9/30/2000) was selected for calibration of the UFORE-Hydro pre-fire model. The NSE, CRF2 and CRF3 were 0.82, 0.64 and 0.88 respectively for the WY 2000 runoff simulation (Figure 5). The Rocky Fire (07/29/2015–08/14/2015) and Jerusalem Fire (08/09/2015–08/25/2015) occurred near the end of WY 2015. There was no precipitation in WY 2015 that occurred after these fires; therefore, the entire water year could be considered a pre-fire water year. The UFORE-Hydro model was validated to WY 2015 (10/1/2014 – 09/30/2015) using the parameters obtained in the model calibration for WY 2000. The model performance metrics produced the following results: NSE = 0.88, CRF2 = 0.63, CRF3 = 0.80. Figure 6 shows the hydrograph for WY 2015 and shows storm events at the Rumsey outlet in the Upper Cache Creek Watershed. The parameters used in the calibrated and validated pre-fire hydrological model are listed in Table 3.

4.2. PFHydro model calibration and validation

The PFHydro model was calibrated for WY 2016 (10/1/2015 – 9/30/2016) (Figure 7), which was the first water year after the Rocky and Jerusalem fires. The three objective functions for the simulation are as follows: NSE = 0.88, CRF2 = 0.78, CRF3 = 0.91. PFHydro was then validated for WY 2017 (10/1/2016 – 9/30/2017) (Figure 8). The three objective functions for the simulation are as follows: NSE = 0.93, CRF2 = 0.81, CRF3 = 0.92. The calibration and validation results indicate good model fit to the observations for the pre- and post-fire runoff simulations.

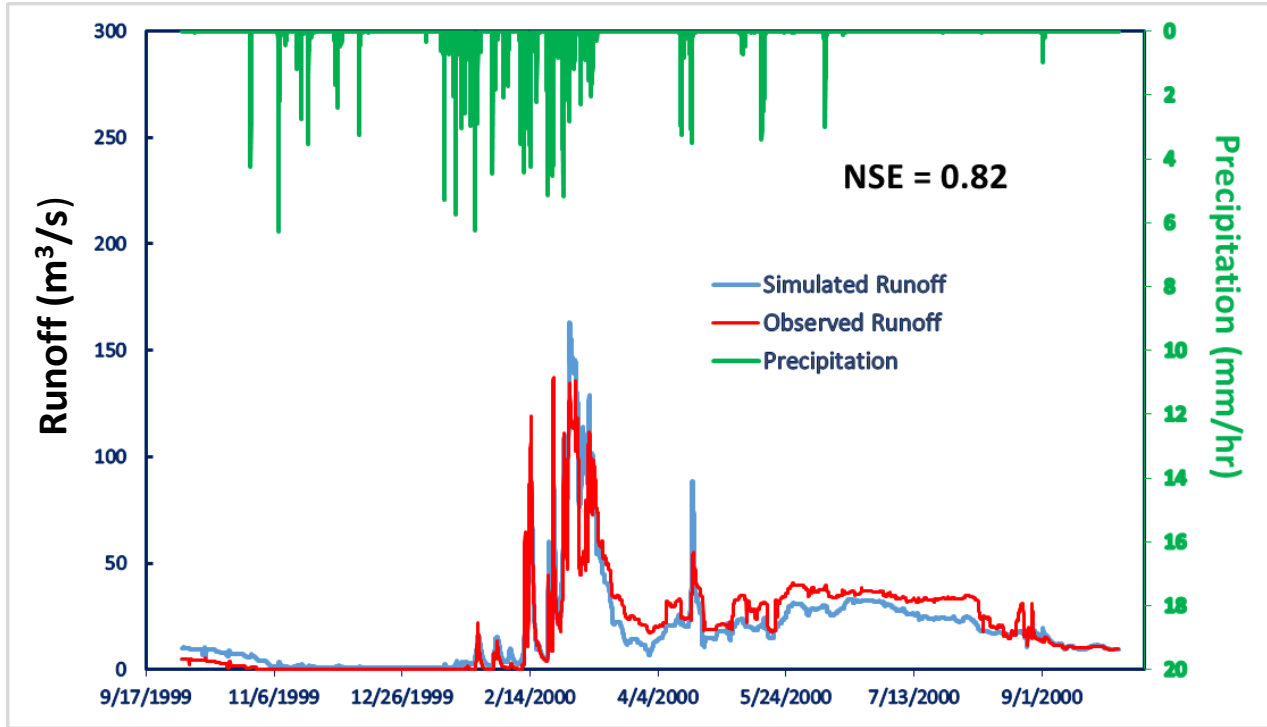


Figure 5. Hydrograph showing comparison of observed and UFORE-Hydro model simulated pre-fire runoff in the Upper Cache Creek Watershed (Rumsey outlet) for WY 2000.

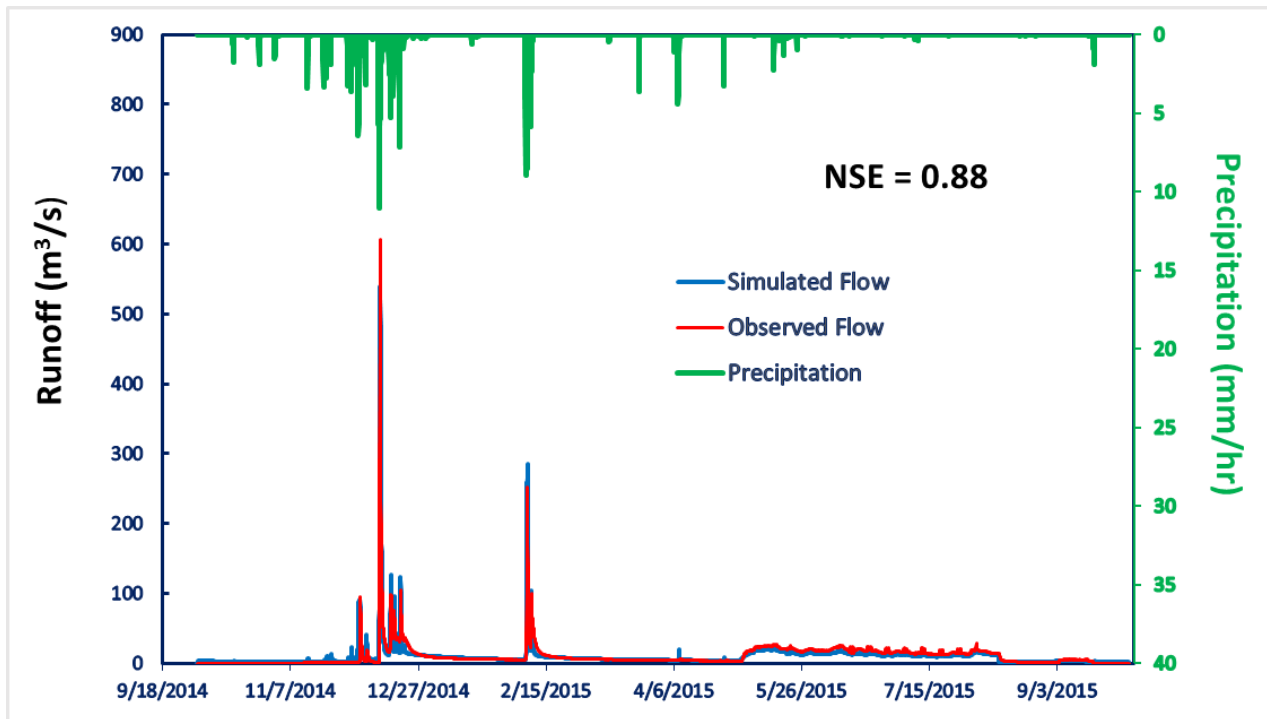


Figure 6. Hydrograph showing comparison of observed and UFORE-Hydro model simulated pre-fire runoff in the Upper Cache Creek Watershed (Rumsey outlet) for WY 2015.

Table 3. Calibrated and validated pre-fire UFORE-Hydro model parameters in the model study area in the Upper Cache Creek Watershed.

Parameter	Value	Parameter	Value
Scale Parameter of Soil: m (m)	0.0116	Main Channel Routing velocity (m/h)	900
Transmissivity at Saturation: T_0 (m^2/h)	0.39	Internal Channel Routing Velocity (m/h)	950
Unsaturated Zone Delay: T_d (h)	10	Fraction of watershed generating infiltration excess overland flow (decimal %)	0.10
Maximum Root Zone Storage Deficit (m)	0.0064	Saturated surface hydraulic conductivity K_0 : (m/h)	0.001
Initial Stream Discharge: (m/h)	3e-06 (WY 2000) 3.5e-06 (WY 2015)	Wetting Front Suction (m)	0.3
Initial Root Zone Deficit (m)	0.006 (WY 2000) 0.006 (WY 2015)	Wetted Moisture Content (decimal %)	0.38

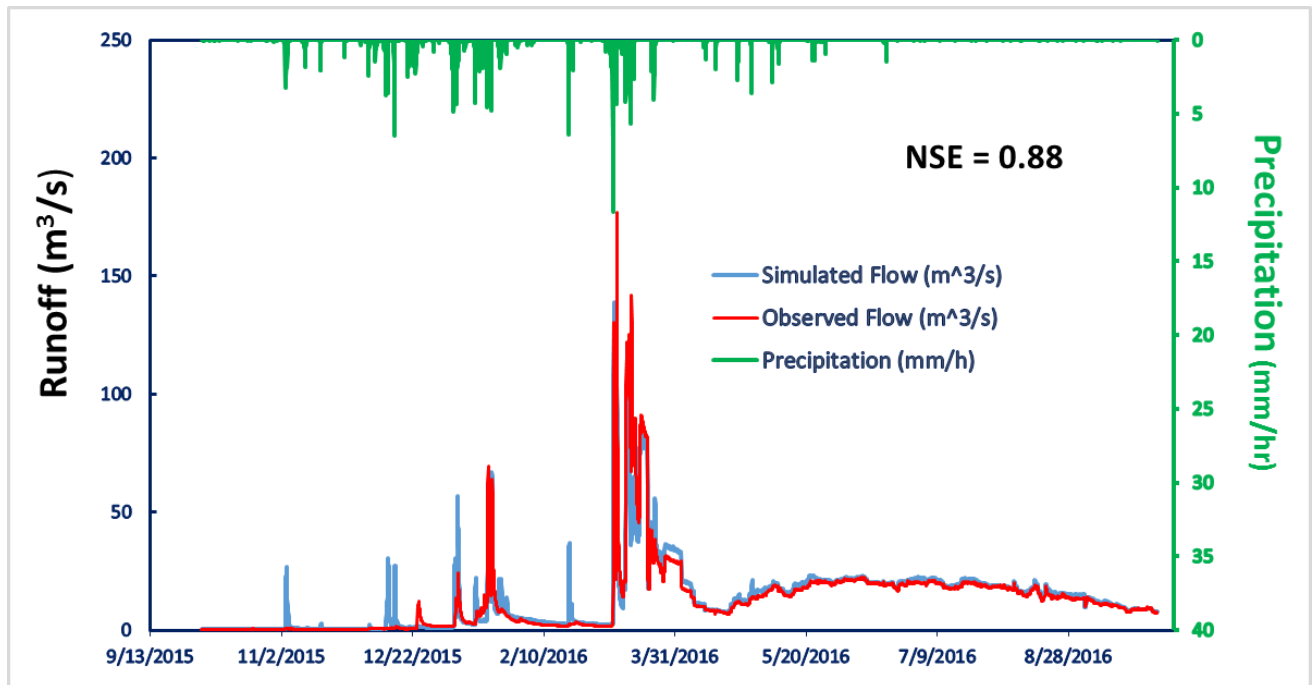


Figure 7. Hydrograph showing a comparison of observed and PFHydro simulated post-fire runoff at Upper Cache Creek Watershed (Rumsey outlet) for WY 2016.

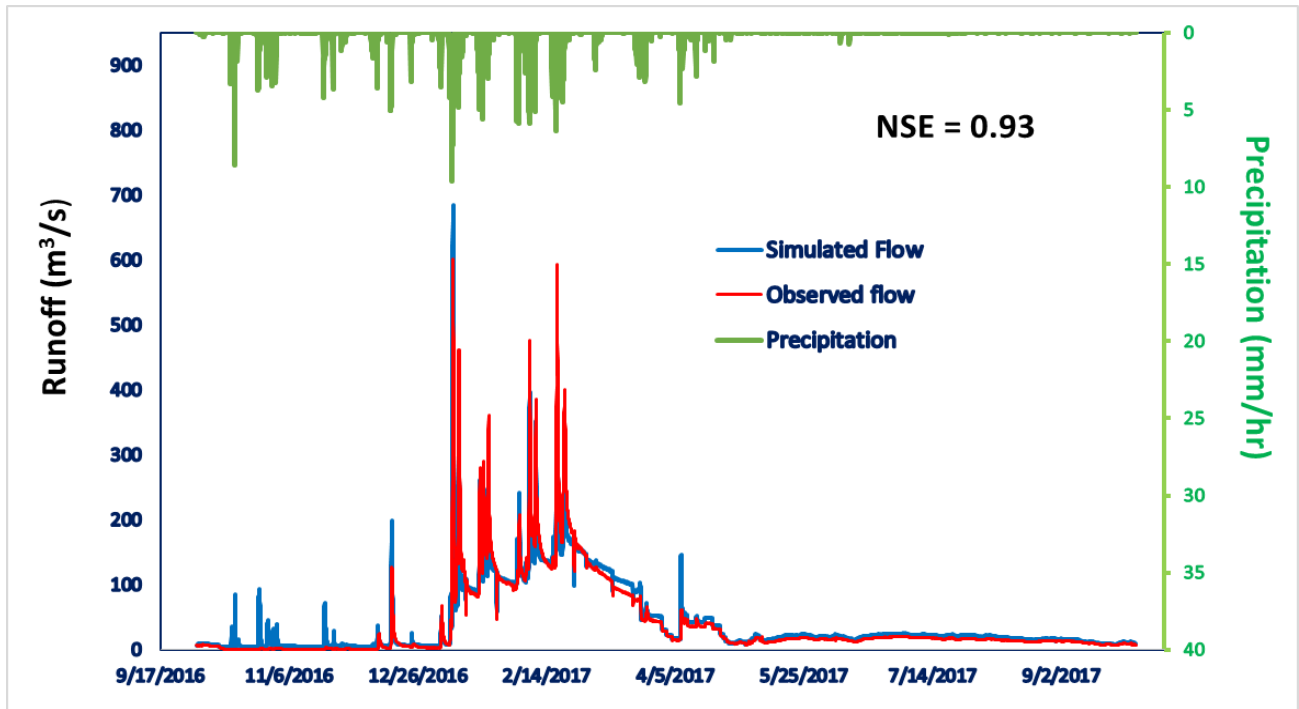


Figure 8. Hydrograph showing a comparison of observed and PFHydro simulated post-fire runoff at Upper Cache Creek Watershed (Rumsey outlet) for WY 2017

The parameters used in simulations with the calibrated and validated PFHydro model are listed in Table 4.

Table 4. Parameters of the PFHydro post-fire model calibration and validation

Parameter	Value	Parameter	Value
Scale Parameter of Soil: m (m)	0.0116	Main Channel Routing Velocity (m/h)	900
Transmissivity at Saturation: T_0 (m^2/h)	0.39	Internal Channel Routing Velocity (m/h)	950
Unsaturated Zone Delay: T_d (h)	10	Fraction of unburned watershed generating infiltration excess overland flow (decimal %)	0.10
Maximum Root Zone Storage Deficit (m)	0.0064	Saturated surface hydraulic conductivity K_0 : (m/h)	0.001
Initial Stream Discharge: (m/h)	2e-06 (WY 2016) 5e-06 (WY 2017)	Wetting Front Suction (m)	0.3
Initial Root Zone Deficit (m)	0.0055 (WY 2016) 0.0055 (WY 2017)	Wetted Moisture Content	0.38
High Burn Severity Fraction of K_0 : μ (decimal %)	0.1 (WY 2016) 0.2 (WY 2017)	Connectivity of SWR Patches: Φ (decimal %)	0.75 (WY 2016) 0.60 (WY 2017)

The PFHydro model assumed that the SWR effects were still present for the WY 2016 and WY 2017. However, the SWR hydrophobic effects were expected to decrease in the 2nd year post-fire (WY 2017) relative to the 1st year post-fire (WY 2016). It follows that the hydraulic conductivity of SWR soil should have increased correspondingly in the 2nd year post-fire compared to the soil hydraulic conductivity exhibited in the 1st year. The connectivity of the SWR Patches (Φ) should have also decreased.

The parameters, including the two new parameters (μ and Φ) were tweaked manually for overall best model performance evaluated in the three objective functions discussed previously during the model calibrations and validations. The parameters of the model calibration for WY 2016 and WY 2017, provided in Table 4, support the assumptions made above. For example, the value of μ in the calibrated hydraulic conductivity parameter μK_0 for WY 2017 doubled compared to WY 2016, to 0.2 from 0.1. The connectivity of SWR patches for WY 2017 ($\Phi = 0.60$) was lower than for WY 2016 ($\Phi = 0.75$). The model parameter values for the pre-fire and post-fire models were identical except for these two values that are used to characterize burned soil (μ and Φ) and the values of two parameters for model initial conditions (Initial Stream Discharge and Initial Root Zone Deficit).

5. Discussion

5.1 Pre-fire and post-fire vegetation interception effects

Vegetation interception of precipitation is a function of the vegetation canopy as well as precipitation intensity and duration. As previously discussed, vegetation interception capacity also depends on vegetation interception storage. Once the available vegetation storage is filled, no additional precipitation can be intercepted. Interception typically resumes after the intercepted water has evaporated and interception storage is made available. Interception is a dynamic process, with vegetation typically intercepting a greater fraction of precipitation for small, scattered storms than for larger, intense storms. The vegetation interception modeling results pre-fire (WY 2000 and WY 2015) and post-fire (WY 2016 and WY 2017) are presented in Table 5.

Table 5. Results of model simulations of vegetation interception (of precipitation) for pre-fire and post-fire

Water Year	Annual Precipitation (mm)	Annual Interception of Trees for Tree-Covered Area (mm)	Annual Interception of Trees for Entire Model Domain	Annual Interception of Short Vegetation for Entire Model Domain	Annual Interception of All Vegetation for Entire Model Domain
2000 (pre-fire)	672	136 (20.2%)	6.3%	3%	9.3%
2015 (pre-fire)	580	82 (14.2%)	4.4%	2.3%	6.7%
2016 (post-fire)	630	125 (19.8%)	2.8%	1.8%	4.6%
2017 (post-fire)	1118	134 (12%)	1.7%	1.1%	2.8%

Water years 2000, 2015, and 2016 had similar annual precipitation totals. For WY 2015 the simulated interception by trees for tree-covered area in the watershed was 82 mm (14.2% of the total precipitation). The high intensity nature of some of the precipitation events and the fact that precipitation during the WY 2015 was concentrated in only two storm events resulted in the lowest interception of the years of precipitation. Annual precipitation during WY 2017 was about 40% higher than the other water years; precipitation intensity was also highest and the percentage of tree interception simulated by the model was the lowest (about 12% of total precipitation) for the tree-covered area.

The total precipitation interception of trees for the tree-covered area in WY 2000 (20.2%) and WY 2016 (19.8%) are very similar. However, the total vegetation (trees + short vegetation) interception of rainfall post-fire (4.6%) for the entire model domain in WY 2016 was about 50% of that pre-fire value (9.3%) in WY 2000 because of reduced vegetation in the modeling area due to the fire.

5.2 Post-fire soil water repellent effects on runoff generation

Simulated runoff for the four water years 2000, 2015, 2016 and 2017 is summarized in Table 6. The results displayed in Table 6 show that the percentage of surface runoff in total runoff was highest (49.8%) in WY 2016 (the 1st year post-fire) and 2nd highest (24.5%) in WY 2017 (the 2nd year post-fire). The simulated annual surface runoff was about 6 times greater in WY 2016 than in WY 2000 with similar total precipitation for the two WYs. The results support the hypothesis that burning causes SWR-related hydrophobic effects that increase surface runoff, and that SWR decreases with time.

The total runoff during WY 2016 (1st year post-fire, was expected to be higher than the runoff during WY 2015, given that the precipitation in WY 2016 was 630 mm compared with precipitation of 580 mm in WY 2015. However, the total observed and simulated runoff was found to be higher in WY 2015 compared with WY 2016 because the precipitation during WY 2015 was concentrated in fewer major storm events than during WY 2016. The simulated surface runoff, on the other hand, was about 1.6 times greater in WY 2016 than in WY 2015, emphasizing the importance of post-fire SWR hydrophobic effects.

Table 6. Simulated surface, subsurface and total runoff of WYs 2000, 2015, 2016, and 2017 for the modeling area in the Upper Cache Creek Watershed

Water Year	Annual Precipitation (mm)	Total Simulated Flow (m ³ /s)	Total Simulated Surface Flow (m ³ /s)	Total Simulated Subsurface Flow (m ³ /s)	Percentage of Surface flow in Total flow
2000 (pre-fire)	672	21445	1852	19419	8.6%
2015 (pre-fire)	580	41071	6264	34619	15.2%
2016 (post-fire)	630	20142	10026	10110	49.8%
2017 (post-fire)	1118	75447	18491	56944	24.5%

Surface runoff simulated by PFHydro for the burned areas is shown in Table 7 (far right column). The normalized precipitation and runoff totals were compared. During WY 2016, the simulated surface runoff of 120 mm over the burned area comprised 47% of the total runoff (257

mm) and 93% of the surface runoff (128 mm). The simulated surface runoff for WY 2017 from the burned area was 186 mm, which was about 17% of total runoff (962 mm) and 79% of the total surface runoff (236 mm). Therefore, the SWR hydrophobic effects on precipitation-induced runoff diminished during the 2nd year post-fire compared to the 1st year post-fire.

Table 7. Comparison of surface and subsurface runoff from burned areas during WYs 2016, 2017.

Water Year	Total Precipitation (mm)	Total Surface and Subsurface Runoff (mm)	Total Subsurface Runoff (mm)	Total Surface Runoff (mm)	Total Surface Runoff from Burned Area (mm)
2016	630	257	129	128	120
2017	1118	962	726	236	186

Given the variation in precipitation volume, intensity, and duration between WY 2016 and WY 2017, it is difficult to draw overarching conclusions from two years of watershed runoff data and the comparison of pre-fire and post-fire conditions as they relate to the total annual runoff.

Two large storm events, one pre-fire (in WY 2015) and one post-fire (in WY 2017), were identified as having the same duration and similar precipitation amounts and intensities. A comparison of model predictions and field observations for the two storm events is shown in Figure 9 and Table 8, which helps validate the previously described conceptual model of post-fire runoff generation.

Table 8. Comparison of model results for the pre-fire and post-fire storm events

Precipitation Start, End (Duration = 58 hrs.)	Total precipitation (mm)	Total observed runoff (m ³ /s)	Total simulated runoff (m ³ /s)	Total simulated surface runoff (m ³ /s)	Surface runoff / total runoff
12/10/14 1:00 am -- 12/12/14 11:00 am (Pre-fire)	123.7	2363	2372	1948	82.1%
01/07/17 1:00 am – 01/09/17 11:00 am (Post-fire)	122.0	3955	3947	3493	88.5%

The two storms analyzed were the first large storms during the wet seasons of WY 2015 and WY 2017 and the two storms had the same precipitation duration (58 hours). The total precipitation for the pre-fire storm (124 mm) and the maximum rainfall intensity (10.9 mm/hr) were higher than for the post-fire storm (122 mm and 9.6 mm/hr, respectively). However, the total post-fire storm event runoff was about 1.7 times that of the total pre-fire storm event.

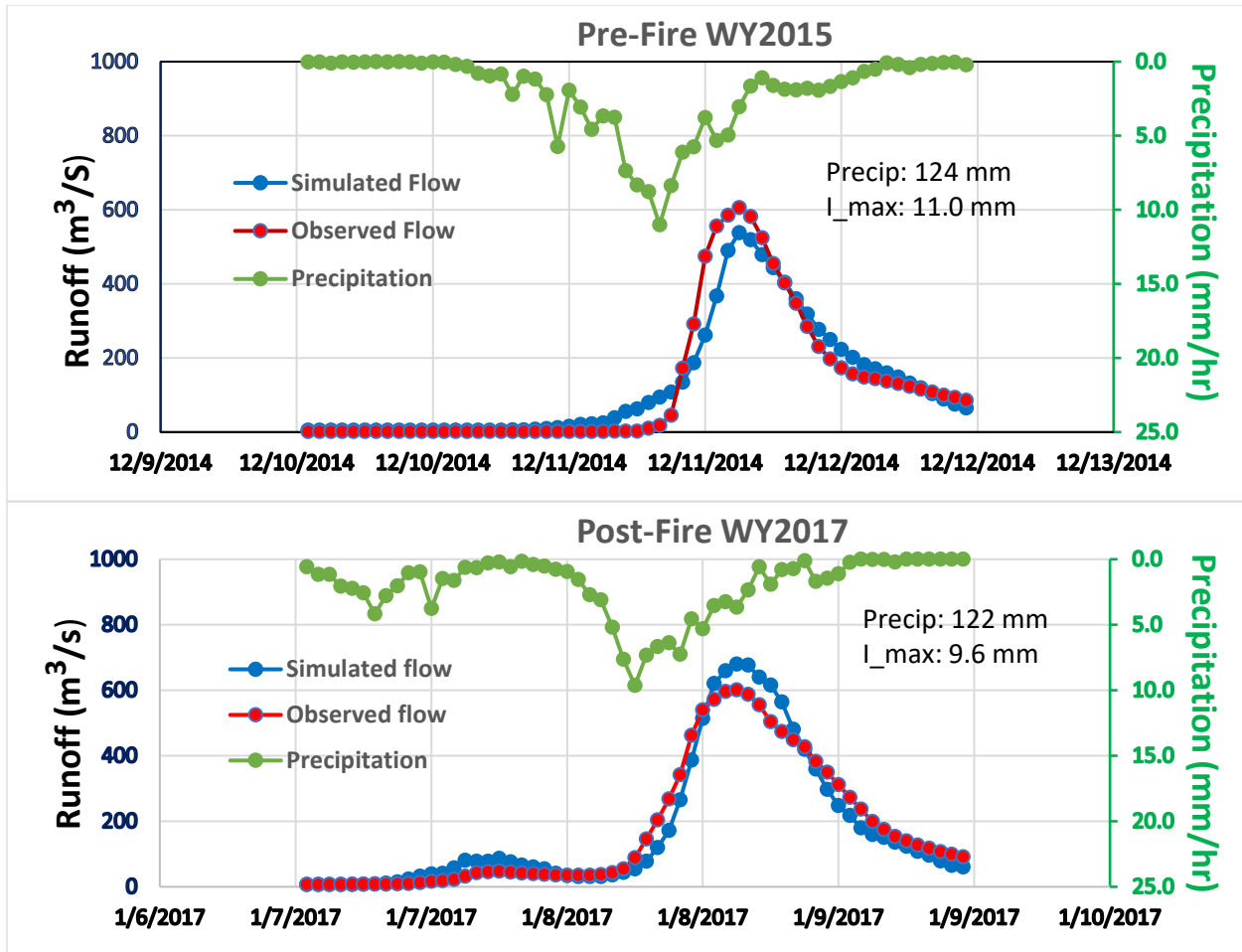


Figure 9. Comparison of model runoff simulations for similar pre-fire and post-fire storm events. “Precip” is total storm event precipitation, “I_max” is the maximum precipitation intensity.

The modeled storm runoff quantities were very close to the observations for both storms (Table 10). Likewise, the modeled pre-fire and post-fire storm runoff volumes, when compared with observations, were only 0.39% higher and 0.21% lower, respectively. The shape of the model-simulated hydrographs for the two storms also show a good match to observations (Figure 9). Although surface runoff from the watershed cannot be directly measured, the excellent match between the quantity and timing of observations and model simulated total runoff suggest a valid conceptual and numerical model. The total surface runoff simulated with the post-fire model simulation was about 1.8 times greater than the surface runoff simulated with the pre-fire model.

The good match between field observations and model simulated runoff values suggests that the post-fire SWR soil hydrophobic effects still existed at the time of this storm, which was about 17 months after the fires occurred. This result supports the model assumption that the soil SWR layer was still present during WY 2017.

5.3 Sensitivity analyses of μ and Φ

Sensitivity analyses of parameters μ and Φ simulating SWR effects are presented in Table 9, 10, respectively.

Table 9. Sensitivity analysis of parameter μ on runoff generation for WY 2016. Δ Surface Flow is the change in surface flow relative to the previous smaller value of μ

μ	Annual Surface Flow (mm)	Annual Subsurface Flow (mm)	Annual Total Flow (mm)	Δ Surface Flow (mm)	Δ Surface Flow (%)
0.1	127.8	128.9	256.7	--	--
0.2	116.3	134.9	251.2	-11.5	-9.0
0.3	99.8	144.6	244.4	-16.5	-14.2
0.4	73.9	162.4	236.3	-25.9	-26.0
0.5	64.1	169.1	233.3	-9.8	-13.3
0.6	58.8	172.8	231.6	-5.3	-8.3
0.7	41.5	185.1	226.6	-17.3	-29.4

Table 10. Sensitivity analysis of parameter Φ on runoff generation for WY 2016. Δ Surface Flow is the change in surface flow relative to the previous smaller value of Φ .

Φ	Annual Surface Flow (mm)	Annual Subsurface Flow (mm)	Annual Total Flow (mm)	Δ Surface Flow (mm)	Δ Surface Flow (%)
0.0	10.6	207.2	217.8	--	--
0.1	26.2	195.6	221.8	15.6	147.2
0.2	41.7	184.7	226.4	15.5	59.2
0.3	57.3	174.0	231.3	15.6	37.4
0.4	72.8	163.6	236.4	15.5	27.1
0.5	88.5	153.3	241.8	15.7	21.6
0.6	104.2	143.3	247.5	15.7	17.7
0.7	119.9	133.6	253.5	15.7	15.1
0.8	135.6	124.4	260.0	15.7	13.1
0.9	151.4	115.4	266.9	15.8	11.7
1.0	167.2	107.0	274.2	15.8	10.4

It can be seen from Table 9 that the surface flow decreases, and subsurface flow increases with increased μ (fraction of K_{sat} in unburned area) because of a higher infiltration. The annual total flow also decreases with increased μ but at a much smaller scale.

The two most sensitive changes of μ are from 0.3 to 0.4 and from 0.6 to 0.7, causing surface runoff decreases of 26.0%, 29.4%, respectively.

It can be seen from Table 10 that the surface flow increases almost constantly (from 15.5 to 15.8 mm) with the increase of Φ (connectivity of burned patches), whereas the percent increase decreases. The SWR effect is minimal or can be neglected when Φ is zero. Note that there is about 42% unburned area which has no SWR effect in the modeling domain.

6. Summary and conclusions

The results of this study suggest that the UFORE-Hydro and PFHydro models were properly calibrated and validated for simulations of pre-fire and post-fire runoff (Table 11). The model performance statistics considered (NSE, CRF2, and CRF3) confirm the agreement between the models and field observations.

Table 11. Model runoff simulation calibration and validation results

Water Year	NSE	CRF2	CRF3	
2000	0.82	0.64	0.88	Pre-fire calibration
2015	0.88	0.63	0.80	Pre-fire validation
2016	0.88	0.78	0.91	Post-fire calibration
2017	0.93	0.81	0.92	Post-fire validation

Model simulations show that precipitation interception by vegetation was reduced by wildfires, as expected (Table 5). When water years with similar annual precipitation volumes and rainfall characteristics were compared, post-fire vegetation interception in WY 2016 was about 50% lower than pre-fire vegetation interception in a comparable year like WY 2000. Fire-induced SWR hydrophobic effects on precipitation-induced runoff generation have been demonstrated using the results of annual model simulations which produced greater surface runoff and a reduction in subsurface flow (Table 6) when pre-fire and post-fire conditions were compared. Two storm events during the modeled period that showed high similarity were selected to compare pre-fire and post-fire conditions, which clearly demonstrated the post-fire SWR effects. The simulation results showed that both surface runoff and total runoff significantly increased post-fire (Table 8).

The UFORE-Hydro model was enhanced to create PFHydro with a new model structure and new algorithms simulating burn effects from wildfire that resulted in a good match between modeling results and measured field observations for post-fire conditions. The PFHydro model provides a unique and reliable way to simulate post-fire watershed scale hydrological process and precipitation-induced runoff.

7. Further work

The current model was applied to the Upper Cache Creek Watershed, which was assumed to be homogenous. The model will be updated so that it can be applied to a heterogeneous watershed. In the natural environment soil water repellency (SWR) significantly decreases with increasing soil moisture. For simplicity, the current model assumes SWR remains for the first

two years post-fire and remains constant within a single year. An algorithm will be developed to simulate the soil moisture content dynamically year-round to simulate post-fire SWR effects more accurately.

Because large fires affected the Upper Cache Creek Watershed during summer 2018, there will be opportunities to use results of planned monitoring during Water Years 2019 and 2020 to further test the PFHydro model. Ongoing work also includes using the HSPF and PFHydro models to simulate the transport of suspended sediment and mercury, a significant contaminant in the Upper Cache Creek Watershed.

8. Acknowledgements

The researchers gratefully acknowledge funding support from the U.S. Bureau of Reclamation through the Science and Technology Program and U.S. Bureau of Land Management. This work is part of the research project: Research and Development of a Watershed-Scale Model/Tool for Simulating the Effects of Wildfires on Mercury Contamination of Land and Water.

References:

- Agnew, W., Labn, R.E., Harding, M.V. (1997). Buffalo Creek, Colorado, fire and flood of 1996. *Land and Water*, 41, 27-29. Beven, K. J. and M. J. Kirkby, (1979), "A Physically Based Variable Contributing Area Model of Basin Hydrology," *Hydrological Sciences Bulletin*, 24(1): 43-69.
- Ambrose, B., Beven, K., Freer, J., 1996. Toward a generalization of the TOPMODEL concepts: topographic indices of hydrological similarity. *Water Resources Research* 32 (7), 2135–2145.
- Benavides-Solorio, JDD., MacDonald, L.H., 2005. Measurement and prediction of post-fire erosion at the hillslope scale, Colorado Front Range. *International Journal of Wildland Fire* 14, 457–474. doi:10.1071/WF05042
- Beven, K.J., Kirkby, M.J., 1979. A Physically based variable contributing area model of basin hydrology. *Hydrological Sciences Bulletin* 24 (1), 43–69.
- Beven, K.J., 1984. Infiltration into a class of vertically non-uniform soils. *Hydrology Science Journal* 29, 425–434.
- Beven, K. (Ed.), 1997a. *Distributed Hydrological Modeling: Applications of the Topmodel Concept Advances in Hydrological Processes*. Wiley, West Sussex, Engla
- Beven, K. J., 1997b. TOPMODEL: A critique. *Hydrological Processes* 11, 1069-1085
- Blake, W.H., Theocharopoulos, S.P., Skoulikidis, N., Clark, P., Tountas, P., Hartley, R., Amaxidis, Y., 2009. Wildfire impacts on hillslope sediment and phosphorus yields. *Journal of Soils and Sediments*, Vol.10, pp. 671-682.
- Bond, R.D., 1964. The influence of the microflora on the physical properties of soils. II. Field studies on water repellent sands. *Aust. J. Soil Res.* 2, 111–122.
- Cawson, J., Sheridan, G., Lane, P., Smith, H., 2010. Characterising fire severity patches to understand how burn patchiness affects runoff connectivity and erosion. *Geophysical Research Abstracts* 12, EGU2010-3009.

- Cerrelli, G.A., 2005. FIRE HYDRO, a simplified method for predicting peak discharges to assist in the design of flood protection measures for western wildfires. In 'Proceedings of the 2005 Watershed Management Conference – Managing Watersheds for Human and Natural Impacts: Engineering, Ecological, and Economic Challenges', July 2005, Williamsburg, VA. (Ed. GE Moglen) pp. 935–941. (American Society of Civil Engineers: Alexandria, VA).
- Chen, L., Berli, M., Chief, K., 2013. Examining modeling approaches for the rainfall-runoff process in wildfire-affected watersheds: Using San Dimas Experimental Forest. *Journal of the American Water Resources Association (JAWRA)* 1-16. DOI: 10.1111/jawr.12043.
- DeBano, L.F., 1966, Formation of non-wettable soils: Involves heat transfer mechanism (Vol. 132). Pacific Southwest Forest & Range Experiment Station.
- DeBano, L.F., 1981. Water repellent soils: a state of the art, Gen. Tech. Rpt. PSW-46. USDA For. Serv., Pacific Southwest Forest and Range Exp. Sta., Berkeley, CA, 21pp
- DeBano, L.F., Krammes, J.S., 1966, Water repellent soils and their relation to wildfire temperatures. *International Association of Scientific Hydrology Bulletin*, 11, pp. 14-19.
- DeBano, L.F., Osborn, J.F., Krammes, J.S., Letey, J., Jr., 1967. Soil wettability and wetting agents...our current knowledge of the problem. Gen. Tech. Rpt. PSW-43. USDA For. Serv., Pacific Southwest Forest and Range Exp. Sta., Berkeley, CA, 13pp
- DeBano, L.F., Neary, D.G., Ffolliott, P.F., 1998. *Fire's Effects on Ecosystems*. John Wiley & Sons, Inc., ISBN 978-0-471-16356-5, New York. 333 p.
- de Jonge, L.W., Jacobsen, O.H., Moldrup, P., 1999. Soil water repellency: Effects of water content, temperature, and particlesize. *Soil Sci. Soc. Am. J.* 63:437–442.
- Dekker, L.W., Ritsema, C.J., 1995. Fingerlike wetting patterns in two water-repellent loam soils. *J. Environ. Qual.* 24, 324–333.
- Dekker, L.W., Doerr, S.H., Oostindie, K., Ziogas, A.K., Ritthesema, C.J., 2001. Water repellency and critical water content in a dune sand. *Soil Sci. Soc. Am. J.* 65:1667–1674.
- van Dijk, A.I.J.M., L.A. Bruijnzeel, 2001. Modeling Rainfall Interception by Vegetation of Variable Density Using an Adapted Analytical Model. Part 1. *Journal of Hydrology* 247:230.
- Doerr, S.H., Moody, J.A., 2004. Hydrological effects of soil water repellency: on spatial and temporal uncertainties. *Hydrological Processes* 18, 829–832.
- Doerr, S.H., and A.D. Thomas. 2000. The role of soil moisture in its classes. Time since burning was a significant control controlling water repellency: New evidence from forest soils in on the strength of soil water repellency at the soil surface. *Portugal. J. Hydrol.* (Amsterdam) 231–232:134–147.
- Dolan, Jack (January 21, 2018). "[Search teams find 21st victim of Montecito mudslide](#)". Los Angeles Times. Retrieved January 21, 2018.
- Dunne, T., 1978. Field studies of hillslope flow processes. In: Kirkby, M.J. (Ed.), *Hillslope Hydrology*. John Wiley & Sons, New York, pp. 227–293.
- Ebel, B.A., Moody, J.A., 2012. Rethinking infiltration in wildfire-affected soils. *Hydrological Processes*. <http://dx.doi.org/10.1012/hyp.9696>.
- Elliot, W.J., Hall, D.E., Robichaud, P.R., 2010. FS Peak Flow Calculator. Version 2010.10.28. U.S. Department of Agriculture, Forest Service, Rocky Mountain Research Station, Moscow, ID (online at <http://forest.moscowfsl.wsu.edu/fswpepp/ermit/peakflow>, last accessed 30 January 2012).

- Elliot, W. J., Miller, I. S., Glaza, B.D., 2006. Using WEPP Technology to Predict Erosion and Runoff Following Wildfire. Presented at the ASAE Annual International Meeting, Jul 9-12, Portland, OR. Paper No. 068011. St. Joseph, MI: ASAE. 12p.
- Flanagan, D. C., Nearing, M. A., 1995. USDA-Water Erosion Prediction Project: Hillslope profile and watershed model documentation, NSERL Report No. 10, West Lafayette, USDA-ARS National Soil Erosion Research Laboratory.
- Flint, A.L. and Childs, S.W., 1991. Use of the Priestley-Taylor evaporation equation for soil water limited conditions in a small forest clear cut. *Agricultural and Forest Meteorology*, 56(3-4), pp.247-260.
- Flint, L.E., Flint, A.L., Thorne, J.H., and Boynton, R., 2013. Fine-scale hydrological modeling for climate change applications; using watershed calibrations to assess model performance for landscape projections. *Ecological Processes* 2:25.
- Foltz, Meg., 2008. A WATBAL watershed program input data and summary report for U.S. Department of Agriculture, Forest Service, Clear water National Forest. Unpublished data supplied to author by M. Foltz, a Clearwater National Forest hydrologist.
- Foltz, R.B., Robichaud, P.R., Rhee, H., 2009. A synthesis of post-fire road treatments for BAER teams: methods, treatment effectiveness, and decision making tools for rehabilitation. US Department of Agriculture, Forest Service, Rocky Mountain Research Station. General Technical Report RMRS-GTR-228 (Fort Collins, CO).
- Frankenberger, J. R., Dun, S., Flanagan, D. C., Wu, J. Q., Elliot, W. J., 2011. Development of a GIS interface for WEPP model application to Great Lakes forested watersheds. In Proc. Intl. Symp. on Erosion and Landscape Evolution, Paper 11139. St. Joseph, Mich.: ASABE
- Garbrecht, J., Martz, L.W. , 1997. TOPAZ Version 1.20: An automated digital landscape analysis tool for topographic evaluation, drainage identification, watershed segmentation and subcatchment parameterization - Overview. Rep.# GRL 97-2, Grazinglands Research Laboratory, USDA, Agricultural Research Service, El Reno, Oklahoma, 21 pp.
- Goodrich, D.C., Canfield, H.E., Burns, I.S., Semmens, D.J., Hernandez, M., Levick, L.R., Guertin, D.P., Kepner, W. 2005. [Rapid post-fire hydrologic watershed assessment using the AGWA GIS-based hydrologic modeling tool](#). Proc. ASCE Watershed Manage. Conf., July 19-22, Williamsburg, VA., 12p., CD-ROM.
- Hamilton, E.L., Rowe, P.B., 1949. Rainfall interception by chaparral in California. USDA and California Dep. Natur. Resour. Div. Forestry. Unnumbered Pub.
- Hawkins, R.H., Greenberg, R.J., 1990. WILDCAT4 Flow Model. University of Arizona, School of Renewable Natural Resources, Tucson, AZ
- Hawkins, R.H., Munoz, A.B., 2011. Wildcat 5 for Windows (W5W): documentation and manual. Tucson, AZ: University of Arizona, School of Natural Resources and Environment.
- Holmes, J.D., 2015. Wind Loading of Structures. 3rd ed. Boca Raton, FL: CRC Press, 413 p.
- Holzhey, C.S., 1969. Water-repellent soil in Southern California. In: DeBano, L.F., Letey, J. (Eds.), *Water-Repellent Soils: Proceedings*, Riverside, CA, pp. 31-41.
- Imeson, A.C., Verstraten, J.M., vanMulligan, E.J., Sevink, J., 1992. The effects of fires and water repellency on infiltration and runoff documented previously, but is consistent with our un- under Mediterranean type forest. *Catena* 19:345-361.
- Huffman, E.L., MacDonald, L.H., Stednick, J.D., 2001. Strength and persistence of fire-induced soil hydrophobicity under pon-derosa and lodgepole pine, Colorado Front Range. *Hydrol. Proc.* 15:2877-2892

- Inbar, M., Tamir, M., Wittenberg, L., 1998. Runoff and erosion processes after a forest fire in Mount Carmel, a Mediterranean area. *Geomorphology* **24**,17–33. doi:10.1016/S0169-555X(97)00098-6
- Iorgulescu, I., Musy, A., 1998. Generalization of TOPMODEL for a power law transmissivity profile. *Hydrological Processes* **11**, 1353–1355.
- Jarrett, R.D., England, J.F., 2002. Reliability of paleostage indicators for paleoflood studies: in House, P.K., Webb, R.H., Baker, V.R., and Levish, D.R., (eds), *Ancient Floods, Modern Hazards, Principles and Applications of Paleoflood Hydrology*, American Geophysical Union, Water and Science Application 5, Washington, D.C., p. 99-110.
- Jenkerson, C. B., Maier-sperger, T.K., Schmidt, G. L., 2010, eMODIS - a user-friendly data source. U.S. Geological Survey (USGS) Open-File Report, Reston, VA, USA. 2010-1055
- Johansen, M.P., Hakonson, T.E., Breshears D.D., 2001, Post-fire runoff and erosion from rainfall simulation: contrasting forests with shrub lands and grasslands. *Hydrological Processes* **15**: 2953– 2965.
- Kean, J.W., Staley, D.M., Cannon, S.H., 2011. In situ measurements of post-fire debris flows in southern California: Comparisons of the timing and magnitude of 24 debris-flow events with rainfall and soil moisture conditions. *Journal of Geophysical Research* **116**. <http://dx.doi.org/10.1029/2011JF002005> (F04019).
- Keizer, J.J., Coelho, C.O.A., Shakesby, R.A., Domingues, C.S.P., Malvar, M.C., Perez, I.M.P., Matias, M.J.S., Ferreira, A.J.D., 2005. The role of soil water repellency in overland flow generation in pine and eucalypt forest stands in coastal Portugal. *Australian Journal of Soil Research* **43**, 337–349.
- Kirkby, M.J., 1997. TOPMODEL: A personal view. *Hydrological Processes* **11**, 1087-1097
- Kinoshita, A.M., Hogue, T.S. Napper, C., 2014. Evaluating Pre-and Post-Fire Peak Discharge Predictions across Western US Watersheds. *JAWRA Journal of the American Water Resources Association*, **50**(6), 1540-1557.
- Letey, J., 2001. Causes and consequences of fire-induced soil water repellency. *Hydrol. Proc.* **15**:2867–2875.
- LACDPW (Los Angeles County Department of Public Works), 1991. Modeling Single Storm Events in Small Urban Areas. <https://www.aquaveo.com/software/wms-modrat>
- Luce, C.H. 2001. FERGI: Fire Enhanced Runoff and Gully Initiation model. Available: <http://fergi.boise.rmrs.fs.fed.us/fergi/> [2 January 2008].
- MacDonald, L.H., Huffman, E.L., 2004. Post-fire soil water repellency: persistence and soil moisture threshold. *Soil Science Society of America Journal* **68**, 1729–1734.
- Martinez-Mena, M., Alvarez, Rogel J., Albaladejo, J., Castillo, V.M., 2000. Influence of vegetal cover on sediment particle size distribution in natural rainfall conditions in a semiarid environment. *Catena* **38**,175–190. doi:10.1016/S0341-8162(99)00073-9
- Meeuwig, R.O., 1971. Infiltration and water repellency in granitic soils. Res. Paper INT-111. USDA For. Serv., Intermountain Res. Sta., Ogden, UT, 10pp.
- Miller, M. E., Billmire, M., Elliot, W. J., Endsley, K. A., Robichaud, P. R., 2015. Rapid response tools and datasets for post-fire modeling: linking Earth Observations and process-based hydrological models to support post-fire remediation, *Int. Arch. Photogramm. Remote Sens. Spatial Inf. Sci.*, **XL-7/W3**, 469-476, doi:10.5194/isprsarchives-XL-7-W3-469-2015.
- Miller, M.E., Elliot, W.J., Billmire, M., Robichaud, P.R., Endsley, K.A., 2016. Rapid response

- tools and datasets for post-fire remediation: Linking remote sensing and process-based hydrologic models. *International Journal of Wildland Fire* (25): 1061-1073.
- Montesinos-Barrios, P. and Beven, K., 2004. Evaluation of TOPMODEL. Southern Cooperative Series Bulletin. <http://www3.bae.ncsu.edu/Regional-Bulletins/Modeling-Bulletin/TOPMODEL.html#837359>.
- Moody, J.A., 2012. An analytical method for predicting post wildfire peak discharges. U.S. Geological Survey Scientific Investigations Report 2011–5236. (36 pp.).
- Moody, J.A., Martin, D.A., 2001. Post-fire, rainfall intensity-peak discharge relations for three mountainous watersheds in the western USA. *Hydrological Processes* **15**, 2981–2993. doi:10.1002/HYP.386
- Moody, J.A., Martin, D.A., Haire, S.L., and Kinner, D.A. 2008. Linking runoff response to burn severity after a wildfire. *Hydrological Processes* **22**, 2063–2074.
- Moody, J.A., Martin, D.A., 2009. Synthesis of sediment yields after wildland fire in different rainfall regimes in the western United States. *International Journal of Wildland Fire* **18**, 96–115.
- Moody, J.A., Shakesby, R.A., Robichaud, P.R., Cannon, S.H., Martin, D.A., 2013. Current research issues related to post-wildfire runoff and erosion processes. *Earth-Science Reviews* **122** : 10–37. DOI: 10.1016/j.earscirev.2013.03.004
- Morris, S.E., Moses, T.A., 1987. Forest fire and the natural soil erosion regime in the Colorado Front Range. *Ann. Assoc. Am. Geog.* **77**:245–254.
- Myneni, R., Knyazikhin, Y., Park, T., 2015, MCD15A2H MODIS/Terra+Aqua Leaf Area Index/FPAR 8-day L4 Global 500m SIN Grid V006. distributed by NASA EOSDIS Land Processes DAAC, <https://doi.org/10.5067/MODIS/MCD15A2H.006>
- Nalder, I.A., Wein, R.W., 1998, Spatial interpolation of climatic normals: test of a new method in the Canadian boreal forest. *Agricultural and Forest Meteorology*, **92**(4), pp.211-225.
- Nash, J.E., Sutcliffe, J.V., 1970. River flow forecasting through conceptual models Part I—a discussion of principles. *Journal of Hydrology* **27** (3), 282–290.
- Neary, D.G., 2011. Impacts of wildfire severity on hydraulic conductivity in forest, woodland and grassland soils. In: Elange, L. (Ed.), *Hydraulic Conductivity—Issues, Determination, and Application*. InTech Publishers, Rijeka, Croatia, pp. 123–142.
- Neary, D.G., G.J. Gottfried, and P.F. Folliott. 2003. Post-wildfire watershed flood responses. Pp. 16–20 in *Proceedings of the 2nd International Fire Ecology Conference*, Orlando, FL.
- Neary, D.G., Ryan, K.C., DeBano, L.F., (Editors) (2005) (Revised 2008). *Wildland fire in ecosystems: Fire effects on soil and water*. General Technical Report RMRS-GTR-42, Volume 4, Fort Collins, CO: U.S. Department of Agriculture, Forest Service, Rocky Mountain Research Station. 250 p.
- Nyman, P., Sheridan, G., Lane, P.N.J., 2010. Synergistic effects of water repellency and macropore flow on the hydraulic conductivity of a burned forest soil, south-east Australia. *Hydrological Processes* **24**, 2871–2887.
- Onda, Y., Dietrich, W.E., Booker, F., 2008. Evolution of overland flow after a severe forest fire. Point Reyes, California. *Catena* **72**, 13–20.
- Owens, M.K., Lyons, R.K., Alejandro, C.L., 2006. Rainfall partitioning within semiarid juniper communities: effects of event size and canopy cover. *Hydrological Processes* **20**, 3179–3189. doi:10.1002/HYP.6326
- Ponce, V.M., 1989, *Engineering hydrology—Principles and practices*: Englewood Cliffs, New Jersey, Prentice-Hall, Inc., 642 p.

- Priestley, C.H.B., Taylor, R.J., 1972. On the Assessment of Surface Heat Flux and Evaporation Using Large-Scale Parameters. *Monthly Weather Review* 100 (2), 81–92. doi:10.1175/1520-0493(1972)100<0081:OTAOSH>2.3.CO;2.
- Perrin, C., Michel, C., Andre´assian, V., 2001. Does a large number of parameters enhance model performance? Comparative assessment of common catchment model structures on 429 catchments. *Journal of Hydrology* 242, 275–301.
- Renschler, C.S., 2003. Designing geo-spatial interfaces to scale process models: the GeoWEPP approach. *Hydrol. Process.* 17, 1005e1017.
- Ritsema, C.J., Dekker, L.W., (Editors) (2003). *Soil Water Repellency: Occurrence, Consequences, and Amelioration*. ISBN-13: 978-0444512697. 358 p.
- Robichaud, P.R., 2000. Fire effects on infiltration rates after prescribed fire in northern Rocky Mountain forests, USA. *Journal of Hydrology*, pp. 220–229.
- Robichaud, P.R., Lewis, S.A., Ashmun, L.E., 2008. New procedure for sampling infiltration to assess post-fire soil water repellency. US Department of Agriculture, Forest Service, Rocky Mountain Research Station, Research Note RMRS-RN-33. (Fort Collins, CO). Available at [http:// forest.moscowfsl.wsu.edu/BAERTOOLS/MDI/](http://forest.moscowfsl.wsu.edu/BAERTOOLS/MDI/) [Verified 14 April 2012]
- Robichaud, P.R., Ashmun, L.E., Foltz, R.B., Showers, C.G., Groenier, J.S., Kesler, J., DeLeo, C., Moore, M., 2013a. Production and aerial application of wood shreds as a post-fire hillslope erosion mitigation treatment. Gen. Tech. Rep. RMRS-GTR-307. Fort Collins, CO: U.S. Department of Agriculture, Forest Service, Rocky Mountain Research Station. 31 p.
- Robichaud, P.R., Lewis, S.A., Wagenbrenner, J.W., Ashmun, L.E., Brown, R.E., 2013b. Post-fire mulching for runoff and erosion mitigation: Part I: Effectiveness at reducing hillslope erosion rates. *Catena*. 105:75-92.
- Rowe, P.B., 1948. Influence of woodland chaparral on water and soil in central California.[N.p.]: State of California Department of Natural Resources, Division of Forestry, in cooperation with the U.S. Department of Agriculture, Forest Service, California Forest and Range Experiment Station. 70 p.
- Rowe, P.B., C.M. Countryman, and H.C. Storey, 1949. Probable Peak Discharge and Erosion Rates from Southern California Watersheds as Influenced by Fire. Department of Agriculture, Forest Service, PacificSouthwest Forest and Range Experiment Station, Berkeley, California.
- Rutter, A.J., A.J. Morton, and P.C. Robins, 1971. A Predictive Model of Rainfall Interception in Forests. I. A Derivative of the Model From Observations in a Plantation of Corsican Pine. *Agricultural Meteorology* 9:367.
- Rutter, A.J., A.J. Morton, and P.C. Robins, 1975. A Predictive Model of Rainfall Interception in Forests. II. Generalization of the Model and Comparison With Observations in Some Coniferous and Hard-Wood Stands. *Journal of Applied Ecology* 12:367.
- Schmidt, K.M., Hanshaw, M.N., Howle, J.F., Kean, J.W., Staley, D.M., Stock, J.D., Bawden, G.W., 2011. Hydrologic conditions and terrestrial laser scanning of post-fire debris flows in the San Gabriel Mountains, CA, U.S.A *Italian Journal of Engineering Geology and Environment*. <http://dx.doi.org/10.4408/IJEGE.2011-03.B-064>.
- Shakesby, R.A., Doerr, S.H., Walsh, R.P.D., 2000. The erosional impact of soil hydrophobicity: current problems and future research directions. *Journal of Hydrology* 231–232, 178–191.

- Shuttleworth, W.J., 1993, Evaporation, in Maidment, D.R. (Ed.), 1993. Handbook of Hydrology. McGraw-Hill, Inc.
- Sacramento River Watershed Program, 2018. Cache Creek Watershed. Available online at <http://www.sacriver.org/aboutwatershed/roadmap/watersheds/westside/cache-creek-watershed>. Accessed 8/22/2018.
- Skau, C.M., 1964 Interception, throughfall, and stemflow in Utah and alligator juniper cover types in northern Arizona. *Forest Science* **10**, 283–287.
- Smith, R. E., Quinton, J. N., 2000. “Dynamics and Scale in Simulating Erosion by Water”. In: Schmidt, J. (Editor). *Soil Erosion: Application of Physically Based Models*. Berlin: Germany, Springer-Verlag, pp.283-294
- Smith, H.G., Sheridan, G.J., Lane, P.N., Nyman, P., Haydon, S., 2011. Wildfire effects on water quality in forest catchments: a review with implications for water supply. *Journal of Hydrology* 396(1–2), 170–192. doi:10.1016/J.JHYDROL.2010.10.043.
- Spigel, K.M., Robichaud P.R., 2007. First-year post-fire erosion rates in the Bitterroot National Forest, Montana. *Hydrological Processes* 21, 998–1005. doi:10.1002/HYP.6295
- Stern, M., Flint, L., Minear, J., Flint, A., Wright, S., 2016, Characterizing changes in streamflow and sediment supply in the Sacramento River basin, California, Using Hydrological Simulation Program—FORTRAN (HSPF). *Water*; 8(10):432.
- Stern, M.A., Flint, A.F., Flint, L.E., 2019. Characterization of hydrology and sediment following drought and wildfire in Cache Creek, California. In preparation.
- Swets, D.L., Reed, B.C., Rowland, J.R., and Marko, S.E., 1999, A weighted least-squares approach to temporal smoothing of NDVI. In Proceedings of the 1999 ASPRS Annual Conference, from Image to Information, Portland, Oregon, May 17-21, Bethesda, Maryland, American Society for Photogrammetry and Remote Sensing, CD-ROM, 1 disc.
- Soil Survey Staff, Natural Resources Conservation Service, United States Department of Agriculture. Soil Survey Geographic (SSURGO) Database. Available online at <https://sdmdataaccess.sc.egov.usda.gov>. Accessed 11/27/2017.
- Soil Survey Staff, Natural Resources Conservation Service, United States Department of Agriculture. U.S. General Soil Map (STATSGO2). Available online at <https://sdmdataaccess.sc.egov.usda.gov>. Accessed 12/14/2017.
- Tromble, J.M., 1983. Interception of rainfall by tarbush. *Journal of Range Management* **36**, 525–526. doi:10.2307/3897960
- U.S. Army Corps of Engineers, 2010. Hydrologic modeling system HEC-HMS: User’s manual version 3.5. Davis, CA: U.S. Army Corps of Engineers, Institute for Water Resources, Hydrologic Engineering Center. 316 p.
- U.S. Department of Agriculture, Natural Resources Conservation Service, 2009. Small watershed hydrology: WinTR-55 U.S. er Guide. Conservation Engineering Division.
- USFS Geospatial Technology and Applications Center, 2018. Frequently Asked Questions. <https://www.fs.fed.us/eng/rsac/baer/barc.html>. Accessed 8/16/2018.
- United States Geological Survey (USGS), National Geospatial-Intelligence Agency (NGA), and National Aeronautics and Space Administration (NASA), 2014. Shuttle Radar Topography Mission 1 Arc-Second Global. Available online at <https://earthexplorer.usgs.gov>. Accessed 10/10/2017.
- Wainwright, J., Parsons, A.J., Abrahams A.D., 1999. Rainfall energy under creosotebush. *Journal of Arid Environments* **43**, 111–120. doi:10.1006/JARE.1999.0540

- Wang, J., Endreny, T.A. and Hassett, J.M., 2005. A Flexible Modeling Package for Topographically Based Watershed Hydrology. *Journal of Hydrology* 314(1-4):78-91.
- Wang, J., Endreny TA., Nowak, DJ., 2008. Mechanistic simulation of tree effects in an urban water balance model. *J. Am. Water. Resour. Assoc.* 44:75–85.
- Westerling, A., Brown, T., Schoennagel, T., Swetnam, T., Turner, M., Veblen, T., 2014. Briefing: Climate and wildfire in western US forests. USDA Forest Service RMRS-P-71.
- Williams, CJ., Pierson, FB., Robichaud, PR., Boll, J., 2014. Hydrologic and erosion responses to wildfire along the rangeland–xeric forest continuum in the western US: a review and model of hydrologic vulnerability. *International Journal of Wildland Fire* **23**, 155–172.
- Wondzell, S.M., King, J.G., 2003. Post-fire erosional processes in the Pacific Northwest and Rocky Mountain regions. *Forest Ecology and Management* 178, 75–87.
- Ye, W., Bates, B.C., Viney, N.R., Silvapan, M., Jakeman, A.J., 1997. Performance of conceptual rainfall runoff models in low-yielding ephemeral catchments. *Water Resources Research* 33 (1), 153–166.